Strength mismatch effects on weld centre cracks under mode-I loading: Analytical and Numerical Investigation

by

Imran Ali Khan

(Enroll. No. ENGG 01200704002)

Bhabha Atomic Research Centre, Mumbai, India

A thesis submitted to the Board of Studies in Engineering Sciences

In partial fulfillment of the requirements

For the Degree of

DOCTOR OF PHILOSOPHY

of

Homi Bhabha National Institute, Mumbai

June, 2012

Homi Bhabha National Institute

Recommendations of the Viva Voce Board

As members of the Viva Voce Board, we certify that we have read the dissertation prepared by Imran Ali Khan entitled "Strength mismatch effects on weld centre cracks under mode-I loading: Analytical and Numerical investigation" and recommend that it may be accepted as fulfilling the dissertation requirement for the Degree of Doctor of Philosophy.

________________________ Date:21st June, 2012
Chairman: Prof. V. K. Suri

________________________ Date: 21st June, 2012
Guide: Prof. A. K. Ghosh

J. Chattopadhyay
________________________ Date: 21st June, 2012
Co-Guide: Dr. J. Chattopadhyay

________________________ Date: 21st June, 2012
Technical Advisor: Mr. V. Bhasin

________________________ Date: 21st June, 2012
Member-1: Prof. P. Chellapandi

________________________ Date: 21st June, 2012
Member-2: Prof. G. R. Reddy

________________________ Date: 21st June, 2012
Examiner: Prof. S. K. Maiti

Final approval and acceptance of this dissertation is contingent upon the candidate's submission of the final copies of the dissertation to HBNI. I hereby certify that I have read this dissertation prepared under my direction and recommend that it may be accepted as fulfilling the dissertation requirement.

Date: 21st June, 2012

Place: Mumbai

Guide: Prof. A. K. Ghosh

STATEMENT BY AUTHOR

This dissertation has been submitted in partial fulfillment of requirements for an advanced degree at Homi Bhabha National Institute (HBNI) and is deposited in the library to be made available to borrowers under rules of the HBNI.

Brief quotations from this dissertation are allowable without special permission, provided that accurate acknowledgement of source is made. Requests for permission for extended quotation from or reproduction of this manuscript in whole or in part may be granted by the Competent Authority of HBNI when in his or her judgment the proposed use of the material is in the interests of scholarship. In all other instances, however, permission must be obtained from the author.

Imran Ali Khan

DECLARATION

I, hereby declare that the investigation presented in the thesis has been carried out by me. The work is original and has not been submitted earlier as a whole or in part for a degree / diploma at this or any other institution / University.

Imran Ali Khan

DEDICATIONS

To my Parents

ACKNOWLEDGEMENT

First I would take this opportunity to express my sincere gratitude to my research adviser Prof. A.K. Ghosh for the encouragement, guidance and support that he has provided during the course of this thesis. Invaluable suggestions emanating from several discussions and his able guidance have finally ensured that this research work sees the light of the day. This work would have not been possible without his enthusiastic involvement in every aspect of it.

I would thank Shri K.K. Vaze, Head, Reactor Safety Division, BARC for permitting me to purse this research work. He has been a source of great inspiration who always advised me to maintain a balance between academic interest and the application aspects of new research. I am also greatly indebted to Mr. H.S. Kushwaha former Director, Health Safety & Environment Group, BARC. He like a true leader realised my inclination towards research work and assigned me the work accordingly. The present thesis is essentially an outcome of one of such assignments. I would also like to express my sincere appreciation to my co-guide Dr. J. Chattopadhyay for several helpful discussions. His constant encouragement and constructive comments have enabled me to focus on key issues related to this research work. I am extremely thankful to my technical adviser Mr. V. Bhasin with whom I have been associated right from day one of my professional carrier. Without his support, work of this magnitude would have been difficult to undertake and finish. He willingly took the pain and shouldered the responsibility of day-to-day office activities and spared me to pursue my research interests.

I greatly acknowledge the contributions of my doctoral committee members Prof. V.K. Suri, Prof. P. Chellapandi and Prof. G.R. Reddy who spared their valuable time for periodical critical assessment of my work. Incorporation of their constructive suggestions has greatly enhanced the technical level of my research work.

Though they may never know, I would like to thank all those researchers whose works provided useful information and understanding related to my research problem. Special thanks are due to Profs. S. Bordas, Y. J. Chao, and A. S. Khan, whom I disturbed several times through my e-mails seeking some technical clarifications. In spite of their extremely busy schedules all these "true gentlemen" showed such a warm and encouraging response that verbal appraise is not sufficient to express my respect towards them. I would also like to thank my close friend Dr. K.K. Singh for providing me help in several ways during the course of this thesis. Direct or indirect support received from BARC is gratefully acknowledged. I thank with apology all those people whose contributions to this work have escaped my attention and, thus, have gone unnoticed.

Words will not be enough to express my thanks to Reshma for exhibiting extraordinary patience which was put to test during last four years. She managed to deal with my self-isolation and neglect of almost all the household chores. Special thanks are due to cute little Sara who often had to wait for long hours due to my late arrival from office. Thanks are due to my parents and elders for their true blessings.

Imran Ali Khan

Contents

Synopsis i

List of publications iv

List of Figures v

List of Tables xi

Nomenclature xii

1. Introduction 1

1.1 Fracture assessment procedures for welds 3

1.2 Identification of issues for investigation 4

1.3 Scope of work 5

1.4 Objectives of the thesis 6

1.5 Organisation of the report 8

2. Literature review 12

2.1. Analytical and numerical studies on plane 2-D fracture specimens 12

2.2. Experimental studies on strength mismatch welds 30

2.3. Plane strain theory of slip line field 33

3. Development of the modified upper bound theorem for rigid plastic body in plane strain 43

3.1. Introduction 43

3.2. Assumption of plastic-rigid material 45

3.3. Virtual work principle 46

3.4. General theorems of limit analysis 49

3.5. Analytical formulation of the modified upper bound theorem 54

4. Application of proposed modified upper bound theorem to plane strain problems in homogeneous materials 63

4.1. Introduction 63

4.2. Equivalence of proposed modified upper bound theorem with slip line field analysis 66

4.2.1. Bending of cantilever 67

4.2.2. Bending of deeply cracked fracture mechanics specimens 75

4.2.3. Compact tension C(T) specimen 93

4.2.4. Single-edge cracked specimen under combined bending and tension 97

4.3. Discussion 102

5. Strength mismatch effects on the limit load and crack tip constraint of pure bending SE(PB) specimen and compact tension C(T) specimen having a weld centre crack 116

5.1. Introduction 116

5.2. Structure of stress fields for a deeply cracked pure bending SE(PB) specimen having a weld centre crack under fully plastic state in mode-I loading 117

5.3. Structure of stress fields for a deeply cracked compact tension C(T) specimen having a weld centre crack under fully plastic state in mode-I loading 141

5.4. Finite element analysis 142

5.5. Results 143

5.6. Discussion 145

6. A study of the limit load and crack tip constraint of middle tension M(T) specimen having a weld centre crack 162

6.1. Introduction 162

6.2. Analysis of overmatched middle tension M(T) specimen having a weld centre crack 164

6.3. Analysis of undermatched middle tension M(T) specimen having a weld centre crack 169

6.4. Results 175

6.5. Discussion 176

7. Aspects related to plastic η factor of plane strain fracture specimens having weld centre crack 187

7.1. Introduction 187

7.2. Analytical evaluation of plastic η-factor 189

7.3. Numerical evaluation of plastic η-factor 190

7.4. Analytical solutions of plastic η-factor of plane strain fracture specimens having weld centre crack 191

7.5. Results 192

7.6. Discussion 192

8. Characterisation of crack tip stresses in elastic-perfectly plastic material under mode-I loading 199

8.1. Introduction 199

8.2. Governing equations 203

8.3. Elastic-plastic crack tip stress field under mode-I loading 207

8.4. Finite element simulation of crack tip stress fields for different constraint levels in incompressible elastic-perfectly plastic material 217

8.5. Results 220

8.6. Discussion 225

9 Conclusions and future work 238

9.1 Conclusions 238

9.2 Future work 241

Bibliography 242

Synopsis

Welding is one of the most widely used fabrication process in the nuclear power plants. It has been observed that weld joint locations are generally critical in comparison to base metal and, thus, their fracture integrity must be assured. Conventional defect assessment procedures that are being used at present were essentially developed for cracks lying in a homogeneous material. In view of the variations in the tensile and fracture properties of base and weld material, the integrity assessment of strength mismatch welds is not straightforward. Extensive studies are required on welds as besides specimen geometry and loading conditions the strength mismatch ratio M (defined as ratio of yield strength of weld to yield strength of base material) and weld slenderness ratio ψ (defined as ratio of uncracked ligament to half weld thickness) are the additional variables affecting the fracture assessment procedures. The present investigation is an effort in that direction.

In this work, detailed theoretical and numerical studies were performed on elastic-perfectly plastic (non-hardening) material. It is well recognized that such idealised model does not adequately represent the real material behaviour, however, insight into the physics of deformation can be obtained by this simplified material response. Thus, in present investigation, both base and weld materials were modeled as elastic-perfectly plastic. The two materials were assumed to have same elastic modulus and Poisson's ratio but mismatch in their yield strength. All the investigations in this work are based on plane-strain assumption. Crack was postulated at the centre of weld. Numerical studies were performed within the framework of continuum scale plasticity (J_2 flow theory) and effects of micro-structural heterogeneity and presence of residual stresses were not accounted.

A new load bounding technique, Modified Upper Bound (MUB) theorem, was proposed. Rigorous mathematical basis of this load bounding technique and its equivalence with the classical Slip Line Field analysis (SLF) was presented. Various simplifications resulting from the use of this new load bounding technique over SLF method were demonstrated. Several standard problems of plane strain analysed by SLF method and validated by experiments in past were examined. As a novel application of the proposed method, a complete analytical formulation for yield locus for the entire range of tensile and bending load was obtained for a single-edge-cracked plate.

Apart from analysing standard homogeneous fracture mechanic specimens in plane-strain condition, the proposed MUB method was used to analyse weld strength mismatch effects. Application of MUB method to the practical problem of evaluation of the limit load, plastic η-factor (used for experimental evaluation of fracture toughness), and crack tip stress fields of fracture specimens having weld centre crack was demonstrated. Aspects related to state of stress at the base-weld interface were discussed in detail. Excellent agreement was observed between the proposed theoretical solutions and those obtained from detailed full-field finite element analysis.

In addition, the important concern of characterization of crack-tip stresses in incompressible elastic-perfectly plastic material under mode-I loading was dealt with. Detailed investigations revealed that the most general elastic-plastic crack-tip fields can be completely described by the 5-sector stress solution proposed in this work. It is well known that the loss of constraint at the crack-tip leads to an elastic sector at the crack flank leading to incomplete crack-tip plasticity. This study has revealed that cases arise where the severe loss of crack-tip constraint can lead to compressive yielding of crack flank that can be described by the 5-sector stress field. Several important applications of the proposed 5-sector stress fields were discussed. A new constraint-indexing parameter T_{CS-2} was proposed which along with hydrostatic stress ahead of crack tip is capable of representing the entire elastic plastic crack-tip stress fields over all angles around a crack tip. Excellent agreement was obtained between the proposed asymptotic crack-tip stress field and the finite element results. It was demonstrated that the proposed constraint parameters are adequate to represent the crack-tip constraint arising due to specimen geometry and loading conditions as well as the additional constraint that arises due to weld mismatch.

Towards the end we would like to briefly address the application aspects of this work. Although finite element analysis may be used to carry out integrity assessment of strength mismatch weld on case by case basis, however, for engineering applications a simplified fracture assessment procedure is invariably preferred. Most of the commonly used fracture assessment procedures developed for welds require the limit load. In addition, evaluation of plastic η-factor is required for experimental evaluation of fracture toughness. The proposed solutions of limit load would be useful for engineering fracture assessment of these strength mismatch welds. Although the proposed solutions of plastic η-factors and crack-tip constraint were evaluated for non-hardening material model, however, the results may still be applicable for materials having low and even moderate strain-hardening. It is expected that the detailed analytical and numerical studies performed in this work would provide a comprehensive understanding of the effects of weld strength mismatch on the limit load, plastic η-factor and crack tip stress fields of plane strain fracture specimens.

List of Publications

International Journals: 04

1. An insight of the structure of stress fields for stationary crack in strength mismatch weld under plane strain mode-I loading- Part I: Pure Bending Specimen. **I.A. Khan**, V. Bhasin, J. Chattopadhyay, and A.K. Ghosh, *International Journal of Mechanical Sciences, 2012, (In Press).*

2. Characterisation of crack-tip stresses in elastic-perfectly plastic material under mode-I loading. **I.A. Khan**, V. Bhasin, J. Chattopadhyay and A.K. Ghosh, *International Journal of Mechanical Sciences, 53, 2011, 207-216.*

3. On the equivalence of slip-line fields and work principles for rigid-plastic body in plane-strain. **I.A. Khan**, V. Bhasin, J. Chattopadhyay and A.K. Ghosh, *International Journal of Solids and Structures, 45, 2008, 6416-6435.*

4. A Modified Upper Bound Approach to limit analysis for plane strain deeply cracked specimens. **I.A. Khan** and A.K. Ghosh, *International Journal of Solids and Structures, 44, 2007, 3114-3135.*

International Conferences: 04

5. Analytical evaluation of crack tip constraint for rigid plastic material using Work principles. **I.A. Khan**, V. Bhasin, J. Chattopadhyay, K.K. Vaze, and A.K. Ghosh, *21st Int. Conf. on Struct. Mech. in Reactor Tech. (SMiRT-21)*, New Delhi, November 6-11, 2011.

6. Two parameter characterisation of crack tip stress field in elastic-perfectly plastic material. **I.A. Khan**, V. Bhasin, J. Chattopadhyay, K.K. Vaze, and A.K. Ghosh, *21st Int. Conf. on Struct. Mech. in Reactor Tech. (SMiRT-21)*, New Delhi, November 6-11, 2011.

7. Fracture mechanics evaluation of similar and dissimilar welded fracture specimens in plane-strain. **I.A. Khan**, V. Bhasin, J. Chattopadhyay, K.K. Vaze, A.K. Ghosh, and H.S. Kushwaha, *20th Int. Conf. on Struct. Mech. in Reactor Tech. (SMiRT-20)*, Espoo, Finland, August 9-14, 2009.

8. Structural Integrity assessment of welds, **I.A. Khan**, V. Bhasin, J. Chattopadhyay and A.K. Ghosh, *Inter-quadrennial Conf. of the Int. Congress on Fracture, IQCICF-08,* IISc., Bangalore, August 4-7, 2008.

List of Figures

1.1 Geometries investigated in present work (a) Pure bending SE(PB) specimen, (b) Middle tension M(T) specimen and (c) Compact tension C(T) specimen having a weld centre crack 11

2.1 Description of slip lines in Cartesian coordinate system 41

2.2 Stresses acting on a plane strain element cut out by slip lines 42

3.1 Schematic used for analytical formulation of Modified Upper Bound (MUB) theorem 62

4.1 (a) Assumed plastic deformation mechanism for a short cantilever under transverse load, Green (1954) 105

(b) Schematic describing the relationship between tangential velocity v^* and the imposed displacement $\dot{\delta}$ 106

(c) Stress and velocity distribution on the elastic-plastic boundary of a short cantilever 107

4.2 Assumed plastic deformation mechanism for a long cantilever under transverse load, Green (1954) 108

4.3 Assumed plastic deformation mechanism for a pure bending SE(PB) specimen, Green (1953) 109

4.4 Asymptotic fully plastic crack tip stress fields for a deeply cracked pure bending SE(PB) specimen and three-point bend SE(B) specimen 110

4.5 Assumed plastic deformation mechanism for a three-point bend SE(B) specimen, Green and Hundy (1956) 111

4.6 Schematic describing the relationship between the tangential velocity and imposed displacement for a three-point bend SE(B) specimen 112
4.7 Effect of indenter width on plastic deformation mechanism for SE(B) specimen, Ewing (1968) 113
4.8 Assumed plastic deformation mechanism for a compact tension C(T) specimen, Ewing and Richards (1974) 114
4.9 Assumed plastic field for a single-edge-cracked specimen under bending with small tensile load, Shiratori and Dodds (1980) 115
5.1 Schematic of (a) an interface crack and (b) a weld centre crack in a strength mismatch weld 148
5.2 Pure bending SE(PB) specimen with a weld centre crack 149
5.3 (a) Proposed structure of stress field-A and (b) plot of equivalent plastic strain obtain from FE analysis 150
5.4 Asymptotic incomplete crack-tip stress field for a deeply cracked SE(PB) specimen and C(T) specimen 151
5.5 Description of stress field-B (a) complete structure of the proposed field (b) zoomed portion of stress field near free surface and (c) plot of equivalent plastic strain obtained from FE analysis 152
5.6 Description of stress field-C (a) complete structure of the proposed field for an over-match weld and (b) plot of equivalent plastic strain as obtained from FE analysis 153
5.7 Description of stress field-D (a) complete structure of the proposed field for an overmatch weld and (b) plot of equivalent plastic strain as obtained

from FE analysis 154

5.8 Description of stress field-E (a) complete structure of the proposed field and (b) plot of equivalent plastic strain as obtained from FE analysis 155

5.9 Compact Tension C(T) specimen with a weld centre crack 156

5.10 Finite element discretisation scheme used in present investigation, (a) global view of the mesh used for a SE(PB) specimen and (b) zoomed view near the crack tip 157

5.11 Comparison of (a) normalised limit moment and (b) crack tip constraint parameter *h*, evaluated at θ=0, obtained from MUB theorem with FE results for SE(PB) specimen 158

5.12 Variation of crack tip constraint parameter *h* with polar angle θ for (a) ψ = 10 and (b) ψ = 3.33 obtained from MUB theorem and FE analysis for SE(PB) specimen 159

5.13 Comparison of (a) normalised limit load and (b) crack tip constraint parameter *h*, evaluated at θ=0, obtained from MUB theorem with FE results for C(T) specimen 160

5.14 Variation of constraint parameter *h* with polar angle θ for ψ = 10 obtained from MUB theorem and FE analysis for C(T) specimen 161

6.1 Middle tension M(T) specimen having a weld centre crack 178

6.2 (a) Proposed stress field for an overmatched M(T) specimen having a weld centre crack 179

6.2 (b) Stress and velocity distribution on the elastic-plastic boundary of an overmatched M(T) specimen having a weld centre crack 180

6.3 Proposed slip line field of extremely undermatched M(T) specimen having a weld centre crack ($1 \leq \psi \leq 3.6$) 181
6.4 Proposed slip line field of extremely undermatched M(T) specimen having a weld centre crack ($3.6 \leq \psi \leq 5.0$) 182
6.5 Comparison of normalised limit load of M(T) specimen, having a weld centre crack, obtained from MUB theorem with FE results 183
6.6 Comparison of normalised limit load of M(T) specimen, having a weld centre crack, provided by Hao et al. (1997) with author's FE results 184
6.7 Comparison of crack tip constraint parameter *h* of overmatched M(T) specimen obtained from MUB theorem with FE results 185
6.8 Comparison of crack tip constraint parameter *h* of extremely undermatched M(T) specimen obtained from proposed SLF with FE results 186
7.1 Determination of area under experimental load-displacement records for J-estimation (a and b) plastic area for SE(PB) and C(T) specimens, (c and d) plastic area for M(T) specimen 194
7.2 Comparison of LLD based plastic η-factor of SE(PB) specimen having a weld centre crack obtained from MUB theorem with FE results 195
7.3 Comparison of CMOD based plastic η-factor of SE(PB) specimen having a weld centre crack obtained from MUB theorem with FE results 196
7.4 Comparison of CMOD based plastic η-factor of C(T) specimen having a weld centre crack obtained from MUB theorem with FE results of Kim et al. (2003) 197
7.5 Comparison of CMOD plastic η-factor of M(T) specimen having a weld

centre crack obtained from MUB theorem with FE results of Kim et al. (2003) 198

8.1 Description of elastic-plastic crack-tip stress fields under mode I loading by (a) Proposed 5-sector field and (b) 4-sector solution of Zhu and Chao (2001) 228

8.2 Comparison of crack-tip stresses for M(T) specimen obtained from present FE analysis with those of Zhu and Chao (2001) (a) under rigid displacement loading condition and (b) under uniformly distributed applied pressure. While continuous line shows present FE results, the open circles refer to FEA of Zhu and Chao (2001) 229

8.3 Comparison of crack-tip stresses for mismatch welded M(T) specimen with ψ=10. (a) M=0.25 and (b) M=0.75. While continuous line shows the results of asymptotic 4-sector stress solution, the open circles refer to FEA 230

8.4 Comparison of crack-tip stresses for mismatch welded M(T) specimen with ψ=10. (a) M=1.25 and (b) M=1.5 that leads to compressive yielding just on crack flank. While continuous line shows the results of asymptotic 4-sector stress solution, the open circles refer to FEA 231

8.5 Comparison of crack-tip stresses for mismatch welded M(T) specimen with ψ=10 and M=1.75. (a) Asymptotic 4-sector stress solution proposed by Zhu and Chao (2001). (b) Proposed 5-sector stress solution. The open circles refer to results obtained from FEA 232

8.6 Comparison of crack-tip stresses for mismatch welded M(T) specimen with ψ=10 and M=2. (a) Asymptotic 4-sector stress solution proposed by Zhu and Chao (2001). (b) Proposed 5-sector stress solution. The open circles refer to results obtained from FEA 233

8.7 Comparison of crack-tip stresses for mismatch welded M(T) specimen with ψ=1.67. (a) M=0.25 and (b) M=0.75. While continuous line shows the results of asymptotic 4-sector stress solution, the open circles refer to FEA 234

8.8 Comparison of crack-tip stresses for mismatch welded M(T) specimen with ψ=1.67 and M=1.75. (a) Asymptotic 4-sector stress solution proposed by Zhu and Chao (2001). (b) Proposed 5-sector stress solution. The open circles refer to results obtained from FEA 235

8.9 Comparison of crack-tip stresses for mismatch welded M(T) specimen with ψ=1.67 and M=2. (a) Asymptotic 4-sector stress solution proposed by Zhu and Chao (2001). (b) Proposed 5-sector stress solution. The open circles refer to results obtained from FEA 236

8.10 Comparison of crack-tip stresses for mismatch welded SE(PB) specimen with. (a) T_p/k=-1.28, T_{CS-2}/k=-1.32 and (b) T_p/k=-1.16, T_{CS-2}/k=-1.48. While continuous line shows the results of asymptotic 4-sector stress solution, the open circles refer to FEA 237

List of Tables

4.1 Comparison of results of SE(PB) specimen obtained from MUB theorem with SLF analysis (Green, 1953) for a/W=0.3 - 1 81

4.2 Comparison of theoretical results of SE(B) specimen obtained from MUB theorem with SLF analysis (Wu et al., 1987) 90

4.3 Effect of indenter width on plastic field parameters and crack tip stresses obtained from MUB theorem and SLF analysis (Ewing, 1968) for a/W=0.2, W=10 mm 92

4.4 Comparison of results obtained from MUB theorem with SLF solutions (Ewing and Richards, 1974) for W=10 mm 97

8.1 Comparison of 4-sector stress field variables in terms of T_π and $T_{CS\text{-}2}$ parameters 216

8.2 Numerical values of T_p, $T_{CS\text{-}2}$ and T_π parameters for a M(T) specimen, having a weld centre crack, obtained from FE analyses 221

Nomenclature

a	Crack length
F_x	Net force in x-direction (i=1)
F_y	Net force in y-direction (i=2)
h	Crack tip constraint parameter
H	Half weld width
k	Shear yield strength
k_B	Shear yield strength of base material
k_w	Shear yield strength of weld material
l	Uncracked length (W-a)
L	Plastic constraint factor
M	Weld strength mismatch factor
M_L	Limit moment
$M_{homog.}$	Limit moment of homogeneous specimen made from base material
n_i	Direction cosines of a unit vector
P_l	Plane strain limit load
R, R_1	Radii of circular arcs
r_p	Plastic rotation factor
S	Support span
dS	Surface of a differential element
T_i	Surface traction
du_i	Actual displacement field

du_i^*	Kinematically admissible displacement field
W	Width of specimen
x, y, z	Parameters describing the plastic fields
ψ	Weld slenderness ratio ($\psi=l/H$)
θ_b	Angle made by α-slip line with respect to some fixed axis in base material
θ_w	Angle made by α-slip line with respect to some fixed axis in weld material
ω	Relative angular velocity
φ, β, γ	Angles describing extent of circular arcs
$\dot{\delta}$	Rate of imposed displacement
σ_{ij}	Stress components (i=1,2)
σ^k	Mean(hydrostatic) stress at a given point 'k'
σ_b^k	Mean(hydrostatic) stress at a given point 'k' in base material
σ_{eq}	Von-Mises stress
σ_y	Yield strength
σ_{yb}	Yield strength of base material
σ_{yw}	Yield strength of weld material
σ_{ij}^*	Kinematically compatible stress field
η_p	Plastic eta function
η_{LLD}	Load line based eta function
η_{CMOD}	Crack mouth opening displacement based eta function
v^*	Tangential velocity (constant in magnitude)

Abbreviations

SE(PB)	Single edge cracked specimen in pure bending
SE(B)	Single edge cracked specimen in three-point bending
M(T)	Middle tension specimen
C(T)	Compact tension specimen
DE(T)	Double edge cracked specimen in tension
CMOD	Crack mouth opening displacement
LLD	Load line displacement
SLF	Slip-Line field
FEA	Finite element analysis
MUB	Modified upper bound

CHAPTER 1

Introduction

The ever increasing demand for power to support and sustain the requirements of world population of 7.0 billion (in 2011) is dictating the optimum use of energy and materials. Fracture of engineering materials is a problem that society has faced for a long. Major airline crashes, failures of high pressure pipe lines, bursting of liquid and gas storage tankers etc are just a few examples of catastrophic failures. An economic study (Duga et al., 1983) estimated the cost of fracture in the United States in 1978 at around $ 120 billion, about 4% of gross national product. This data is sufficient to indicate that how detrimental these catastrophic failures are to the economy. Moreover, this study also provided an estimate of the annual cost that could be reduced if further research is directed towards understanding and predicting the failure behaviour of materials. Thus, it is a little surprise that substantial efforts are being made worldwide in this direction with a broad objective of developing more robust structural integrity assessment methods so that the safety and integrity of the load bearing components/structures can be reliably assured.

Nuclear power generation is considered to be one of the clean and sustainable sources of energy. At present around 20% of electricity in US and 74% in France is generated through nuclear energy. India has an ambitious plan to extend its power generation capacity through nuclear energy to 20,000 MWe by 2020. Safe and reliable operation of nuclear power plants is an essential requirement to satisfy the public concern of safety besides the obvious economic aspects.

Welding is one of the most widely used fabrication process in the nuclear power plants. It is used to join permanently two, usually metallic, components by the application of heat and/or pressure. The range of pressure and temperature used may vary a lot depending up on the particular welding technique but heating and cooling are integral parts of most welding process. The particular combination of these variables results in a joint that is unique in terms of material variation, potential flaws, and residual stresses. Material variations occur across a weld joint because each region of weld is subjected to a different thermal history, with temperatures rising, in some cases, above those required for phase transformation and grain growth. In a typical multi-pass weld in steels, for instance, several regions may develop in the heat affected zone, each with its own microstructure and mechanical and fracture properties. In cases where filler metals are used the weld metal may have significantly different chemical composition than the base metal and, hence, may possess different mechanical properties. Such material variations can affect significantly both the fracture toughness and the crack driving force in a weld joint. The welding process also largely controls the potential for weld defects which may develop during fabrication. The common defects developed during welding include lack of penetration, lack of fusion, which are planar defects, and slag inclusions and porosity, which are volumetric defects. Cracks may also develop during welding. Planar defects and cracks have direct consequences on the structural integrity of weldment, while volumetric defects may eventually pose problems due to fatigue crack initiation during service.

Conventional defect assessment procedures that are being used at present were essentially developed for cracks lying in a homogeneous material. In view of the variations in the tensile and fracture properties of base and weld material, the integrity assessment of strength mismatch welds is not straightforward. Here mismatch means that the weld and base material differ in yield strength and in hardening behaviour. In addition the difference in elastic modulus and Poisson's ratio also occurs in certain cases. However, for engineering materials that are used in bridges, offshore equipments, piping and pressure vessels, the difference in the elastic properties is usually small (Hao et al., 1997). Thus, these structures need specific attention on the mismatch problem under elastic-plastic condition. Although finite element analysis may be used to carry out integrity assessment of strength mismatch weld on case by case basis, however, for engineering applications a simplified fracture assessment procedure is invariably preferred. In this study accurate analytical solutions of the limit load, plastic η-factor and crack tip stress fields of plane strain fracture specimens having weld centre crack are presented. Proposed analytical solutions were validated by detailed elastic-plastic finite element analyses. It is expected that the detailed analytical and numerical studies performed in this work would provide a comprehensive understanding of the effects of weld strength mismatch on the limit load, plastic η-factor and crack tip stress fields of plane strain fracture specimens.

1.1 Fracture assessment procedures for welds

Most of the commonly used fracture assessment procedures developed for welds require an accurate evaluation of the limit load. For materials having high fracture toughness the net-section collapse occurs prior to crack growth initiation and, thus, the limit load provides a good estimate of the load bearing capacity of the component. However, for materials having moderate or low fracture toughness the criterion of net section yielding is not adequate and detailed fracture mechanics calculations are required. Apart from accurate evaluation of crack driving force like J-integral, the material fracture toughness is also required for such integrity assessment calculations. In general, plastic η-factor is used for the experimental evaluation of fracture toughness. Fracture testing standards like ASTM E-1820 provides the plastic η-factor for standard homogeneous fracture specimens. Effects of weld strength mismatch on the plastic η-factor have not been incorporated till date.

Conventionally, fracture toughness tests are performed on small size standard fracture specimens. Detailed analytical and experimental studies conducted in past two decades have revealed that the crack-tip stresses play an important role in the fracture process. Since the state of stress near the crack tip in a standard fracture specimen is very different from that of the component/structure under investigation, significant variations in the fracture toughness of standard fracture specimen and the actual component have been observed.

Thus, extensive studies are required on welds as besides specimen geometry and loading conditions the strength mismatch ratio M (defined as ratio of yield strength of weld to yield strength of base material) and weld slenderness ratio ψ (defined as ratio of uncracked ligament to half weld thickness) are the additional variables affecting the fracture assessment parameters.

1.2 Identification of issues for investigation

A detailed literature survey (presented in Chapter 2) revealed that in the past two decades several detailed numerical (FE) and experimental studies have been performed on weld centre crack. Although the effect of strength mismatch ratio M and weld slenderness ratio ψ on fracture assessment parameters has been numerically as well as experimentally examined, however, the detailed insight of the mechanics of deformation in a strength mismatch weld is still lacking. The detailed structure of global plastic fields that occurs in commonly used fracture specimens, having weld centre crack, under fully plastic condition has not been worked out. Aspects related to the state of stress at the base-weld interface need a more thorough investigation. The general structure of crack tip stress field and particularly the angular variation of these local stresses need a detailed examination. The important concern of characterisation of crack tip stresses for weld centre crack under mode I loading needs to be studied. It remains to be established that the effect of specimen geometry, loading condition and weld strength mismatch can be suitably represented by appropriate crack tip constraint parameters. The present work is intended to address these issues.

1.3 Scope of work

In this work, detailed analytical and numerical studies were envisaged on weld centre crack under mode I loading. Both base and weld materials were modeled as elastic-perfectly plastic (non-hardening). It is well recognized that such idealised model does not adequately represent the real material behaviour, however, this material model was chosen for the present study because of three prime reasons; (i) an insight into the physics of deformation of solids can be obtained by this simplified material response. (ii) Limit load has been widely used as an important design parameter. It is worth to note that the assumption of non-hardening plasticity is a necessary requirement for limit analysis. The effect of strain hardening is accounted indirectly by adjusting the reference stress, in general, as an average of yield and ultimate tensile strength. In addition, the experimental evaluation of fracture toughness requires a proportionality factor, often referred as the plastic η-factor. Analytical evaluation of plastic η-factor also invokes the assumption of non-hardening plasticity. (iii) The results of crack tip stresses obtained from this idealized material model may still be applicable for materials having low and even moderate strain-hardening. For homogeneous standard fracture mechanics specimens it has been demonstrated by O' Dowd and Shih (1991) that the constraint parameter Q is a weak function of material strain hardening behaviour.

Thus, in the present investigation, both base and weld materials were modeled as elastic-perfectly plastic. The two materials were assumed to have same elastic modulus and Poisson's ratio but mismatch in their yield strength. All the investigations in this work were carried out on deeply cracked fracture specimens under plane-strain condition. A schematic of geometries investigated in present work is shown in Fig.1. Crack was postulated at the centre of weld. Numerical studies were performed within the framework of continuum scale plasticity (J_2 flow theory) and effects of micro-structural heterogeneity and presence of residual stresses were not accounted.

1.4 Objectives of the thesis

The objectives of the present thesis are as follows

- To develop a robust analytical method for plane-strain problems that can account for weld strength mismatch effects.
- To develop accurate analytical solutions of the limit load for commonly used fracture mechanics specimens having weld centre cracks.
- To study the effects of strength mismatch ratio M and weld slenderness ratio ψ on the state of stress near the crack tip in high as well as in low constraint geometries namely pure bending SE(PB) specimen, compact tension C(T) specimen, and middle tension M(T) specimen having weld centre crack.
- To propose analytical solutions of the plastic η-factor (used for experimental evaluation of fracture toughness) for fracture specimens having weld centre cracks.
- To propose the general structure of crack tip stress field in an elastic-perfectly plastic material under mode I loading. To study the suitability of 4-sector stress field proposed by Zhu and Chao (2001) for the problem of weld centre crack. To examine whether the combined effects of specimen geometry, loading conditions and weld strength mismatch can be suitably represented by a general structure of crack tip stress field.
- To develop constraint parameters that can be used to characterize the crack tip stresses in an elastic-perfectly plastic material under mode I loading. To study the suitability of the proposed constraint parameters for a wide range of crack tip constraint. To identify whether the proposed constraint parameters are adequate to represent the effects of specimen geometry, loading conditions and weld strength mismatch on crack tip stresses.

- To perform detailed 2-D elastic-plastic full field finite element analysis on both high constraint and low constraint geometries having weld centre crack under mode I loading. To validate the structure of proposed general elastic plastic crack tip stress field with the results of crack tip stresses obtained from FE analysis.

1.5 Organisation of the report

The work carried out in this thesis is organised in nine chapters. The structure of the remaining part of this report is as follows:

Chapter 2 of this thesis describes a detailed literature survey that is conducted to understand the studies performed by various researchers on fracture aspects of strength mismatch welds under monotonic loading. Both analytical and experimental studies are covered. For the sake of completeness a brief description of the studies performed on homogeneous fracture specimens is also provided.

In chapter 3 of this thesis, general aspects related to the assumption of rigid plastic material model, virtual work principle, and limit theorems of classical plasticity are introduced. The concept of proposed Modified Upper Bound (MUB) theorem and its analytical formulation are presented. It is demonstrated that the method (MUB) is actually a new form of already existing extremum/work principle.

In chapter 4, the equivalence of proposed MUB theorem with the classical Slip line Field (SLF) analysis, for a rigid-plastic body in plane strain, is discussed. It is demonstrated that minimization of this new form of general work principle automatically leads to global equilibrium equations, as obtained from SLF analysis. Both cracked and uncracked configurations are analysed to establish this equivalence in general. As a novel application a complete analytical formulation for yield locus for the entire range of tensile and bending load, for a single edge notched specimen, is presented.

In chapter 5, weld strength mismatch effects on the limit load and crack tip constraint is examined. The detailed structure of global plastic fields for pure bending SE(PB) specimen, and compact tension C(T) specimen having weld centre crack, under fully plastic condition, is presented. Aspects related to the state of stress at the base-weld interface are discussed. Effect of strength mismatch ratio M and weld slenderness ratio ψ is systematically examined. Using the proposed MUB theorem accurate analytical solutions of the limit load, and crack tip constraint parameter h are obtained. It is shown that a family of five fields proposed in this work is adequate to cover all practical cases of weld mismatch. Proposed analytical solutions are confirmed with detailed FE results.

In chapter 6, weld strength mismatch effects on low constraint geometries is analysed. As a representative of such a case, a middle tension M(T) specimen is analysed. A discontinuous stress solution is proposed to analyse M(T) specimen having a weld centre crack. Discontinuity is incorporated in the proposed solution by assuming an unknown value of normal stress at the base-weld interface. MUB theorem along with global equilibrium equations is utilised to obtain this unknown normal stress and hence the whole plastic field. The results obtained are found to be in excellent agreement with the known FE solutions available in literature. In addition to limit load, detailed evaluation of crack tip constraint is performed.

In chapter 7, the effects of weld strength mismatch on fracture toughness testing are discussed. Analytical solutions of plastic η-factor for pure bending specimen, compact tension specimen and middle tension specimen having weld centre cracks are proposed and compared with finite element results.

In chapter 8, the important concern of characterisation of crack tip stresses in an elastic-perfectly plastic material under mode-I loading is discussed. A novel 5-sector asymptotic crack tip stress field is developed for a stationary crack under plane strain condition. Detailed 2-D elastic plastic finite element analyses are performed to examine validity of the proposed 5-sector stress field. A new constraint-indexing parameter T_{CS-2} is proposed which along with hydrostatic stress ahead of crack tip is capable of representing the entire elastic plastic crack tip stress fields over all angles around a crack tip. Finally, it is demonstrated that the proposed constraint parameters are adequate to represent the crack tip constraint arising due to combined effect of specimen geometry, loading conditions, and weld strength mismatch effects.

In chapter 9, a brief summary of the entire work and salient conclusions drawn from the present investigation are presented. In addition, further possible extension of the present study that may be carried out in future is also discussed.

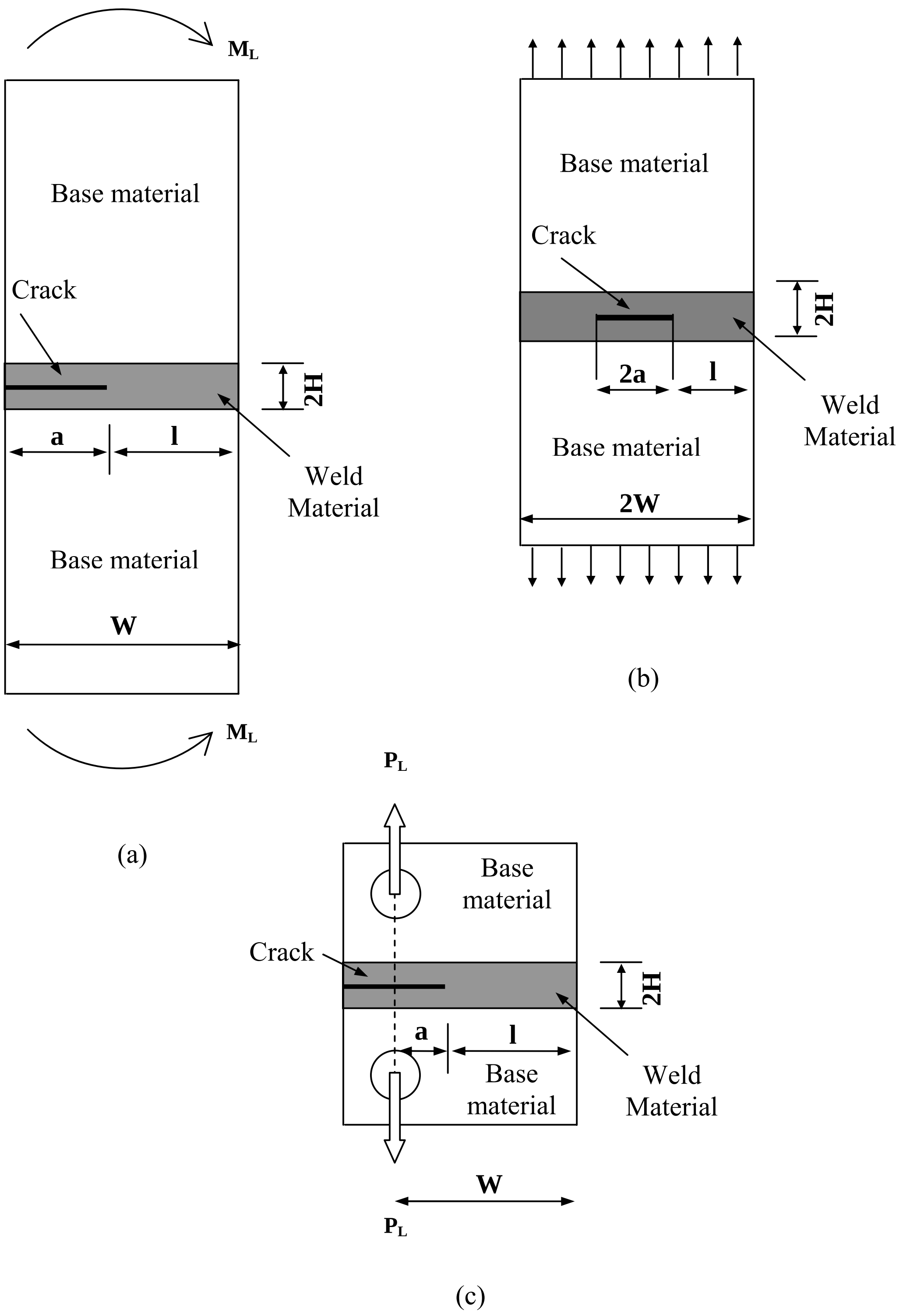

Fig. 1.1: Geometries investigated in present work (a) Pure bending SE(PB) specimen, (b) Middle tension M(T) specimen and (c) Compact tension C(T) specimen having a weld centre crack

CHAPTER 2

Literature review

In the following sections literature describing the investigations performed to understand the effects of weld strength mismatch on the fracture assessment parameters is presented. For the sake of completeness a brief description of the studies performed on homogeneous fracture specimens is also provided. These investigations are covered under two main headings: Analytical and numerical studies, and experimental studies.

2.1 Analytical and numerical studies on plane 2-D fracture specimens

A brief review of analytical and numerical studies on the limit load, plastic η-factor and crack tip stress fields performed on plane 2-D fracture specimens is presented in the following paragraphs. The review comprises of studies on homogeneous specimens as well as on fracture specimens having strength mismatch welds.

2.1.1 Studies on limit load

The two-criteria approach for flaw assessment like R-6 (Milne et al., 1986) provides a method for interpolation between plastic collapse and fracture governed by linear elastic fracture mechanics. A realistic assessment of plastic collapse should take into account the material strain hardening, the finite strain and the finite deformation effects. In practice, however, a simpler assessment is performed using the limit analysis, where these effects are ignored. Limit analysis may also be used for evaluation of other fracture assessment parameters. The elastic-plastic parameter J (Rice, 1968) may be assessed by the reference stress method (Ainsworth, 1984) using the limit load. If it is assumed that the creep stress distribution is similar to that of the reference stress obtained from the limit load, the reference stress itself may be used to evaluate the creep crack growth parameter, that is, the C^* integral. In view of these considerations it becomes apparent that the limit analysis plays an important role in integrity assessment of components subjected to different loading conditions.

Limit analysis calculates the maximum load that a given structure made of elastic-perfectly plastic material can sustain. The loading is assumed to vary proportionally with a single factor. When the limit load is reached the deformations become unbounded and the structure behaves like a mechanism. As complete solutions are difficult to obtain, bounds are arrived on the limit load using the two limit theorems. In the following paragraphs few salient studies related to the limit load of homogeneous fracture specimens and fracture specimens having strength mismatch welds are described.

2.1.1.1 Limit load of homogeneous fracture specimens

The notched specimens are nowadays frequently used in fracture mechanics analysis. In low strength metal specimens the remaining ligament is normally fully yielded before crack growth initiation occurs. Under these conditions the slip-line field (SLF) analysis, assuming that the material is rigid-plastic, can provide sufficiently accurate estimates of stresses in plastic region and the corresponding limit load. Applications of the SLF theory to fracture related problems in Charpy and Izod test specimens are discussed in detail by Green and Hundy (1956), Green (1953, 1956), Alexander and Komoly (1962) and Ewing (1968). Effect of notch root radius and flank angle on the limit load and the corresponding crack tip stresses was accounted in these solutions. An excellent survey of limit loads of structures containing defects was presented by Miller (1988).

2.1.1.2 Effect of weld strength mismatch on the limit load of fracture specimens

In many practical applications, flaws are located within the welds. In these cases, the assumptions on which the conventional flaw assessment procedures are based are generally not valid. As a result flaw assessment procedures have been developed for welds that can account for weld strength mismatch effects. Most of these methods require an accurate evaluation of the limit load.

Analytical studies on the limit load of fracture specimens having weld centre cracks were carried out by Joch et al. (1993) and Burstow and Ainsworth (1995). These authors quantified the influence of strength mismatch ratio M and weld slenderness ratio ψ on the limit load of middle tension M(T) and three-point bend SE(B) specimens. Classical upper bound theorem of limit analysis was used to derive analytical solutions. Proposed analytical solutions were compared with FE results. Hao et al. (1997, 2000) examined the effect of weld strength mismatch on the limit load of M(T) and pure bending SE(PB) specimen having weld centre crack. They performed analytical studies on rigid-plastic material model. Using classical approach of Slip-line theory, they provided sufficiently detailed analytical solutions of limit load and crack-tip stresses for the cases where plasticity was confined only in weld material. For the cases where the yield strength of base and weld material was comparable approximate solutions were proposed using results obtained from finite element (FE) analyses.

Kim and Schwalbe (2001a, b and c) in a series of papers numerically examined the effect of weld strength mismatch on the limit load of commonly used fracture specimens: M(T), SE(PB), SE(B), C(T) and double edge cracked tensile DE(T) specimen. Results of the limit load obtained from FE analyses were presented in closed-form solutions. Both plane strain and plane stress cases were analysed. Limit load solutions were provided for weld centre crack, interfacial crack and for asymmetrically located crack in the weld region.

The effect of weld undermatch on the plastic limit load and fully plastic stress triaxilities for flat plates and round bar specimens was studied by Kim and Oh (2006) using FE analysis. Elastic-perfectly plastic material model was assumed and for flat plate both plane stress and plane strain cases were analysed. It was observed that the effect of weld strength mismatch was significant for flat plate under plane strain and round bar specimens whereas the effect was less significant for plate under plane stress condition. The effect of weld slenderness ratio was also quantified.

Limit load solution for a M(T) specimen having a highly undermatch weld with an arbitrary crack in the weld region is recently proposed by Alexandrov (2010). Plane strain condition was assumed. Using the slip line field for the Prandtl's problem (compression of a plastic layer between two rough parallel plates), a closed form expression of the limit load was proposed.

2.1.2 Studies on plastic η-factor

The evaluation of fracture toughness is an integral part of structural integrity assessment procedures which are based on fracture mechanics concepts. In fact fracture toughness essentially provides the criterion through which the severity of crack like flaws can be related to the operating conditions in terms of a critical applied load or a critical crack size. Fracture toughness, in terms of J-integral, is measured using the experimental load-displacement data and a proportionality factor, often referred as the plastic η-factor (Rice et al., 1973). These authors proposed to split the total J-integral into elastic (J_e) and plastic components (J_p). While the elastic part J_e is related to the stress intensity factor (K), the plastic part J_p is associated with the plastic area under the load-displacement data obtained from experiments, as described by the following equation

$$J = J_e + J_P = \frac{K^2}{E'} + \eta_P \int_0^{\Delta_P} P d\Delta_P \tag{2.1}$$

Here E'= E for plane stress and E'=E/(1-ν^2) for plane strain condition. A γ-factor was proposed by Hutchinson and Paris (1979) and later generalised by Ernst et al. (1979) and Ernst and Paris (1980) to incorporate the correction term due to crack growth. The following paragraphs summarizes some of the important studies related to plastic η-factor for standard homogeneous fracture specimens as well as fracture specimens having strength mismatch welds.

2.1.2.1 Plastic η-factor of homogeneous fracture specimens

Conventionally, fracture toughness is evaluated by performing tests on small size standard fracture specimens like deeply cracked SE(B) and C(T) specimens. Commonly used fracture testing standards like ASTM E-1820 and ESIS P1-92 use the experimental load versus load line displacement (LLD) data of deeply cracked specimens for evaluation of fracture toughness. Values of plastic η-factor to be used are also suggested by theses standards which are based on investigations performed by many researchers. For deeply cracked geometries expressions of plastic η-factor have been obtained either using dimensional analysis or load separation criterion. Solutions of plastic η-factor for middle tension M(T) specimen have been proposed by Rice (1973), Landes et al. (1979) and Roos et al. (1986). However, for cases where gross-section yielding occurs prior to net section yielding the fracture toughness procedures based on load versus load line displacement data are not adequate. This is the case particularly for specimens having short cracks. Sumpter (1987) proposed the idea to determine the fracture toughness J_c from three-point bend specimen having a shallow crack using load versus crack mouth opening displacement (CMOD) data. Elastic plastic FE analysis was used to show the adequacy of the proposed method. For M(T) specimen Hoshide et al. (1982) also proposed to evaluate J from the area under load versus CMOD data. Based on FE calculations, Wang and Gordon (1992) proposed expressions of CMOD based plastic η-factor for SE(PB) specimen. In a more general work, Chattopadhyay et al. (2001) derived limit load based general expressions of plastic η and γ factors. The advantage of these general expressions is that the plastic η and γ factors for any cracked geometry and loading condition can be readily obtained using the limit load expression. Based on slip line field and detailed FE analysis, Kim (2002b) provides the plastic η factor for single-edge cracked specimen, subjected to four-point bending load. Both LLD based and CMOD based η factors were proposed. In accordance with previous studies, it was observed that the use of CMOD based η factors provide a more robust experimental J estimation procedure, particularly for shallow cracked geometries. The effect of in-plane and out-of-plane constraint on the plastic η factor of double edge cracked tensile specimen DE(T) was examined by Kim et al. (2004) using detailed 3-D FE analysis. Investigations were performed for both hardening and non-hardening material models. It was observed that in contrast to M(T) specimen, the J estimation scheme for a DE(T) specimen depends on whether the specimen is in plane strain or plane stress.

2.1.2.2 Effect of weld strength mismatch on plastic η-factor of fracture specimens

Existing fracture testing standards are mainly applicable to fracture specimens made of homogeneous materials. In order to assess fracture integrity of a cracked welded structure, accurate estimation formulas for fracture toughness evaluation, which can account for weld strength mismatch effects, are required.

Analytical studies to quantify the effect of weld strength mismatch on plastic η-factors were performed by Joch et al. (1993) and Burstow and Ainsworth (1995). Using classical upper bound theorem of limit analysis solutions of limit load were obtained by these authors. The limit load solutions were in turn used to derive the plastic η-factors for M(T) and SE(B) specimens. Crack was postulated at the centre of weld and the effect of mismatch ratio M and weld slenderness ratio ψ was systematically examined. Proposed analytical solutions of η-factors were compared with FE results and reasonably good agreement was obtained between the two solutions. It was demonstrated that weld strength overmatch ($M>1$) would reduce the plastic η-factors below that of standard homogeneous specimens while under match welds lead to higher plastic η-factors. Obtained results were used to provide guidance for testing weldments using standard bend specimens. Burstow and Ainsworth (1995) discussed that the crack growth in the undermatched specimen can be characterised by J-integral for the weld metal. However, for overmatched specimen J-integral can be used to characterise only small amount of crack growth.

Sumpter (1987) presented a method for determination of fracture toughness J_c from SE(B) specimen having a shallow crack using load versus CMOD data. For the weld geometry and the range of weld strength mismatch considered, he demonstrated that the method can be applied to specimens containing weld joints also. Eripret and Hornet (1992, 1994) discussed that for an overmatched weld plastic deformation can occur at the base-weld interface even before starting at the crack tip. Under such condition the LLD increases without causing any real loading of the crack. They suggested that commonly used toughness estimation procedures based on area under the load versus LLD curves are not valid particularly for overmatched welds. Based on analytical considerations, Hornet and Eripret (1995) proposed a new procedure for evaluation of fracture toughness from the area under the load versus CMOD curve. The proposed method was compared with experimental results and FE calculations.

Based on FE analysis, Gordon and Wang (1994) suggested an expression for CMOD based plastic η-factor incorporating the weld strength mismatch effect, however, their proposed expression was not in good agreement with their FE results. Kim (2002b) proposed solutions of plastic η-factor for bi-material SE(PB) specimen having an interface crack. Based on FE results both LLD based and CMOD based η-factors were proposed. It was demonstrated that the proposed CMOD based η-factor of homogeneous SE(PB) specimen can also be used for a bi-material specimen with an interface crack.

The effect of weld strength mismatch on plastic η-factor of fracture specimens having weld centre crack was also examined by Kim et al. (2003). Detailed 2-D FE analyses were performed to account the effect of strength mismatch ratio M and weld slenderness ratio ψ on plastic η-factor of commonly used fracture specimens namely M(T), SE(B), and C(T) specimens. Investigations were performed on deeply cracked specimens and the effect of material strain hardening was accounted. However, same value of strain hardening index was used for both base and weld material. Based on proposed solutions a window was provided, within which the plastic η-factor of homogeneous specimens may be used for fracture toughness evaluation of weldments.

In a recent study, Dunato et al. (2009) examined the effect of weld strength mismatch on fracture toughness parameters such as J-integral and crack tip opening displacement CTOD for SE(B) specimen. Detailed non-linear FE analyses were performed on plane strain SE(B) specimen with a crack located at the centre of weld and in heat affected zone along the fusion line of weldment. The study provided a database of plastic η-factor and plastic rotation r_p factor for a wide range of crack sizes and strength mismatch ratio. It was concluded that for the range of mismatch ±20% J-integral and CTOD estimation expressions are not significantly affected and, thus, the weld mismatch effects can be ignored.

2.1.3 Studies on crack tip stress fields

The application of conventional fracture mechanics to assess the integrity of a cracked structure is based on the assumption that a single parameter uniquely characterizes the resistance of a material to fracture. Material resistance to catastrophic brittle fracture is characterized by a critical value of the stress intensity factor, K_{Ic} while resistance to the onset of ductile fracture is characterized by a critical value of the J-integral, J_{Ic}. Fracture testing standards like ASTM E-1820 imposes certain restrictions on the size of fracture specimens to be tested and on crack depth. These requirements are intended to ensure that the crack tip is essentially in a state of plane strain and a high stress tri-axiality (constraint) exists ahead of crack tip. Under these conditions it can be demonstrated that the state of stress near the crack tip and the resulting fracture is controlled by Hutchinson-Rice-Rosengren (HRR) asymptotic fields. The requirements of the testing standards thereby guarantee that K_{Ic} and J_{Ic} are lower bound, geometry independent measures of fracture toughness. However, cracks in civil, nuclear and marine structures are seldom this highly constrained, which makes predictions of structural fracture resistance based on laboratory fracture toughness values overly conservative. Excessive conservatism in structural assessment can lead to the unwarranted repair or decommissioning of engineering structures to protect the public safety at a great, and often unneeded, cost and inconvenience.

Experimental studies by Sumpter (1989) and by Kirk and Dodds (1991) demonstrated that the use of geometry dependent fracture toughness values allows more accurate prediction of the fracture performance of structures than is possible using conventional fracture mechanics. However, the task of characterizing fracture toughness becomes more complex as testing of non-standard specimens is required, and different fracture toughness data are needed for each geometry of interest. Further, this approach cannot be applied economically to thick section structures (e.g. nuclear pressure vessels). As a result many detailed numerical and experimental studies were performed to identify the parameters responsible for the variation of fracture toughness with specimen geometry and loading conditions. These studies revealed that the geometry dependence of fracture toughness arises essentially due to difference in state of stress ahead of crack tip. Thus, special emphasis is laid on the understanding of these local fields and characterisation of crack tip stresses has been an area of active research for many decades. This is not only useful in structural design but also helps in understanding material failure by throwing light on potential fracture mechanisms (e.g. brittle cleavage or ductile void coalescense). Further, the information on the state of stress near the crack tip, obtained from a continuum analysis, can be suitably combined with a local (micro-mechanical based) fracture criterion that may help in predicting the fracture toughness and the potential direction of crack propagation especially under mixed mode loading conditions.

In the following paragraphs a few salient investigations describing the near tip stress fields of a stationary crack, in pressure-insensitive solids (yield criterion independent of hydrostatic stress), is presented. More details on stationary crack tip stress fields in elastic plastic solids can be found in a recent article by Narasimhan et al. (2009).

2.1.3.1 Crack-tip stress fields in homogeneous fracture specimens

The first general study regarding the state of stress ahead of crack tip, in a linear elastic material, was performed by Williams (1957), though Westergaard (1939) in an earlier work has provided a means for connecting the local stress fields to the global boundary conditions in certain configurations. In his landmark paper, Williams (1957) showed that the crack tip stress fields in an isotropic elastic material can be expressed as an infinite series where the leading term exhibit a $1/\sqrt{r}$ singularity and the second term is independent of r. Classical fracture mechanics theory neglects all but the singular term and, thus, came the concept of characterisation of crack tip stresses by a single parameter. Although the third and higher order terms of the Williams's series vanish near the crack tip, the second term (that is constant) remains finite and has a strong effect on the stresses in the plastic zone near the crack tip (Larsson and Carlsson, 1973). This second term has been referred in the literature as T-stress (Rice, 1974). The single parameter characterisation is rigorously correct only for $T > 0$. In nuclear power plants, particularly for class-I components, special emphasis is laid on the use of high toughness materials so that the possibility of brittle fracture is remote. For such materials the size of plastic zone, ahead of crack tip, is quite large and T-stress being an elastic parameter has no physical meaning under such large scale plasticity. By idealising the actual elastic-plastic behaviour of material as non-linear elastic, Hutchinson (1968), Rice and Rosengren (1968) proposed the dominant term of the singularity field (often referred as HRR solution) for plane strain mode-I crack based on the *J*-integral (Rice, 1968). Thus, the HRR singularity is the natural extension of one-parameter characterisation concept to a non-linear elastic material. The HRR solution, revealed several important features about the structure of stress and strain fields near the crack tip and paved the way for the development of the field of elastic-plastic fracture mechanics. It was pointed out by Hutchinson (1983) that in order to use J as a valid fracture characterizing parameter, it is essential that the region of dominance of HRR field must exceed the size of the fracture process zone where microscopic processes such as void growth and coalescence occur. This requirement has been referred in the literature as the condition of the J-dominance. Shih (1974) and Hutchinson and Shih (1975) extended the HRR solution to include combined I and II loading under conditions of plane strain and plane stress, respectively.

It has been realized, however, that the specimen geometry and loading conditions have significant effect on the region of J-dominance. For shallow cracks, tensile dominated loads etc it has been observed that the actual structure of crack tip stress fields is very different from those predicted by HRR fields (Al-Ani and Hancock, 1991) and, thus, the HRR field have limited application to real cracked structures. For a Ramberg-Osgood material model, the crack tip fields in the plastic zone can be expressed in terms of a power series where the HRR solution is the leading term. Analytical studies aimed at determining the higher order terms in the asymptotic solution for the crack tip fields were conducted by Sharma and Aravas (1991) and Xia et al. (1993). The higher order terms of this power series were grouped together and its amplitude was denoted as Q by O'Dowd and Shih (1991). Other representative two-parameters that are used to characterise the crack tip stress fields are J-T of Betegon and Hancock (1991) and J-A_2 of Chao et al. (1994). The objective of all these investigations is to develop a suitable fracture criterion that can be used to characterise crack growth initiation in ductile materials.

2.1.3.2 Crack-tip stress fields in fracture specimens having strength mismatch welds

In-service inspection of many nuclear power plants have revealed that cracks are most likely to occur in or the regions near welds that invariably occur in reactor coolant piping. Although welding is done as per qualified welding procedure it is quite probable that small cracks at the fusion line of base-weld interface or in the filler material may occur. These initials flaws may grow during service due to combined effects of environment and fatigue loading and may pose a serious threat to the integrity of these components. From integrity assessment point of view the problem of crack lying at the interface of two materials or in the centre of weld is of equal importance. The behaviour of crack lying anywhere else in the weld region is likely to be explained by these two limiting crack locations. In the following sub-sections studies conducted on crack tip stress fields for interfacial crack as well as for weld centre crack are presented.

2.1.3.2.1 Crack-tip stress fields for interface cracks

The problem of elastic dissimilar materials with a semi-infinite crack at the interface was first analysed by Williams (1959). He discovered that the crack tip stresses possess an oscillatory character of the type $r^{-1/2}$ *sin* (or *cos*) of the argument $\varepsilon \log r$, where r is the radial distance from the crack tip and ε is a function of material constants. This problem was later extended to the case of bending loads by Sih and Rice (1964). In a later work Rice and Sih (1965) analysed this problem using the complex variable method combined with eigenfunction expansion. They demonstrated that the stress intensity factor of an interfacial crack between two elastic dissimilar materials is in mixed mode even when the geometry is symmetric with respect to crack, and loading is pure mode I. Solutions to specific problems of interface crack have been given by Cherepanov (1962), England (1965), and Erdogan (1965). The concern of crack face contact that is predicted by analytical studies based on the assumption of linear elastic materials was discussed by Comninou (1977) and Comninou and Schmueser (1979). All these studies were performed on elastic isotropic materials. Willis (1971) analysed this problem for anisotropic materials. Rice (1988) reexamined this elastic interface crack problem and proposed the complete form of near tip fields based on analytic function theory. A complex stress intensity factor was proposed and its validity as the crack tip characterising parameter was discussed.

Fracture in most structural materials, however, is often accompanied by plastic flow near the crack tip, invalidating the assumption of linear elasticity. When the plastic deformation takes place over a large size scale, then the linear elastic solution may not be useful to characterise the stresses and deformations near a crack tip, and the elastic-plastic solutions for such crack problems are essential. An elastic-plastic finite element analysis for a crack at the interface between a power-law hardening material and a rigid substrate has been given by Zywicz and Park (1989, 1992). Shih and Asaro (1988, 1989) and Shih et al. (1991) performed a series of investigations and showed that the crack tip fields are members of a family parametrised by plastic mode mixity factor and are scaled by J-integral. Under plane-strain condition, the problem of a stationary and quasi-statically growing interface crack between an elastic-perfectly plastic solid and a rigid substrate has been analysed by Guo and Keer (1990a). For a stationary crack a one-parameter family of asymptotic near tip stress fields was proposed by these authors. A complete asymptotic near tip stress and deformation field for a quasi-statically growing crack was also proposed. Under anti-plane deformation Guo and Keer (1990b) presented an asymptotic solution for a crack at the interface of two power-law hardening elastic-plastic materials. It was demonstrated that the stress singularity near the crack tip was $-1/(1+n)$ where n is the maximum of the strain hardening index of the two materials. The problem of interface crack between two yield strength mismatched solids, under remote mode I loading, was analysed by Ganti and Parks (1997) and Zhang et al. (1997a, 1997b). These authors investigated the effect of yield strength mismatch between the two materials on the crack tip constraint. The study of Ganti and Parks (1997) was focused on elastic-perfectly plastic materials while Zhang et al. (1997a, 1997b) incorporated the effect of strain hardening also. Two-parameter description of crack tip stress field for a crack located at the fusion line was given by Ranestad et al. (1997). The asymptotic crack tip stress fields for the general case of remote mixed mode loading were developed by Sham et al. (1999). The authors characterised the local stress field by a phase angle which quantified the ratio of normal to shear tractions on the interface at the crack tip and the yield strength ratio of the two materials. The effect of mismatch in yield strength as well as in strain hardening index of the two materials on interfacial crack tip fields was examined by Lee and Kim (2001) using detailed FE analysis.

2.1.3.2.2 Crack-tip stress fields for weld centre cracks

The problem of crack lying at the centre of weld is (theoretically) less understood. This case was first systematically studied by Varias et al. (1991). They numerically (finite element) examined the case where a crack was postulated at the centre of ductile metal foil sandwiched between two rigid ceramic blocks. The focus of this study was to understand the ductile failure mechanisms that are likely to occur in the metal foil under such a high constraint state. It was demonstrated that for such an extreme mismatch case, under small-scale yielding condition, under uni-axial tensile load a high tri-axial stress exists ahead of crack tip at a distance several times the foil thickness. A formula for evaluating the stress intensity factor was also suggested. In welds that are typically encountered in many engineering applications the mismatch in yield strength, however, is not so high. Thus, in the more general case both the materials are elastic-plastic and plasticity passes through the interface of two materials. This was the focus of a numerical study by Burstow et al. (1998). They performed a series of two-dimensional finite element analyses within the framework of modified boundary layer formulation. Both base and weld materials were assumed to have same elastic properties and were modeled as elastic-perfectly plastic.

Elastic T-stress was applied to model different constraint at the crack-tip arising due to actual specimen geometry and loading conditions. The effect of strength mismatch on crack-tip constraint was studied systematically by changing the yield strength of base material. It was demonstrated that a normalised load parameter, $J/h\sigma_{yw}$, scales the size of the plastic zone with the width of the weld material and can be used to quantify the level of constraint for a given degree of mismatching. The effect of strength mismatch on constraint of SE(B) specimen under small scale yielding, for a wide variety of weld geometries, was examined by Kirk and Dodds (1993). A constraint parameter for quantifying the crack tip stress fields in weld joints, under small scale yielding, was suggested by Betegon and Penuelas (2006). All these numerical studies demonstrated that under small-scale yielding condition the weld strength mismatch effects have a strong influence on the state of stress (constraint) near the crack tip.

The small-scale yielding assumption is valid only as long as the remotely applied elastic displacement field is not influence by the plastic behavior at the crack-tip. Since welded structures are intended to withstand sufficiently high loading such an assumption of small-scale yielding strictly does not hold good. Analytical studies of crack tip stresses under fully plastic condition (at limit state) were performed by Hao et al. (1997). Using classical approach of Slip-line theory, they obtained analytical solutions of crack-tip stresses for the case where plasticity was confined only in the weld material. In cases where the yield strength of base and weld material is comparable plastic deformation occurs in both the materials. To construct crack tip stress fields for such cases, information about the state of tractions at the interface is needed. Although Hao et al. (1997) briefly discussed aspects related to state of stress at the base-weld interface, however, no detailed solutions were provided for this general case. Based on comparison of their analytical results with finite element studies they indicated the possibility of jump in tractions at the interface of the two materials. Since many plastic deformation patterns and variables are involved in mismatch welds, comprehensive analytical solutions of crack tip stresses, based on SLF analysis, are difficult to obtain. In addition to above-mentioned problems the possibility of discontinuity of tractions at the material interfaces is also a matter of concern. At this point it is necessary to clarify that the concept of continuity of tractions at the interface has been successfully utilised to examine the structure of crack-tip stress fields, for an interfacial crack, under small-scale-yielding (Guo and Keer, 1990a, Ganti and Parks, 1997, Sham et al., 1999). However, no such detailed study has yet been reported for the case of weld centre crack under large-scale plasticity. This general case was numerically examined by Kim and Schwalbe (2004). They performed detailed finite element analysis to examine the strength mismatch effect on crack-tip stresses under fully plastic condition. FE Studies were performed on M(T) and SE(PB) specimen for an elastic-perfectly plastic material. Variation of constraint parameter *h* was presented for different mismatch ratio M and weld slenderness ratio ψ. Both plane-strain and plane stress cases were accounted.

2.2 Experimental studies on strength mismatch welds

Initial studies on crack growth in welded specimens were carried out by Garwood (1985) and de Verdia (1989). The effect of heterogeneity of the mechanical properties on the crack growth resistance was also examined by Homma et al. (1995). In this experimental study two types of welded C(T) specimens were used to relate the crack growth behavior near to and in a welding bead. The initial fatigue crack was introduced perpendicular to the weld bead. The crack growth resistance curves were evaluated for various positions of initial crack tip. For the case where the difference in mechanical properties of base metal, weld metal, and heat affected zone was relatively small, the crack growth resistance curves spread over a narrow range. For C(T) specimens fabricated from A-533B-HT80 welds exhibiting large strength mismatch, the crack growth resistance was strongly affected by the relative positions of the steels in the specimen and the width ratio of each steel to the specimen.

The influence of strength mismatch and crack depth on the triaxial state of stress at the crack tip, crack tip opening displacement, and fracture toughness of welded SE(B) specimen was examined by Tang and Shi (1995). It was demonstrated that there exists a fracture toughness peak in the curve of fracture toughness versus crack depth. It was discussed that the location of fracture toughness peak is influenced by the yield strength for a homogeneous specimen and is also influenced by the strength mismatch for the welded specimen. The variation of observed fracture toughness with weld strength mismatch was explained in terms of the size of plastic zone ahead of crack tip. It was concluded that the fracture toughness of an undermatched specimen is lower than that of overmatched specimen for the same crack depth.

The fracture behavior of M(T) specimen having a strength mismatch weld was examined by Neale (1999). Experiments were performed to measure the J-Δa behavior. The mismatched specimens were fabricated from two steel plates joined by electron beam welding technique. The J-Δa data for the mismatched specimens were compared with the results obtained from the individual plates. It was demonstrated that the use of mismatch corrected plastic η-factor provided J-Δa data that was in excellent agreement with the J-Δa data for the individual plates.

An et al. (2003) examined the effect of strength mismatch and loading rate on ductile fracture initiation using a two-parameter criterion. Experimental studies revealed that the relationship between the critical equivalent plastic strain to initiate ductile fracture and stress triaxiality for a strength mismatch weld was equivalent to that obtained on homogeneous specimens under static loading. Moreover the two parameter criterion was shown to be independent of the loading rate.

The effect of mismatch in plastic properties on initiation and propagation of an interface crack in a ferrite-austenite joint was examined by Besson et al. (2005). Tests were performed on various specimens including smooth and notched tensile bars, Charpy V-notched specimens, and single-edge notch bend specimens. The effect of distance between the notch root and interface on fracture initiation and crack propagation direction was examined. These studies revealed that when the crack is located in ferrite, the overall ductility increases as the distance of the crack from the interface decreases whereas the load carrying capacity decreases. Opposite effects were observed when the crack was located in the austenite. The observed variations of the ductility can be explained by the alterations of the stress state in the vicinity of crack due to strength mismatch. Compared to homogeneous structure, the stress triaxility ratio close to crack is smaller when the crack lies in the harder material and vice-versa.

Experimental studies of interface crack growth, where plastic yielding occurs in at least one of the solids joined at the interface have been reported by Cao and Evans (1989), Liechti and Chai (1992) and O'Dowd et al. (1992). These studies have shown a strong dependence on mode mixity, such that the measured fracture toughness is much higher in cases where mode II loading dominates at the crack tip than in cases where mode I loading dominates. This was also predicted by the numerical computations of Tvergaard and Hutchinson (1993), and it was concluded that the observed strong dependence on the mode of loading is due to plastic yielding.

Recently an experimental study was conducted by Saxena (2007) to assess the structural performance of repair welds in 1Cr-1Mo-0.25V turbine casing material. The tests conducted include tensile tests, creep tests, fracture toughness tests, fatigue crack growth rate tests, creep crack growth rate tests, and creep-fatigue crack growth tests on base and weld metal. The effects of weld strength mismatch and the location of crack (with respect to fusion line and in weldment) on the various aspects related to these tests were discussed. In addition, the analytical framework of non linear fracture mechanics for assessing the behavior of welds was examined and suggestions for future work in this direction were made.

2.3 Plane strain theory of slip line field

In plane strain the displacement of particles of the body are parallel to the x, y plane, and are independent of z:

$$u_x = u_x\left(x, y\right) \qquad u_y = u_y\left(x, y\right) \qquad u_z = 0 \tag{2.2}$$

In any section $z = const.$ there will be the same stress-strain configuration. The components of stress depend only on x, y, and τ_{xz}, τ_{yz} are zero on account of the absence of the corresponding shears. Thus, σ_z is one of the principal stresses. In elasticity theory the above conditions are known to be sufficient for formulating the plane strain problem. In plasticity theory, however, additional simplifications are needed, since otherwise it is not possible to derive an acceptable mathematical formulation of the problem (Kachanov, 1971).

In general, the rigid plastic material model is used to formulate the theory for plane strain problems. As discussed earlier, this assumption introduces an error which is difficult to estimate. On the other hand, as pointed by Kachanov (1971), it is extremely difficult to undertake any systematic analysis of the plane strain problem without using the rigid plastic model. In most of the plane strain problems, the limit state is usually reached with some regions of the body still in an elastic state. Thus, it is really necessary to consider the elastic-plastic problem, but the difficulties of solving it (analytically) are enormous. Complete neglect of the elastic regions deprives the formulation of determinacy and makes physical interpretation of solutions difficult.

It is far more expedient to proceed from the rigid plastic model. This allows the stress field and the displacement field to be investigated simultaneously, the latter being related to the displacement of the rigid (elastic) regions. In this way meaningful approximate solutions of elastic-plastic problems can be constructed. The error so introduced will, however, depend on the type of problem being considered.

2.3.1 Governing equations

For plane strain problems $\varepsilon_z = 0$. Using this condition it can be easily demonstrated that both the deformation theory and the flow theory equations, after neglecting the elastic strain, lead to the following relation

$$\sigma_z - \sigma = 0 \tag{2.3}$$

And hence

$$\sigma = \frac{1}{2}\left(\sigma_x + \sigma_y\right) \tag{2.4}$$

As noted earlier, σ_z is one of the principal stresses. The other two principal stresses are given by the following relation

$$\left.\begin{array}{l}\sigma_{\max}\\ \sigma_{\min}\end{array}\right\} = \frac{1}{2}\left(\sigma_x + \sigma_y\right) \pm \frac{1}{2}\sqrt{\left(\sigma_x - \sigma_y\right)^2 + 4\tau_{xy}^2} \tag{2.5}$$

It is clear that σ_z is the intermediate principal stress, so that the maximum tangential stress will be

$$\tau_{\max} = \frac{1}{2}\left(\sigma_{\max} - \sigma_{\min}\right) = \frac{1}{2}\sqrt{\left(\sigma_x - \sigma_y\right)^2 + 4\tau_{xy}^2} \equiv \tau \tag{2.6}$$

Thus, the principal stresses are

$$\sigma_1 = \sigma + \tau \qquad \sigma_2 = \sigma \qquad \sigma_3 = \sigma - \tau \tag{2.7}$$

Eq. (2.7) describes that the state of stress at every point is characterized by superposition of the hydrostatic pressure σ on the maximum shear stress τ.

The angle made by the first principal stress σ_1 with the x-axis can be obtained from the following relation

$$\tan 2(1, x) = \frac{2\tau_{xy}}{\sigma_x - \sigma_y} \tag{2.8}$$

The directions of the surfaces on which the maximum shear stresses act make angles ± π/4 with the principal directions. This brings an important concept of the so called "slip lines". A slip line is a line which is tangent at every point to the surface of maximum shear stress. It is obvious that there are two orthogonal families of slip lines, often referred as the α-slip line and β-slip line. The α-line is inclined to the right of first principal direction at 45°, the β-line is inclined to the left of first principal direction at the same angle (Fig. 2.1). The direction of the α and β lines may be fixed by using the standard convention that clockwise shear stress is taken as positive. Thus, α- lines are all associated with a positive shear stress (+ τ) and β-lines with a negative shear stress (- τ). The angle of inclination of the tangent to the α- line, measured in the positive x-direction will be denoted by θ. Thus, the differential equations of the α and β families are respectively

$$\frac{dy}{dx} = \tan\theta \quad , \quad \frac{dy}{dx} = -\cot\theta \tag{2.9}$$

The slip lines cover the region with an orthogonal grid. An infinitesimal element cut out by slip lines experiences identical tension (σ) in the directions of the slip line (Fig. 2.2).

2.3.1.1 Yield condition

As discussed earlier, the material is assumed to be perfectly plastic (non-hardening). Thus, the yield criterion may be expressed as follows

$$\tau = const. = k \tag{2.10}$$

or

$$\sigma_{\max} - \sigma_{\min} = 2k \tag{2.11}$$

Thus,

$$\left(\sigma_x - \sigma_y\right)^2 + 4\tau_{xy}^2 = 4k^2 \tag{2.12}$$

2.3.1.2 Hencky's theorems

In the absence of body forces, the differential equations of equilibrium can be expressed as

$$\frac{\partial \sigma_x}{\partial x} + \frac{\partial \tau_{xy}}{\partial y} = 0 \quad , \quad \frac{\partial \tau_{xy}}{\partial x} + \frac{\partial \sigma_y}{\partial y} = 0 \tag{2.13}$$

From elementary stress transformation equations, the relation between the Cartesian components of stresses and the principal stresses can be expressed as follows

$$\sigma_x = \frac{1}{2}(\sigma_1 + \sigma_2) + \frac{1}{2}(\sigma_1 - \sigma_2)\cos 2(1, x) \tag{2.14}$$

$$\sigma_y = \frac{1}{2}(\sigma_1 + \sigma_2) - \frac{1}{2}(\sigma_1 - \sigma_2)\cos 2(1, x) \tag{2.15}$$

$$\tau_{xy} = \frac{1}{2}(\sigma_1 - \sigma_2)\sin 2(1, x) \tag{2.16}$$

On substituting σ for half the sum of the principal stresses, k for half their difference (yield criterion) and transform to the angle θ = (1, x)-π/4. Then

$$\sigma_x = \sigma - k \sin 2\theta \tag{2.17}$$

$$\sigma_y = \sigma + k \sin 2\theta \tag{2.18}$$

$$\tau_{xy} = k\cos 2\theta \tag{2.19}$$

On substituting eqs. (2.17-2.19) in the equilibrium equations, we obtain two non-linear partial differential equations of first order with respect to unknown functions σ (x, y) and θ (x, y).

$$\frac{\partial\sigma}{\partial x} - 2k\left(\cos 2\theta\frac{\partial\theta}{\partial x} + \sin 2\theta\frac{\partial\theta}{\partial y}\right) = 0 \tag{2.20}$$

$$\frac{\partial\sigma}{\partial y} - 2k\left(\sin 2\theta\frac{\partial\theta}{\partial x} - \cos 2\theta\frac{\partial\theta}{\partial y}\right) = 0 \tag{2.21}$$

Since the equilibrium equations and yield criterion remain unchanged in transforming from co-ordinate system x, y to any other system, a local co-ordinate system is chosen in which s_1 and s_2 are measured along the tangent and normal to any point P on the slip line, respectively then $\theta = 0$. Thus, the differential equations, eq. (2.20) and eq. (2.21), take the simple form

$$\frac{\partial}{\partial s_\alpha}\left(\sigma - 2k\theta\right) = 0 \tag{2.22}$$

$$\frac{\partial}{\partial s_\beta}\left(\sigma + 2k\theta\right) = 0 \tag{2.23}$$

Where $\partial/\partial s_\alpha$ and $\partial/\partial s_\beta$ are derivatives along the α and β lines, respectively. Since P is an arbitrary point on the slip line, it follows that along slip lines of α and β families we have respectively the following relations

$$\left.\begin{array}{l}\dfrac{dy}{dx}=\tan\theta \\ \\ \dfrac{\sigma}{2k}-\theta=const.=\xi\end{array}\right\} \qquad \left.\begin{array}{l}\dfrac{dy}{dx}=-\cot\theta \\ \\ \dfrac{\sigma}{2k}+\theta=const.=\eta\end{array}\right\} \tag{2.24}$$

The above equations of plasticity for plane strain problems were first obtained by Hencky (1923).

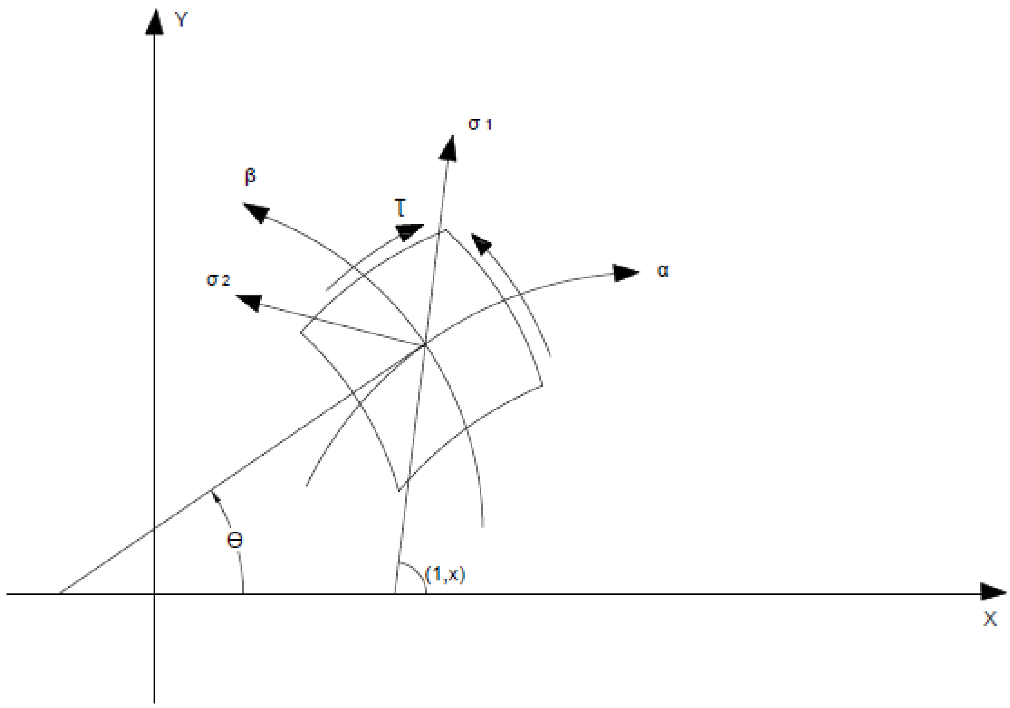

Fig. 2.1: Description of slip lines in Cartesian coordinate system.

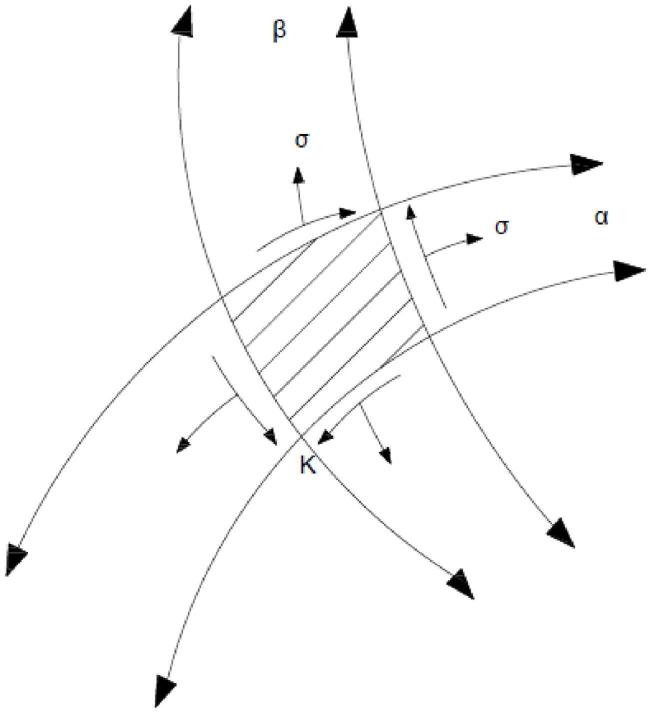

Fig. 2.2: Stresses acting on a plane strain element cut out by slip lines.

CHAPTER 3

Analytical formulation of Modified Upper Bound theorem

3.1 Introduction

In the mathematical theory of elasticity, the principles of minimum potential energy and minimum complimentary energy are powerful tools for obtaining approximate solutions to difficult boundary value problems. In plasticity exact solutions are harder to obtain than in elasticity. Accordingly the extremum theorems of plasticity play an equally, or even more important role in arriving at solutions of problems of practical interest. Apart from their general nature, these theorems provide a way to a direct construction of solutions, by-passing the integration of the differential equations. In the non-linear problems which constitute the plasticity theory this possibility is extremely important as emphasized by Prager and Hodge (1951) and Kachanov (1971). Fundamental results on extremum principles for a plastic-rigid body are mainly due to Markov (1947), Hill (1950), Prager and Hodge (1951) and Koiter (1960). The extremum theorems for a plastic-rigid body provide an efficient method of obtaining the limit load using successive approximations by means of upper and lower bound estimates. More details regarding these load bounding techniques can be found in the work of Hill (1950), Prager and Hodge (1951), Kachanov (1971), and Johnson and Mellor (1973) etc.

Of the two general limit theorems, the upper bound theorem, in particular, has been extensively used in metal forming operations where no exact solutions for the load to cause unconstrained plastic deformation are available. It needs a kinematically admissible velocity field which may have discontinuities in the tangential component but normal component must be the same to maintain plastic volume constancy. The assumption which is often invoked to simplify the analysis is to consider the rigid mode of deformation, that is, the material is assumed to move in rigid blocks separated by lines of tangential displacement discontinuity (see Johnson and Mellor, 1973). This results in considerable simplification and useful upper bounds can be easily obtained. Unfortunately, as a result of this simplifying assumption, particularly for the problems involving predominant bending loads, this upper bound theorem provides (unacceptable) higher estimates of the limit loads. Thus, despite its efficiency the use of this upper bound analysis is quite restricted. In other words, the usefulness and the general nature of these work principles have not been fully exploited and to an extent, till date, they remain merely as a crude method of obtaining the bounds on the limit load.

The organization of this chapter is as follows: first the assumption of plastic-rigid material which is often made in the analytical solutions of many practical problems is discussed. This is followed by a discussion on virtual work principle which is the basis of general theorems of limit analysis. Concepts of statically admissible stress field and kinematically admissible velocity fields which are closely connected with the lower and upper bound theorems of limit analysis are introduced. Finally, the analytical formulation of the proposed Modified Upper Bound (MUB) theorem is presented.

3.2 Assumption of plastic-rigid material

In finding the analytical solutions of many problems of practical interest we are often compelled by mathematical difficulties to disregard the elastic component of strain. For consistency we must also disregard the purely elastic strain in the non-plastic region. In effect, therefore, we work with a material that is rigid when stressed below the yield-point and in which the Young's modulus has an infinitely large value. This hypothetical material may be referred to as a plastic-rigid material, in contrast to the elastic-plastic material.

The distribution of stress in the plastic-rigid body is only likely to approximate that in a real metal under similar external conditions when the plastic material has freedom to flow in some direction. If the plastic material is severely constrained by adjacent elastic material, neglect of the elastic component of strain introduces serious errors in some of the calculated stress components. On the other hand, even though an easy direction of flow is available, so that the elastic strain increments soon become negligible throughout most of the plastic zone, there must still be a certain boundary layer, or transition region, bordering the elastic zone, in which the elastic and plastic strain increments are comparable. The narrower this transition region, the better should be the overall approximation. Since the allowable error depends very much on the intended field of application of the solution, no more explicit rule can be laid down (Hill, 1950). In many metal forming processes like rolling, drawing, forging etc., where large plastic deformation occurs, experience shows that the assumption of a plastic-rigid material does not lead to any significant errors. Another type of problem is that characterized by small deformations. These are problems on limit loads and are closely related to the questions of strength. In this case the regions of plastic deformation for plastic-rigid and elastic-plastic bodies can be quite different. To estimate the error it is desirable to have experimental data. It has been seen that the tests are in good agreement with many of the results obtained from the plastic-rigid model.

3.3 Virtual work principle

The principle of virtual work has proved very powerful as a technique in solving problems and in providing proofs for general theorems in solid mechanics. In the following the virtual work equation is derived. This equation is needed for considerations of stability and uniqueness of general stress-strain relations, which may be irreversible and path dependent. In the derivation the following assumption is made: the displacements are sufficiently small so that the changes in the geometry of the body are negligible and the original undeformed configuration can be used in setting up the equations for the system. This implies that nonlinear contributions in the compatibility of strains and displacements are neglected.

The principle of virtual work deals with two separate and unrelated sets: the equilibrium set and the compatible set. The equilibrium set and the compatible set are brought together, side by side but independently, in the equation of virtual work

$$\int_A T_i u_i^* dA + \int_V F_i u_i^* dV = \int_V \sigma_{ij} \varepsilon_{ij}^* dV \tag{3.1}$$

Here integration is over the whole area, A, or volume, V, of the body. The quantities T_i and F_i are external surface and body forces, respectively. The stress field σ_{ij} is any set of stresses, real or otherwise, in equilibrium with body forces F_i within the body and with the surface forces T_i on the surfaces where the forces T_i are prescribed. Similarly the strain field ε_{ij}^* represents any set of strains or deformation compatible with the real or imagined (virtual) displacements u_i^* of the points of application of the external forces T_i and F_i.

The important point to keep in mind is that neither the equilibrium set T_i, F_i and σ_{ij} nor the compatible set u_i^* and ε_{ij}^* need be the actual state, nor need the equilibrium and compatible sets be related in any way to each other. In eq. (3.1) asterisks are used for the compatible set to emphasise the point that these two sets are completely independent. When the actual or real states (which satisfy both equilibrium and compatibility) are substituted in eq. (3.1), the asterisks are omitted.

3.3.1 Proof of virtual work equation

Consider the external virtual work, W_{ext}, given by the expression on the left-hand side of eq. (3.1). With $T_i = \sigma_{ji} n_j$ on A, we can write

$$W_{ext} = \int_A \sigma_{ji} n_j u_i^* dA + \int_V F_i u_i^* dV \tag{3.2}$$

The first integral can be transformed into a volume integral using the divergence theorem. Thus, we have

$$W_{ext} = \int_V \left(\sigma_{ji} u_i^*\right)_{,j} dV + \int_V F_i u_i^* dV \tag{3.3}$$

$$W_{ext} = \int_V \left(\sigma_{ji,j} u_i^* + \sigma_{ji} u_{i,j}^* \right) dV + \int_V F_i u_i^* dV \qquad (3.4)$$

$$W_{ext} = \int_V \left[\left(\sigma_{ji,j} + F_i \right) u_i^* + \sigma_{ji} u_{i,j}^* \right] dV \qquad (3.5)$$

The first term in parenthesis in eq. (3.5) vanishes for the equilibrium set, which satisfies the equilibrium equations. Therefore, eq. (3.5) reduces to

$$W_{ext} = \int_V \sigma_{ij} u_{i,j}^* dV \qquad (3.6)$$

Now consider the internal virtual work, W_{int}, given by the expression on the right-hand side of eq. (3.1). Using the compatibility relations, we have

$$W_{int} = \int_V \sigma_{ij} \varepsilon_{ij}^* dV = \int_V \frac{1}{2} \sigma_{ij} \left(u_{i,j}^* + u_{j,i}^* \right) dV \qquad (3.7)$$

$$W_{int} = \int_V \left(\frac{1}{2} \sigma_{ij} u_{i,j}^* + \frac{1}{2} \sigma_{ij} u_{j,i}^* \right) dV \qquad (3.8)$$

Which can be written as (i, j are dummy indices)

$$W_{int} = \int_V \left(\frac{1}{2} \sigma_{ij} u_{i,j}^* + \frac{1}{2} \sigma_{ji} u_{i,j}^* \right) dV \qquad (3.9)$$

Finally using the symmetry of σ_{ij},

$$W_{int} = \int_V \sigma_{ij} u^*_{i,j} dV \tag{3.10}$$

Thus, from eqs. (3.6) and (3.10), $W_{ext} = W_{int}$, and the virtual work principle, eq. (3.1) is established.

3.4 General theorems of limit analysis

A complete elastic-plastic analysis is generally quite complicated. The complexities arise mainly from the necessity of carrying out an analysis in an iterative and incremental manner. The development of efficient alternative methods that can be used to obtain the collapse load of a structural problem in a simple and more direct manner without recourse to an iterative and incremental analysis is, therefore, of great value to practicing engineers, despite the fact that the information so obtained is just a part of the total solution. Limit analysis is concerned with the development and applications of such methods that can furnish the engineer with an estimate of the collapse load of a structure in a direct manner. The estimation of the collapse load is of great value, not only as a simple check for a more refined analysis, but also as a basis for engineering design.

It should be emphasized here that the collapse load as calculated in limit analysis is different from the actual plastic collapse load, as it occurs in a real structure or body. Herein, we shall calculate the plastic collapse load of an ideal structure, at which the deformation of the structure can increase without limit while the load is held constant. This, of course rarely happens in a real structure, and hence, the limit analysis calculations apply strictly, not to the real structure, but to the idealised one, in which neither work hardening of the material nor significant changes in geometry of the structure occurs. Nevertheless a load computed on the basis of this definition or idealisation may give a good approximation to the actual plastic collapse load of a real structure.

3.4.1 Admissible stress and velocity fields

It is well known that there are three basic relations that must be satisfied for a valid solution of any problem in the mechanics of deformable solids, namely, the equilibrium equations, the constitutive relations, and the compatibility equations. In general in a limit analysis problem, only the equilibrium equations and yield criterion need be satisfied for a lower-bound solution, and only the compatibility equations and the flow rule associated with a yield criterion need be satisfied for an upper-bound solution. However, an infinite number of stress states will generally satisfy the equilibrium equations and the yield criterion alone, and an infinite number of displacement modes will satisfy the kinematic conditions associated with the flow rule and the displacement boundary conditions. Like other dual principles in structural mechanics, the two theorems of limit analysis are obtained by comparing first only the conditions imposed on the solution by the equilibrium requirements and the constitutive relations, and second the conditions imposed only by the kinematic requirements and the constitutive relations, with the complete or exact solution to be satisfied by all three requirements: equilibrium, kinematics, and constitutive relations.

3.4.1.1 Statically admissible stress field

The stress field which (i) satisfies the equations of equilibrium, (ii) satisfies the stress boundary conditions, and (iii) nowhere violates the yield criterion is termed a statically admissible stress field for the problem under consideration. The external loads determined from a statically admissible stress field alone are not greater than the actual collapse load according to the lower-bound theorem of limit analysis.

3.4.1.2 Kinematically admissible velocity field

An assumed deformation mode (or velocity field) that satisfies (a) velocity boundary conditions, and (b) strain rate and velocity compatibility conditions is termed a kinematically admissible velocity field. The loads determined by equating the external rate of work to the internal rate of dissipation for this assumed deformation mode are not less than the actual collapse load according to the upper bound theorem of limit analysis.

3.4.2 Lower bound theorem

According to lower-bound theorem, “If an equilibrium distribution of stress σ_{ij} can be found which balances the body force F_i in V and the applied loads T_i on the stress boundary A_T and is everywhere below yield, then the body at the loads T_i, F_i will not collapse". Thus, it can be seen that the lower-bound theorem considers only the equilibrium and yield conditions. It gives no consideration to kinematics.

The lower-bound theorem of limit analysis follows directly from the basic material stability postulate (Drucker, 1951). Assume that there are no body forces and define the limit state as one for which deformation occurs under constant surface tractions on the boundary of the body. Then, in the limit state

$$0 = \int_S dT_i du_i dS = \int_V d\sigma_{ij} d\varepsilon_{ij} dV = \int_V d\sigma_{ij} d\varepsilon_{ij}^p dV \tag{3.11}$$

Virtual work and normality of plastic strain increments have been employed. The last integrand is positive definite, so that stresses and elastic strains are constant in the limit state; $d\varepsilon_{ij}=d\varepsilon_{ij}^p$. Let σ_{ij}^E be any stress field in equilibrium with T_i^E on the boundary and nowhere violating the yield condition. As per material stability postulate

$$\left(\sigma_{ij} - \sigma_{ij}^E\right) d\varepsilon_{ij}^p \geq 0 \tag{3.12}$$

Where σ_{ij} and $d\varepsilon_{ij}^p=d\varepsilon_{ij}$ refer to the limit state,

$$\int_V \sigma_{ij} d\varepsilon_{ij} dV \geq \int_V \sigma_{ij}^E d\varepsilon_{ij} dV \tag{3.13}$$

Therefore,

$$\int_S T_i du_i dS \geq \int_S T_i^E du_i dS \tag{3.14}$$

This is the lower bound theorem. When tractions are proportional to some positive parameter P, the value at limit load exceeds any value P^E corresponding to an equilibrium stress field nowhere violating the yield condition

3.4.3 Upper bound theorem

According to upper-bound theorem, "If a kinematically admissible velocity field can be found then the loads T_i and F_i determined by equating the rate at which the external forces do work to the rate of internal dissipation will be either higher than or equal to the actual limit load". Thus, the upper-bound theorem considers only the velocity field and energy dissipation. The stress distribution need not be in equilibrium, and is only defined in the deforming regions of the assumed failure mode.

Consider a strain increment field $d\varepsilon_{ij}^*$derivable from a kinematically admissible displacement increment field du_i^* (that is, the displacement increment field satisfies any prescribed boundary conditions and compatibility equations). Let σ_{ij}^* be any stress state corresponding to a plastic strain increment $d\varepsilon_{ij}^*$. Since

$$\left(\sigma_{ij}^* - \sigma_{ij}\right) d\varepsilon_{ij}^* \geq 0 \tag{3.15}$$

$$\int_V \sigma_{ij}^* d\varepsilon_{ij}^* dV \geq \int_V \sigma_{ij} d\varepsilon_{ij}^* dV \tag{3.16}$$

therefore,

$$\int_V \sigma_{ij}^* d\varepsilon_{ij}^* dV \geq \int_S T_i du_i^* dS \tag{3.17}$$

This is the upper-bound theorem. When tractions are proportional to some positive parameter P and du_i^* is chosen so that the surface integral is positive, the value at limit load is less than the value P^* defined by equality of the surface and volume integrals. Discontinuous displacement increment fields are permissible, but sliding type discontinuities alone are admissible when incompressibility is assumed. In this case, work done on sliding displacement increments by the shear stress corresponding to a shear strain increment in the sliding direction must be added to the volume integral. Thus, the final expression for an upper bound load can be expressed as follows:

$$\int_S T_i du_i^* dS \leq \int_V \sigma_{ij}^* d\varepsilon_{ij}^* dV + \int_S \tau v^* dS_p \tag{3.18}$$

Here v^* denotes the tangential displacement increment discontinuity on a surface S_p for the kinematically admissible velocity field du_i^*, and τ the shear stress.

3.5 Analytical formulation of the modified upper bound theorem

We proceed in a manner similar to that used for formulation of work principle. Let us consider a body, as shown in Fig. 3.1, which occupies a volume V and is bounded by surface $S = S_F + S_V$. Suppose that on the portion S_F of the surface the traction vector T is given whose components with respect to global axes x_i ($i=1,2,3$) are denoted by T_i. Stress field is assumed to be consistent with the prescribed traction vector on the boundary S_F in the sense of Cauchy's formula

$$\sigma_{ij} n_j = T_i \tag{3.19}$$

where n_j are the direction cosines. On the portion S_V of the surface we suppose that velocity v_o is prescribed, its components are denoted by v_{oi}. Assume some continuous velocity field v_i (later we shall remove this restriction) which satisfies the prescribed conditions, that is, $v_i = v_{oi}$ on S_V. Now the strain rate components are related to this velocity field by

$$d\xi_{ij} = \frac{1}{2}\left(\frac{\partial v_i}{\partial x_j} + \frac{\partial v_j}{\partial x_i}\right) \tag{3.20}$$

For a complete solid body the following equation based on virtual work principle holds (Kachanov, 1971)

$$\int_s T_i v_i dS = \int_V \sigma_{ij} d\xi_{ij} dV \tag{3.21}$$

where the second integration extends over the whole volume of the body, and the first over the whole surface S. When we consider discontinuities in the velocity field we note that the discontinuities can occur only in the tangential velocity components. The stresses acting on the surface of velocity discontinuity develop a rate of work

$$-\sum \int_{s_p} \tau v^* dS_p \tag{3.22}$$

where the summation covers all surfaces of discontinuity. τ is the shearing stress component of σ_{ij} in the direction of displacement increment discontinuity. This rate of work when inserted in the virtual work principle, that is, eq. (3.1) would lead to following expression (Kachanov, 1971)

$$\int_s T_i v_i dS = \int_V \sigma_{ij} d\xi_{ij} dV + \int_{s_p} \tau v^* dS_p \tag{3.23}$$

We now proceed to apply this virtual work principle to a rigid-plastic body. Let the quantities σ_{ij}, $d\xi_{ij}$, v_i be the actual solution of the problem in which case the stresses and strain-rates are connected by the Saint Venant-Von Mises relations and satisfy all the conditions of equilibrium and continuity. Together with the actual state we consider another kinematically possible velocity field v_i^*, satisfying the incompressibility condition and the prescribed boundary conditions on S_V. The velocities have associated with them strain-rates $d\xi_{ij}^*$, and to these there corresponds a stress deviator s_{ij}^* for $d\xi_{ij}^* \neq 0$. Finally, let the kinematically possible field v_i^*, be discontinuous on certain surfaces. If σ_{ij}^* is a stress field, not necessarily statically admissible, derivable by way of the concept of the plastic potential from the strain increment field $d\xi_{ij}^*$, then as per material stability postulate (Drucker, 1951),

$$\int_V \left(\sigma_{ij}^* - \sigma_{ij}\right) d\xi_{ij}^* dV \geq 0 \tag{3.24}$$

If the virtual work principle, that is, eq. (3.23) is applied to the actual stress distribution σ_{ij} and the kinematically possible velocity field v_i^*, we have,

$$\int_s T_i v_i^* dS = \int_V \sigma_{ij} d\xi_{ij}^* dV + \int_{s_p} \tau v^* dS_p \tag{3.25}$$

Using eq. (3.24) in eq. (3.25) we get

$$\int_s T_i v_i^* dS \leq \int_V \sigma_{ij}^* d\xi_{ij}^* dV + \int_{s_p} \tau v^* dS_p \tag{3.26}$$

If we replace τ by k the shear yield strength of material we only strengthen the inequality. Thus, finally we have,

$$\int_s T_i v_i^* dS \leq \int_V \sigma_{ij}^* d\xi_{ij}^* dV + \int_{s_p} k v^* dS_p \tag{3.27}$$

The equality sign is achieved only when the kinematically possible field v_i^* coincides with the actual field v_i. The expression on the right-hand side may be interpreted as the total rate of work. Thus, the total rate of work attains an absolute minimum for the actual field.

We further assume that this body actually comprises of two distinct regions viz. Region I consisting of a set of volumes, say V_m (*m=1, 2, 3…)*, comprising of rigid blocks of materials separated by surfaces of tangential displacement discontinuity S_{Vm} (similar to the assumption made in classical upper bound theorem) and Region II consisting of another set of volumes say V_n (*n=1, 2, 3…)*, having deforming zone. The bounding surfaces of the volumes V_n are denoted as S_{Vn}. Applying the work principle as expressed by eq. (3.27) over this entire body we can write

$$\int_s T_i v_i^* dS \leq \sum \int_{V_m} \sigma_{ij}^* d\xi_{ij}^* dV_m + \sum \int_{s_{Vm}} kv^* dS_m + \sum \int_{V_n} \sigma_{ij}^* d\xi_{ij}^* dV_n + \sum \int_{s_{Vn}} kv^* dS_n \qquad (3.28)$$

The assumption of rigid mode of deformation, in region I, makes the first integral term of RHS of eq. (3.28) equal to zero. Similarly the assumption of deforming zone, in region II, vanishes the fourth integral term. As a result eq. (3.28) can finally be expressed as

$$\int_s T_i v_i^* dS \leq \sum \int_{s_{Dm}} kv^* dS_m + \sum \int_{V_n} \sigma_{ij}^* d\xi_{ij}^* dV_n \qquad (3.29)$$

Of course eq. (3.29) seems just to be a rearranged form of general expression of work principle but it would soon become evident that it leads to considerable simplifications and allows us to obtain a general solution. In general, in most of the plastic deformation fields that typically occurs in plane strain problems, the deforming zone, that is, Region II usually lies near the free surface and is in the form of either *uniform stress state* or *simple stress state.* This immediately allows us to use some of the standard results of stress distributions as obtained from SLF. These stress distributions obtained from SLF satisfies the differential equations of equilibrium at each and every point in this plastically deformed zone, that is,

$$\frac{\partial \sigma_{ij}^{*}}{\partial x_i} = 0 \quad \text{in region II} \tag{3.30}$$

It is worth to note that, till now, neither information regarding the state of stress in region I is required nor is it necessary to prove that the stress distribution there satisfies the equilibrium equations. The evaluation of first term on RHS of eq. (3.29) is rather straightforward and needs no further discussion. However, the second term requires some more attention. Using Green Gauss's theorem this second term can be expressed in the form of surface integral as follows

$$\int_{S_n} \sigma_{ij}^{*} v_i^{*} n_j dS_n = \int_{V_n} v_i^{*} \frac{\partial \sigma_{ij}^{*}}{\partial x_i} dV_n + \int_{V_n} \sigma_{ij}^{*} d\xi_{ij}^{*} dV_n \tag{3.31}$$

The first integral on RHS of eq. (3.31) becomes zero because of differential equation of equilibrium expressed by eq. (3.30). Thus,

$$\int_{S_n} \sigma_{ij}^{*} v_i^{*} n_j dS_n = \int_{V_n} \sigma_{ij}^{*} d\xi_{ij}^{*} dV_n \tag{3.32}$$

Substituting eq. (3.32) in eq. (3.29) we can write

$$\int_{s} T_i v_i^* dS \leq \sum \int_{s_{Dm}} kv^* ds_m + \sum \int_{S_n} \sigma_{ij}^* v_i^* n_j dS_n \tag{3.33}$$

If the assumption of rigid mode of deformation (Johnson & Mellor, 1973) was invoked over the whole body then second integral term of eq. (3.33) becomes zero and hence eq. (3.33) would reduce to the conventional form of upper bound theorem that is widely used in load bounding estimates.

In passing it may be mentioned that the proposed solution is incomplete in so far as no attempt is made to extend the stress field into the rigid zones. It has not been shown that an equilibrium stress distribution satisfying the boundary conditions and not exceeding the yield point exists in the assumed rigid regions. Thus, the solution does not meet the requirements of the lower bound theorem. However, the velocity field is that required by the upper bound theorem and, therefore, the MUB theorem is strictly speaking an upper bound solution. These arguments are very much in line with those establishing the upper bound nature of SLF solution. It is important to note that, additionally, inside a SLF the equation of incompressibility and equilibrium conditions are satisfied. In the MUB theorem, neither information regarding the state of stress in region-I is required nor is it necessary to prove that the stress distribution there satisfies the equilibrium equations.

To evaluate this integral, that is, eq. (3.33) we need to know the extent of rigid and deforming zones over which the first and second integral term of RHS of eq. (3.33) should be evaluated respectively. For an assumed kinematically admissible velocity fields, the MUB theorem itself provides the extent of the rigid and deforming zones. This aspect would become clear in chapters 4 and 5 where we deal with specific problems. The only thing that remains is to relate the rate of imposed velocity field v_i^* with the tangential velocity, v^*, with which the rigid parts slide relative to each other. New kinematically compatible velocity fields are proposed in chapter 4 for three-point bending, SE(B) and compact tension, C(T) specimens. These proposed velocity fields when incorporated in MUB theorem have provided results that are in exact agreement with SLF solutions.

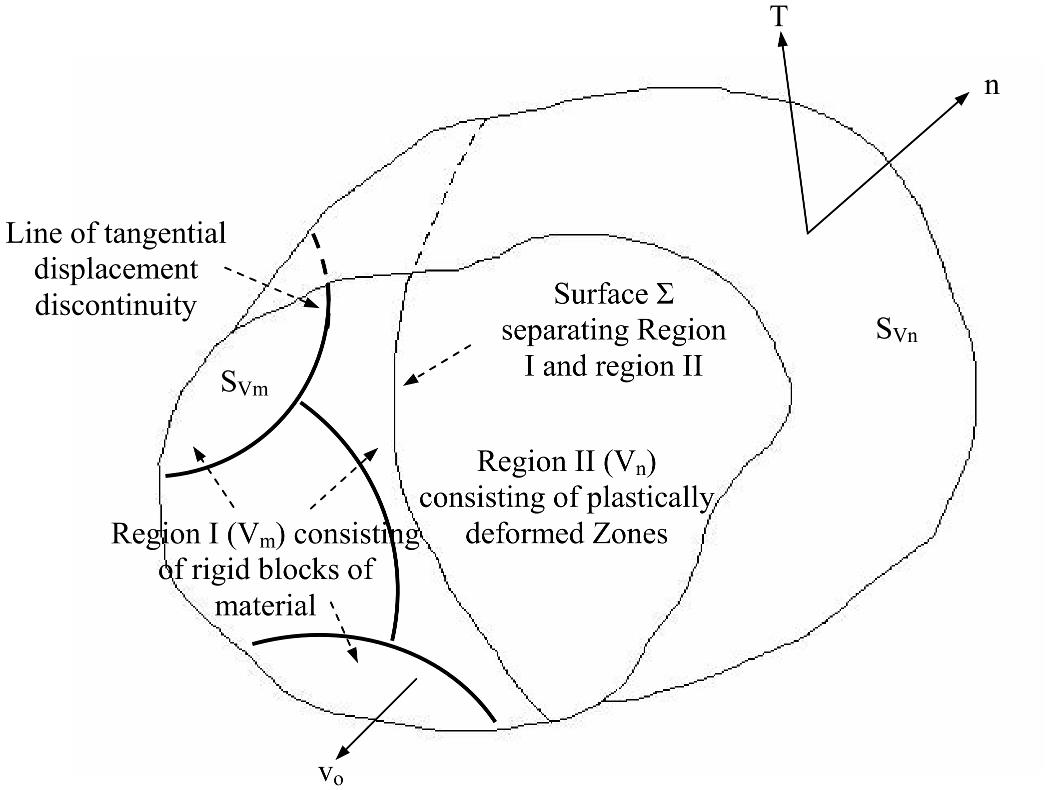

Fig. 3.1: Schematic used for analytical formulation of Modified Upper Bound (MUB) theorem.

CHAPTER 4

Application of proposed modified upper bound theorem to plane strain problems in homogeneous materials

4.1 Introduction

In the previous chapter the significance of extremum theorems/work principles for a plastic-rigid body was emphasised. Apart from their general applicability to many boundary value problems, these theorems provide a way to a direct construction of solutions, by-passing the integration of the differential equations. In the non-linear problems which constitute the plasticity theory this possibility is extremely important as emphasized by Kachanov (1971). Unfortunately, till now, these extremum theorems have been used only as a crude method of obtaining the limit load, of a plastic-rigid body, using successive approximations by upper and lower bound estimates. On the other hand, slip-line field (SLF) analysis, which also assumes that the material is rigid-plastic, can provide sufficiently accurate estimates of the stresses in the plastic region as well as near the notch tip and the corresponding limit loads. Constructing complete SLF for plane strain, non-hardening plasticity, involves discovering a field that satisfies (i) the Hencky equations for equilibrium and yield condition in the deformed region, (ii) the Geiringer equations for incompressibility and (iii) equilibrium and yield inequality in the rigid regions. As a result constructing a complete SLF is relatively difficult and theoretical solutions exist only for limited geometries and loading conditions. Applications of the SLF theory to fracture related problems in Charpy and Izod test specimens are discussed in detail by Green (1953, 1956), Green and Hundy (1956), Alexander and Komoly (1962) and Ewing (1968). Till now, these two methods of plastic analysis, that is, the limit theorems and SLF have remained more or less independent apart from the fact that both are upper bounds as they use kinematically admissible velocity fields.

The analytical formulation of a new load bounding technique, Modified Upper Bound (MUB) theorem, was presented in the previous chapter. It was demonstrated that the method (MUB) is actually a new form of already existing extremum/work principle. In this chapter the equivalence of this new form of work principle, that is, the MUB theorem with the classical SLF analysis, for a rigid-plastic body in plane strain, is discussed in detail. Since plastic deformation fields depend on specimen geometry and type of loading, specific cases were considered. Both cracked and uncracked configurations were analysed to establish this equivalence in general. For cracked bodies only deeply cracked configurations were considered so that the plastic deformation remains confined to the uncracked ligament and does not spread to the cracked flanks. At this point it is worth to mention that Kim (2002) has also shown the global equilibrium of least upper bound circular arcs and evaluated fully plastic crack tip stresses. He assumed a plane strain deformation field consisting of rigid-body rotation across a circular arc extending from a crack tip across the remaining ligament. However, such an assumed deformation field has very limited applications.

In the subsequent sections it would be demonstrated that minimization of this new form of general work principle automatically leads to global equilibrium equations, as obtained from SLF analysis. Once this global equilibrium is established, the kinematically admissible velocity field allows us to use Hencky's equation for evaluation of stresses at any point in the plastically deformed region and in the vicinity of crack tip. Solutions of crack tip stresses obtained from MUB theorem were compared with detailed SLF solutions. Prandtl (1920) first developed the well-known Prandtl slip-line field for a semi-infinite plane strain mode-I crack. Detailed crack tip SLF solutions have already been provided by Rice & Johnson (1970) for blunted crack tip and Hutchinson (1968) for plane stress condition. Various simplifications resulting from the use of the proposed MUB theorem over SLF method are discussed in this chapter.

As a novel application of the proposed method, single-edge-cracked specimen under combined bending and tensile load was analysed. For plates with deep, single edge cracks, slip line fields are known under pure tension and under opening bending with compression or small tension (Shiratori and Miyoshi, 1980; Shiratori and Dodds, 1980). For such plates under opening bending and large tension, Rice (1972) gave an analytical-graphical formulation for sliding along the circular arc giving the least upper bound to the limit load. He also proposed an approximate elliptical yield locus for all ranges of positive tension and net section moments. Kim et al. (1995) provided a complete analytical formulation for Rice's least upper bound. They also proposed an improved approximate elliptical yield locus (based on numerical fitting) and compared it with the finite element limit analyses of Lee and Parks (1993). Thus, while SLF solutions are available only for bending with small tensile load, classical upper bound solutions are valid for bending with large tensile load. In this chapter a completely analytical formulation for yield locus for the entire range of tensile and bending load is presented.

4.2 Equivalence of proposed modified upper bound theorem with slip line field analysis

As mentioned earlier, the modified upper bound (MUB) theorem is actually a new form of already existing extremum/work principle. In this section equivalence of SLF analysis and MUB theorem would be established in terms of global equilibrium equations for a wide variety of plastic deformation fields. While SLF method requires integration of stress distribution of plastically deformed regions the MUB method minimizes plastic work with respect to unknown parameters of assumed plastic field to arrive at global equilibrium equations. Standard results of stress distribution in plastically deformed zones, that is, Region II (see Fig. 3.1), obtained from SLF analysis would be utilized. It is obvious that if we can obtain stress distribution that satisfies equilibrium conditions in the deforming region by any method (experimental or analytical) we need not to refer to SLF results. Moreover, no information is required regarding the state of stress in region I comprising of rigid blocks of material.

As demonstrated in subsequent sections, the expression of MUB theorem itself provides an equation of global equilibrium for force or bending moment. Minimum work principle is then invoked to evaluate the unknown parameters of the plastic deformation field. This process of minimization automatically leads to other equations of global equilibrium which are identical to those obtained from the SLF analysis. It may be emphasized that this equivalence in terms of global equilibrium equations means that the state of stress in the regions having rigid mode of deformation and hence throughout the body is identical with that obtained from detailed SLF analyses. Thus, the plastic deformation field assumed in MUB analysis is in fact SLF and Hencky's theorem can now be used at any point in the plastically deformed regions to evaluate the state of stress. For the sake of simplicity we begin with uncracked configurations.

4.2.1 Bending of cantilever

We start with this classical problem that was first analysed by Green (1954). Let a cantilever beam of rectangular cross-section and length l be bent by a force P (per unit width), applied at the end; the left-hand end of the beam is rigidly clamped. The width b in the horizontal direction is constant and at least six times (Green, 1954) than the height $2h$. In these circumstances plane strain condition can be safely assumed. Depending on $l/2h$ two types of plastic deformation patterns are possible.

4.2.1.1 Short cantilever ($l/2h \leq 13.73$)

In this case the possible plastic deformation field, assumed by Green (1954), is shown in Fig. 4.1(a). Let d be the length of AD, ε the angle DAC and 2ψ the angle subtended by the arc DD′. The right hand part of the cantilever slides along this arc in the limit state. Following the standard results of SLF analysis, (Green, 1954), we have uniaxial tension $+2k$ in ABC and compression $-2k$ in A′B′C′. Adjoining these triangles are the central fields ACD, A′C′D′, which are linked by circular slip line DD′ of radius R. The mean pressure on slip line AD is $p=k\,(1+2\varepsilon)$; the tangential stress on AD is clearly equal to k.

This much information regarding the state of stress distribution, in plastically deformed region, is required for MUB analysis.

The scheme used to relate the relative velocity, v^*, (with which rigid parts rotate) to the rate of imposed displacement, $\delta^{\cdot}$, is shown in Fig. 4.1(b). Since the undeformed material is assumed to slide over the circular arc, therefore, its instantaneous centre must lie at the centre of this arc DD′. At instantaneous centre the tangential velocity is zero. As the undeformed portions are moving rigidly, linear variation of velocity (between instantaneous centre and the point of application of imposed load) can be assumed. As a result the Y-component of imposed displacement at D or D′ can be expressed as follows:

$$\delta^{\cdot}_{D} = \frac{\delta^{\cdot} R\cos\psi}{\left(l + R\cos\psi - d\sin\psi\right)} \tag{4.1}$$

For kinematic admissibility the Y-component of tangential velocity, v^*, at D, must be equal to the Y-component of imposed displacement. Thus, the tangential velocity can be expressed as follows

$$v^* = \frac{\delta^{\cdot} R}{\left(l + R\cos\psi - d\sin\psi\right)} \tag{4.2}$$

The angular velocity ω with which the rigid part of the beam rotate about the instantaneous centre O can be obtained from the following relation

$$\omega = \frac{v^*}{R} = \frac{\delta^{\cdot}}{\left(l + R\cos\psi - d\sin\psi\right)} \tag{4.3}$$

Now invoking work principle, that is, eq. (3.33), limit load can be expressed as,

$$P_L\delta^{\cdot} = 2\left[\int_0^{\psi} kv^* R d\theta + \int_{DC} \sigma_{ij} n_j v_i dS + \int_{CB} \sigma_{ij} n_j v_i dS\right] \tag{4.4}$$

The velocity *v* of any point *P* lying on the circular arc *DC* or on the segment *CB* can be simply obtained as the product of radial distance *r* between the instantaneous centre *O* and point *P* and the angular velocity *ω*. In order to evaluate the work done by the stresses on the elastic-plastic boundary, the velocity *v* is resolved into two components: v_t that is along the slip line and v_n which is normal to it, as shown in Fig. 4.1(c).

The work done by the stresses on the circular arc *DC* (of radius *d*) can be expressed as follows

$$\int_{DC} \sigma_{ij} n_j v_i dS = -\int_0^{\varepsilon} k dv_t d\theta + \int_0^{\varepsilon} k\left(1 + 2\theta\right) dv_n d\theta \tag{4.5}$$

$$\int_{DC} \sigma_{ij} n_j v_i dS = -\int_0^{\varepsilon} kdr\omega \sin\lambda d\theta + \int_0^{\varepsilon} k\left(1 + 2\theta\right) dr\omega \cos\lambda d\theta \tag{4.6}$$

From simple geometry , Fig. 4.1(c), it can be readily shown that along circular arc *DC*

$$r\sin\lambda = d\left[1-\cos\left(\varepsilon-\theta\right)\right]+R\sin\left(\varepsilon-\theta\right) \tag{4.7}$$

$$r\cos\lambda = R\cos\left(\varepsilon-\theta\right)+d\sin\left(\varepsilon-\theta\right) \tag{4.8}$$

On substituting eqs. (4.7 & 4.8) in eq. (4.6), followed by integration, it can be shown that

$$\begin{aligned}\int_{DC}\sigma_{ij}n_jv_i dS = &-k\omega d\left[\varepsilon d+R-d\sin\varepsilon-R\cos\varepsilon\right]\\&+k\omega d\left[d\left(1+2\varepsilon\right)+2R+R\sin\varepsilon-d\cos\varepsilon-2R\cos\varepsilon-2d\sin\varepsilon\right]\end{aligned} \tag{4.9}$$

Similarly, the work done by the stresses on the segment *CB* can be expressed as follows

$$\int_{CB}\sigma_{ij}n_jv_i dS = -\int_0^x kv_t dx+\int_0^x kv_n dx \tag{4.10}$$

$$\int_{CB}\sigma_{ij}n_jv_i dS = -\int_0^x kr\omega\sin\lambda dx+\int_0^x kr\omega\cos\lambda dx \tag{4.11}$$

As per the geometry shown in Fig. 4.1(c), it can be readily shown that along segment *CB*

$$r\sin\lambda = d\left(1-\cos\varepsilon\right)+R\sin\varepsilon \tag{4.12}$$

$$r\cos\lambda = R\cos\varepsilon+d\sin\varepsilon+x \tag{4.13}$$

Substitution of eqs. (4.12 & 4.13) in eq. (4.11), followed by integration, lead to the following relation

$$\int_{CB} \sigma_{ij} n_j v_i dS = -k\omega d\left[d\left(1-\cos\varepsilon\right)+R\sin\varepsilon\right]+k\omega d\left[R\cos\varepsilon + d\sin\varepsilon + \frac{d}{2}\right] \qquad (4.14)$$

Finally, substitution of eqs. (4.9 & 4.14) in eq. (4.4), using the value of ω as given by eq. (4.3), lead to the following relation for the limit load of a short cantilever

$$P_L = \frac{2k}{\left(l - d\sin\psi + R\cos\psi\right)}\left[R^2\psi + dR + \left(1+2\varepsilon\right)\frac{d^2}{2}\right] \qquad (4.15)$$

It may be noted that eq. (4.15) is in fact the condition of global moment equilibrium about hinge point *O*. From geometry it may be easily observed that $\psi = \frac{\pi}{4} - \varepsilon$ and $d = \frac{h - R\sin\psi}{\cos\psi}$.

Here ε and R are the two independent unknown parameters that would be evaluated using minimum work principle. Minimizing eq. (4.15) with respect to these two unknown parameters we have

$$\begin{aligned} \frac{\partial P_L}{\partial \varepsilon} = & \frac{2k}{\left(l - d\sin\psi + R\cos\psi\right)}\left[-R^2 + R\frac{\partial d}{\partial \varepsilon} + \left(1+2\varepsilon\right)d\frac{\partial d}{\partial \varepsilon} + d^2\right] + \\ & \left[R^2\psi + dR + \left(1+2\varepsilon\right)\frac{d^2}{2}\right]\left[\frac{-2k\left(d\cos\psi - \sin\psi\frac{\partial d}{\partial \varepsilon} + R\sin\psi\right)}{\left(l - d\sin\psi + R\cos\psi\right)^2}\right] = 0 \end{aligned} \qquad (4.16)$$

$$\frac{\partial P_L}{\partial R} = \frac{2k}{\left(l - d\sin\psi + R\cos\psi\right)}\left[2R\psi + d + R\frac{\partial d}{\partial R} + \left(1+2\varepsilon\right)d\frac{\partial d}{\partial R}\right] + \left[R^2\psi + dR + \left(1+2\varepsilon\right)\frac{d^2}{2}\right]\left[\frac{-2k\left(-\sin\psi\dfrac{\partial d}{\partial R} + \cos\psi\right)}{\left(l - d\sin\psi + R\cos\psi\right)^2}\right] = 0 \tag{4.17}$$

After a few algebraic simplifications the resulting expressions can be written as follows

$$\left[\left(1+2\varepsilon\right)R\cos\psi + d\cos\psi - R\sin\psi - \left(1+2\varepsilon\right)d\sin\psi\right] = \frac{\left[R^2\psi + dR + \left(1+2\varepsilon\right)\dfrac{d^2}{2}\right]}{\left(l - d\sin\psi + R\cos\psi\right)} = \frac{P_L}{2k} \tag{4.18}$$

$$\left[2R\psi\cos\psi + d\cos\psi - R\sin\psi - \left(1+2\varepsilon\right)d\sin\psi\right] = \frac{\left[R^2\psi + dR + \left(1+2\varepsilon\right)\dfrac{d^2}{2}\right]}{\left(l - d\sin\psi + R\cos\psi\right)} = \frac{P_L}{2k} \tag{4.19}$$

Comparison of eqs. (4.18) and (4.19) provides $1+2\varepsilon = 2\psi$ that can also be obtained from SLF analysis using Hencky's theorem of constancy of ξ along the continuous α-slip-line ADD′A′ (Green, 1954). Thus $2\varepsilon=\pi/4-1/2$. If SLF analysis is performed then unknown radius R is determined from the condition of force equilibrium. Along the arc DD′, the normal stress is equal to $2k\chi$ (Kachanov, 1971), where the angle χ is measured from the horizontal as shown in Fig. 4.1(a). Thus,

$$\left[d\cos\psi - \left(1+2\varepsilon\right)d\sin\psi + R\int_0^{\psi}\cos\chi\, d\chi - 2R\int_0^{\psi}\chi\sin\chi\, d\chi\right] = \frac{P_L}{2k} \tag{4.20}$$

After simplification eq. (4.20) can be finally expressed as

$$\left[d\cos\psi-(1+2\varepsilon)d\sin\psi-R\sin\psi+2R\psi\cos\psi\right]=\frac{P_L}{2k} \tag{4.21}$$

Thus, it is proved that the MUB theorem automatically leads to equations of global equilibrium which are identical to those obtained from SLF analyses. Moreover, the method inherently satisfies Hencky's theorem along a continuous slip line.

4.2.1.2 **Long cantilever** ***(l/2h> 13.73)***

For the case of a long cantilever the possible slip field, assumed by Green (1954), is shown in Fig. 4.2. State of stress in plastically deformed regions ABCD, A′B′C′D′, is identical to that obtained for short cantilever. The shape of assumed plastic field clearly reveals that there is no region in which rigid mode of deformation can be assumed, thus, the first integral term of eq. (3.33) becomes zero. In the limit state a rotation of the rigid part of the cantilever (to the right of BDB′) takes place with respect to point D. Using the stress distribution of plastically deformed region, and evaluating the work done by the stresses on the elastic-plastic boundary DCB, eq. (3.33) can be finally expressed as

$$P_L=\frac{\left[k(1+2\varepsilon)d^2\right]}{\left(l-d\sin\left(\frac{\pi}{4}-\varepsilon\right)\right)} \tag{4.22}$$

It may be noted that the limit load of a long cantilever expressed by eq. (4.22) can be directly obtained by substituting R=0 in eq. (4.15). From geometry it can be readily obtained that *d=h/cos(π/4-ε)*. Here *ε* is the only unknown parameter that would be evaluated using minimum work principle. Minimizing eq. (4.22) with respect to *ε* we have

$$\begin{aligned}\frac{\partial P_L}{\partial \varepsilon} &= \left(l - d\sin\left(\frac{\pi}{4}-\varepsilon\right)\right)\left[2d^2k + k\left(1+2\varepsilon\right)2d\frac{\partial d}{\partial \varepsilon}\right] - \\ &\left[k\left(1+2\varepsilon\right)d^2\right]\left[-\sin\left(\frac{\pi}{4}-\varepsilon\right)\frac{\partial d}{\partial \varepsilon} + d\cos\left(\frac{\pi}{4}-\varepsilon\right)\right] = 0\end{aligned} \tag{4.23}$$

After a few algebraic re-arrangements the following expression can be easily obtained

$$\cos\left(\frac{\pi}{4}-\varepsilon\right) - \left(1+2\varepsilon\right)\sin\left(\frac{\pi}{4}-\varepsilon\right) = \frac{\left[\left(1+2\varepsilon\right)d\right]}{2\left(l - d\sin\left(\frac{\pi}{4}-\varepsilon\right)\right)} \tag{4.24}$$

Using eq. (4.22), eq. (4.24) can be re-written as follows

$$\cos\left(\frac{\pi}{4}-\varepsilon\right) - \left(1+2\varepsilon\right)\sin\left(\frac{\pi}{4}-\varepsilon\right) = \frac{P_L}{2kd} \tag{4.25}$$

Eq. (4.25) represents the condition of force equilibrium which is identical to that obtained from SLF analysis (Kachanov, 1971). As per SLF procedure, for the case of long cantilever, *2ε<π/4-1/2*, the plastic deformation field shown in Fig. 4.2 is valid. When *2ε=π/4-1/2*, SLF shown in Fig. 4.1(a) leads to a smaller, and therefore more appropriate, value of the limit load. The first type of field, Fig. 4.1(a), arises with short cantilever *(l/2h*

≤ 13.73), when ($l/2h = 13.73$) the two fields coincided, since $R=0$. All these conditions can be directly obtained from the proposed MUB theorem. Thus, for both short and long cantilever MUB theorem and SLF analysis finally provide identical results. Numerical values of ε, R, d and P_L for both these configurations were already provided by Green (1954).

4.2.2 Bending of deeply cracked fracture mechanics specimens

In order to demonstrate equivalence of proposed MUB theorem and SLF analysis for cracked bodies, standard fracture mechanics specimens (plane-strain) viz. pure bending specimen, SE(PB), three-pint bend specimens, SE(B) and compact tension specimen, C(T) were analysed. These cracked bend specimens are nowadays frequently used in fracture mechanics analysis. To ensure that a high crack tip constraint exists in these specimens the testing standards usually recommend deeply cracked geometries subjected to predominant bending load. This recommendation ensures that the fracture toughness so obtained would be a conservative estimate of the fracture toughness of the actual structure under investigation. In low strength metal specimens the remaining ligament is normally fully yielded before crack growth initiation. The plastic deformation, therefore, gets confined to the uncracked ligament and does not spread to the cracked flanks. Under these conditions the proposed MUB theorem, assuming that the material is rigid-plastic, can provide sufficiently accurate estimates of the crack tip stresses and, hence, the crack tip constraint parameters like Q, q or h. Which of these constraint parameters is more appropriate to characterise ductile fracture process has been the topic of many detailed investigations (e.g.

Roos et al., 1993). In the remaining part of this chapter results of crack tip constraint is expressed in terms of Q, though q or h can also be easily obtained. The parameter Q is defined by O' Dowd and Shih (1991) in the form

$$Q = \left. \frac{\sigma_{\theta\theta} - \sigma_{\theta\theta,Prandtl}}{\sigma_Y} \right|_{\theta=0, \frac{r\sigma_Y}{J}=2} \tag{4.26}$$

for a rigid-plastic material; where θ is the angle in polar co-ordinate system centered at the crack tip and the subscript Prandtl denotes the stress component calculated from the solution of Prandtl crack tip field. In addition, parameters like the limit load, plastic eta factors (η_p) and plastic rotation factor (r_p) were also evaluated. These parameters may serve as an essential preliminary aspect of the subsequent fracture analysis.

In conventional fracture mechanics J-integral has been widely used as a parameter (though it has its own limitations) to characterize stress and strain field in the vicinity of crack tip for a non-linear elastic material. Its experimental evaluation requires a calibration factor (η_p) either based on load-load line displacement (η_{LLD}) records or on load-crack mouth opening displacement (η_{CMOD}) records. For a given specimen geometry and loading condition, MUB theorem provides the plastic limit load solution, P_L, as a function of crack length a/W, which then provides η_{LLD} and subsequently η_{CMOD}, (see chapter 7 for details).

4.2.2.1 Single edge cracked specimen in pure bending, SE(PB)

For a deeply cracked SE(PB) specimen (a/W>0.3), the plastic deformation mechanism, as shown in Fig. 4.3, was assumed. This is exactly the same deformation mode that was assumed by Green (1953) in his slip line field analysis. Instead of SLF method, here MUB theorem (eq. 3.33) was used to evaluate the limit moment and other useful fracture mechanics parameters. In the proposed solution it is assumed that at limit moment, there is a central pivot OPQ that remains rigid, around which the rigid parts of the specimen on either side rotate by shearing over the circular arcs, OPQ. Near free surface, there is a region of constant compressive stress, RQR, due to traction free boundary condition at the edge A-A. Circular arcs, OPQ, merge in this compressive zone tangentially. The line, OPQR', consisting of a straight line segment, QR', and a circular arc, OPQ, has a continuous tangent and therefore the corresponding velocity field is kinematically admissible (Kachanov, 1971). From Hundy's field (1954), the stress distribution in this compressive zone can be expresses as

$$\sigma_{11} = 0,\ \ \sigma_{22} = -2k \ \text{ and } \ \sigma_{12} = 0 \tag{4.27}$$

Here k is the shear yield strength ($\sigma_y/\sqrt{3}$, according to Von-Mises yield criterion). As far as kinematics is concerned it is assumed that, at limit state, the relative angular velocity, v^*, with which rigid parts rotate becomes equal to the rate of imposed rotation i.e. $v^*=\omega$. Using stress distribution of compressive zone and evaluating the work done by the stresses on the elastic-plastic boundary QR, the resulting expression for limit moment, using eq. (3.33), can be expressed as

$$M_L = k\left[R^2(\beta + \frac{\pi}{4}) + x(R + 0.5x) \right] \tag{4.28}$$

Eq. (4.28) represents the condition of global moment equilibrium about the hinge point. From geometry following relation can be easily obtained

$$R = \frac{l - \frac{x}{\sqrt{2}}}{(\sin\beta + \frac{1}{\sqrt{2}})} \tag{4.29}$$

Here x and β are the two independent unknown parameters that would be evaluated using minimum work principle. Since the algebra involved is quite standard only important steps/equations are provided. Minimizing eq. (4.28) with respect to these two unknown parameters we have

$$\frac{\partial M_L}{\partial x} = k\left[\left(\beta + \frac{\pi}{4}\right) 2R\frac{\partial R}{\partial x} + R + x\frac{\partial R}{\partial x} + x \right] = 0 \tag{4.30}$$

$$\frac{\partial M_L}{\partial \beta} = k\left[R^2 + \left(\beta + \frac{\pi}{4}\right) 2R\frac{\partial R}{\partial \beta} + x\frac{\partial R}{\partial \beta} \right] = 0 \tag{4.31}$$

On further simplification, these two equations can be expressed as

$$\left(\sin\beta+\cos\beta\right)=2\cos\beta\left(\beta+\frac{\pi}{4}\right) \tag{4.32}$$

$$x=\frac{R}{\sqrt{2}}\left[\cos\beta-\sin\beta+2\sin\beta\left(\beta+\frac{\pi}{4}\right)-\sqrt{2}\right] \tag{4.33}$$

Eqs. (4.32) & (4.33) actually represent global equilibrium conditions which can also be obtained from detailed SLF analysis (Chakrabarty, 1987). In addition to limit moment, plastic eta factor, η_{LLD}, and plastic rotation factor, r_p, were also evaluated and were found to be in exact agreement with SLF solution. Numerical values of these parameters are presented in Table 4.1. In Table 4.1, the values of the limit moment M_L were normalised with the limit moment of an uncracked bar M_o.

It is important to note that if presence of compressive zone is neglected then eq. (4.28) would reduce to the classical upper bound solution proposed by Prager (1955), that is, $M_L = 0.398\sigma_y l^2$ which is about 10% higher than that obtained from detailed SLF/MUB solution. In addition to limit moment, plastic eta factor, η_{LLD}, and plastic rotation factor, r_p, were also compared with the classical SLF solution. MUB theorem provides η_{LLD} =2 and r_p =0.37 which are in exact agreement with Green's (1953) SLF solution.

4.2.2.1.1 Fully plastic crack-tip stress fields for SE(PB) specimen

In the previous section, it was established that, for the assumed plastic deformation field, minimum work principle automatically satisfies the global equilibrium equations. It means that the state of stress in the regions having rigid mode of deformation and hence through out the body is identical with that obtained from detailed SLF analyses. Thus, the assumed plastic deformation field is in fact SLF and Hencky's theorem can now be used at any point in the plastically deformed regions to evaluate the state of stress. However, from the stress distribution we cannot determine the constraint parameter Q at the crack tip directly as the assumed plastic field can only give the stress components along the slip lines which radiate from the crack tip and which are inclined to the horizontal line with an angle larger than 45° (Hao et al., 2000). From this kind of slip line fields the stress field surrounding the crack tip is not uniquely obtainable. Following Hao et al. (2000), possible crack-tip stress field is illustrated in Fig. 4.4. In this figure we assume, asymptotically, that a small segment of straight slip line OO' exists. It radiates from the crack tip and is connected to the arc OP in the global slip line field. Thus, the stress components on these small lines are constant and equal to the components at the point O' on the arc O'P. The plastic deformation expand from the line OO' ahead of the crack tip, as shown in Fig. 4.4 and form a diamond-like plastic zone OBXB like that in Prandtl field. In Fig. 4.3, OPQR' is a β slip line along which $\frac{\sigma}{2k}+\theta=\eta$. At point Q, σ=-k and θ=$\pi/4$. Thus, $\eta_Q=\eta_O=\frac{\pi}{4}-\frac{1}{2}$. At point O, θ=-β and on substituting ψ=$\pi/4$+β, $\sigma_O=k(2\psi-1)$. Also O'BX is α-slip line along which $\frac{\sigma}{2k}-\theta=\xi$. Thus, $\xi_{O'}=\xi_B=\psi-\frac{1}{2}+\beta$. At point B, θ=-$\pi/4$ and the normal pressure (hydrostatic stress) can be expressed in terms of slip angle β as follows.

$$\sigma_B=\sigma_X=k(2\psi-1)+2k\left(\beta-\frac{\pi}{4}\right) \tag{4.34}$$

In triangle OBX (that is actually a uniform stress zone) lying just below the crack tip, maximum tensile stress is given by the following expression

$$\sigma_{\theta\theta} = \sigma_B + k \tag{4.35}$$

Comparison of these local stresses near the crack tip and, hence, the constraint factor obtained using MUB theorem and those from detailed SLF solution (Green, 1953) is given in Table 4.1.

Table 4.1: Comparison of results of SE(PB) specimen obtained from MUB theorem with SLF analysis (Green, 1953) for a/W=0.3 - 1.

	R/l	ψ°	x/l	M_L/M_o	r_p	η_{LLD}	(σ_m/σ_y) at θ=0	$(\sigma_{\theta\theta}/\sigma_y)$ at θ=0	Q
SLF	0.388	117.04	0.502	1.26	0.369	2.0	2.326	2.903	-0.064
MUB	0.388	117.04	0.502	1.26	0.369	2.0	2.326	2.903	-0.064

4.2.2.2 Single edge cracked specimen in three-point bending, SE(B)

For a deeply cracked SE(B) specimen (a/W > 0.177), the plastic deformation mechanism suggested by Green and Hundy (1956), as shown in Fig. 4.5, was used. In constructing this field it was assumed that the crack is sufficiently deep for initial overall yielding not to spread to the surface on the cracked side and that there is a stress singularity at the point R on the flat surface. In practice, the central load is supported over a finite length of the surface spanning the point R and local deformation would fit the load 'point' to this surface. Thus, the singularities shown coinciding at R in Fig. 4.5 should be separated by a small distance; in fact, with them coinciding, the yield criterion is certainly violated in the rigid corner QRQ (Hill, 1954). However, as Ewing (1968) has demonstrated, the effect of neglecting this local disturbance does not lead to much error in the overall pattern or limit load, or in the stress distribution near the crack tip. The effect of finite indenter width would be dealt in more detail in the later part of this sub-section.

In the proposed solution it was assumed that at limit moment, there is a region OPQQPO that remains rigid, around which the rigid parts of the specimen on either side rotate by shearing over the circular arcs, OPQ. Near free surface, we have uniaxial compression in the region RST. Adjacent to it is the central field QRT which merges with the circular slip line of radius R. From Hundy's field (1954), the stress distribution in this compressive zone can be expressed as $\sigma_{11} = 0$, $\sigma_{22} = -2k$ and $\sigma_{12} = 0$. In the central field QRT, the shear stress along RT is k and the normal pressure acting on the segment RQ is $k(1+2\gamma)$. The scheme used to relate the relative velocity, v^*, (with which rigid parts rotate) to the rate of imposed displacement, $\dot{\delta}$, is shown in Fig. 4.6. In an actual SE(B) specimen supports are fixed and load is applied at the center that causes an imposed displacement. However, for a kinematic analysis it can be assumed that load point is fixed and a displacement, $\dot{\delta}$, is imposed at the supports. From kinematics, it is well known that the instantaneous centre of a body sliding on a curved surface lies at the center of curvature. Since the undeformed material is assumed to slide over the circular arcs, therefore, their instantaneous centre must lie at the centre of these arcs. At instantaneous centre the tangential velocity is zero. As the undeformed portions are moving rigidly, linear variation of velocity (between instantaneous centre and support) can be assumed. As a result, x-component of imposed displacement (see Fig. 4.6) at crack tip can be expressed as follows:

$$\delta^{\cdot}_{c} = \frac{\delta^{\cdot} R\cos\beta}{\left(S/2 + R\cos\beta\right)} \tag{4.36}$$

For kinematic admissibility the x-component of tangential velocity, v^{*}, at crack tip, must be equal to the x-component of imposed displacement i.e.

$$\delta^{\cdot}_{c} = \frac{\delta^{\cdot} R\cos\beta}{\left(S/2 + R\cos\beta\right)} = v^{*}\cos\beta \tag{4.37}$$

Thus, the tangential velocity can be expressed in terms of imposed displacement, $\delta^{\cdot}$, as given by following equation.

$$v^{*} = \frac{R\delta^{\cdot}}{\left(S/2 + R\cos\beta\right)} \tag{4.38}$$

The angular velocity ω with which the rigid part of the beam rotate about the hinge H can be obtained from the following relation

$$\omega = \frac{v^{*}}{R} = \frac{\delta^{\cdot}}{\left(S/2 + R\cos\beta\right)} \tag{4.39}$$

Now invoking work principle, that is, eq. (3.33), limit load can be expressed as,

$$P_L\delta^{\cdot} = \int_0^{\left(\beta+\frac{\pi}{4}-\gamma\right)} kv^* R d\theta + \int_{QT} \sigma_{ij} n_j v_i dS + \int_{TS} \sigma_{ij} n_j v_i dS \tag{4.40}$$

Since the stress and velocity distribution on the elastic-plastic boundary QTS are quite similar to that of short cantilever, Fig. 4.1 (c), the details are omitted and the resulting expression for the limit load can be expressed as

$$P_L = \frac{2k}{\left(\frac{S}{2} + R\cos\beta\right)} \left[R^2 \left(\beta + \pi/4 - \gamma\right) + \left(1 + 2\gamma\right)\frac{x^2}{2} + xR \right] \tag{4.41}$$

for

$$R = \frac{l - x\cos\left(\frac{\pi}{4} - \gamma\right)}{\sin\beta + \sin\left(\frac{\pi}{4} - \gamma\right)} = \frac{x\sin\left(\frac{\pi}{4} - \gamma\right)}{\cos\left(\frac{\pi}{4} - \gamma\right) - \cos\beta} \tag{4.42}$$

Eq. (4.41) represents the global moment equilibrium, about the hinge point, that needs to be minimized with respect to unknown parameters, that is, x, γ and β. These three parameters are not independent but are subjected to a geometrical constraint as specified by eq. (4.42). In the present case, Lagrange's method of undetermined multiplier was used. Application of this optimization technique requires the geometrical constraint to be re-expressed in following form

$$\phi(x,\beta,\gamma) = x\sin\left(\frac{\pi}{4} - \gamma\right)\left(\sin\beta + \sin\left(\frac{\pi}{4} - \gamma\right)\right) - \left(\cos\left(\frac{\pi}{4} - \gamma\right) - \cos\beta\right)\left(l - x\cos\left(\frac{\pi}{4} - \gamma\right)\right) \tag{4.43}$$

Following Lagrange's multiplier method, we have

$$\frac{\partial P_L}{\partial x}+\lambda\frac{\partial\phi}{\partial x}=0\ ;\ \frac{\partial P_L}{\partial\beta}+\lambda\frac{\partial\phi}{\partial\beta}=0\ ;\ \frac{\partial P_L}{\partial\gamma}+\lambda\frac{\partial\phi}{\partial\gamma}=0 \qquad (4.44)$$

On elimination of undetermined multiplier, λ, from the above equations we have

$$\frac{\partial P_L}{\partial x}\frac{\partial\phi}{\partial\beta}-\frac{\partial P_L}{\partial\beta}\frac{\partial\phi}{\partial x}=0 \qquad (4.45)$$

$$\frac{\partial P_L}{\partial\beta}\frac{\partial\phi}{\partial\gamma}-\frac{\partial P_L}{\partial\gamma}\frac{\partial\phi}{\partial\beta}=0 \qquad (4.46)$$

$$\frac{\partial P_L}{\partial x}\frac{\partial\phi}{\partial\gamma}-\frac{\partial P_L}{\partial\gamma}\frac{\partial\phi}{\partial x}=0 \qquad (4.47)$$

Minimizing eq. (4.41) with respect to unknown parameters and after a few algebraic simplifications, we have

$$\frac{\partial P_L}{\partial x}=\frac{2k}{x}\left[\frac{2\psi R^2+\left(1+2\gamma\right)x^2+2Rx}{\left(\frac{S}{2}+R\cos\beta\right)}\right]-\frac{P_L\cos\beta R}{x\left(\frac{S}{2}+R\cos\beta\right)} \qquad (4.48)$$

$$\frac{\partial P_L}{\partial \beta} = \frac{2k}{\left(\frac{S}{2} + R\cos\beta\right)}\left[R^2 - \frac{2\psi R^2 \sin\beta}{\left\{\cos\left(\frac{\pi}{4} - \gamma\right) - \cos\beta\right\}} - \frac{xR\sin\beta}{\left\{\cos\left(\frac{\pi}{4} - \gamma\right) - \cos\beta\right\}}\right] \tag{4.49}$$
$$+ \frac{P_L}{\left(\frac{S}{2} + R\cos\beta\right)}\left[R\sin\beta + \frac{R\sin\beta\cos\beta}{\left\{\cos\left(\frac{\pi}{4} - \gamma\right) - \cos\beta\right\}}\right]$$

$$\frac{\partial P_L}{\partial \gamma} = \frac{2k}{\left(\frac{S}{2} + R\cos\beta\right)}\left[-R^2 - \frac{2\psi xR\left\{1 - \cos\beta\cos\left(\frac{\pi}{4} - \gamma\right)\right\}}{\left\{\cos\left(\frac{\pi}{4} - \gamma\right) - \cos\beta\right\}^2} + x^2 - \frac{x^2\left\{1 - \cos\beta\cos\left(\frac{\pi}{4} - \gamma\right)\right\}}{\left\{\cos\left(\frac{\pi}{4} - \gamma\right) - \cos\beta\right\}^2}\right] \tag{4.50}$$
$$+ \frac{P_L}{\left(\frac{S}{2} + R\cos\beta\right)}\left[\frac{x\cos\beta\left\{1 - \cos\beta\cos\left(\frac{\pi}{4} - \gamma\right)\right\}}{\left\{\cos\left(\frac{\pi}{4} - \gamma\right) - \cos\beta\right\}^2}\right]$$

Here,

$$\psi = \beta + \frac{\pi}{4} - \gamma \tag{4.51}$$

Also

$$\frac{\partial \phi}{\partial x} = 1 - \cos\psi \tag{4.52}$$

$$\frac{\partial \phi}{\partial \beta} = x\sin\left(\frac{\pi}{4} - \gamma\right)\cos\beta - R\left[\sin^2\beta + \sin\beta\sin\left(\frac{\pi}{4} - \gamma\right)\right] \tag{4.53}$$

$$\frac{\partial \phi}{\partial \gamma} = -x\sin\left(\frac{\pi}{4} - \gamma\right)\cos\left(\frac{\pi}{4} - \gamma\right) - x\sin\psi - R\left[\sin\beta + \sin\left(\frac{\pi}{4} - \gamma\right)\right]\sin\left(\frac{\pi}{4} - \gamma\right) \tag{4.54}$$

Substitution of eqs. (4.49) & (4.50) and eqs. (4.53) & (4.54) in eq. (4.46) finally leads to following equation

$$\begin{aligned}\frac{P_L}{2} &= kx\left[\sin\left(\frac{\pi}{4}+\gamma\right)-(1+2\gamma)\cos\left(\frac{\pi}{4}+\gamma\right)\right]+ \\ &kR\left[\{2\psi-(1+2\gamma)\}\sin\left(\psi+\frac{\pi}{4}+\gamma\right)+\cos\left(\psi+\frac{\pi}{4}+\gamma\right)+(1+2\gamma)\sin\left(\frac{\pi}{4}+\gamma\right)-\cos\left(\frac{\pi}{4}+\gamma\right)\right]\end{aligned} \tag{4.55}$$

Similarly, substitution of eqs. (4.48) & (4.54) and eqs. (4.50) & (4.52) in eq. (4.47) provides the following expression

$$\begin{aligned}&kx\left[(1+2\gamma)\sin\left(\frac{\pi}{4}+\gamma\right)+\cos\left(\frac{\pi}{4}+\gamma\right)\right]+ \\ &kR\left[\{2\psi-(1+2\gamma)\}\cos\left(\psi+\frac{\pi}{4}+\gamma\right)-\sin\left(\psi+\frac{\pi}{4}+\gamma\right)+(1+2\gamma)\cos\left(\frac{\pi}{4}+\gamma\right)+\sin\left(\frac{\pi}{4}+\gamma\right)\right]=0\end{aligned} \tag{4.56}$$

Eqs. (4.55) & (4.56) represent the global force equilibrium equations (identical to those obtained from SLF analysis, Wu et al., 1987). This in turn again establishes equivalence of MUB theorem and SLF analysis. For the case of standard deeply cracked SE(B) specimen, Wu et al. (1987) have presented SLF solution and expressed the results of limit load in the form of plastic constraint factor L that gives the measure of load enhancement due to presence of notch. Limit load, thus can be expressed in the following form

$$P_L = L(a/W)\frac{2\sigma_y l^2}{\sqrt{3}S} \tag{4.57}$$

In addition to plastic constraint factor, *L(a/W)*, *x*, β and γ, plastic eta factor, η_{LLD}, and plastic rotation factor, r_p, were also compared with the classical SLF solution and their numerical values are given in Table 4.2.

It is worth to note that Joch et al. (1993) have also proposed an upper bound solution for standard SE(B) specimen. They have neglected the constant stress region RST and the fan field QRT (see Fig. 4.5) and assumed a deformation mechanism consisting of circular arcs emanating from the crack tip up to the free surface. The tangential velocity and the load point displacement was related by the following expression

$$v^* = \frac{2R\dot{\delta}}{S} \tag{4.58}$$

The resulting expression of upper bound limit load (Joch et al., 1993), with Von-Mises plasticity, is given below

$$P_l = \frac{1.593\sigma_y l^2}{S} \tag{4.59}$$

It can be noted that the solution provided by Joch et al. (1993) does not explain the dependence of limit load on a/W ratio. For a/W=0.5, the limit load is about 10% higher that that obtained from SLF solution (Wu et al., 1987). Similarly, the plastic constraint factor obtained is about 13.5% higher than that obtained from the SLF solution.

4.2.2.2.1 Fully plastic crack-tip stress fields for SE(B) specimen

In Fig. 4.5, assuming Δ RST to be in a state of compression, ST is α-slip line along which $\frac{\sigma}{2k}-\theta=\xi$. At point S, $\sigma=-k$ and $\theta=\pi/4$. Thus, $\xi_S=\xi_Q=-\left(\frac{\pi}{4}+\frac{1}{2}\right)$. At point Q, $\theta=\frac{\pi}{4}-\gamma$ and thus the normal pressure is $\sigma_Q=-k\left(1+2\gamma\right)$. Now, RQPO is β-slip line along which $\frac{\sigma}{2k}+\theta=\eta$. Thus, $\eta_Q=\eta_O=\frac{\pi}{4}-2\gamma-\frac{1}{2}$. At point O, $\theta=-\beta$ and on substituting $\psi=\pi/4+\beta-\gamma$, $\sigma_O=k\left(2\psi-2\gamma-1\right)$. Also O′BX is α-slip line along which $\frac{\sigma}{2k}-\theta=\xi$. Thus, $\xi_{O'}=\xi_B=\psi-\gamma-\frac{1}{2}+\beta$. At point B, $\theta=-\pi/4$ and the normal pressure (hydrostatic stress) can be expressed in terms of slip angle β as follows.

$$\sigma_B=\sigma_X=k\left(2\psi-2\gamma-1\right)+2k\left(\beta-\frac{\pi}{4}\right) \tag{4.60}$$

In triangle OBX (that is actually a uniform stress zone) lying just below the crack tip, maximum tensile stress is given by the following expression

$$\sigma_{\theta\theta}=\sigma_B+k \tag{4.61}$$

Comparison of hydrostatic stress, near the crack tip, obtained using MUB theorem and that from detailed SLF solution (Wu et al., 1987) is given in Table 4.2.

Table 4.2: Comparison of theoretical results of SE(B) specimen obtained from MUB theorem with SLF analysis (Wu et al., 1987).

a/W	Method	$R/(W-a)$	ψ°	γ°	$x/(W-a)$	L	r_p	η_{LLD}	(σ_m/k) at $\theta=0$
0.2	SLF	0.5	102.38	7.37	0.3	1.215	0.455	1.937	3.006
	MUB	0.5	102.31	7.35	0.3	1.215	0.455	1.921	3.00
0.3	SLF	0.49	103.99	7.28	0.31	1.227	0.451	1.945	3.118
	MUB	0.49	104.08	7.3	0.31	1.227	0.450	1.935	3.124
0.4	SLF	0.48	105.63	7.18	0.32	1.238	0.447	1.953	3.233
	MUB	0.48	105.66	7.17	0.32	1.238	0.447	1.948	3.235
0.5	SLF	0.47	107.29	7.07	0.34	1.248	0.443	1.961	3.349
	MUB	0.47	107.29	7.07	0.34	1.248	0.443	1.959	3.346
0.6	SLF	0.47	108.96	6.96	0.35	1.258	0.439	1.969	3.466
	MUB	0.47	108.96	6.94	0.35	1.258	0.439	1.97	3.462
0.7	SLF	0.46	110.65	6.84	0.36	1.267	0.435	1.977	3.584
	MUB	0.46	110.64	6.81	0.36	1.267	0.435	1.979	3.582
0.8	SLF	0.45	112.35	6.71	0.37	1.275	0.431	1.985	3.702
	MUB	0.45	112.34	6.71	0.37	1.275	0.431	1.988	3.701
0.9	SLF	0.44	114.05	6.58	0.38	1.282	0.427	1.987	3.821
	MUB	0.44	114.05	6.53	0.38	1.282	0.427	1.994	3.821

4.2.2.2.2 <u>Effect of indenter width on the limit load and local stresses near the crack tip for SE(B) specimen</u>

In actual practice, SE(B) specimen is loaded in three-point bending by an indenter of finite width. This requires evaluation of correction to be expected due to finite indenter width. The indenter surface in practice is a circular arc of about 2.5 mm radius but following the suggestions of Alexander and Komoly (1962), Ewing (1968) replaced it by a flat punch of width *2b* and analyse the effects on the SLF by varying this small dimension *b*. The plastic deformation field (as suggested by Ewing, 1968) is shown in Fig. 4.7. The stress distribution in compressive zone and central field remain same as obtained earlier. Application of MUB theorem, eq. (3.33), yields the following expression for limit load (same as eq. (4.41)).

$$P_L = \frac{2k}{\left(\frac{S}{2}+R\cos\beta\right)}\left[R^2\left(\beta+\pi/4-\gamma\right)+\left(1+2\gamma\right)\frac{x^2}{2}+xR\right] \tag{4.62}$$

for

$$R = \frac{b+x\sin\left(\frac{\pi}{4}-\gamma\right)}{\left\{\cos\left(\frac{\pi}{4}-\gamma\right)-\cos\beta\right\}} \tag{4.63}$$

$$\left(b+x\sin\left(\frac{\pi}{4}-\gamma\right)\right)\left(\sin\beta+\sin\left(\frac{\pi}{4}-\gamma\right)\right)=\left(\cos\left(\frac{\pi}{4}-\gamma\right)-\cos\beta\right)\left(l-x\cos\left(\frac{\pi}{4}-\gamma\right)\right) \tag{4.64}$$

Rest of the analysis is exactly same as discussed under sub-section 4.2.2.2 and we proceed directly to results. Effect of finite indenter width on plastic constraint factor, *L(a/W)*, *R*, *x,* β and ψ, and on local stresses near the crack tip is quantified in Table 4.3. Again, both MUB theorem and SLF analysis provides identical results.

Table 4.3: Effect of indenter width on plastic field parameters and crack tip stresses obtained from MUB theorem and SLF analysis (Ewing, 1968) for a/W=0.2, W=10 mm.

Span	b (mm)	Method	R (mm)	ψ°	γ°	x (mm)	β	$(\sigma_{\theta\theta}/2k)_{\theta=0}$
S=44 (mm)	0	SLF	3.9629	103.548	7.309	2.4779	1.224	2.044
		MUB	3.9627	103.538	7.312	2.4786	1.224	2.043
	0.5	SLF	4.0881	103.755	9.431	2.2456	1.251	2.051
		MUB	4.0879	103.769	9.419	2.2453	1.251	2.051
	1.0	SLF	4.2173	104.119	11.532	2.0322	1.287	2.064
		MUB	4.2163	104.128	11.531	2.0335	1.287	2.064
S=40 (mm)	0	SLF	4.0219	102.375	7.376	2.4078	1.215	2.003
		MUB	4.0221	102.364	7.375	2.4077	1.215	2.002
	0.5	SLF	4.1475	102.590	9.510	2.1757	1.243	2.01
		MUB	4.1480	102.591	9.499	2.1746	1.243	2.01
	1.0	SLF	4.2771	102.957	11.625	1.9624	1.279	2.023
		MUB	4.2766	102.960	11.622	1.9630	1.279	2.023

4.2.3 Compact tension C(T) specimen

Theoretical solution proposed here is valid for a deeply cracked C(T) specimen (*a/W* ≥ 0.1). The same plastic deformation mechanism that was suggested by Green (1953) for SE(PB) specimen was used by Ewing and Richards (1974) in their SLF analysis of C(T) specimen. The stress distribution in compressive zone is assumed to be same as that in case of SE(B) specimen i.e. $\sigma_{11} = 0,\ \sigma_{22} = -2k$ and $\sigma_{12} = 0$.

The scheme used to relate the relative velocity, v^*, (with which rigid parts rotate) to the rate of imposed displacement, $\delta^{\cdot}$, is similar to that used for SE(B) specimen. Since the undeformed material is assumed to slide over the circular arcs, therefore, their instantaneous centre must lie at the centre of these arcs. At instantaneous centre the tangential velocity is zero. As the undeformed portions are moving rigidly, linear variation of velocity (between instantaneous centre and pin) can be assumed. As a result, Y-component of imposed displacement (see Fig. 4.6) at the crack tip can be expressed as follows

$$\delta^{\cdot}_c = \frac{\delta^{\cdot} R \sin\beta}{2\left(a + R\sin\beta\right)} \tag{4.65}$$

For kinematic admissibility, Y-component of the tangential velocity, v^*, at the crack tip, must be equal to Y-component of imposed displacement i.e.

$$\delta^{\cdot}_c = \frac{\delta^{\cdot} R \sin\beta}{2\left(a + R\sin\beta\right)} = v^* \sin\beta \tag{4.66}$$

Thus, the tangential velocity can be expressed in terms of imposed displacement, $\delta^{\cdot}$, as given by the following equation.

$$v^{*} = \frac{R\delta^{\cdot}}{2\left(a + R\sin\beta\right)} \tag{4.67}$$

Using the stress distribution of compressive zone and the proposed velocity field in the MUB theorem, eq. (3.33), the resulting expression for limit load can be expressed as

$$P_L = \frac{k}{\left(a + R\sin\beta\right)}\left[R^2(\beta + \pi/4) + x(R + 0.5x)\right] \tag{4.68}$$

Eq. (4.68) represents the condition of global moment equilibrium about the hinge point. From geometry following relation can be easily obtained

$$R = \frac{l - \frac{x}{\sqrt{2}}}{(\sin\beta + \frac{1}{\sqrt{2}})} \tag{4.69}$$

Similar to the case of SE(PB) specimen, here x and β are the two independent unknown parameters that would be evaluated using minimum work principle. Minimizing eq. (4.68) with respect to these two unknown parameters and after a few algebraic re-arrangements we have

$$\sqrt{2}\left(\beta+\frac{\pi}{4}\right)R=\left[\left(l-\sqrt{2}x\right)+x\left(\sin\beta+\frac{1}{\sqrt{2}}\right)\right]+\frac{P_L\sin\beta}{k\sqrt{2}} \tag{4.70}$$

$$1-\frac{2\cos\beta\left(\beta+\frac{\pi}{4}\right)}{\left(\sin\beta+\frac{1}{\sqrt{2}}\right)}-\frac{P_L\cos\beta}{k\sqrt{2}R\left(\sin\beta+\frac{1}{\sqrt{2}}\right)}=\frac{x\cos\beta}{R\left(\sin\beta+\frac{1}{\sqrt{2}}\right)} \tag{4.71}$$

On further simplification, these two equations can be rearranged to give

$$\left(\sin\beta+\cos\beta\right)=2\cos\beta\left(\beta+\frac{\pi}{4}\right) \tag{4.72}$$

$$x=R\left(\frac{1-\sqrt{2}\cos\beta}{\sqrt{2}\cos\beta}\right)-\frac{P_L}{k\sqrt{2}} \tag{4.73}$$

Solution of eq. (4.72) provides $\beta=72.04°$, that is, the angle subtended by the circular arc *OQ* to its centre (see Fig. 4.8) is always $117.04°$ for all $a/W \geq 0.1$. This leads to considerable simplification and a closed-form expression for the limit load can be expressed as follows

$$\frac{l}{2W}=\left(1.26\sqrt{m^2+m}\right)-m \tag{4.74}$$

Here, $m=\frac{P_L}{4kW}$, thus results obtained from MUB theorem are in exact agreement with SLF solution (Ewing and Richards, 1974). In addition to factor *m*, plastic eta factor, η_{LLD}, and plastic rotation factor, r_p, were also compared with the classical SLF solution and their comparison is given in Table 4.4. It is worth to note that for deep notches as $a/W \rightarrow 1$, results obtained from eq. (4.60) reduces to the case of pure bending specimen, SE(PB), as discussed by Ewing and Richards (1974).

Following the procedure used to evaluate the fully plastic crack tip stresses, for a pure bending specimen SE(PB), the pressure (hydrostatic stress) in the diamond shaped plastic zone OBXB (see Fig. 4.4) can be expressed in terms of slip angle β as follows:

$$\sigma_B = \sigma_X = k\left(2\psi - 1\right) + 2k\left(\beta - \frac{\pi}{4}\right) \tag{4.75}$$

In triangle OBX (that is actually a uniform stress zone) lying just below the crack tip, maximum tensile stress is given by the following expression

$$\sigma_{\theta\theta} = \sigma_B + k \tag{4.76}$$

For a deeply cracked C(T) specimen ($a/W \geq 0.1$), the angle subtended by the circular arc at its centre is *117.04°* and, thus, the hydrostatic stress near the crack tip, that is, $\sigma_m/2k$ is *2.014* and the tensile stress at the tip of crack ($\sigma_{\theta\theta}/\sigma_o$) is *2.903* (the same as found for a deeply cracked pure bending specimen).

Table 4.4: Comparison of results obtained from MUB theorem with SLF solutions (Ewing and Richards, 1974) for W=10 mm.

a/W	m (SLF)	m (MUB)	R (mm) (SLF)	R (mm) (MUB)	η_p (MUB)	η_p (SLF)	r_p (MUB)	r_p (SLF)
0.1	0.244	0.244	5.3959	5.3955	2.63	2.63	0.57	0.57
0.2	0.179	0.179	4.5050	4.5033	2.591	2.59	0.53	0.53
0.3	0.127	0.127	3.7124	3.7105	2.531	2.53	0.50	0.50
0.4	0.087	0.087	3.0075	3.0061	2.458	2.453	0.47	0.47
0.5	0.056	0.056	2.3785	2.3776	2.377	2.376	0.45	0.45
0.6	0.033	0.033	1.8136	1.8126	2.295	2.293	0.43	0.43
0.7	0.017	0.017	1.3019	1.3008	2.214	2.212	0.41	0.41
0.8	0.007	0.007	0.8344	0.8334	2.137	2.133	0.39	0.39
0.9	0.0017	0.0017	0.4038	0.4017	2.06	2.045	0.38	0.38

4.2.4 Single-edge-cracked specimen under combined bending and tension

Shiratori and Dodds (1980) discussed that the plastic deformation mechanism that was suggested by Green (1953) for SE(PB) specimen can also be used for single-edge- cracked specimen under combined bending and tension but with modification to account for the tensile load. Thus, in the proposed solution, for opening bending with small tension, it is assumed that at limit state, there is a region OPQQPO that remains rigid, around which the rigid parts of the specimen on either side rotate by shearing over the circular arcs, OPQ.

Near free surface, we have uni-axial compression in the region RQR′. Thus, plastic deformation mechanism (as shown in Fig. 4.9) consists of a circular arc that merges into the constant stress region tangentially. The stress distribution in this constant region is already known from Hundy's field (1954).

Before proceeding further let us introduce two non-dimensional parameters $\hat{N}_n$ and $\hat{M}_n$ representing net section tension and bending moment normalized in terms of an uncracked plate with the shear strength *k* and remaining ligament *l*:

$$\hat{N}_n = \frac{N_n}{2kl} \tag{4.77}$$

$$\hat{M}_n = \frac{M_n}{0.5kl^2} \tag{4.78}$$

The condition $-1 \le \hat{N}_n < 0.5512$ is generally referred as small tension for which compressive zone near the free surface exists and SLFs are well known. $\hat{N}_n > 0.5512$ is referred as large tension for which compressive zone vanishes and SLFs are unknown.

The scheme used to relate the relative angular velocity, ω, (with which rigid parts rotate) to the rate of imposed displacement, $\dot{\delta}$, was proposed by Kim et al. (1995). Thus, the relative velocity, ω, can be expressed in terms of imposed displacement, $\dot{\delta}$, as given by following equation.

$$\omega = \frac{\delta^{\cdot}}{\left(R\sin\beta - \frac{l}{2}\right)} \tag{4.79}$$

Using the stress distribution of compressive zone and the proposed velocity field in the MUB theorem, eq. (3.33), the resulting expression for limit moment can be expressed as

$$M_L = k\left[R^2(\beta + \frac{\pi}{4}) + x(R + 0.5x)\right] - N_L\left(R\sin\beta - \frac{l}{2}\right) \tag{4.80}$$

Eq. (4.80) represents the condition of global moment equilibrium about the hinge point. From geometry following relation can be easily obtained

$$R = \frac{l - \frac{x}{\sqrt{2}}}{(\sin\beta + \frac{1}{\sqrt{2}})} \tag{4.81}$$

Here x and β are the two independent unknown parameters that would be evaluated using minimum work principle. Minimizing eq. (4.80) with respect to these two unknown parameters we have

$$\frac{\partial M_L}{\partial x} = k\left[\left(\beta + \frac{\pi}{4}\right)2R\frac{\partial R}{\partial x} + R + x\frac{\partial R}{\partial x} + x\right] - N_L\sin\beta\frac{\partial R}{\partial x} = 0 \tag{4.82}$$

$$\frac{\partial M_L}{\partial \beta} = k\left[R^2 + \left(\beta + \frac{\pi}{4}\right)2R\frac{\partial R}{\partial \beta} + x\frac{\partial R}{\partial \beta}\right] - N_L\left(R\cos\beta + \sin\beta\frac{\partial R}{\partial \beta}\right) = 0 \tag{4.83}$$

On further simplification, these two equations can be expressed as

$$\left(\sin\beta+\cos\beta\right)=2\cos\beta\left(\beta+\frac{\pi}{4}\right) \tag{4.84}$$

$$x=R\left(\frac{1-\sqrt{2}\cos\beta}{\sqrt{2}\cos\beta}\right)-\frac{N_L}{k\sqrt{2}} \tag{4.85}$$

Eqs. (4.84) & (4.85) actually represent global equilibrium conditions which can also be obtained from detailed SLF analysis (Shiratori and Dodds, 1980). Solution of eq. (4.84) provides *β=72.04°* , that is, the angle subtended by the circular arc *OQ* to its centre (see Fig. 4.9) is always *117.04°* for all *a/W>0.35 and small tension*. This leads to considerable simplification and a closed-form expression for resulting yield locus that is in exact agreement with SLF solution (Shiratori and Dodds, 1980) can be expressed as follows

$$\Phi_{MUB}=\hat{M}_n+0.7394\,\hat{N}_n^{\,2}-0.5212\,\hat{N}_n-1.2606=0 \tag{4.86}$$

for $-1\le\hat{N}_n<0.5512$

For deeply cracked specimens subjected to opening bending with large tensile load compressive zone region i.e. *x* becomes zero and hence MUB theorem would reduce to the classical upper bound theorem of limit analyses. The plastic field for this case can be approximated by a circular arc emanating from the crack tip and extending up to the free surface (Rice, 1972). Using this deformation mechanism, as suggested by Rice (1972), Kim et al. (1995) and Kim (2002) have already provided a complete analytical formulation for Rice's least upper bound yield locus that can be obtained directly by substituting *x=0* in eq. (4.78). It may be observed that now there is no way to impose traction free boundary condition and, therefore, the total angle subtended by circular arc is simply β+ γ. The resulting expression for limit moment can then be expressed as

$$M_L = kR^2(\beta+\gamma) - N_L\left(R\sin\beta - \frac{l}{2}\right) \tag{4.87}$$

for

$$R = \frac{l}{(\sin\beta + \sin\gamma)} \tag{4.88}$$

Minimizing eq. (4.87) with respect to the two unknown parameters, that is, β and γ we have

$$\frac{\partial M_L}{\partial \beta} = k\left[R^2 + (\beta+\gamma)2R\frac{\partial R}{\partial \beta}\right] - N_L\left[R\cos\beta + \sin\beta\frac{\partial R}{\partial \beta}\right] = 0 \tag{4.89}$$

$$\frac{\partial M_L}{\partial \gamma} = k\left[R^2 + (\beta+\gamma)2R\frac{\partial R}{\partial \gamma}\right] - N_L\left[\sin\beta\frac{\partial R}{\partial \gamma}\right] = 0 \tag{4.90}$$

On further simplification, these two equations can be expressed as

$$(\beta+\gamma)\cos\beta - \frac{1}{2}(\sin\beta + \sin\gamma) + \frac{N_L\cos\beta\sin\gamma}{2kR} = 0 \tag{4.91}$$

$$\left(\beta+\gamma\right)\cos\gamma-\frac{1}{2}\left(\sin\beta+\sin\gamma\right)-\frac{N_L\cos\gamma\sin\beta}{2kR}=0 \tag{4.92}$$

As expected, eqs. (4.91) and (4.92) are in exact agreement with the classical upper bound solution proposed by Kim et al. (1995). Thus, for the case of deeply cracked specimens subjected to opening bending with small tensile load MUB theorem has provided yield locus that is in exact agreement with detailed SLF solutions where as for opening bending with large tensile load MUB theorem reduces to the classical upper bound solution.

The procedure used to evaluate the fully plastic crack tip stresses for a pure bending specimen SE(PB) can be used for the case of opening bending with small tensile load (for which SLF exists). As the angle subtended by the circular arc at its centre is *117.04°* thus the hydrostatic stress near the crack tip, that is, $\sigma_m/2k$ is *2.014* and the tensile stress at the tip of crack ($\sigma_{\theta\theta}/\sigma_o$) is *2.903* (same as found for a deeply cracked pure bending specimen). For the case of opening bending with large tensile load SLF breakdown and thus the Hencky's equations cannot be used directly to evaluate stress distribution in plastically deformed region. For this case Kim (2002) has suggested an approximate procedure that can be used to estimate fully plastic crack tip stresses based on equilibrium condition of the least upper bound for plane strain deformation fields consisting of rigid-body rotation.

4.3 Discussion

In this chapter an analytical formulation of MUB theorem is presented and it is demonstrated that MUB theorem is actually a new form of already existing general work principle. The most important consideration in the proposed method (as well as in SLF analysis) is the choice of assumed plastic deformation field which is subjected to restrictions imposed by kinematic admissibility and boundary conditions. Once this plastic field is chosen then either the concept of global static equilibrium (the SLF method) or minimum work principle (the MUB theorem) can be invoked to evaluate the dimensions of this plastic field. Unfortunately, till now these extremum/work principles have normally been utilized as a crude method of load bounding mainly in metal forming operations. Thus, whenever it was required to analytically evaluate the stress distribution near the tip of crack or any crack tip constraint parameter, SLF analysis was the only choice.

In the present context it is worth to discuss the work performed by Kim (2002). He has presented a simple method to estimate fully plastic crack tip stresses based on equilibrium condition of the least upper bound for plane strain deformation fields consisting of rigid-body rotation across a circular arc extending from the crack tip across the remaining ligament. However, such an assumed plastic field has very limited application and no attempt was made to establish the general equivalence of work principle and SLF analysis. In the present work it was established, for a wide variety of cases, that consideration of minimum work principle automatically leads to global equilibrium and, thus, the two methods, that is, MUB theorem and SLF analysis would give identical results. A wide variety of plastic deformation fields were analysed to establish this equivalence in general. The proposed MUB theorem was used to obtain theoretical solutions of the limit load, plastic eta factor (η_p), plastic rotation factor (r_p), and crack tip constraint parameter Q for standard deeply cracked SE(PB), SE(B) and C(T) specimens, under plane strain condition. In addition, standard problem of bending of cantilever was also analysed. Results of these standard homogeneous specimens were found to be in exact agreement with those obtained by detailed SLF analyses. The case of single-edge-cracked specimen under combined bending and tensile load was also analysed. A complete analytical formulation of yield locus for the entire range of tensile and bending load was obtained using the proposed MUB theorem. These findings have demonstrated that the proposed MUB theorem is a promising technique to solve a class of plane strain plasticity problems in rigid-plastic materials.

In SLF analysis, in addition to equilibrium considerations, Hencky's theorem is invoked to set up additional equations which need to be solved simultaneously to evaluate the unknown parameters. As these equations are generally transcendental considerable mathematics is involved in SLF analysis. No such calculations are involved in the proposed method. Standard optimization algorithms can be readily used to minimize the plastic work done and thus the present method becomes very amenable to computational analysis. It is worth to note that MUB theorem automatically satisfies Hencky's theorem. This work has shown one successful application of the proposed theorem and it is expected that similar other cases, particularly in metal forming processes, where in one region rigid plastic flow of the material is occurring and in other region statically governed stress field exists, may also be treated.

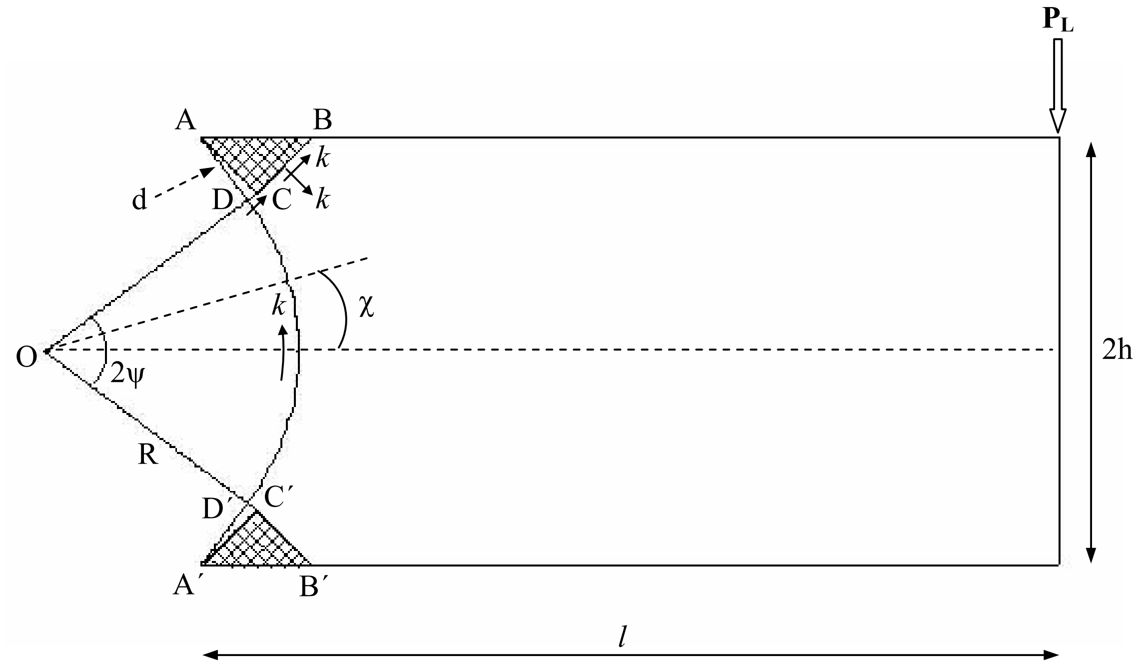

Fig. 4.1 (a): Assumed plastic deformation mechanism for a short cantilever under transverse load, Green (1954).

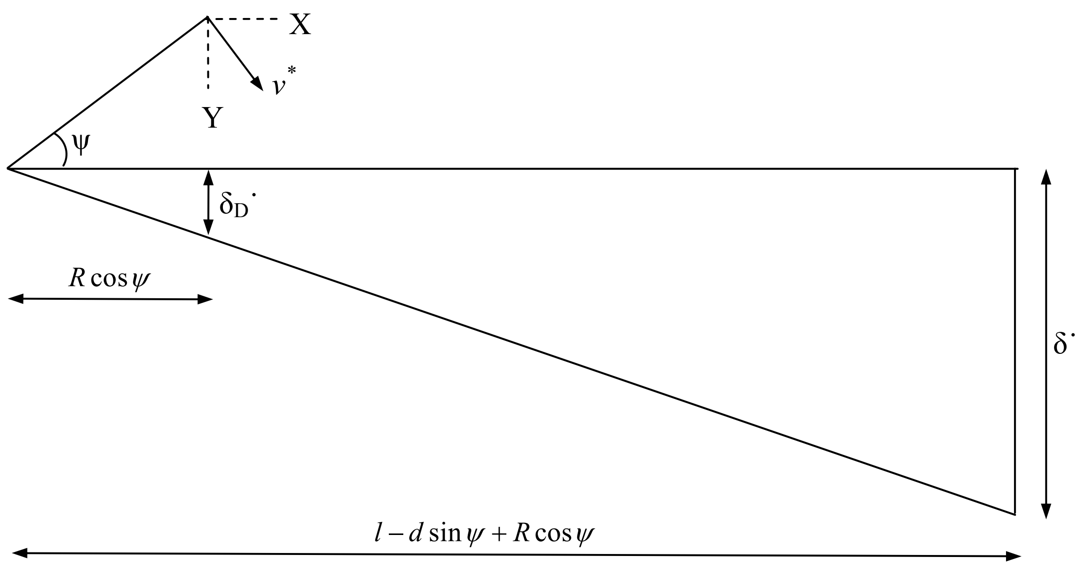

Fig. 4.1 (b): Schematic describing the relationship between tangential velocity v^* and imposed displacement $\delta^{\cdot}$.

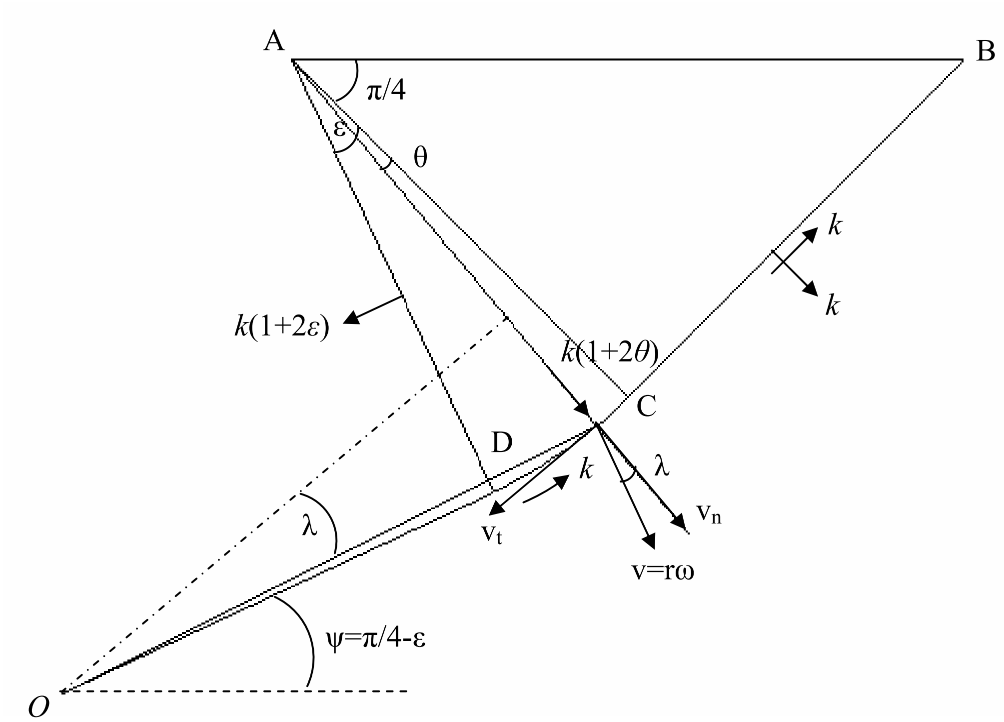

Fig. 4.1 (c): Stress and velocity distribution on the elastic-plastic boundary of a short cantilever.

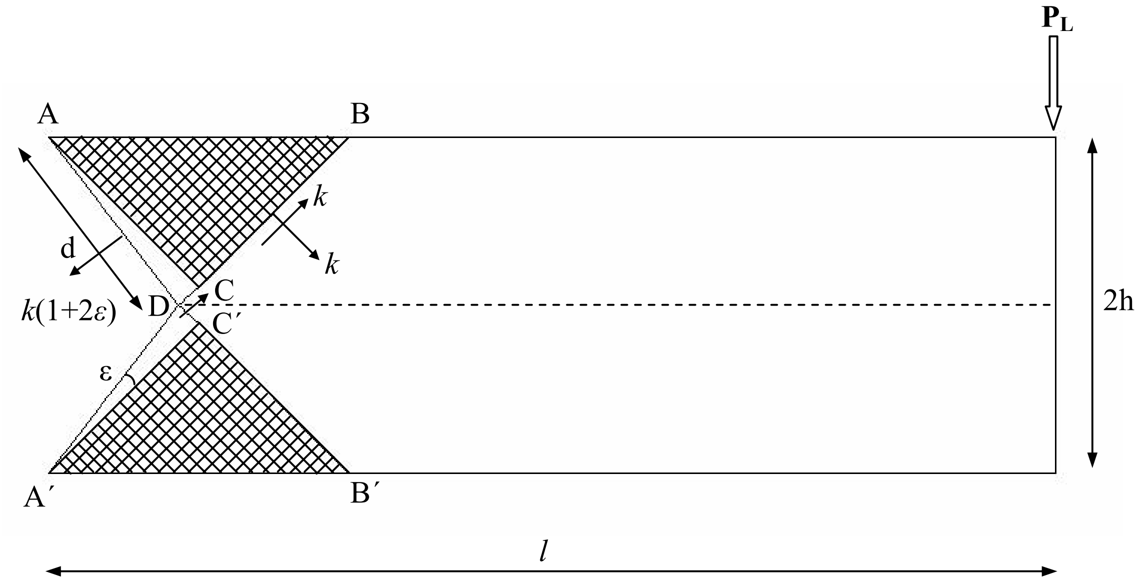

Fig. 4.2: Assumed plastic deformation mechanism for a long cantilever under transverse load, Green (1954).

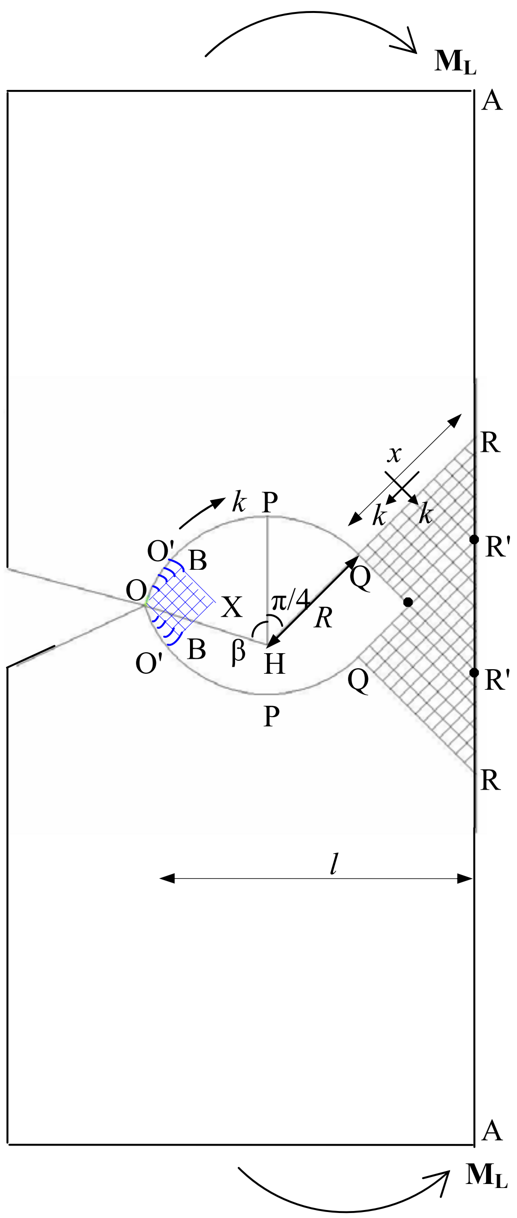

Fig. 4.3: Assumed plastic deformation mechanism for SE(PB) specimen, Green (1953).

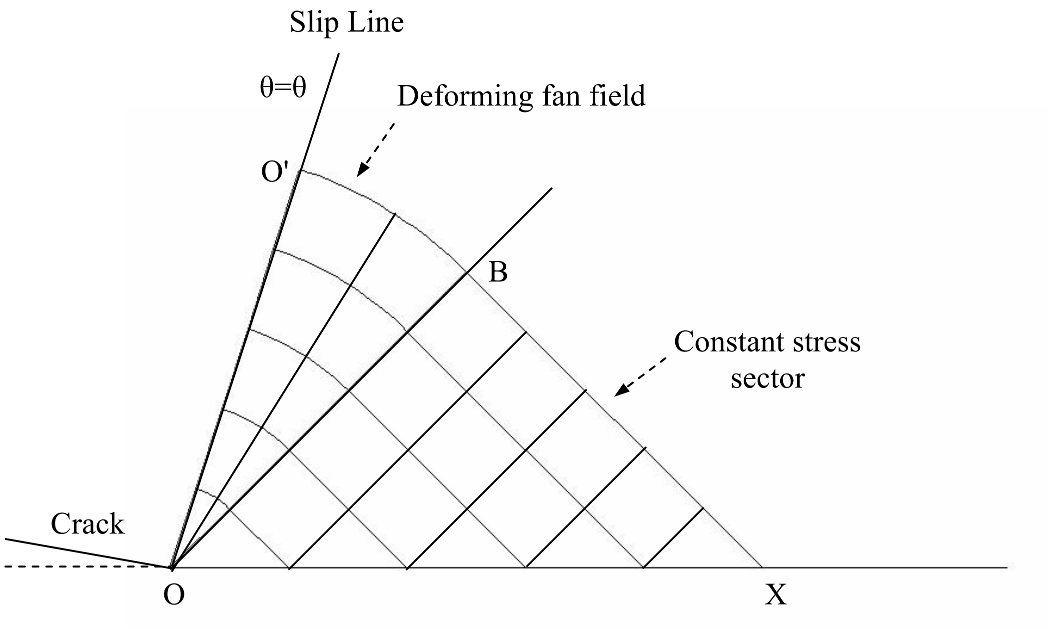

Fig. 4.4: Asymptotic fully plastic crack-tip stress fields for a deeply cracked pure bending SE(PB) and three-point bend SE(B) specimen.

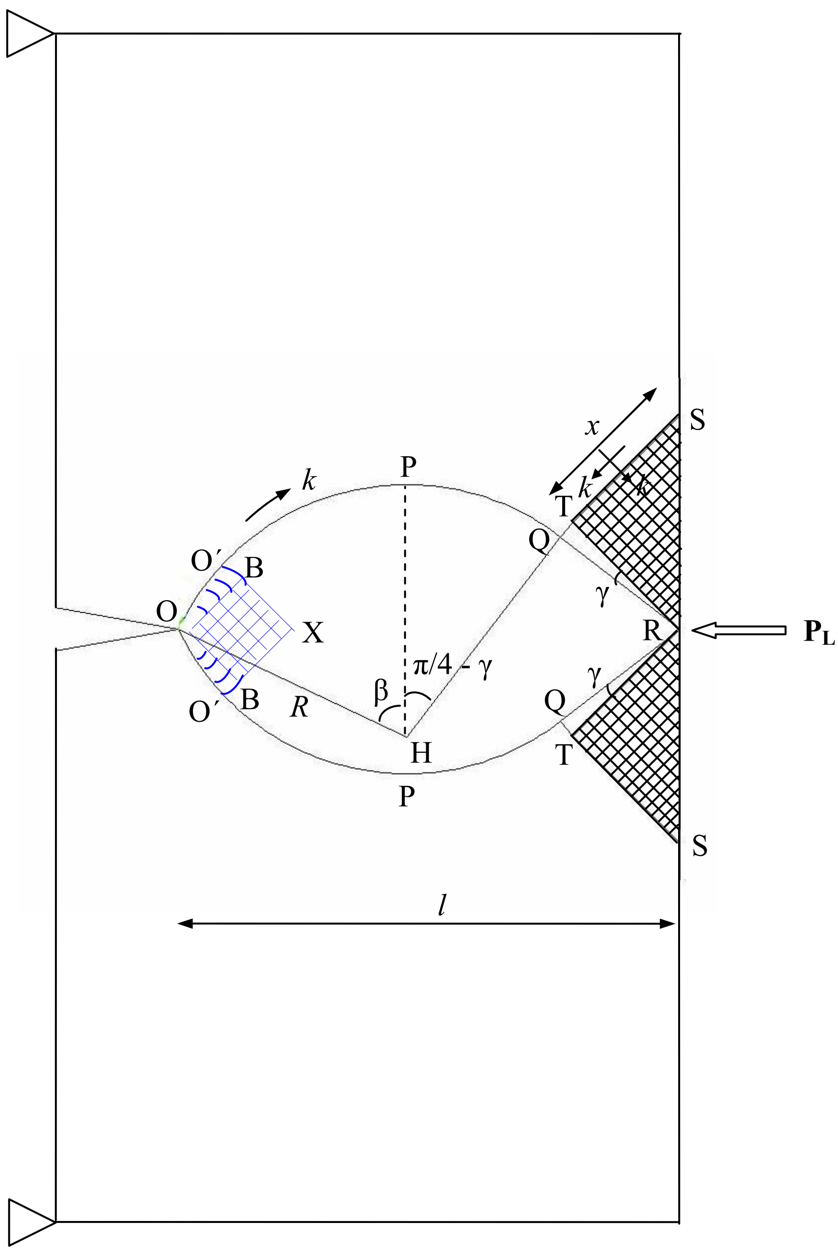

Fig. 4.5: Assumed plastic deformation mechanism for a three-point bend SE(B) specimen, Green and Hundy (1956).

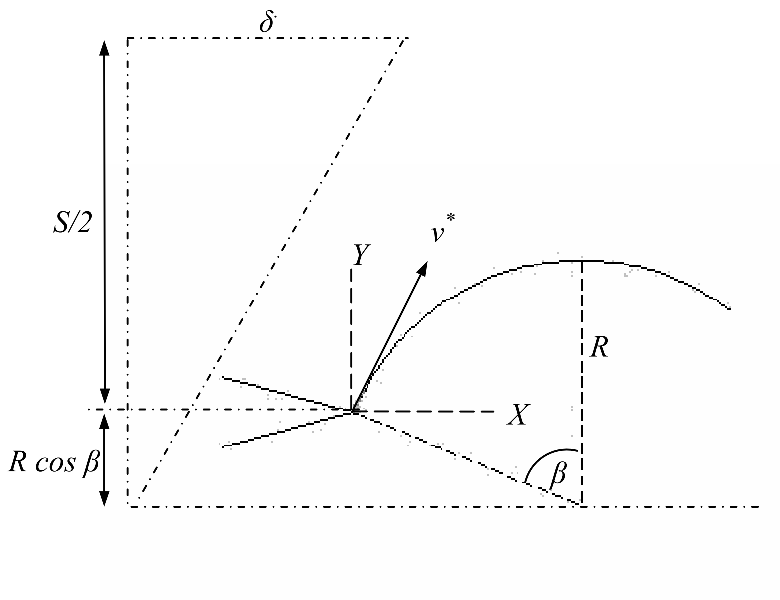

Fig. 4.6: Schematic describing the relationship between the tangential velocity and imposed displacement for a three-point SE(B) specimen.

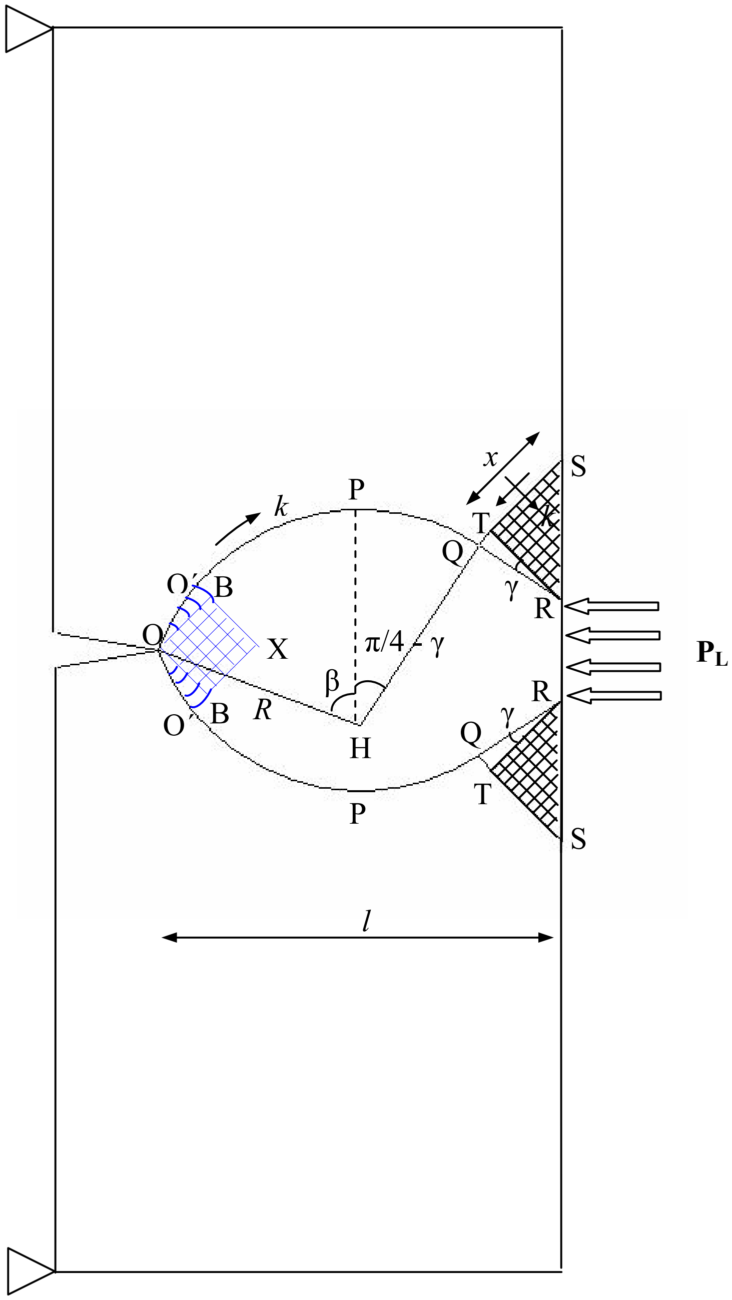

Fig. 4.7: Effect of indenter width on plastic deformation mechanism for SE(B) specimen, Ewing (1968).

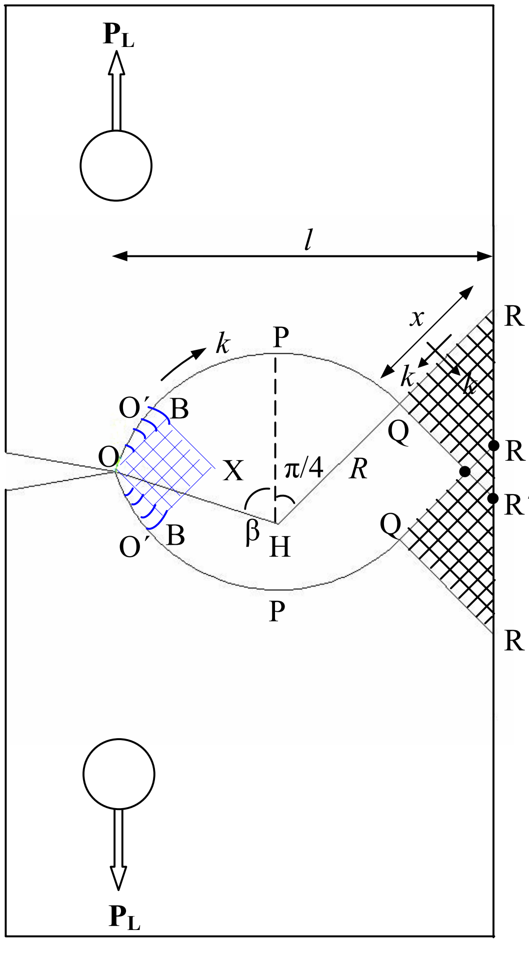

Fig. 4.8: Assumed plastic deformation mechanism for a compact tension C(T) specimen, Ewing and Richards (1974).

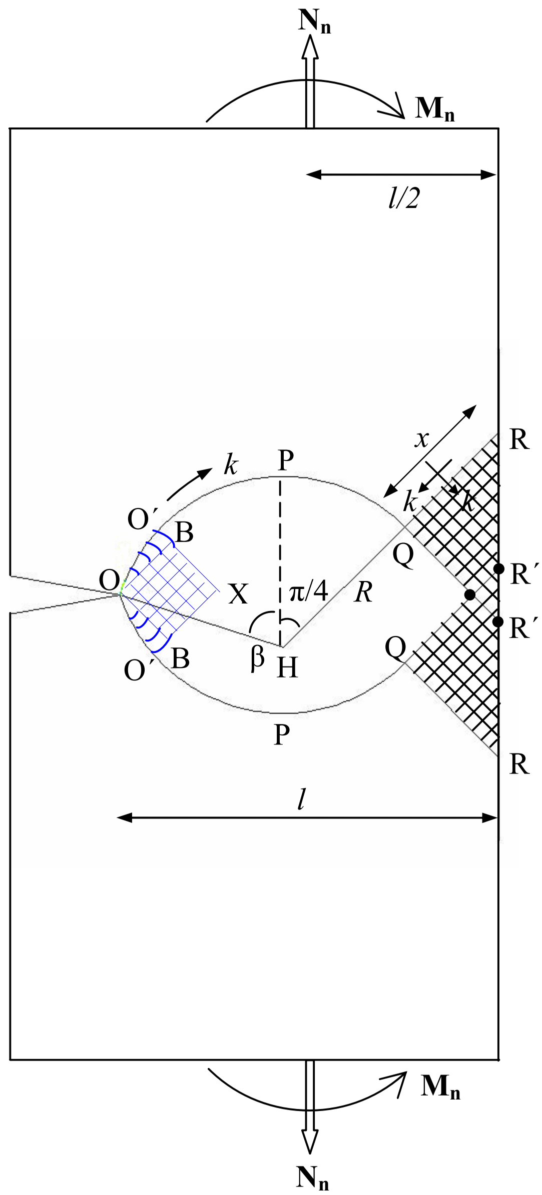

Fig. 4.9: Assumed plastic field for a single-edge-cracked specimen under bending with small tensile load, Shiratori and Dodds (1980).

CHAPTER 5

Strength mismatch effects on the limit load and crack tip constraint of pure bending SE(PB) specimen and compact tension C(T) specimen having a weld centre crack

5.1 Introduction

In-service inspections of many nuclear power plants have revealed that cracks are most likely to occur in or the regions near the weld. Interfacial cracks (Fig. 5.1a) under elastic as well as in elastic-plastic conditions have already been extensively discussed in literature. However, the problem of crack lying at the centre of weld (Fig. 5.1b) is (theoretically) less understood. Though several detailed numerical and experimental studies have been performed in past to investigate the influence of weld strength mismatch on the limit load, plastic η-factor, and crack-tip stress fields, however, the detailed insight of the structure of stress fields under large scale plasticity is still lacking.

In this chapter, the detailed structure of the global plastic fields that occur in high constraint geometries like deeply cracked pure bending SE(PB) specimen, and compact tension, C(T) specimen having weld centre crack is presented. Both the base and weld materials were modeled as elastic-perfectly plastic. The two materials were assumed to have same elastic modulus and Poisson's ratio but mismatch in their yield strength. All the investigations in this work were based on plane strain assumption. Crack was postulated at the centre of weld. Aspects related to the state of stress at the interface of two materials are discussed in detail. It is shown that a family of five stress fields proposed in this work is adequate to cover all practical cases of weld mismatch. Extreme under-match cases where plastic fields get fully confined in the weld material were not considered as sufficiently detailed results for these cases already exist in literature (Hao et al., 1997, 2000). The proposed fields were utilized to obtain analytical solutions of the limit moment/load, and crack-tip constraint using the Modified Upper Bound (MUB) theorem, developed in chapter 3. One of the most striking features of this new load bounding technique is that it requires no information about the state of stress in the rigid regions, the stress field only in the deforming zones should be statically admissible. This important feature of the proposed theorem has enabled us to theoretically examine the problem of a crack lying at the centre of a strength mismatch weld. Proposed fields were confirmed by detailed full-field finite element analysis. Numerical studies were performed within the framework of continuum scale plasticity (J_2 flow theory) and effects of micro-structural heterogeneity and presence of residual stresses were not accounted. Excellent agreement was observed between the proposed theoretical solutions and the numerical results.

5.2 Structure of stress fields for a deeply cracked pure bending SE(PB) specimen having a weld centre crack under fully plastic state in mode-I loading

We consider here a stationary crack lying at the centre of weld in a pure bending SE(PB) specimen, as shown in Fig. 5.2. Generally, an actual weld joint is very complicated both metallurgically and mechanically. In order to simplify the analysis the effects of heat affected zone, residual stresses and other kinds of heterogeneity (except material) were not considered and weld joint was modeled as a sandwich like bi-material structure. The mismatch in yield strength between the weld (σ_{yw}) and base material (σ_{yb}) is quantified by the mismatch factor *M*:

$$M = \frac{\sigma_{yw}}{\sigma_{yb}} = \frac{k_w}{k_b} \tag{5.1}$$

where $k_w = \sigma_{yw}/\sqrt{3}$ and $k_b = \sigma_{yb}/\sqrt{3}$ are the shear yield strengths of base and weld material, respectively. For an under match weld, $M < 1$ and for an over match weld, $M > 1$. Another important parameter for the strength mismatched welds is the weld slenderness ratio which is defined as

$$\psi = \frac{(W - a)}{H} \tag{5.2}$$

where *a* denotes the crack length, *W* is the width of the specimen and *H* is half weld width. Only deeply cracked configuration ($a/W > 0.3$) is considered so that the plastic fields are confined in the ligament and do not spread up to the crack flank. We present here the detailed structure of the family of five stress fields that occur in case of pure bending SE(PB) specimen, under fully plastic state, in mode-I loading. These five stress fields cover all practical cases of weld mismatch except for the extreme under-match cases where the plastic fields get fully confined in the weaker weld material. For such a case sufficiently detailed results already exist in literature. Only plane strain case was considered for all theoretical and numerical calculations. The basic assumption invoked to construct these stress fields is that in cases where the slip line passing through the interface of two materials lies in deforming zones, continuity of traction is respected. For other cases where the slip line passing through the interface separates the two rigid (elastic) regions both shear and normal traction undergoes a jump at this interface. It would be demonstrated in the subsequent sections that such an assumption was in excellent agreement with the results obtained from detailed finite element analysis. In passing it may be mentioned that the proposed solutions are incomplete in so far as no attempt is made to extend the stress fields into the rigid zones. It has not been shown that an equilibrium stress distribution satisfying the boundary conditions and not exceeding the yield point exists in the assumed rigid regions. Thus, the solution does not meet the requirements of the lower bound theorem. However, the velocity fields, as per the requirement of upper bound theorem, are kinematically admissible and, therefore, the proposed solutions strictly speaking are in fact upper bound.

5.2.1 Stress field-A

Detailed structure of this stress field is shown in Fig. 5.3(a). It is symmetric with respect to weld centre line. It is worth to note that the structure of this field is similar to that suggested by Ewing (1968) to analyse the Charpy specimen loaded by a finite width indenter. Hao et al. (2000) discussed that this field is responsible for plastic yielding of an over-matched SE(PB) specimen, however, the authors did not present any details of its analysis. In the proposed solution, it is assumed that at limit state, there is a region OPQ that remains rigid, around which the rigid parts of the specimen on either side rotate by shearing over the circular arc, OPQ at an angular velocity ω. Near the free surface, we have uni-axial compression in the region RST. Adjacent to it is the central field QRT which merges with the circular slip line OPQ of radius R.

It is easy to establish that the slip line OPQR belongs to α–family (Katchanov, 1971). Using the free surface condition and the yield criterion in the constant stress region the stress distribution in Δ RST can be expressed as $\sigma_{11} = 0,\ \sigma_{22} = -2k_b$ and $\sigma_{12} = 0$. Here minus sign indicates the compressive nature of stress. In the central field QRT, the shear stress along QR is k_b and the mean stress (pressure) acting on it is $-k_b(1+2\gamma)$. Stress distribution along the circular arc OPQ can be easily obtained, up to point P, using the well-known Hencky's relation. Thus, the mean stress just above point P, that is, in the base material can be simply expressed in terms of angles φ and γ (see Fig. 5.3) as given below

$$\sigma_b^P = 2k_b\left(\phi + \frac{\pi}{4} - \gamma\right) - k_b\left(1 + 2\gamma\right) \tag{5.3}$$

At point P, that is, at the interface of two materials we propose that the continuity of tractions is violated. Thus, both the in-plane shear stress σ_{12} as well as the mean stress undergoes a sudden jump at the interface. As a result, the stress distribution in the weld region cannot be readily obtained. This problem can be overcome by the use of modified upper bound (MUB) theorem. Unlike slip line field (SLF) analysis this technique does not require any information about the mean stress along the arc (slip line) separating the two rigid regions. This is simply because only plastic dissipation of energy in the rigid domain is needed for the application of this work principle (see Chapter 3 for details). Since the tangential velocity and the shear stress (by virtue of yield criterion) are known along the circular arc OPQ, plastic dissipation of energy can be easily computed. As the mean stress acting on the circular arc OPQ and, hence, the unknown mean stress at the interface, does not enter in MUB analysis problem becomes amenable to a fully analytical treatment. We now proceed to analyse this field. Using the stress and velocity distributions on the elastic-plastic boundary QTS, the work done by the stresses can be easily evaluated (the method is similar to that discussed in section 4.1). The resulting expression for limit moment, using eq. (3.33), can be finally expressed as

$$M_L = k_B \left[R^2 \left(\phi + \pi/4 - \gamma \right) + MR^2 \left(\beta - \phi \right) + \left(1 + 2\gamma \right) \frac{x^2}{2} + xR \right] \tag{5.4}$$

for

$$R = \frac{l - x\cos\left(\frac{\pi}{4} - \gamma\right)}{\sin\beta + \sin\left(\frac{\pi}{4} - \gamma\right)} = \frac{x\sin\left(\frac{\pi}{4} - \gamma\right)}{\cos\left(\frac{\pi}{4} - \gamma\right) - \cos\beta} \tag{5.5}$$

and

$$\phi = \cos^{-1}\left(\cos\beta + \frac{lK}{R} \right) \tag{5.6}$$

Eq. (5.4) represents the global moment equilibrium, about the hinge point, that needs to be minimized with respect to the unknown parameters, that is, x, γ and β. These three parameters are not independent but are subjected to a geometrical constraint as specified by eq. (5.5). Due to considerable algebra involved, minimization of the limit moment, that is, eq. (5.4) was carried out numerically. This minimization process gives us the required unknown parameters of the plastic field. It may be noted that as far as evaluation of the limit moment is concerned, the unknown value of the mean stress at the base-weld interface does not enter in the analysis. However, for evaluation of crack tip stress field the jump in the value of mean stress that occurs at the base-weld interface must be quantified. For several cases of cracked as well as uncracked geometries of homogeneous material, it was demonstrated in chapter 4 that the MUB theorem and SLF analysis are equivalent. It was established that the minimization process finally leads to equations of global equilibrium. Since the problem of a mismatch weld with mismatch ratio close to one cannot differ substantially from a corresponding homogeneous problem, it is expected that the MUB theorem when applied to fracture specimens having strength mismatch welds should also satisfy global equilibrium equations. We now need to establish this assumption rigorously. If the unknown mean stress at the base-weld interface (at point P) is denoted by σ_w^*, Hencky's equations may be used to describe stress distribution along the circular arc OP in the weld region. Mean stress at point O, on the circular arc, near the crack tip can be obtained from the following expression

$$\sigma^O = \sigma_w^* + 2k_w\left(\beta - \phi\right) \tag{5.7}$$

Once the state of stress is described the global equilibrium equations can be simply expressed as follows.

$$\sum F_x = \int_{OPQR} \sigma_{1i} n_i dS = 0 \tag{5.8}$$

$$\sum F_y = \int_{OPQR} \sigma_{2i} n_i dS = 0 \tag{5.9}$$

Here n_i are the direction cosines of the vector which is normal to the infinitesimal line segment on OPQR. If the plastic stress field is extended into the rigid region to form two fictitious fans, that is, QHP and PHO (see Fig. 5.3) the global equilibrium equations can be essentially written by inspection. According to Ewing (1968) this simple artifice was first suggested to him by Hill. Resulting equilibrium equations can, thus, be expressed as follows

$$\begin{aligned}\sum F_x &= k_b x \sin\left(\frac{\pi}{4}+\gamma\right) - k_b\left(1+2\gamma\right)x\cos\left(\frac{\pi}{4}+\gamma\right) - k_b R\sin\left(\frac{\pi}{4}-\gamma\right) + k_b\left(1+2\gamma\right) \\ &R\cos\left(\frac{\pi}{4}-\gamma\right) - k_b R\sin\phi + \sigma_b^P R\cos\phi + k_w R\sin\phi - \sigma_w^* R\cos\phi - k_w R\sin\beta + \sigma^O R\cos\beta\end{aligned} \tag{5.10}$$

$$\begin{aligned}\sum F_y &= -k_b x \cos\left(\frac{\pi}{4}+\gamma\right) - k_b\left(1+2\gamma\right)x\sin\left(\frac{\pi}{4}+\gamma\right) - k_b R\cos\left(\frac{\pi}{4}-\gamma\right) - k_b\left(1+2\gamma\right) \\ &R\sin\left(\frac{\pi}{4}-\gamma\right) + k_b R\cos\phi + \sigma_b^P R\sin\phi - k_w R\cos\phi - \sigma_w^* R\sin\phi + k_w R\cos\beta + \sigma^O R\sin\beta\end{aligned} \tag{5.11}$$

Now if the assumption that MUB analysis also satisfies the global equilibrium equations holds good than by substituting the parameters of the plastic field obtained from it, both eqs (5.10) and (5.11) should become zero. Except for the unknown mean stress at the base-weld interface, denoted by σ_w^*, rest all the other parameters of this plastic field are known from MUB analysis. In fact σ_w^* can not be evaluated directly from work principle (MUB analysis) as it plays no role in the plastic dissipation of energy. So an easy way to prove the validity of this assumption is to calculate σ_w^* from one of these two equations, say eq. (5.10) and then ensure that with the value of σ_w^* so obtained the other equation, that is eq. (5.11), is satisfied identically. For all the cases analysed it was observed that wherever the proposed plastic field was responsible for full yielding of the ligament, the values of the field parameters obtained from MUB analysis and σ_w^* obtained from eq. (5.10) always satisfies the other equilibrium condition, that is, eq. (5.11). This essentially validates our assumption that for the case of a strength mismatch weld also (having two different material interfaces) the parameters of plastic field as obtained from MUB theorem also satisfies the global equilibrium equations. This is really an important finding, particularly for the problem of strength mismatch welds, as it allows a complete analytical evaluation of stress distribution in the plastic regions.

Once σ_w^* is known the mean stress at point O on the slip line OPQ, near the crack tip, can be obtained from eq. (5.7). From the stress distribution so obtained the state of stress ahead of crack tip can not be directly evaluated as discussed by Hao et al. (2000). To evaluate crack tip stress distribution, the plastic field is extended in the rigid region ahead of crack tip as shown in Fig. 5.4. In this figure we assume, asymptotically, that a small segment of straight slip line OO′ exists. It radiates from the crack tip and is connected to the arc OP in the global slip line field. Thus, the stress components on this small line OO' are constant and equal to the components at the point O′ on the arc O′P. The plastic deformation expands from the line OO′ ahead of the crack tip and forms a diamond-like plastic zone OBX like that in Prandtl field. Using Hencky's relations, the pressure (hydrostatic stress), directly ahead of crack tip, can be expressed in terms of slip angle β as follows.

$$\sigma^{X} = \sigma^{B} = \sigma^{O} + 2k_{w}\left(\beta - \frac{\pi}{4}\right) \tag{5.12}$$

This incomplete crack tip stress field can be used to obtain stress distribution in the plastic sectors, that is, in the constant stress sector OBX and in fan field O′OB. Such a construction cannot be extended beyond O′O as the elastic-plastic boundary is unknown. Thus, the proposed MUB theorem, assuming that the material is rigid-plastic, can provide estimates of the crack tip stresses (in the plastic sectors) and hence the constraint parameters. In the literature the effect of weld strength mismatch on crack tip constraint has been quantified, by many investigators, in terms of constraint parameter *h.* The parameter *h,* for a rigid-plastic material, is defined as follows (Kim and Schwalbe, 2004)

$$h = \left.\frac{\sigma_{m}}{\sigma_{yw}}\right|_{\theta=0} = \frac{\sigma^{X}}{\sigma_{yw}} \tag{5.13}$$

5.2.2 Stress field-B

Detailed structure of this stress field is shown in Fig. 5.5. For clarity enlarged view of the stress fields occurring in the region near the free surface is shown in Fig. 5.5 (b). It is assumed that at the limit state, there is a region GFE that remains rigid, around which the rigid parts of the specimen on either side rotate by shearing over the circular arc, GE at an angular velocity ω. Near the free surface, we have uni-axial compression in the region ABL. This constant stress sector is followed by a circular arc BC and another constant stress sector CDM till point D that lies on the interface of two materials. In the region lying in the base material, just adjacent to the interface, there is a constant stress sector DEN that merges with the circular arc GFE tangentially. It can be shown easily that the slip line GFEDCBA belongs to α–family. Using the free surface condition and the yield criterion in the constant stress region the stress distribution in Δ ABL can be expressed as $\sigma_{11} = 0$, $\sigma_{22} = -2k_w$ and $\sigma_{12} = 0$. Thus, the mean stress at point B, σ^B, is simply $-k_w$.

Since point D at the interface lies in deforming zone it is assumed, as discussed in section 5.2, that both the shear and normal traction are continuous. Due to continuity of shear traction a sudden jump occurs in the angle θ made by α-slip-line at the interface as the shear yield strength of the materials lying on either side of interface (base and weld material) are different. Careful examination of the stress fields obtained from detailed FE studies and physical considerations related to mechanics of deformation have revealed that the in-plane shear stress acting in the two constant stress sectors, that is, in CDM and DEN, lying on either side of interface can be simply expressed as follows

$$\sigma_{12} = (M-1)k_b \tag{5.14}$$

We would like to emphasise here that eq. (5.14) is quite general and holds good for both over-matched and under-matched welds. It was observed that eq. (5.14) is able to describe adequately the shear stress distribution near the base-weld interface for other plastic fields also proposed in this work. Shear stress σ_{12} and the angle, θ, made by α-slip line with respect to some fixed axis are related by the following expression (Kachanov, 1971)

$$\sigma_{12} = k\cos 2\theta \tag{5.15}$$

Thus, the angle made by α-slip line on either side of interface can be obtained from the following expressions

$$\theta_w = \frac{1}{2}\cos^{-1}\frac{(M-1)}{M} \tag{5.16}$$

$$\theta_b = \frac{1}{2}\cos^{-1}(M-1) \tag{5.17}$$

Using Hencky's relation, the mean stress at point C can be expressed as

$$\sigma^C = \sigma^B + 2k_w\gamma_w \tag{5.18}$$

$$\sigma^C = -k_w\left[1-\left\{\frac{\pi}{2}-\cos^{-1}\left(\frac{M-1}{M}\right)\right\}\right] \tag{5.19}$$

Continuity of normal traction at the interface, at point D, can be expressed in the following form (Kachanov, 1971)

$$\sigma_b^D + k_b\sin 2\theta_b = \sigma_w^D + k_w\sin 2\theta_w \tag{5.20}$$

$$\sigma_b^D - k_b\sqrt{M(2-M)} = \sigma^C - k_w\frac{\sqrt{2M-1}}{M} \tag{5.21}$$

Thus, the mean stress acting in the constant stress sector DEN lying in the base material, just adjacent to the interface, can be expressed as follows

$$\sigma_b^D = -k_b\left[M - M\left\{\frac{\pi}{2} - \cos^{-1}\left(\frac{M-1}{M}\right)\right\} + \sqrt{2M-1} - \sqrt{M\left(2-M\right)}\right] \tag{5.22}$$

Stress and velocity distributions on the elastic-plastic boundary GFEDCBA, were utilized to evaluate the work done. The resulting expression for limit moment, using eq. (3.33), can be finally expressed as

$$\begin{aligned}
&M_L = k_w R^2\left(\beta - \phi\right) + k_B R^2\left(\phi + \pi/4 - \gamma_b\right) + k_B zR + 0.5\sigma_b^D z^2 + k_w y R_1 + \\
&\sigma^C y\left(z_1 + 0.5y\right) - k_w R_1\left(z_1 + y\right) - 0.5\sigma^C R_1^2 + k_w R_1\left(z_1 + y\right)\cos\gamma_w + \\
&k_w R_1\left\{0.5R_1 + \left(z_1 + y\right)\sin\gamma_w\right\} + k_w y\left\{R_1 + \left(z_1 + y\right)\sin\gamma_w\right\} + k_w y\left\{\left(z_1 + y\right)\cos\gamma_w + 0.5y\right\}
\end{aligned} \tag{5.23}$$

From geometry the following relations can be easily established

$$\gamma_w = \frac{\pi}{4} - \theta_w = \frac{\pi}{4} - \frac{1}{2}\cos^{-1}\left(\frac{M-1}{M}\right) \tag{5.24}$$

$$\gamma_b = \frac{\pi}{4} - \theta_b = \frac{\pi}{4} - \frac{1}{2}\cos^{-1}\left(M-1\right) \tag{5.25}$$

$$\delta = \gamma_b - \gamma_w \tag{5.26}$$

$$\phi = \cos^{-1}\left(\cos\beta + \frac{lK}{R}\right) \tag{5.27}$$

$$R_1 = \frac{R}{\cos\delta} + \left(z - R\tan\delta\right)\sin\delta \tag{5.28}$$

$$z_1 = \left(z - R\tan\delta\right)\cos\delta \tag{5.29}$$

$$y = \frac{\left(lK - x\right) - \left(z\sin\delta + R\cos\delta\right)\left\{\sin\left(\frac{\pi}{4} + \gamma_w\right) - \frac{1}{\sqrt{2}}\right\}}{\left\{\sin\left(\frac{\pi}{4} - \gamma_w\right) + \frac{1}{\sqrt{2}}\right\}} \tag{5.30}$$

$$R = \frac{l - \left(lK - x\right)\dfrac{\left\{\frac{1}{\sqrt{2}} + \cos\left(\frac{\pi}{4} - \gamma_w\right)\right\}}{\left\{\frac{1}{\sqrt{2}} + \sin\left(\frac{\pi}{4} - \gamma_w\right)\right\}} - z\left\{\cos\left(\frac{\pi}{4} - \gamma_b\right) + c_1\sin\delta\right\}}{\left\{\sin\beta + \sin\left(\frac{\pi}{4} - \gamma_b\right) + c_1\cos\delta\right\}} \tag{5.31}$$

where

$$c_1 = \left[\left\{\frac{1}{\sqrt{2}} - \cos\left(\frac{\pi}{4} + \gamma_w\right)\right\} - \frac{\left\{\sin\left(\frac{\pi}{4} + \gamma_w\right) - \frac{1}{\sqrt{2}}\right\}\left\{\frac{1}{\sqrt{2}} + \cos\left(\frac{\pi}{4} - \gamma_w\right)\right\}}{\left\{\frac{1}{\sqrt{2}} + \sin\left(\frac{\pi}{4} - \gamma_w\right)\right\}}\right] \tag{5.32}$$

Also

$$lK + z\sin\left(\frac{\pi}{4} - \gamma_b\right) = R\left\{\cos\left(\frac{\pi}{4} - \gamma_b\right) - \cos\beta\right\} \tag{5.33}$$

Eq. (5.23) was minimized with respect to the unknown parameters, that is, x, z and β accounting for the geometrical constraint that is represented by eq. (5.33). Once the parameters of the assumed plastic field are obtained we can proceed to establish that the resulting stress field also satisfies global equilibrium equations. Stress distribution along the circular arc GFE can be easily obtained, up to point F, using the well-known Hencky's relation. Thus, the mean stress just above point F, that is, in the base material can be simply expressed in terms of angles φ and γ_b (see Fig. 5.5(a)) as given below

$$\sigma_b^F = 2k_b\left(\phi + \frac{\pi}{4} - \gamma_b\right) + \sigma_b^D \tag{5.34}$$

At point F, that is, at the interface of two materials we propose that the continuity of tractions is violated. If the unknown mean stress at the base-weld interface (at point F) is denoted by σ_w^*, Hencky's equations may be used to describe stress distribution along the arc GF in the weld region. Mean stress at point G, on the circular arc, near the crack tip can be obtained from the following expression

$$\sigma^G = \sigma_w^* + 2k_w\left(\beta - \phi\right) \tag{5.35}$$

The global equilibrium equations can be easily obtained by extending the plastic stress field into the rigid region to form two fictitious fans, that is, EHF and FHG. The resulting equations can be expressed as follows

$$\sum F_x = k_w R_1 \cos\left(\frac{\pi}{4}+\gamma_w\right) - \sigma^C R_1 \cos\left(\frac{\pi}{4}-\gamma_w\right) + k_w y \cos\left(\frac{\pi}{4}-\gamma_w\right) - \sigma^C y \sin\left(\frac{\pi}{4}-\gamma_w\right)$$
$$+\left(k_b z + \sigma_b^D R\right)\cos\left(\frac{\pi}{4}-\gamma_b\right) - \left(\sigma_b^D z + k_b R\right)\sin\left(\frac{\pi}{4}-\gamma_b\right) - k_b R\sin\phi + \sigma_B R\cos\phi + k_w R\sin\phi \quad (5.36)$$
$$-\sigma_w^* R\cos\phi - k_w R\sin\beta + \sigma^G R\cos\beta$$

$$\sum F_y = \left(\sigma^C R_1 - k_w y\right)\sin\left(\frac{\pi}{4}-\gamma_w\right) + \left(k_w R_1 - \sigma^C y\right)\cos\left(\frac{\pi}{4}-\gamma_w\right) - \left(k_b R + \sigma_b^D z\right)\cos\left(\frac{\pi}{4}-\gamma_b\right)$$
$$-k_w y\sqrt{2} - \left(\sigma_b^D R + k_b z\right)\sin\left(\frac{\pi}{4}-\gamma_b\right) - k_w R_1\sqrt{2} + k_b R\cos\phi + \sigma_b^F R\sin\phi - k_w R\cos\phi - \sigma_w^* R\sin\phi \quad (5.37)$$
$$+k_w R\cos\beta + \sigma^G R\sin\beta$$

The procedure used to evaluate σ_w^* and constraint parameter *h*, ahead of crack tip, is similar to that described in section 5.2.2.

5.2.3 Stress field-C

Structure of this stress field, for an over-match weld, is shown in Fig. 5.6(a). It may be observed that the proposed field is quite similar to the stress field described in Fig. 5.5(a). Stress distribution in the deforming zone is, thus, identical to that of Stress field-B. As a result, eqs. (5.14-5.22) derived in section 5.2.2 are equally applicable for stress field-C also. The unknown parameters of this plastic field can be obtained from MUB analysis. The resulting expression for the limit moment is as follows

$$\begin{aligned}
&M_L = k_w R^2(\beta-\phi) + k_B R^2(\phi+\pi/4-\gamma_b) + k_B zR + 0.5\sigma_b^D z^2 + k_w cR_1 + \sigma^C c(z_1+0.5c) \\
&-k_w R_1(z_1+c) - 0.5\sigma^C R_1^2 + k_w R_1(z_1+c)\cos\gamma_w + k_w R_1\{0.5R_1 + (z_1+c)\sin\gamma_w\} + \\
&k_w c\{R_1 + (z_1+c)\sin\gamma_w\} + k_w c\{(z_1+c)\cos\gamma_w + 0.5c\} + k_w y\{(z_1+c)\cos\gamma_w + c\} + \\
&k_w y\{R_1 + (z_1+c)\sin\gamma_w + 0.5y\}
\end{aligned} \tag{5.38}$$

It may be noted that eqs. (5.24-5.33), except eqs. (5.31) and (5.32), describing the geometrical relations among different field parameters are equally valid here. Moreover, for this case

$$c = \frac{lK - (z\sin\delta + R\cos\delta)\left\{\sin\left(\frac{\pi}{4}+\gamma_w\right) - \frac{1}{\sqrt{2}}\right\}}{\left\{\sin\left(\frac{\pi}{4}-\gamma_w\right) + \frac{1}{\sqrt{2}}\right\}} \tag{5.39}$$

and

$$R = \frac{\left(l - \frac{y}{\sqrt{2}}\right) - lK\dfrac{\left\{\frac{1}{\sqrt{2}} + \cos\left(\frac{\pi}{4}-\gamma_w\right)\right\}}{\left\{\frac{1}{\sqrt{2}} + \sin\left(\frac{\pi}{4}-\gamma_w\right)\right\}} - z\left\{\cos\left(\frac{\pi}{4}-\gamma_b\right) + c\sin\delta\right\}}{\left\{\sin\beta + \sin\left(\frac{\pi}{4}-\gamma_b\right) + c\cos\delta\right\}} \tag{5.40}$$

Eq. (5.38) was minimized numerically to evaluate the limit moment and the unknown parameters of the assumed plastic field. Stress distribution along the circular arc GFE can be obtained from eqs (5.34) and (5.35) derived in section 5.2.2. Since the stress distribution of sector PAP (near the free surface) produces no force in X-direction, force equilibrium in this direction can be described by eq. (5.36). Force equilibrium equation in Y-direction is given by the following equation

$$\begin{aligned}\sum F_y &= \left(\sigma^C R_1 - k_w c\right)\sin\left(\frac{\pi}{4}-\gamma_w\right)+\left(k_w R_1 - \sigma^C c\right)\cos\left(\frac{\pi}{4}-\gamma_w\right)-\left(k_b R+\sigma_b^D z\right)\cos\left(\frac{\pi}{4}-\gamma_b\right)\\ &-k_w c\sqrt{2}-\left(\sigma_b^D R+k_b z\right)\sin\left(\frac{\pi}{4}-\gamma_b\right)-k_w R_1\sqrt{2}+k_b R\cos\phi+\sigma_B R\sin\phi-k_w R\cos\phi-\sigma_w^* R\sin\phi\\ &+k_w R\cos\beta+\sigma^G R\sin\beta-k_w y\sqrt{2}\end{aligned} \tag{5.41}$$

For an under-match weld it can be seen from eqs. (5.16) and (5.17) that the angles made by α-slip line in weld θ_w and base material θ_b are greater than π/4. This essentially means that the centre of curvature of the circular arc BC (in weld region) would lie to the right of elastic-plastic boundary DCBA to maintain continuity of slope of tangents drawn at point B and C. Thus, the angle subtended by circular arc EF (in base region) is $\phi+\dfrac{\pi}{4}+\gamma_b$.

Except for these changes rest of the analysis is same as discussed for the case of an over-match weld.

5.2.4 Stress field-D

The complete structure of this stress field, for an over match weld, is shown in Fig. 5.7(a). Stress field in the deforming zone up to point D is identical to that described in Fig. 5.5(a). At point D the straight slip line CD merges with the circular arc GFED tangentially. The resulting expression for the limit moment can be expressed as follows

$$\begin{aligned} M_L &= k_w R^2 (\beta - \phi) + 2k_b R^2 \phi + k_w R^2 (\pi/4 - \gamma_w - \phi) + k_w y R + 0.5\sigma^C y^2 + k_w R y \cos\gamma_w \\ &-k_w R y + k_w R\{0.5R + y\sin\gamma_w\} - 0.5\sigma^C R^2 + k_w y\{R + y\sin\gamma_w\} + k_w y\{y\cos\gamma_w + 0.5y\} \\ &+k_w z\{y\cos\gamma_w + y\} + k_w z\{R + y\sin\gamma_w + 0.5z\} \end{aligned} \tag{5.42}$$

From geometry followings relations can be easily obtained

$$R = \frac{l - \left\{ y\cos\left(\frac{\pi}{4} - \gamma_w\right) + \frac{(y+z)}{\sqrt{2}} \right\}}{\left\{ \sin\beta + \sin\left(\frac{\pi}{4} - \gamma_w\right) + \frac{1}{\sqrt{2}} - \cos\left(\frac{\pi}{4} + \gamma_w\right) \right\}} \tag{5.43}$$

$$\gamma_w = \frac{\pi}{4} - \theta_w = \frac{\pi}{4} - \frac{1}{2}\cos^{-1}\left(\frac{M-1}{M}\right) \tag{5.44}$$

$$\phi = \cos^{-1}\left(\cos\beta + \frac{lK}{R}\right) \tag{5.45}$$

Also

$$y\left\{\frac{1}{\sqrt{2}}+\sin\left(\frac{\pi}{4}-\gamma_w\right)\right\}=R\left\{\cos\left(\frac{\pi}{4}-\gamma_w\right)-\cos\beta-\sin\left(\frac{\pi}{4}+\gamma_w\right)+\frac{1}{\sqrt{2}}\right\} \tag{5.46}$$

Eq. (5.42) was minimized numerically to evaluate the limit moment and the unknown parameters of the plastic field. The mean stress just below point E, that is, in the weld material can be simply expressed in terms of angles φ and γ_w (see Fig. 5.7(a)) as given below

$$\sigma_w^E = 2k_w\left(\frac{\pi}{4}-\gamma_w-\phi\right)-\sigma^C \tag{5.47}$$

At points E and F, that is, at the base-weld interface, it is proposed that continuity of tractions is violated. If the unknown mean stresses at points E and F are denoted by σ_E^* and σ_w^* respectively, Hencky's equations may be used to describe stress distribution to obtain mean stress at point F and G (near the crack tip) in terms of the two unknowns as follows.

$$\sigma^F = \sigma_E^* + 4k_b\phi \tag{5.48}$$

$$\sigma^G = \sigma_w^* + 2k_w\left(\beta-\phi\right) \tag{5.49}$$

Resulting equilibrium equations can be expressed as follows

$$\sum F_x = k_w y\cos\left(\frac{\pi}{4}-\gamma_w\right)-\sigma^C y\sin\left(\frac{\pi}{4}-\gamma_w\right)+\sigma_w^E R\cos\phi+4k_b R\phi\cos\phi+2\left(k_w-k_b\right)R\sin\phi \\ -\sigma_w^* R\cos\phi-k_w R\sin\beta+\sigma^G R\cos\beta \tag{5.50}$$

$$\sum F_y = -\left[k_w\left(z+y\right)\sqrt{2}+\left(k_w y+\sigma^C R\right)\sin\left(\frac{\pi}{4}-\gamma_w\right)+\left(\sigma^C y+k_w R\right)\cos\left(\frac{\pi}{4}-\gamma_w\right)\right]+k_w R\sin\left(\frac{\pi}{4}+\gamma_w\right) \\ +\sigma^C R\sin\left(\frac{\pi}{4}-\gamma_w\right)-k_w R\sqrt{2}+\left(\sigma_E^*-\sigma_w^E\right)R\sin\phi+\left(\sigma^F-\sigma_w^*\right)R\sin\phi+k_w R\cos\beta+\sigma^G R\sin\beta \tag{5.51}$$

Eqs. (5.50) and (5.51) contain two unknowns namely σ_w^* and σ_E^*, which can not be evaluated from MUB analysis. The procedure used for evaluation of σ_w^* and constraint parameter *h* has been described in section 5.2.1. The other unknown, that is, σ_E^* can be determined from eq. (5.51). If the field parameters as obtained from MUB analysis are correct than both σ_w^* and σ_E^* should be in agreement with FE results.

For an under-match weld the centre of curvature of the circular arc BC (in weld region) would lie to the right of elastic-plastic boundary DCBA and the angle subtended by circular arc EF (in base region) is $\phi+\frac{\pi}{4}+\gamma_w$.

5.2.5 Stress field-E

The structure of this proposed stress field, for an overmatch weld, is shown in Fig. 5.8(a). Stress field comprises of a rigid region MLJ, around which the rigid parts of the specimen rotate at an angular velocity ω. Near the free surface, we have uni-axial compression in the region ABP lying in the base material. This constant stress sector is followed by a circular arc BC and another constant stress sector till point D that lies at the base-weld interface. It is assumed that the interface lies in deforming zone and continuity of both shear and normal traction is respected. Due to continuity of shear traction a sudden jump occurs in the angle θ made by α slip-line at the interface. In the region lying in the weld material, just adjacent to the interface, there is another constant stress sector that merges with the circular arc EF tangentially. Using the free surface condition and the yield criterion the stress distribution in Δ ABP can be expressed as $\sigma_{11} = 0,\ \sigma_{22} = -2k_b$ and $\sigma_{12} = 0$. The in-plane shear stress acting in the constant stress sectors, lying in the weld material, can be simply expressed as follows

$$\sigma_{12} = (M-1)k_b \tag{5.52}$$

As a result, eqs. (5.16) and (5.17) describing the angles made by α-slip line in the weld and base material respectively, hold good. If it is assumed that continuity of tractions is maintained at point I also then the stress distribution in the entire deforming zone, up to point J, can be easily obtained using Hencky's relations. The resulting expression for limit moment can be expressed as follows

$$\begin{aligned}
M_L &= k_w R^2(\beta-\phi) + k_b R^2(\phi+\pi/4) + k_b\left(y-\sqrt{2}lK\right)R + 0.5k_b\left(y-\sqrt{2}lK\right)^2 + k_w\sqrt{2}lKR \\
&+(2-M)k_b\sqrt{2}lK\left(y-\frac{lK}{\sqrt{2}}\right) + k_w cy + (2-M)k_b c(R+0.5c) - k_w R(R+c) + k_w Rd \\
&+(2-M)k_b R(0.5R-y) + \sigma_w^D R(e-0.5R) + k_w ce + \sigma_w^D c(d+0.5c) + k_b cf + \sigma_b^D c(g-0.5c) \\
&+k_b Rg + \sigma_b^D R(f+0.5R) - k_b Rh - k_b R(m-0.5R) + k_b z(m-R) + k_b z(h+0.5z)
\end{aligned} \tag{5.53}$$

Here,

$$\sigma_w^D = -k_b\left[(2-M) + M\left\{\frac{\pi}{2} - \cos^{-1}\left(\frac{M-1}{M}\right)\right\}\right] \tag{5.54}$$

$$\sigma_b^D = -k_b\left[(2-M) + M\left\{\frac{\pi}{2} - \cos^{-1}\left(\frac{M-1}{M}\right)\right\} + \sqrt{2M-1} - \sqrt{M(2-M)}\right] \tag{5.55}$$

From geometry the followings relations can be easily obtained

$$c = \frac{\left[lK - R\left\{\frac{1}{\sqrt{2}} - \sin\left(\frac{\pi}{4} - \gamma_w\right)\right\}\right]}{\left\{\frac{1}{\sqrt{2}} + \sin\left(\frac{\pi}{4} + \gamma_w\right)\right\}} \tag{5.56}$$

$$R = \frac{\left(l - \frac{z}{\sqrt{2}}\right)\left[\frac{1}{\sqrt{2}} + \sin\left(\frac{\pi}{4} + \gamma_w\right)\right] - lk\left[\frac{1}{\sqrt{2}} + \cos\left(\frac{\pi}{4} + \gamma_w\right) + \cos\left(\frac{\pi}{4} + \gamma_b\right)\right]}{\left\{\sin\beta - \cos\beta + \cos\left(\frac{\pi}{4} - \gamma_w\right) + \cos\left(\frac{\pi}{4} - \gamma_b\right)\right\}\left\{\frac{1}{\sqrt{2}} + \sin\left(\frac{\pi}{4} + \gamma_w\right)\right\} - \{b_1\}} \tag{5.57}$$

where

$$b_1 = \left\{\frac{1}{\sqrt{2}} - \sin\left(\frac{\pi}{4} - \gamma_w\right)\right\}\left\{\cos\left(\frac{\pi}{4} + \gamma_w\right) + \cos\left(\frac{\pi}{4} + \gamma_b\right) + \frac{1}{\sqrt{2}}\right\} \tag{5.58}$$

$$y = R\left\{1 - \sqrt{2}\cos\beta\right\} \tag{5.59}$$

$$d = (R + c)\cos\gamma_w + (R - y)\sin\gamma_w \tag{5.60}$$

$$e = R - \frac{(R-y)}{\cos\gamma_w} + (R+c)\sin\gamma_w + \frac{(R-y)\sin^2\gamma_w}{\cos\gamma_w} \tag{5.61}$$

$$f = f_1 + f_2 \tag{5.62}$$

$$f_1 = \frac{\left\{R - \frac{(R-y)}{\cos\gamma_w}\right\}\left[\cos\left(\frac{\pi}{4}-\gamma_w\right)+\sin\left(\frac{\pi}{4}-\gamma_w\right)\right]}{\left[\cos\left(\frac{\pi}{4}-\gamma_b\right)+\sin\left(\frac{\pi}{4}-\gamma_b\right)\right]} + c\frac{\left[\cos\left(\frac{\pi}{4}+\gamma_w\right)-\sin\left(\frac{\pi}{4}+\gamma_w\right)+\cos\left(\frac{\pi}{4}+\gamma_b\right)-\sin\left(\frac{\pi}{4}+\gamma_b\right)\right]}{\left[\cos\left(\frac{\pi}{4}-\gamma_b\right)+\sin\left(\frac{\pi}{4}-\gamma_b\right)\right]} \tag{5.63}$$

$$f_2 = (R+c)\sin\gamma_b + (R-y)\tan\gamma_w\sin\gamma_b + \left[\sqrt{2}\left\{\left[R-\frac{(R-y)}{\cos\gamma_w}\right]\cos\left(\frac{\pi}{4}-\gamma_w\right)+c\left[\cos\left(\frac{\pi}{4}+\gamma_w\right)+\cos\left(\frac{\pi}{4}+\gamma_b\right)\right]-f_1\cos\left(\frac{\pi}{4}-\gamma_b\right)\right\}\right]\sin\gamma_b \tag{5.64}$$

$$g = f_2\frac{\cos\gamma_b}{\sin\gamma_b} \tag{5.65}$$

$$h = \frac{f_2}{\sin\gamma_b} + (R+f_1)\sin\gamma_b \tag{5.66}$$

$$m = (R+f_1)\cos\gamma_b \tag{5.67}$$

$$\phi = \cos^{-1}\left(\cos\beta + \frac{lK}{R}\right) \tag{5.68}$$

Eq. (5.53) was minimized with respect to the unknown parameters z, and β. At point L that is at the interface of two materials, it is proposed that continuity of tractions is violated. If the unknown mean stress at point L is denoted by σ_w^*, the mean stress at point M (near the crack tip) can be expressed as follows.

$$\sigma^M = \sigma_w^* + 2k_w\left(\beta - \phi\right) \tag{5.69}$$

Resulting equilibrium equations can be expressed as follows

$$\begin{aligned}\sum F_x = {} & 2k_b\left(M-1\right)lK - k_w\frac{c}{\sqrt{2}} + \left(2-M\right)k_b\frac{c}{\sqrt{2}} - k_w\frac{R}{\sqrt{2}} + k_w R\cos\left(\frac{\pi}{4}-\gamma_w\right) + \\ & \left(2-M\right)k_b\frac{R}{\sqrt{2}} - \sigma_w^D R\cos\left(\frac{\pi}{4}+\gamma_w\right) - k_w c\cos\left(\frac{\pi}{4}+\gamma_w\right) + \sigma_w^D c\cos\left(\frac{\pi}{4}-\gamma_w\right) \\ & -k_b c\cos\left(\frac{\pi}{4}+\gamma_b\right) + \sigma_b^D c\cos\left(\frac{\pi}{4}-\gamma_b\right) + k_b R\cos\left(\frac{\pi}{4}-\gamma_b\right) - \sigma_b^D R\cos\left(\frac{\pi}{4}+\gamma_b\right) \\ & +k_b\left(M-1\right)R\sin\phi + k_b\left[2\left(\phi+\frac{\pi}{4}\right)-1\right]R\cos\phi - \sigma_w^* R\cos\phi - k_w R\sin\beta + \sigma^M R\cos\beta\end{aligned} \tag{5.70}$$

$$\begin{aligned}\sum F_y = {} & -\left[\begin{array}{l} k_b\left(z+y\right)\sqrt{2} + \sqrt{2}k_b c - \sqrt{2}k_b R + k_w R\sin\left(\frac{\pi}{4}-\gamma_w\right) + \sigma_w^D R\sin\left(\frac{\pi}{4}+\gamma_w\right) + k_w c\sin\left(\frac{\pi}{4}+\gamma_w\right) \\ +\sigma_w^D c\sin\left(\frac{\pi}{4}-\gamma_w\right) + k_b c\sin\left(\frac{\pi}{4}+\gamma_b\right) + \sigma_b^D c\sin\left(\frac{\pi}{4}-\gamma_b\right) + k_b R\sin\left(\frac{\pi}{4}-\gamma_b\right) \end{array}\right] \\ & -\sigma_b^D R\sin\left(\frac{\pi}{4}+\gamma_b\right) + k_B\left(1-M\right)R\cos\phi + k_B\left[2\left\{\phi+\frac{\pi}{4}\right\}-1\right]R\sin\phi - \sigma_w^* R\sin\phi + k_w R\cos\beta + \sigma^M R\sin\beta\end{aligned} \tag{5.71}$$

For an under-match weld, the centres of curvature of the circular arc BC (in the base region) and EF (in the weld region) would lie to the left and right of elastic-plastic boundary BCDEF respectively.

5.3 Structure of stress fields for a deeply cracked compact tension C(T) specimen having a weld centre crack under fully plastic state in mode-I loading

We consider here a stationary crack lying at the centre of weld in a compact tension C(T) specimen, as shown in Fig. 5.9. The effects of strength mismatch ratio M and weld slenderness ratio ψ on the limit load and the crack tip constraint parameter h were analysed. It is well known that the global stress field of a homogeneous SE(PB) specimen is also applicable to a C(T) specimen, though the kinematic conditions are different in the two cases. The present study has revealed that a family of five stress fields proposed for a SE(PB) specimen having a weld centre crack, is also applicable to a C(T) specimen having a weld centre crack. The proposed stress fields cover all practical cases of weld mismatch except for the extreme under-match case where the plastic field gets fully confined in the weaker weld material. The detailed structure of these five stress fields has already been presented in section 5.2 and we now emphasise on the kinematic aspects of the associated velocity fields as they are required in MUB analysis.

The relation between the relative velocity, v^*, (with which the rigid parts rotate) and the rate of imposed displacement, $\dot{\delta}$, is the same proposed for a homogeneous C(T) specimen and can be expressed as

$$v^* = \frac{R\dot{\delta}}{2\left(a + R\sin\beta\right)} \tag{5.72}$$

The above kinematic relation along with the stress distribution of deforming zones for each of the five stress fields (proposed in section 5.2) was used to obtain the limit load expression using the modified upper bound theorem, eq. 3.33. Since rest of the analysis used to obtain the limit load and the crack tip constraint parameter *h* is very similar to that of SE(PB) specimen, we skip the details and proceed directly to results.

5.4 Finite element analysis

In sections 5.2 and 5.3, detailed structure of the stress fields was proposed for a stationary crack lying at the centre of weld in a pure bending specimen and in a compact tension specimen under plane strain condition. To verify the proposed analytical solutions of the limit moment and crack tip constraint, finite element analyses were performed on the above-mentioned specimens, under large-scale plasticity (at limit state). Numerical solutions of the limit moment/load and crack-tip constraint parameter *h* were compared with analytical results. In finite element analysis both base and weld materials were modeled as isotropic, elastic-perfectly plastic. The two materials were assumed to have same elastic modulus (E=203 GPa) and Poisson's ratio (ν=0.3) but mismatch in their yield strength. Stationary crack at the centre line of weld, parallel to base-weld interface, was modeled. Fig. 5.10 shows the FE discretisation scheme used in present investigation. To avoid problems associated with incompressibility eight-noded plane strain element with reduced integration were employed in all finite element calculations. 16 eight-noded elements comprised the upper-half of crack tip and forty circumferential rings of element were surrounding the crack tip. The innermost ring of the elements had one side collapsed on to the crack-tip. All the collapsed nodes got separated after the loading was applied. Due to symmetry only one-half of SE(PB) and C(T) specimen was modeled. This one-half model contains about 1400, 8-noded elements and 4000 nodes. The radial extent of the elements in the first ring was $\approx 2\text{x}10^{-4}\ l$ where l is the uncracked ligament. Numerical model employs the small-strain formulation with J_2 flow theory. For SE(PB) specimen rotation was applied on the top edge of this FE model and the specimen was loaded to its limit state. Material mismatch ratio M and weld slenderness ratio ψ were systematically varied to create a wide range of crack-tip constraint. For over matched welds analyses were performed for $1 \leq M \leq 2$. This range of mismatch covers practically the entire range of over matching that is likely to occur in most engineering applications. For under matched welds finite element analyses were performed only for $0.8 \leq M \leq 1$ so that the plastic fields are not fully confined in weld material. Weld slenderness ratio was also varied ($1.667 \leq \psi \leq 10$) to account for both conventional and narrow grove welds.

5.5 <u>Results</u>

We present here the comparison of the limit moment/load, and crack tip constraint parameter h of SE(PB) and C(T) specimen, having a weld centre crack, obtained from the proposed MUB theorem with our numerical (FE) results. For each mismatch ratio M and weld slenderness ratio ψ out of the five stress fields, described in 5.2.1-5.2.5, only one of them governs the plastic yielding of the remaining ligament. The stress field producing the lowest limit moment represents the correct solution (for details see section 5.6). Thus, the limit moment and constraint parameter h was evaluated from the equations relevant to that particular stress field. It may be noted that Kim and Schwalbe (2001a, 2001b, 2004) have also investigated the effect of weld strength mismatch on the limit moment/load and crack-tip constraint parameter h of the above-mentioned specimens by finite element analysis. Fig. 5.11 shows the variation of normalised limit moment M_{lr} and constraint parameter h with mismatch factor M and weld slenderness ratio ψ for a SE(PB) specimen. The normalised limit moment M_{lr} is defined as the ratio of the limit moment of a SE(PB) specimen, having a weld centre crack, to the limit moment of homogeneous SE(PB) specimen of base material. Fig. 5.13 shows the variation of normalised limit load P_{lr} and constraint parameter h with mismatch factor M and weld slenderness ratio ψ for a C(T) specimen. The normalised limit load P_{lr} is defined as the ratio of the limit load of a C(T) specimen, having a weld centre crack, to the limit load of homogeneous C(T) specimen of the base material.

It can be seen from Figs. 5.11(a) and 5.13(a) that all the three solutions of the limit moment/load seem to be in good agreement with each other. Closed form solutions proposed by Kim and Schwalbe (2001a, 2001b) shows a small difference with our finite element results as these are based on fitting of finite element results of these authors. Constraint parameter h, shown in Fig. 5.11(b) and 5.13(b), was evaluated ahead of crack tip, that is, at $\theta=0$. In finite element analysis, h was evaluated at a distance of $5\text{x}10^{-3}\ l$ which is sufficiently close to the crack tip. Here l is the uncracked ligament. Both theoretical and finite element results clearly indicate that weld overmatch reduces crack tip constraint while undermatch increases it. This observation has been made by many other investigators and more detailed comments can be found in the work of Kim and Schwalbe (2004).

Figs. 5.12 and 5.14 shows the variation of constraint parameter *h* with polar angle θ for SE(PB) and C(T) specimen, respectively. For SE(PB) specimen, results are presented here for two representative cases, that is, for $\psi = 10$ and $\psi = 3.33$. As discussed in section 5.1, proposed analytical solutions, due to lack of information about the elastic plastic boundary near the crack tip, can provide crack tip stresses only in the plastic sectors, that is, for $0 \leq \theta \leq \beta$. The angle β is shown in Figs. (5.1-5.8). For this range of θ analytical solutions of *h* were found to be in good agreement with finite element results. From Fig. 5.12 it can be observed that as weld slenderness ratio ψ decreases (large weld width), the effect of weld strength mismatch on crack tip constraint parameter *h* becomes less pronounced.

5.6 Discussion

In the past two decades, the problem of a stationary crack lying at the centre of a strength mismatched weld has been extensively investigated. However, the detailed insight of the structure of stress fields under large scale plasticity is still lacking. In this work the problem was examined from a more fundamental perspective. It is generally felt that unlike numerical results the classical approaches like slip line field provides a better understanding of the aspects related to mechanics of deformation. However, constructing such analytical solutions for mismatch welds requires some special considerations over and above those needed for a standard boundary value problem involving single material. In the present investigation, stress fields were constructed by assuming that in the cases where the slip line passing through the interface of two materials lies in deforming zones, continuity of traction is respected. For the cases where the slip line passing through the interface separates two rigid (elastic) regions both the shear and normal tractions undergo a jump at this interface. This assumption which was the basis of the proposed solutions was in good agreement with observations from detailed finite element analysis. To evaluate the unknown parameters of the plastic field, the modified upper bound (MUB) theorem developed in chapter 3 was used. Minimization of the limit moment/load expressions obtained from MUB analysis provided us the required unknown parameters of the plastic fields. It may be noted that as far as the evaluation of limit moment/load is concerned the unknown value of the mean stress at the base-weld interface does not enter in the analysis. For several cases of homogeneous cracked as well as uncracked geometries, the equivalence of MUB theorem with slip line field analysis was demonstrated in chapter 4. It was established that the minimization process finally leads to equations of global equilibrium. Studies presented in this chapter have established that this equivalence holds good for mismatch welds also. This is really an important finding, particularly for the problem of strength mismatch welds, as it allows a complete analytical evaluation of stress distribution in the plastic regions.

For homogeneous fracture specimens, it is well established that plastic deformation fields depend on specimen geometry and loading condition (McClintock, 1971). For a fracture specimen having a strength mismatch weld, mismatch ratio M and weld slenderness ratio ψ are the additional parameters affecting the plastic fields. Thus, in comparison to the slip line fields describing the stress distribution in homogeneous cracked specimens, fields for mismatched welds are more complicated. In this work, a family of five stress fields is proposed to cover all practical cases of weld mismatch. It is worth to discuss that all the five fields are similar to each other in the rigid zones where they are in the form of circular arcs. However, significant differences do occur in the structure of these fields in the deforming zones. Depending upon the mismatch ratio M and weld slenderness ratio ψ only one of these fields governs the plastic yielding of the remaining ligament. The criterion adopted to choose which of these fields is relevant for a particular case is similar to that used for the homogeneous cases. Since all the proposed solutions are upper bound the one giving the least value of limit load/moment is nearer to the exact solution (Katchanov, 1971). Our study revealed that out of the five proposed fields the one leading to the least value of limit moment also satisfies the global equilibrium equations and was close to the actual plastic field obtained from FE analysis.

It is also worth to discuss that the present article was focused mainly on weld centre crack. In an actual weld joint crack may lie, however, anywhere also. MUB theorem may be used to analyse such cases but the structure of global plastic fields need to be established. Such studies may be carried out in future.

It is widely accepted that the weld mismatch effects not only change the limit moment/load and crack driving force (J-integral) but also influence the materials fracture behaviour. This is simply because the weld mismatch effects change the stress fields near the crack tip and, hence, the crack tip constraint. Detailed numerical studies performed by many investigators have clearly established that weld over match produces a "shielding effect" on the crack tip and reduces the crack tip constraint. Similarly under match causes a significant increase in crack tip constraint. The detailed structure of stress fields presented in this chapter has provided a more elaborate explanation to this well-known influence of weld mismatch on crack-tip constraint.

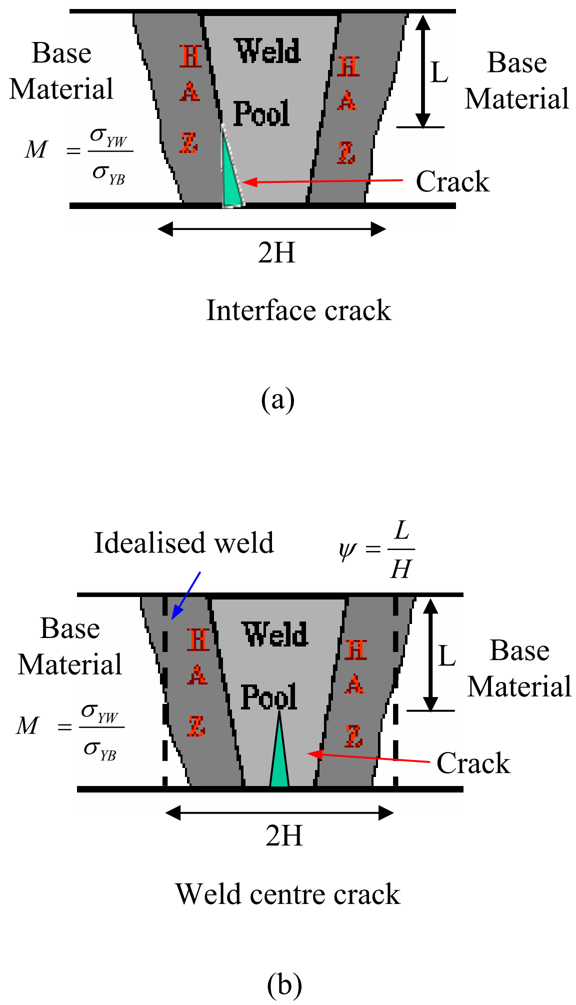

Fig. 5.1: Schematic of (a) an interface crack and (b) a weld centre crack in a strength mismatch weld.

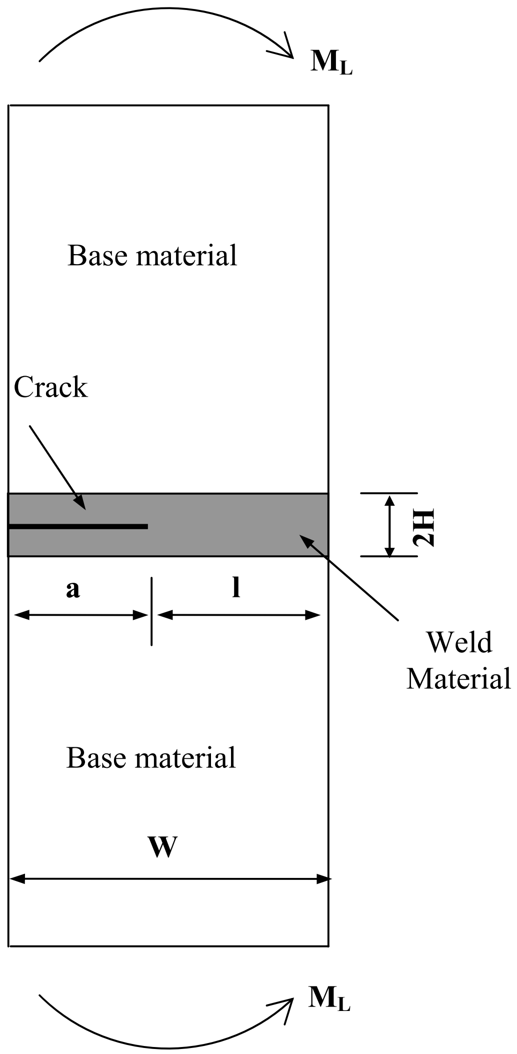

Fig. 5.2: Pure bending SE(PB) specimen with a weld centre crack.

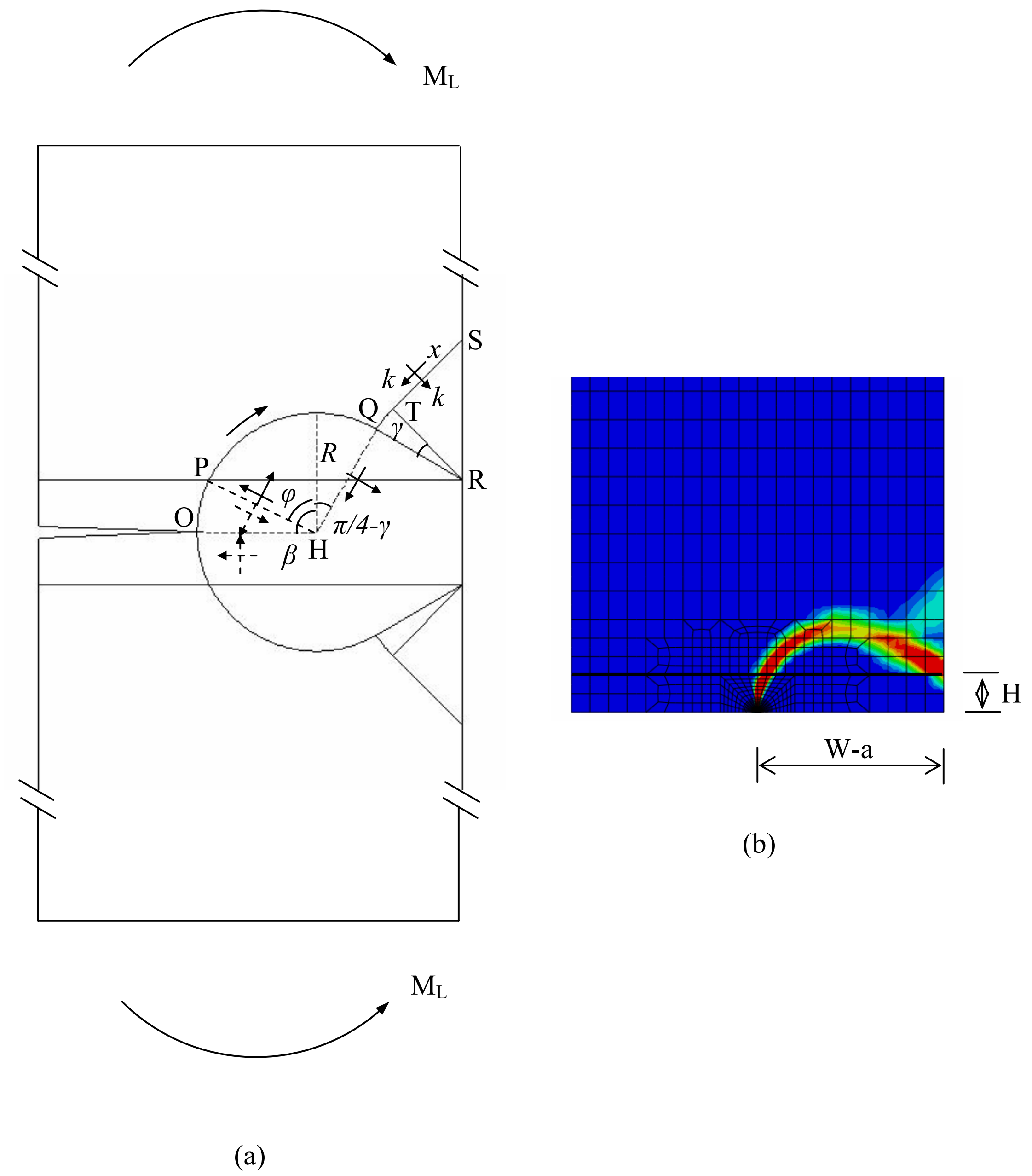

Fig. 5.3: (a) Proposed structure of stress field-A and (b) plot of equivalent plastic strain obtain from FE analysis.

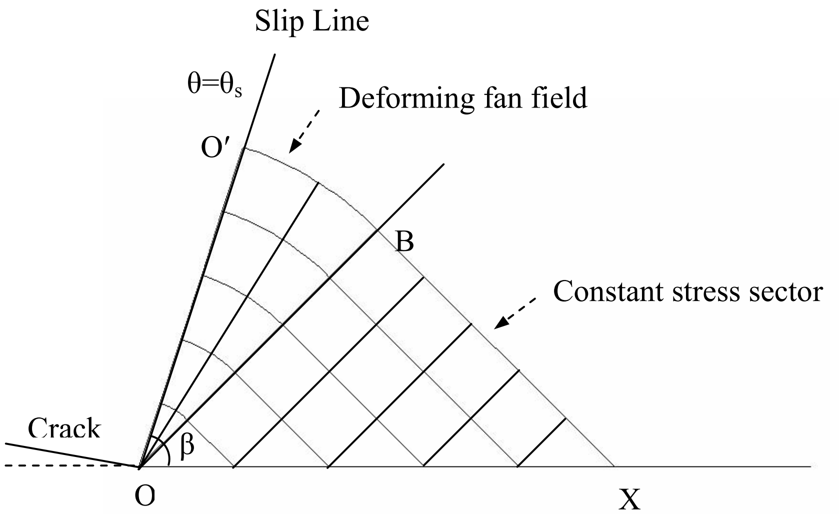

Fig. 5.4: Asymptotic incomplete crack-tip stress field for a deeply cracked SE(PB) specimen and C(T) specimen.

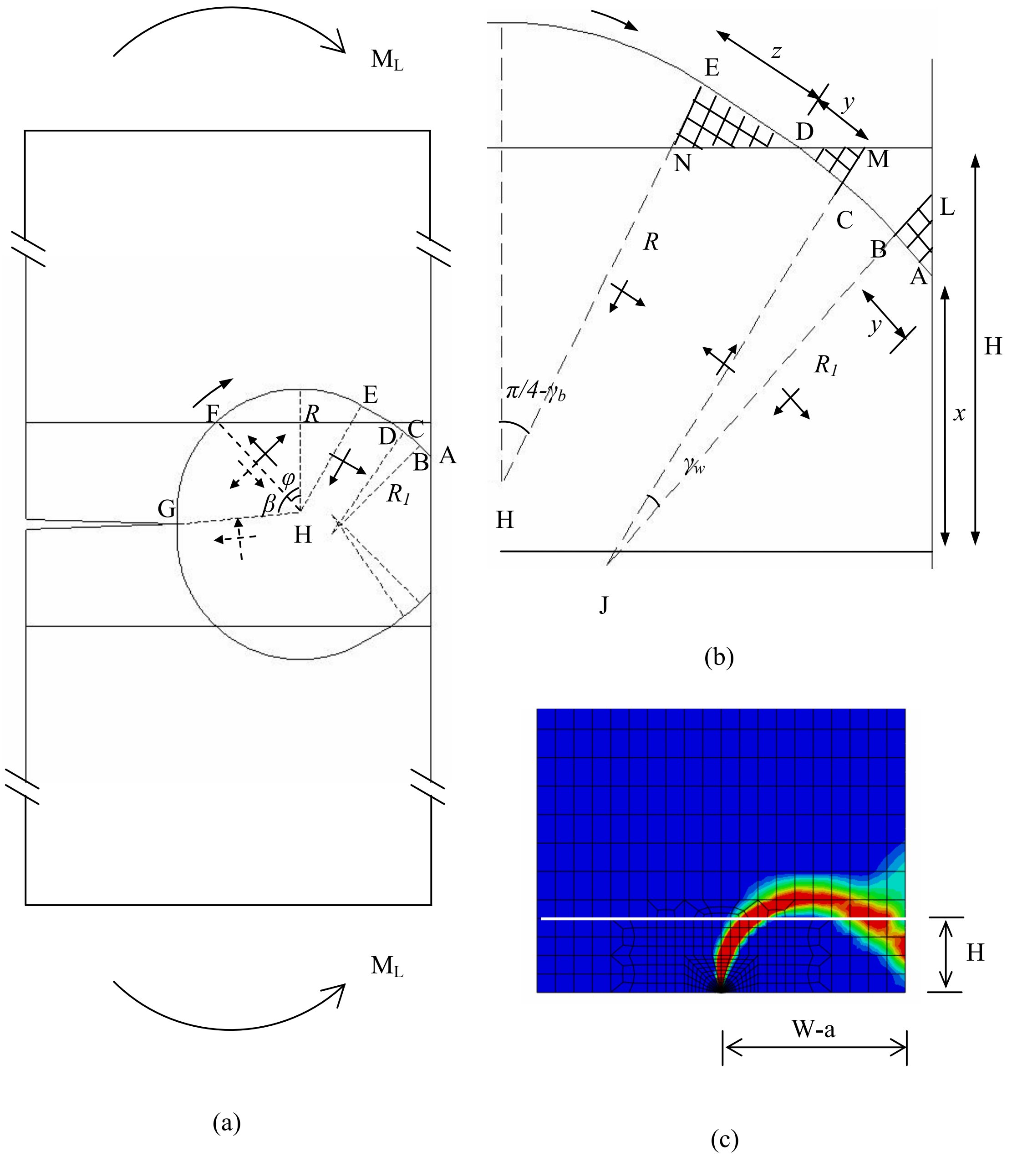

Fig. 5.5: Description of stress field-B (a) complete structure of the proposed field (b) zoomed portion of stress field near free surface and (c) plot of equivalent plastic strain obtained from FE analysis.

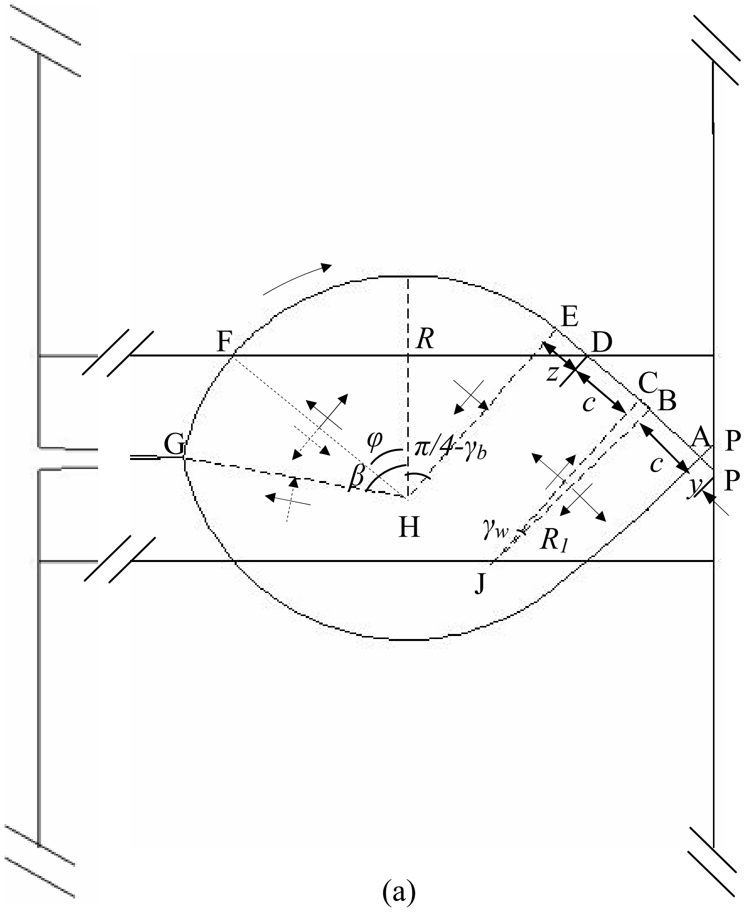

(a)

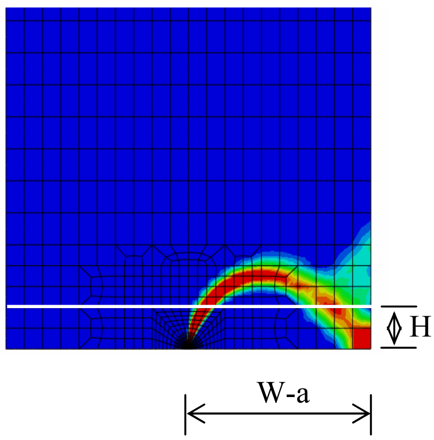

(b)

Fig. 5.6: Description of stress field-C (a) complete structure of the proposed field for an over-match weld and (b) plot of equivalent plastic strain as obtained from FE analysis.

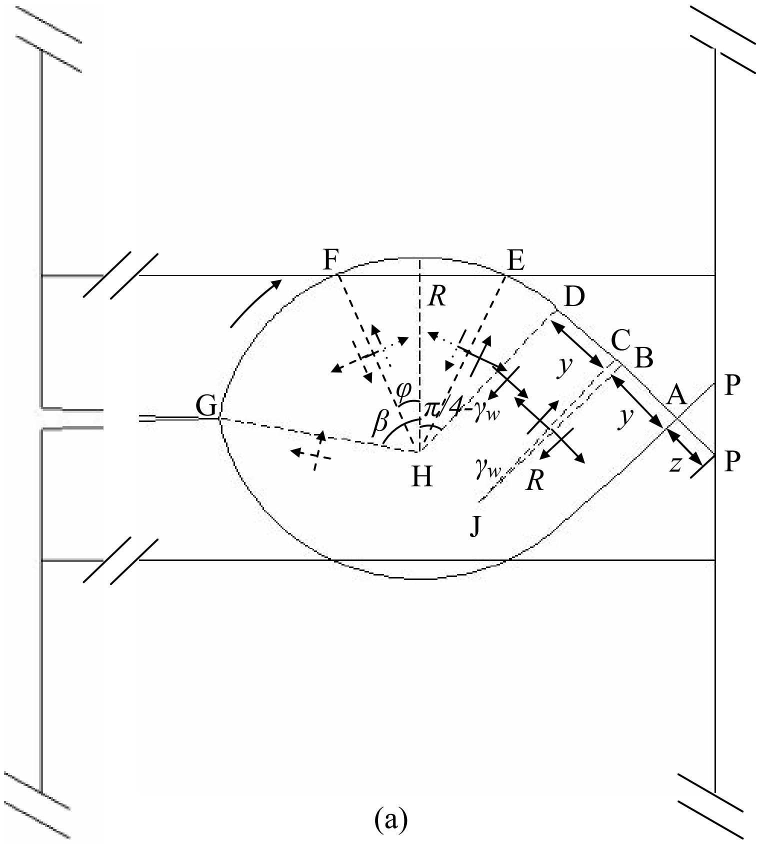

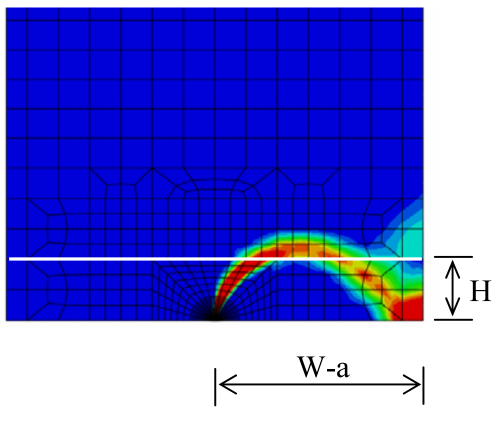

Fig. 5.7: Description of stress field-D (a) complete structure of the proposed field for an overmatch weld and (b) plot of equivalent plastic strain as obtained from FE analysis.

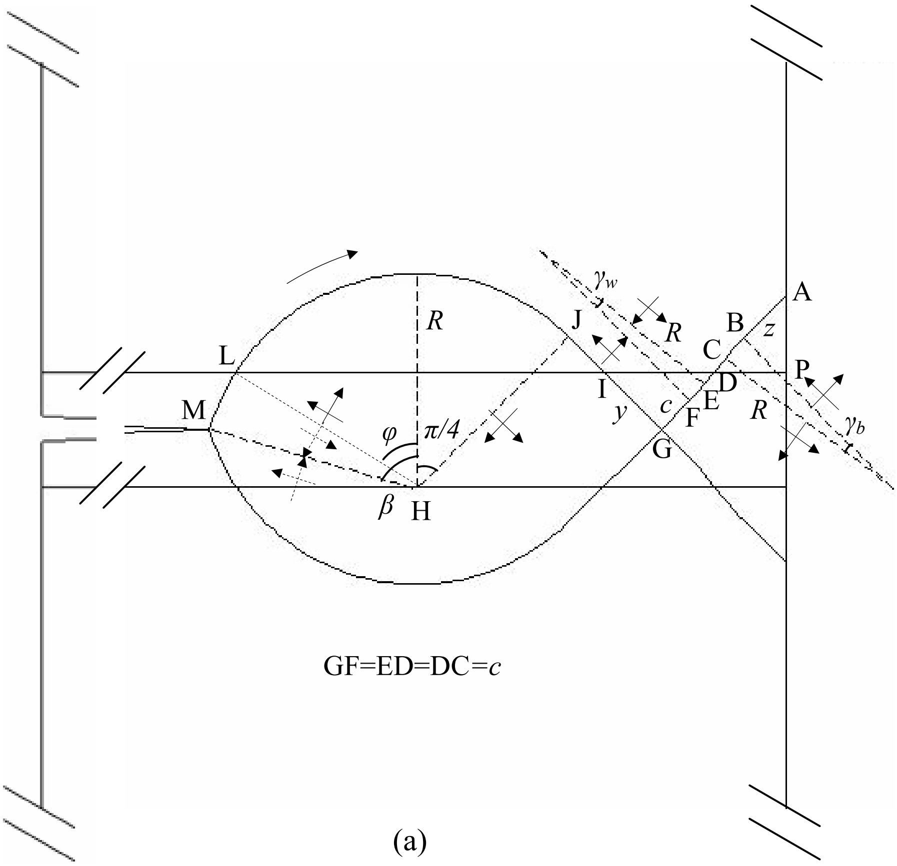

(a)

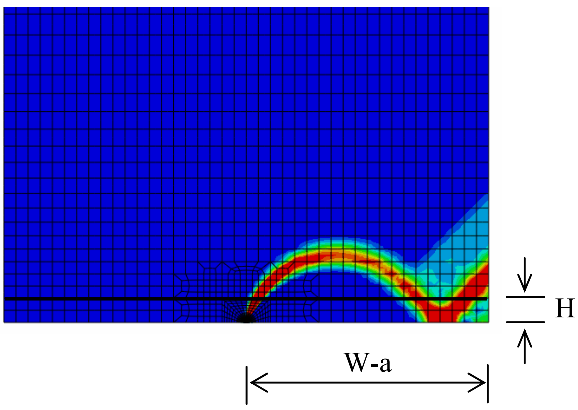

(b)

Fig. 5.8: Description of stress field-E (a) complete structure of the proposed field and (b) plot of equivalent plastic strain as obtained from FE analysis.

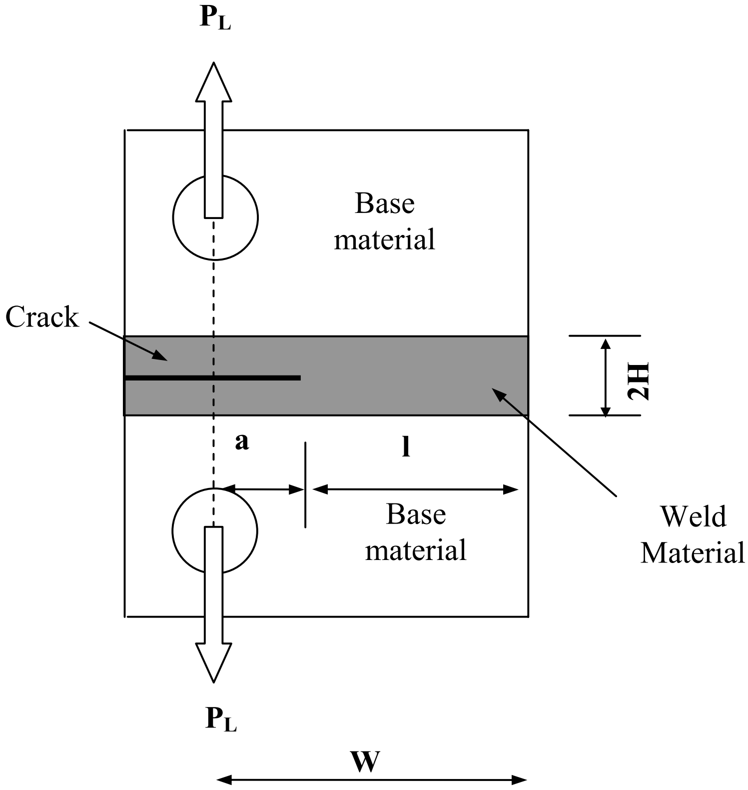

Fig. 5.9: Compact Tension C(T) specimen with a weld centre crack.

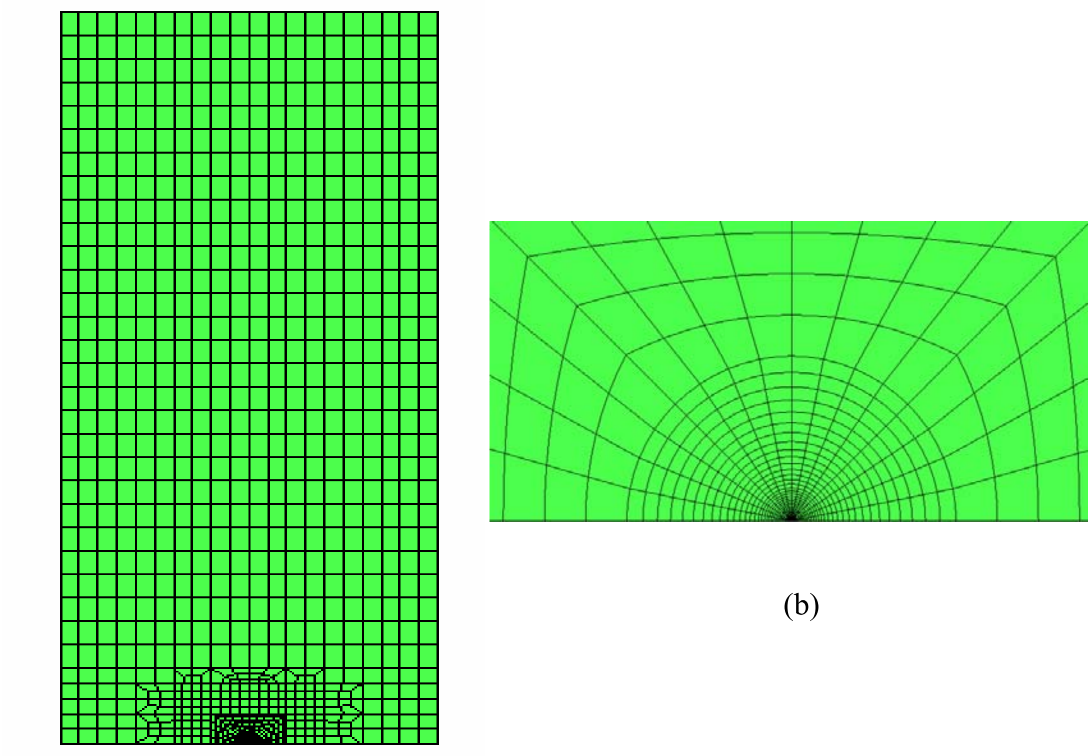

(b)

(a)

Fig. 5.10: Finite element discretisation scheme used in present investigation, (a) global view of the mesh used for a SE(PB) specimen and (b) zoomed view near the crack tip

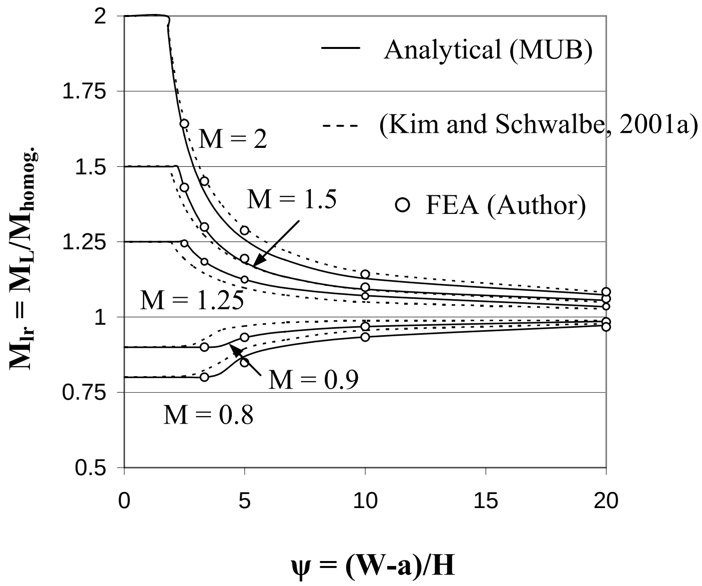

(a)

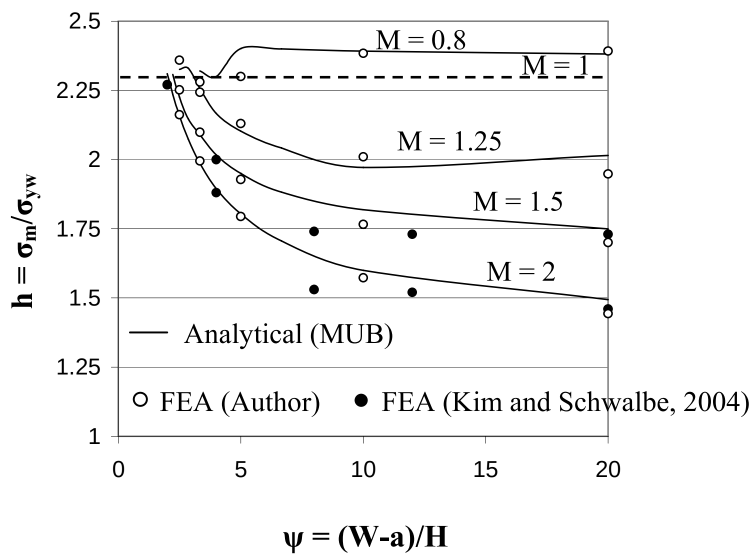

(b)

Fig. 5.11: Comparison of (a) normalised limit moment and (b) crack tip constraint parameter *h*, evaluated at θ=0, obtained from MUB theorem with FE results for SE(PB) specimen.

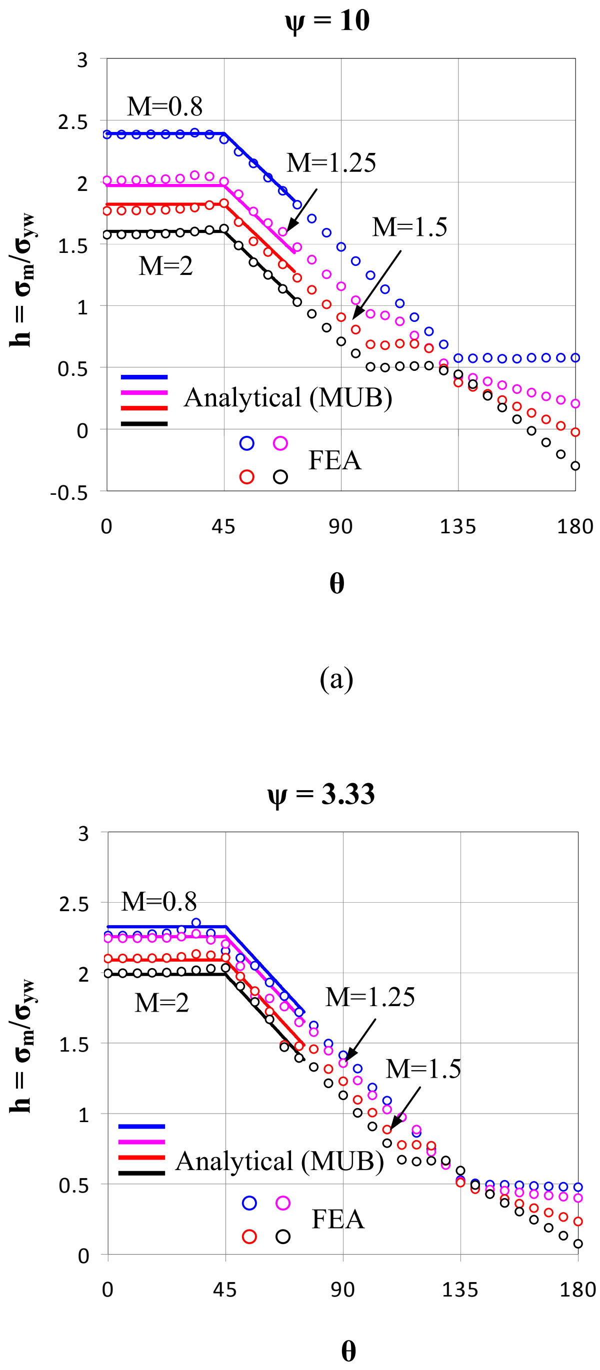

(a)

(b)

Fig. 5.12: Variation of constraint parameter *h* with polar angle θ for (a) $\psi = 10$ and (b) $\psi = 3.33$ obtained from MUB theorem and FE analysis for SE(PB) specimen.

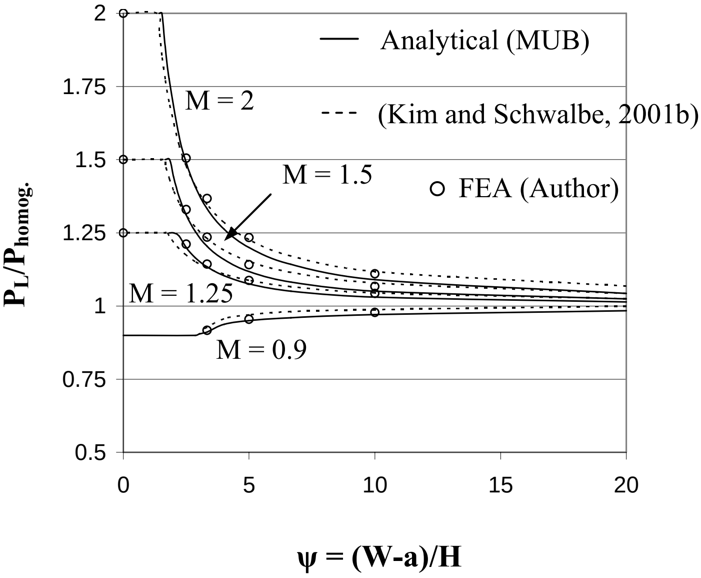

(a)

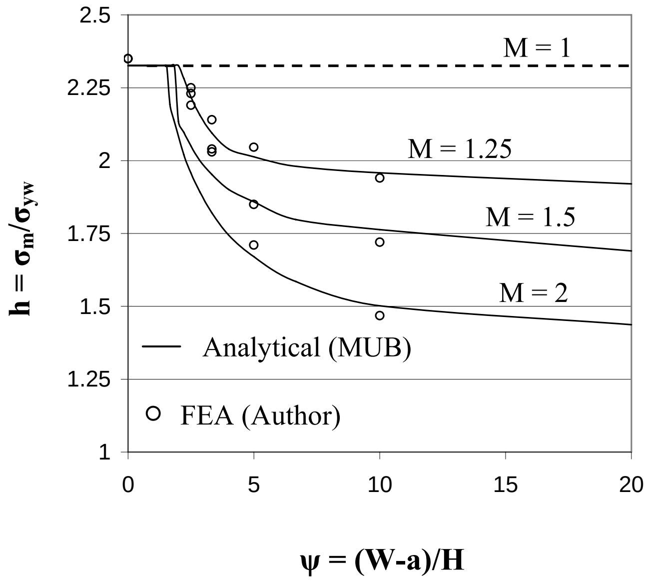

(b)

Fig. 5.13: Comparison of (a) normalised limit load and (b) crack tip constraint parameter *h*, evaluated at θ=0, obtained from MUB theorem with FE results for C(T) specimen.

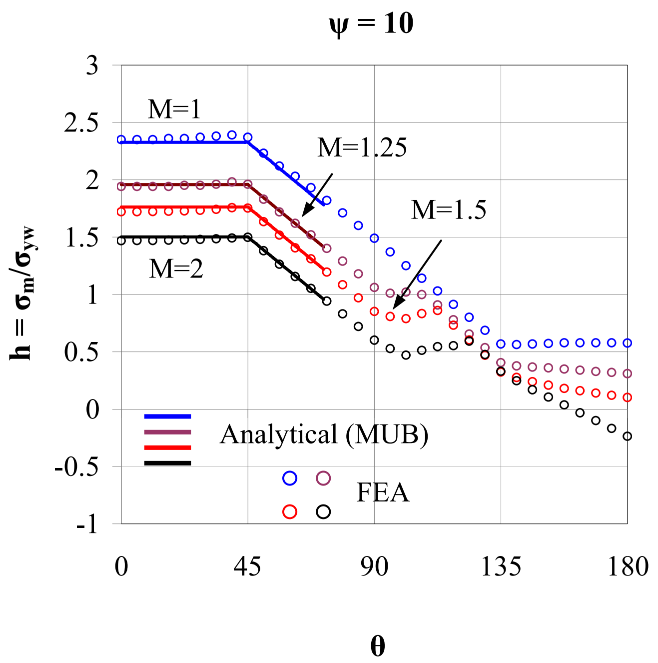

Fig. 5.14: Variation of constraint parameter h with polar angle θ for ψ = 10 obtained from MUB theorem and FE analysis for C(T) specimen.

CHAPTER 6

A study of the limit load and crack tip constraint of middle tension M(T) specimen having a weld centre crack

6.1 Introduction

The problem of middle tension M(T) specimen having a weld centre crack has been studied extensively. It was first systematically analysed by Varias et al. (1991). They numerically (finite element) examined the case where a crack was postulated at the centre of ductile metal foil sandwiched between two rigid ceramic blocks. The focus of this study was to understand the ductile failure mechanisms that are likely to occur in the metal foil under such a high constraint state. It was demonstrated that for such an extreme mismatch case, under small-scale yielding condition, under uni-axial tensile load a high tri-axial stress exists ahead of crack tip at a distance several times the foil thickness. A formula for evaluating the stress intensity factor was also suggested.

On analytical front, initial study on M(T) specimen having a weld centre crack, under large-scale plasticity, was carried out by Joch et al. (1993). Main objective of this study was to quantify the influence of weld strength mismatch on the limit load and plastic η-factor. Classical upper bound theorem of limit analysis was used to derive analytical solutions. However, more detailed description of this problem was presented by Hao et al. (1997). Using classical approach of Slip-line theory, they provided sufficiently detailed analytical solutions of the limit load and crack tip stresses for the case where plasticity was confined only in the weld material. In case where the yield strength of base and weld material is comparable plastic deformation occurs in both the materials. Constructing SLF solutions for such cases is not straightforward as the stress connections conditions at the base-weld interface are unknown.

Hao et al. (1997) made an attempt to solve this problem analytically by assuming continuity of normal and shear stress along the slip line passing through the interface of base and weld material. However, this assumption was not well supported by the results obtained from detailed elastic-plastic finite element analysis. Based on comparison of their analytical results with finite element (FE) studies they indicated the possibility of jump in tractions at the interface of the two materials. This problem was then re-examined numerically by Kim and Schwalbe (2001, 2004). Based on extensive FE analyses, these authors proposed closed-form expressions of the limit load of M(T) specimen for weld centre crack, interfacial crack, and asymmetrically located crack in the weld region. They also performed detailed numerical studies to examine the strength mismatch effect on crack tip constraint parameter h under fully plastic condition (2004). The problem of M(T) specimen having an asymmetric crack in the weld region was also analysed by Lei et al. (1999). The classical upper bound theorem of limit analyses was used to obtain analytical solutions of the limit load. Using the concept of equivalent stress-strain relation proposed by Lei and Ainsworth (1997) these authors also provided an estimation of J-integral. Analytical solutions of the limit load of an overmatched M(T) specimen were also provided by Alexandrov et al. (1999). Based on kinematically admissible velocity fields and statically admissible stress fields corresponding upper and lower bound estimates of limit load were arrived. Their numerical results for upper bound limit load were identical to those provided by Joch et al. (1993), however, Alexandrov et al. (1999) demonstrated that the upper bound limit load depends on a single parameter that can account for the effects of weld strength mismatch M as well as weld slenderness ratio ψ.

In this chapter, a discontinuous stress solution is proposed to analyse M(T) specimen having a weld centre crack. Discontinuity is incorporated in the proposed solution by assuming an unknown value of the mean (hydrostatic) stress at the base-weld interface. Modified upper bound (MUB) theorem along with global equilibrium equations was utilised to obtain this unknown mean stress and hence the whole stress field. The results obtained were found to be in excellent agreement with the known FE solutions available in literature. In addition to the limit load, effect of weld strength mismatch on crack tip constraint parameter h was quantified.

6.2 Analysis of overmatched middle tension M(T) specimen having a weld centre crack

Consider the case of a M(T) specimen having a weld centre crack as shown in Fig. 6.1. Assumption of plane strain was made and analysis was carried out on an idealised weld without any heat affected zone (HAZ). The two materials (base and weld) were considered as rigid-plastic having mismatch in their yield strength. The effects of weld geometry were modeled by changing the weld slenderness ratio ψ while the strength mismatch effects were incorporated by changing the mismatch ratio M. These two parameters are defined as follows

$$M = \frac{\sigma_{YW}}{\sigma_{YB}} \qquad\qquad \psi = \frac{W-a}{H} = \frac{l}{H} \tag{6.1}$$

Material strength mismatch ratio M and weld slenderness ratio ψ were systematically varied to account all practical cases. M>1 corresponds to an overmatch weld while M<1 refers to an undermatch weld.

For a M(T) specimen, having a weld centre crack, the assumed plastic field for an overmatch weld is shown in Fig. 6.2. In this field it was assumed that a straight slip line APB emanated from the crack tip and crossed the base-weld interface. It was then merged into the fan field BEC of angular extent γ whose centre E lied at the base-weld interface. Near the free surface there was a region of constant stress (uniform tension) CDE which merged with the fan field tangentially. It may be mentioned that this type of field was first suggested by Hao et al. (1997), however, the authors did not provide any details of its analysis. The stress distribution in the constant stress region, CDE, can be expressed as

$$\sigma_{11} = 0,\ \sigma_{22} = -2k \text{ and } \sigma_{12} = 0 \tag{6.2}$$

In the central field BEC, the shear stress along BE was k and the pressure acting on it, as per Hencky's relation, was $k(1+2\gamma)$. Thus, the stress distribution in the plastic region of the base material up to point P was readily known. At point P, that is, at the interface of two materials we propose that the continuity of tractions is violated. Thus, both the in-plane shear stress σ_{12} as well as the mean stress undergoes a sudden jump at the interface. As a result, the stress distribution cannot be obtained directly for the weld region. As discussed in chapter 5, this problem was solved by the use of MUB theorem. Unlike SLF analysis this technique does not require any information about the mean stress along the slip line separating the two rigid regions. Since the tangential velocity and the shear stress (by virtue of yield criterion) were known along the slip line APB, plastic dissipation of energy can be easily computed. As the mean stress acting on the slip line APB and, hence, the unknown mean stress at the interface, does not enter in MUB analysis problem becomes amenable to a fully analytical treatment. We now proceed to analyse this field.

From kinematics the relation between the rate of imposed displacement $\delta^{\cdot}$ and the tangential velocity v^* along the slip line APB can be easily established, that is,

$$v^* = \frac{\delta^{\cdot}}{\sin\left(\frac{\pi}{4}+\gamma\right)} \tag{6.3}$$

Now invoking work principle, that is, eq. (3.33), limit load can be expressed as,

$$P_L\delta^{\cdot} = 2\left[\int_{AP} k_w v^* dS + \int_{PB} k_b v^* dS + \int_{BC} \sigma_{ij} n_j v_i dS + \int_{CD} \sigma_{ij} n_j v_i dS\right] \tag{6.4}$$

The work done by the stresses on the circular arc BC (of radius x), Fig. 6.2 (b), can be expressed as follows

$$\int_{BC} \sigma_{ij} n_j v_i dS = \int_0^{\gamma} kxv_t d\theta + \int_0^{\gamma} k\left(1+2\theta\right)xv_n d\theta \tag{6.5}$$

$$\int_{BC} \sigma_{ij} n_j v_i dS = \int_0^{\gamma} kx\delta^{\cdot} \sin\left(\frac{\pi}{4}+\theta\right) d\theta + \int_0^{\gamma} k\left(1+2\theta\right) x\delta^{\cdot} \cos\left(\frac{\pi}{4}+\theta\right) d\theta \tag{6.6}$$

$$\int_{BC} \sigma_{ij} n_j v_i dS = kx\delta^{\cdot} \cos\left(\frac{\pi}{4}+\gamma\right) + k\left(1+2\gamma\right) x\delta^{\cdot} \sin\left(\frac{\pi}{4}+\gamma\right) - \sqrt{2}kx\delta^{\cdot} \tag{6.7}$$

Similarly, work done by the stresses on the segment CD can be expressed as follows

$$\int_{CD} \sigma_{ij} n_j v_i dS = \int_{CD} kv_t dS + \int_{CD} kv_n dS = \sqrt{2}kx\delta^{\cdot} \tag{6.8}$$

Finally, substitution of eqs. (6.7) & (6.8) in eq. (6.4), using the value of v^* as given by eq. (6.3), lead to the following relation for the limit load

$$F_y = \frac{2\sigma_{yb} l}{\sqrt{3}} \left[\begin{array}{l} \dfrac{\left(M-1\right)H/l}{\sin^2\left(\pi/4+\gamma\right)} + \dfrac{\left(1-\dfrac{x}{l}\cos\left(\pi/4-\gamma\right)\right)}{0.5\cos 2\gamma} \\ +\dfrac{x}{l}\left\{\left(1+2\gamma\right)\sin\left(\pi/4+\gamma\right)+\sin\left(\pi/4-\gamma\right)\right\} \end{array} \right] \tag{6.9}$$

Since γ is the only independent variable, as per MUB theorem

$$\frac{dF_y}{d\gamma} = 0 \tag{6.10}$$

Thus, the limit load F_y and all the unknown parameters of the assumed plastic field can be easily evaluated. When γ=0 the field reduces to that of homogeneous M(T) specimen (McClintock, 1971). As far as evaluation of the limit load is concerned, the unknown value of the mean stress at the base-weld interface does not enter in the analysis. However, for evaluation of crack tip stress field the jump in the value of mean stress that occurs at the base-weld interface must be quantified.

For a wide variety of specimen geometry and loading conditions it has been established in chapter 4 that the MUB theorem provides results that are identical to those obtained from SLF analysis. Moreover, it was demonstrated in chapter 5 that MUB theorem when applied to SE(PB) and C(T) specimen having a weld centre crack satisfy global equilibrium equations. We now proceed to establish this for a M(T) specimen also. If it is assumed that σ_w^* is the unknown value of hydrostatic stress that occurs at point P, in the weld material, then the equations of global equilibrium can be expressed as follows

$$\frac{F_y}{2} = 2k_b x\cos\left(\pi/4+\gamma\right) + \frac{k_b\left(1+2\gamma\right)x}{\sin\left(\pi/4+\gamma\right)} + k_w H + \frac{\sigma_w{}^* H}{\tan\left(\pi/4+\gamma\right)} \tag{6.11}$$

$$\frac{F_x}{2} = \frac{-k_b x\sin 2\gamma}{\sin\left(\pi/4+\gamma\right)} + \frac{k_w H}{\tan\left(\pi/4+\gamma\right)} - \sigma_w{}^* H = 0 \tag{6.12}$$

Thus, if the equivalence of MUB theorem and SLF analysis is assumed to hold good for a M(T) specimen also then the value of assumed plastic field parameters (x and γ) obtained from the MUB theorem may be used to obtain σ_w^* from eq. (6.12). As a cross check, the value of σ_w^* was substituted in eq. (6.11) to confirm that the limit load so obtained is quite close to that obtained directly from the MUB theorem. This again has validated our assumption that for the case of a strength mismatch weld also (having two different material interfaces) the parameters of plastic field as obtained from MUB theorem also satisfies the global equilibrium equations.

As discussed in chapter 5, from the stress distribution so obtained the state of stress ahead of crack tip can not be directly evaluated. A construction similar to that shown in Fig. 5.4 was used to evaluate the crack tip stress distribution. Thus, the mean (hydrostatic) stress, directly ahead of crack tip, can be expressed as follows.

$$\sigma^X = \sigma^B = \sigma_w^* + 2k_w\gamma \qquad (6.13)$$

The crack tip constraint parameter *h* (eq. 5.15) was used to describe the effect of weld strength mismatch on the local stress tri-axiality.

6.3 Analysis of undermatched middle tension M(T) specimen having a weld centre crack

For a M(T) specimen having a crack at the centre of an undermatched weld, in general, plasticity passes through both base and weld material. Detailed FE analyses performed by the author revealed that in comparison to an overmatch case the global stress fields for an undermatch case are more complex. No detailed global stress field could be developed for such a case. Limit load solution for such cases were obtained using the simple kinematically admissible velocity field that was first proposed by Joch et al. (1993).

However, it is important to mention that such simplified velocity field can not be used for evaluation of crack tip constraint as it has not been demonstrated that the global equilibrium equations are satisfied.

When the yield strength of weld material is sufficiently low (with respect to base metal), the entire plastic deformation gets confined in the weaker weld material and, thus, the weld slenderness ratio ψ is the only important parameter affecting the plastic deformation. For such cases Hao et al. (1997) proposed slip line fields for various values of ψ and obtained analytical solution of the limit load and crack tip constraint parameter *h*. The case of extreme undermatch was also analysed by Kim and Schwalbe (2001a). Based on SLF analyses a different expression of the limit load was proposed, however, no details of solution were provided. It was discussed that their solutions provide slightly different value of the limit load than that suggested by Hao et al. (1997).

In the following sections detailed analyses of the proposed slip line fields for the case of a M(T) specimen having a crack at the centre of an extreme undermatch weld are presented. The proposed fields were used to obtain analytical solutions of the limit load and crack tip constraint parameter *h*.

6.3.1 **Slip Line Field-1** ($1 \leq \psi \leq 3.6$)

The complete structure of the proposed field is shown in Fig. 6.3. At point C lying at the base-weld interface, near the free surface, it was assumed that a singularity exist and the stress distribution in the plastic sector BCD is described by a fan field of radial extent *x* and angular extent γ. Adjacent to the fan field is the constant stress region CED in which a uniform tensile stress of magnitude *2k* exists. It is assumed, asymptotically, that a small segment of straight slip line AA' exists. It radiates from the crack tip at an angle of π/4 with the horizontal axis. The fan field BCD is connected to the straight slip line AA' by a circular arc A'B of radius *y* and angular extent γ. The stress components on the small line AA' are constant and equal to the components at the point A' on the arc A'B. The global stress field is completely described by the three unknown parameters, that is, *x*, *y*, and *γ*.

It can be easily established that ABC is an α-slip line and the mean (hydrostatic) stress at point B is $k(1+2\gamma)$. From Hencky's relation, the hydrostatic stress at point A' can be expressed by the following equation

$$\sigma_w^{A'} = k_w\left[\left(1+2\gamma\right)-\frac{\pi}{2}+2\left(\frac{\pi}{4}+\gamma\right)\right] \tag{6.14}$$

From geometry the following two relations can be easily obtained

$$y\left[\cos\left(\frac{\pi}{4}-\gamma\right)-\frac{1}{\sqrt{2}}\right]+x\sin\left(\frac{\pi}{4}-\gamma\right)=H \tag{6.15}$$

$$y\left[\frac{1}{\sqrt{2}}-\sin\left(\frac{\pi}{4}-\gamma\right)\right]+x\cos\left(\frac{\pi}{4}-\gamma\right)=l \tag{6.16}$$

The remaining third equation can be obtained from the equilibrium consideration, that is

$$\sum F_x = \int_{ABC} \sigma_{1i} n_i dS = 0 \tag{6.17}$$

Eqs. 6.15-6.17 may be used to obtain the values of the three unknown parameters of the plastic field and the stress distribution in the plastic sectors can be easily evaluated. The resulting limit load can be obtained from the following expression

$$\sum F_y = \int_{ABC} \sigma_{2i} n_i dS = 0 \tag{6.18}$$

Once the hydrostatic stress at point A' is known, the crack opening stress directly ahead of crack tip can be obtained from the following relation

$$\sigma_{\theta\theta}\big|_{\theta=0} = \sigma_w^{A'} + k_w \tag{6.19}$$

It is worth to mention that the proposed slip line field is applicable for $1 \leq \psi \leq 3.6$. As the weld slenderness ratio ψ increases the angle γ describing the angular extent of fan field BCD increases. This results in a increase of hydrostatic stress at point *A* near the crack tip. When ψ=3.6, the angle γ becomes equal to $\pi/4$ and the hydrostatic stress ahead of crack tip is high enough to cause complete yielding of the crack tip and the Prandtl's field develops.

6.3.2 **Slip Line Field-2** ($3.6 \le \psi \le 5$)

The construction of this field is guided by the consideration that for $\psi \ge 3.6$, the stress tri-axiality ahead of crack tip is sufficient enough to cause complete yielding of the crack tip. As a result the asymptotic distribution of stresses near the crack tip can be completely described by the Prandtl field which extends up to a distance z from the crack tip in the radial direction as shown in Fig. 6.4. At point J lying at the base-weld interface, near the free surface, it is assumed that a singularity exist and the stress distribution in the plastic sector EFJ is described by a fan field of radial extent x and angular extent of $\pi/4$. Adjacent to the fan field is the constant stress region JFG in which a uniform tensile stress of magnitude $2k$ exists. The fan field EFJ is connected to the Prandtl field by a circular arc DE of radius y that intersects the horizontal axis at an angle of $\pi/4$. The radial extent of the Prandtl field is described by z. The global stress field is, thus, completely described by the three unknown parameters, that is, x, y, and z.

From Hencky's relation, the hydrostatic stress at point D can be expressed by the following equation

$$\sigma_w^D = k_w \left(1 + \pi\right) \tag{6.20}$$

Eq. (6.20) indicates that the stress distribution at point D is the same as that obtained from the Prandtl field. The crack opening stress directly ahead of crack tip in the Prandtl field can be expressed as

$$\sigma_{\theta\theta}\big|_{\theta=0} = \sigma_w^D + k_w = k_w\left(2+\pi\right) \tag{6.21}$$

Now from geometry the following two relations can be easily obtained

$$y\left[1-\frac{1}{\sqrt{2}}\right] = H \tag{6.22}$$

$$\frac{2z}{\sqrt{2}} + \frac{y}{\sqrt{2}} + x = l \tag{6.23}$$

The equilibrium equation in horizontal direction remain same as expressed by eq. (6.12) as the presence of Prandtl field near the crack tip does not effect the force equilibrium in X-direction. Thus, eqs. (6.17), (6.22) and (6.23) may be used to evaluate the unknown parameters of the plastic field and, hence, the stress distribution in the plastic regions. The resulting limit load can be obtained from the following expression.

$$\sum F_y = \int_{DEJ} \sigma_{2i} n_i dS + \sqrt{2}\left(2+\pi\right)k_w z \tag{6.24}$$

As the weld slenderness ratio ψ increases the size of the Prandtl field near the crack tip, as measured by the distance z, increases monotonically and at ψ=5 the Prandtl field just touches the base-weld interface. For $\psi \geq 5$ the stress fields of the weld zone become complicated and numerical construction of slip line fields is required. Slip line fields for such cases were constructed by Hao et al. (1997), and Kim and Schwalbe (2001a).

6.4 Results

For the case of M(T) specimen having a weld centre crack the limit load solutions have been provided by various authors. However, the solutions provided by Kim and Schwalbe (2001a) which are based on detailed FE analysis are most accurate and are widely accepted. Thus, in the present study analytical solutions of the limit load obtained from MUB theorem were compared with detailed FE analyses performed by the author and with the solutions provided by Kim and Schwalbe (2001a) as shown in Fig. 6.5. As mentioned earlier, analytical solutions of the limit load based on continuity of tractions at the base-weld interface were proposed by Hao et al. (1997). A comparison of their limit load solutions with FE results is shown in Fig. 6.6. In Figs. 6.5 and 6.6, the normalised limit load represent the ratio of limit load of M(T) specimen having a weld centre crack to that of homogeneous M(T) specimen. It may be observed from Fig. 6.6 that as the weld strength mismatch ratio M increases the difference between the limit load solutions of Hao et al. (1997) and FE results becomes higher. This actually suggests that the assumption of continuous stress solution is not valid particularly for higher mismatch ratios. On the other hand the limit load obtained from MUB theorem is in very good agreement with FE results (see Fig. 6.5) for all mismatch ratios. In Fig. 6.7 analytical solution of crack tip constraint parameter h obtained from MUB theorem is compared with FE results of Kim and

Schwalbe (2004). For an extremely undermatched M(T) specimen having a weld centre crack analytical solutions of crack tip constraint parameter *h* obtained from the proposed slip line fields were compared with the solutions provided by Kim and Schwalbe (2004) in Fig. 6.8. Very good agreement was obtained between the two solutions.

6.5 Discussion

In this chapter analytical solutions of the limit load and crack tip constraint parameter *h* for a rigid-plastic material under mode-I loading were described. For standard homogeneous fracture specimens MUB theorem provides results that are in exact agreement with SLF solutions. Classical methods like SLF analysis are, however, applicable to macroscopically homogeneous/single material. Welded structures have an abrupt material discontinuity at the base weld interface. Constructing SLF solutions for such problems is not straightforward as the stress connections conditions at the interface are unknown. Detailed FE analysis performed by Hao et al. (1997) and Kim and Schwalbe (2001a) have revealed that SLF solutions based on continuity of stress at base-weld interface are not in good agreement with FE results. In this chapter MUB theorem was successfully used to obtain analytical solution of the limit load and crack tip constraint parameter *h* for M(T) specimen having a weld centre crack. At this point it is worth to discuss that while the analytical solutions of the limit load obtained from MUB theorem are in excellent agreement with the widely accepted solutions of Kim and Schwalbe (2001a) and detailed FE results performed by the author, however, analytical results of crack tip constraint parameter *h* do not show such a good match with FE solutions. Such kind of differences in the crack tip stresses obtained from SLF analysis and FE results have also been observed for a homogeneous M(T) specimen (Zhu and Chao, 2000). These authors performed detailed FE studies and observed that there exist tensile and compressive stresses along the vertical centerline of M(T) specimen which result in a bending moment M_V. The difference between M_V and the moment generated by the applied far-field load makes the crack opening stress non-uniform along the remaining ligament. However the slip line field for M(T) specimen (McClintock, 1971) comprises of a constant stress sector creating uniform opening stress along the ligament. These authors, thus, concluded that at the limit load the crack tip stress fields obtained from FE analysis can only approach to, but cannot attain to, the slip-line fields of homogeneous M(T) specimen. A closer look of Fig. 6.7 reveals that for higher weld overmatch ratios ($M \rightarrow 2$), FE results were close to analytical solutions, however, as M approaches unity (homogeneous case) difference between FE results and analytical predictions increases as noted by Zhu and Chao (2000).

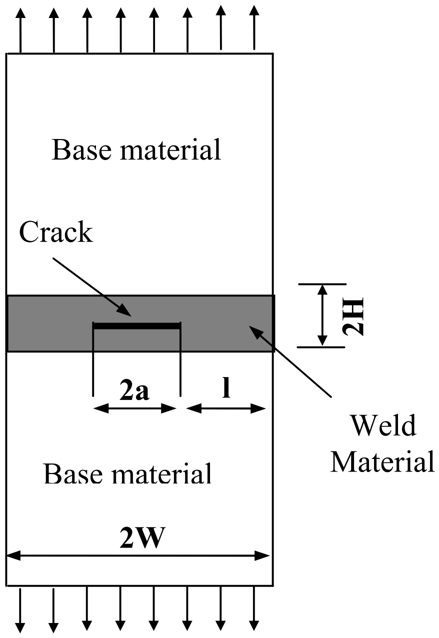

Fig. 6.1: Middle tension M(T) specimen having a weld centre crack.

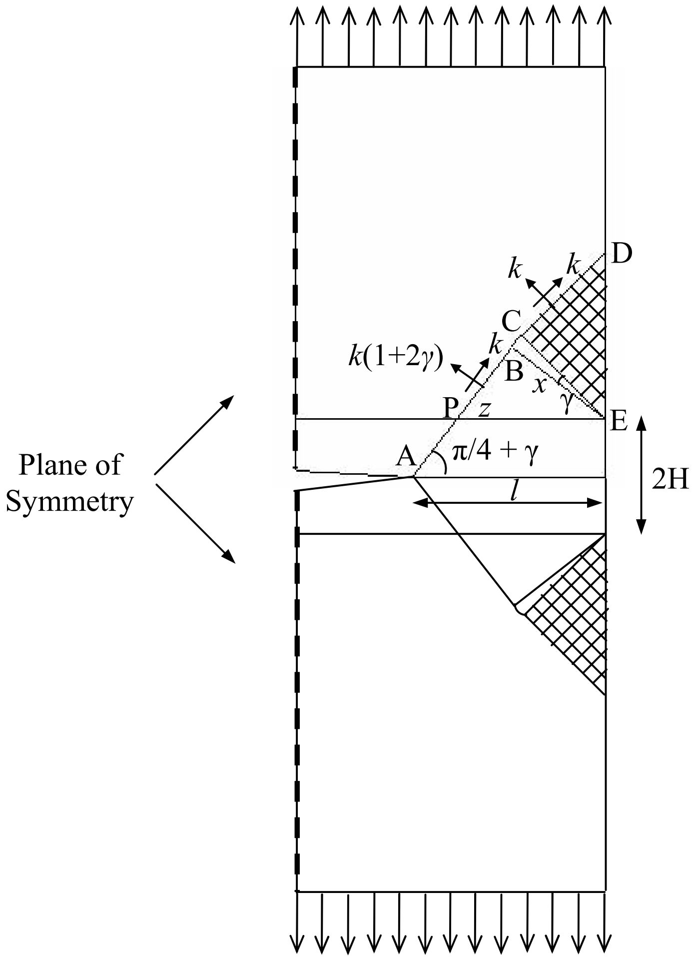

Fig. 6.2 (a): Proposed stress field for an overmatched M(T) specimen having a weld centre crack.

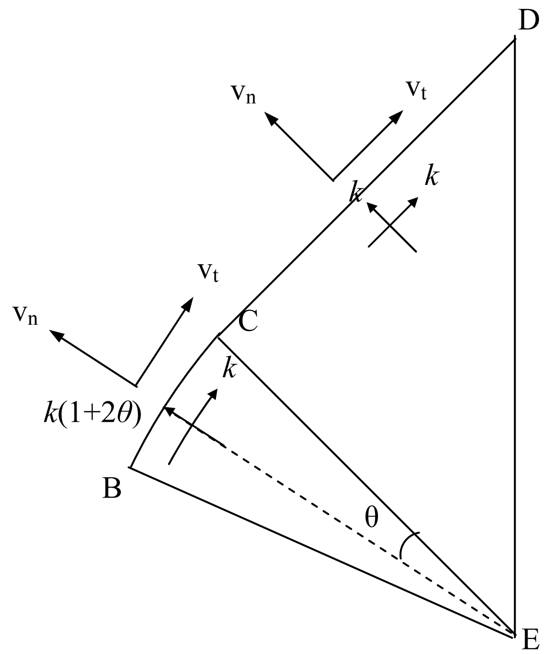

Fig. 6.2 (b): Stress and velocity distribution on the elastic-plastic boundary of an overmatched M(T) specimen having a weld centre crack.

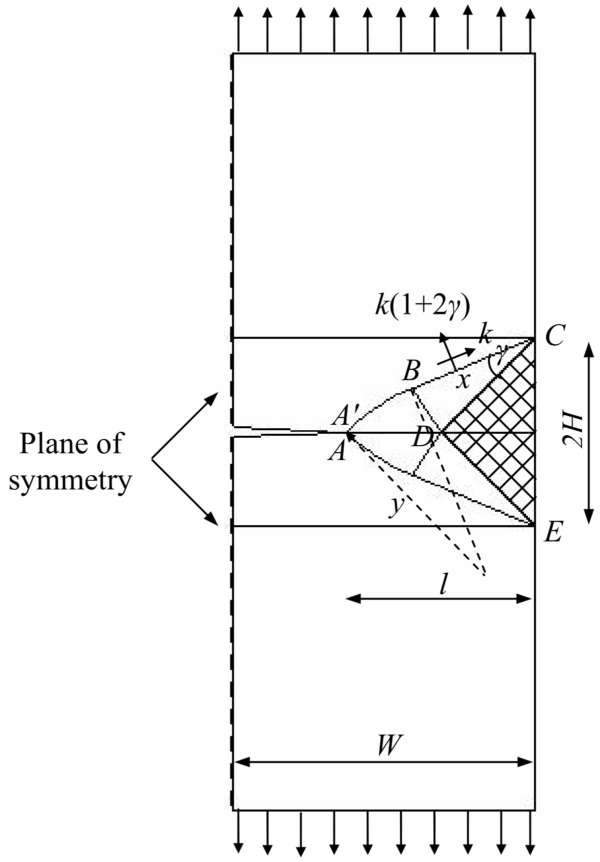

Fig. 6.3: Proposed slip line field of extremely undermatched M(T) specimen having a weld centre crack ($1 \leq \psi \leq 3.6$).

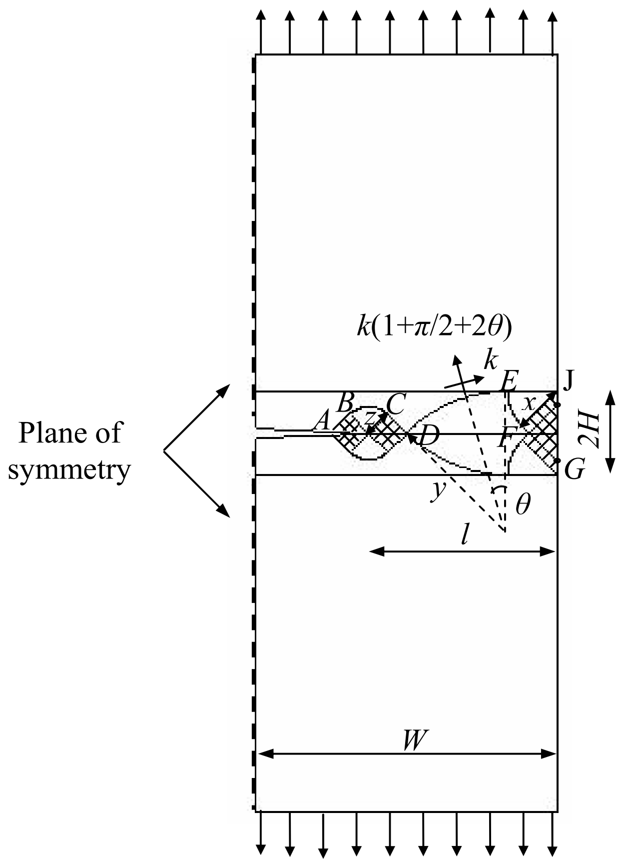

Fig. 6.4: Proposed slip line field of extremely undermatched M(T) specimen having a weld centre crack ($3.6 \leq \psi \leq 5$).

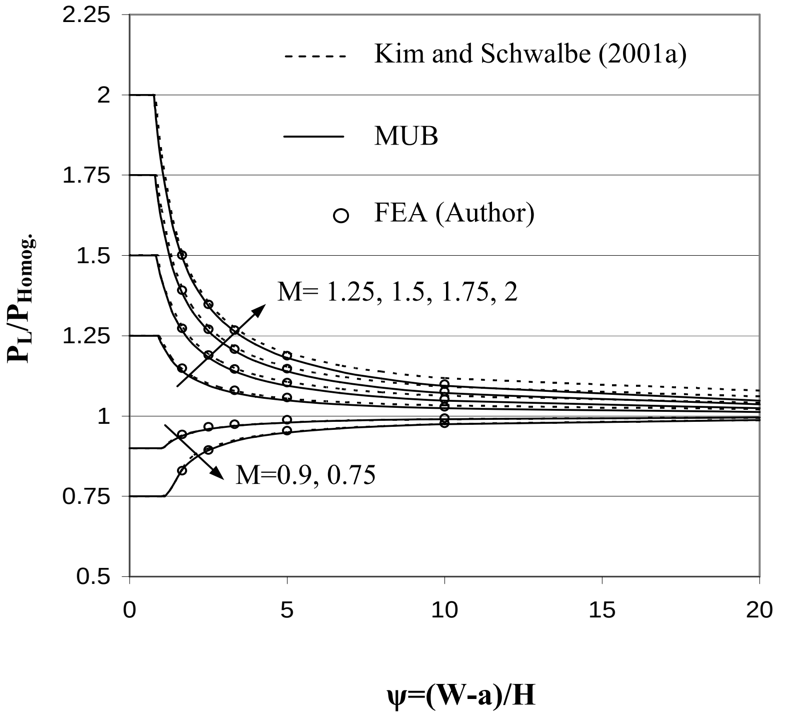

Fig. 6.5: Comparison of normalised limit load of M(T) specimen, having a weld centre crack, obtained from MUB theorem with FE results.

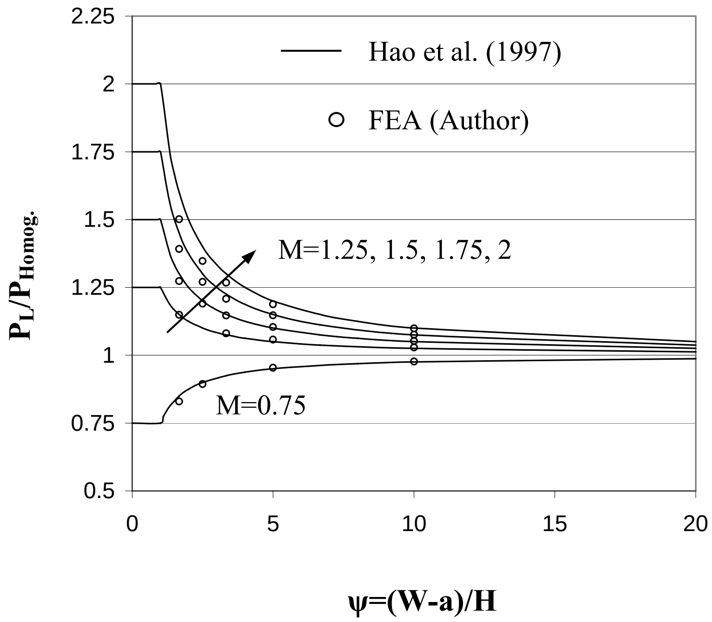

Fig. 6.6: Comparison of normalised limit load of M(T) specimen, having a weld centre crack, provided by Hao et al. (1997) with author's FE results.

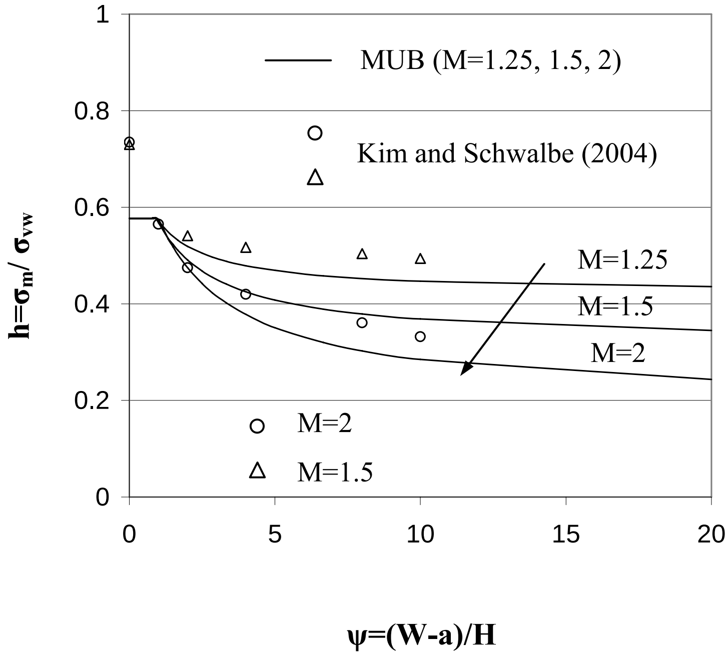

Fig. 6.7: Comparison of crack tip constraint parameter *h* of overmatched M(T) specimen obtained from MUB theorem with FE results.

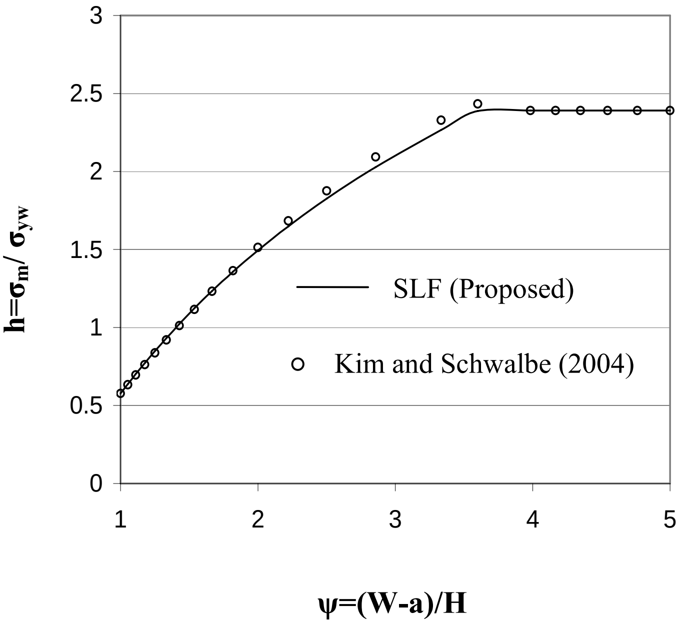

Fig. 6.8: Comparison of crack tip constraint parameter *h* of extremely undermatched M(T) specimen obtained from proposed SLF with FE results.

CHAPTER 7

Aspects related to plastic η factor of plane strain fracture specimens having weld centre crack

7.1 Introduction

The evaluation of fracture toughness is an integral part of structural integrity assessment procedures which are based on fracture mechanics concepts. In fact, fracture toughness essentially provides the criterion through which the severity of crack like flaws can be related to the operating conditions in terms of a critical applied load or a critical crack size. Fracture toughness, in terms of J-integral, is measured using the experimental load-load line displacement (LLD) data and a proportionality factor, often referred as the plastic η-factor (Rice et al., 1973). These authors proposed to split the total J-integral into elastic (J_e) and plastic components (J_p). While the elastic part J_e is related to the Stress intensity factor (K), the plastic part J_p is associated with the plastic area under the load-displacement data obtained from experiments, Fig. 7.1a, as described by the following equation

$$J = J_e + J_P = \frac{K^2}{E'} + \eta_P \int_0^{\Delta_P} P d\Delta_P \tag{7.1}$$

Here E' = E for plane stress and E' = E/(1-ν^2) for plane strain condition. ν is the Poisson's ratio, P is the total applied load and Δ_p is the plastic component of load line displacement due to crack only.

Recently it has been observed that the J-integral estimated from experimental crack mouth opening displacement (CMOD) records provide more robust and accurate J-estimation, particularly for shallow cracked geometries (Wang and Gordon, 1992, Kim and Schwalbe, 2001d). Moreover, the measurement of CMOD is more robust and easier than that of LLD. The expression used to evaluate J-integral from CMOD data is as follows

$$J = J_e + J_P = \frac{K^2}{E'} + \eta_P^{CMOD} \int_0^{\Delta_P^{CMOD}} P d\Delta_P^{CMOD} \tag{7.2}$$

Here Δ_p^{CMOD} is the plastic component of CMOD (Fig. 7.1b). Existing fracture testing standards like ASTM E-1820 are mainly applicable to fracture specimens made of homogeneous materials. In order to assess fracture behaviour of a cracked welded structure accurate estimation formulas for fracture toughness evaluation, which can account for weld strength mismatch effects, are required.

Analytical studies to quantify the effect of weld strength mismatch on plastic η-factors were performed by Joch et al. (1993) and Burstow and Ainsworth (1995). Sumpter (1987) presented a method for determination of fracture toughness J_c from three-point bend specimen having a shallow crack using load versus CMOD data. Based on analytical considerations Hornet and Eripret (1995) proposed a new procedure for evaluation of fracture toughness from the area under the load versus CMOD curve. Gordon and Wang (1994) suggested an expression for CMOD based plastic η-factor incorporating the weld strength mismatch effect using FE analyses. The effect of weld strength mismatch on plastic η-factor of fracture specimens having weld centre crack was also examined by Kim et al. (2003). In a recent study, Dunato et al. (2009) examined the effect of weld strength mismatch on fracture toughness parameters such as J and CTOD for three-point bend specimen. All these analytical and numerical investigations revealed that the weld strength overmatch (M>1) would reduce the plastic η-factors below that of standard homogeneous specimens while under match welds lead to higher plastic η-factors.

In this chapter analytical solutions of plastic η-factor are developed using the accurate limit load solutions proposed in chapter 5 and 6. Pure bending specimen, SE(PB), Compact tension specimen, C(T) and middle tension specimen, M(T) having weld centre crack were considered. The effects of strength mismatch ratio M and weld slenderness ratio ψ on plastic η-factor are discussed.

7.2 Analytical evaluation of plastic η-factor

The computation of plastic η-factor for evaluation of plastic part of J-integral, J_p, requires a limit load expression. Ernst et al. (1979) have shown that η_p will always exist if and only if a separation of variables can be found for the expression of load P in terms of crack length a and plastic load-line displacement Δ_p. If it is assumed that the material behavior can be represented as ideal-plastic then under conditions of constant load-line displacement, a straight forward derivation based on the general definition of J-integral provides following expression (Roos et al. , 1986, Chattopadhyay et al. , 2001)

$$\eta_P = \frac{-1}{P_L}\left(\frac{\partial P_L}{\partial a}\right) \tag{7.3}$$

By this expression η_p can be calculated in principle if the limit load equation as a function of crack size *a* is available. It is important to note that the limit load as mentioned in the above equation corresponds to the global limit load. Chattopadhyay et al. (2001, 2004) conducted further studies and obtained limit load based general expression of γ-factor (correction factor to account for crack growth). Using the limit load based expressions these authors derived plastic η_p and γ factors for various geometries of practical interest. The η_p^{CMOD} solution can also be obtained from limit analysis using the following expression

$$\eta_P^{CMOD} = f\left(\frac{a}{W}, r_p\right)\eta_P \tag{7.4}$$

Here r_p denotes the plastic rotation factor and can be obtained from the limit analysis. The explicit form of the function f (a/W, r_p) depends on the geometry of the specimen (Kim, 2002b).

7.3 Numerical evaluation of plastic η-factor

Analytical solutions of plastic η-factors (both LLD and CMOD based) obtained from limit analyses are applicable to a rigid-plastic (non-hardening) material model. In order to assess the influence of material strain hardening on plastic η-factors, finite element analysis is required. The J-integral can be easily obtained using the post-processing techniques (like Rice's contour integral, Virtual crack extension method, or domain integral method) which are typically available in all commercial finite element codes. In addition, the FE results provide other required data like load-LLD and load-CMOD values from which the plastic η-factors can be computed using the estimation formulae (eqs. 1 and 2). Further details on calculation of plastic η-factors from FE results are available in Kim (2002b). Detailed finite element studies have revealed that for homogeneous fracture specimens the effect of material strain-hardening on plastic factors is weak (Kim and Schwalbe, 2001e).

7.4 Analytical solutions of plastic η-factor of plane strain fracture specimens having weld centre crack

The limit load based general expression of plastic η-factor (eq. 7.3), derived for homogeneous fracture specimens, is applicable for fracture specimens having strength mismatch weld provided the limit load formulas accounting weld mismatch effects are used (Kim et al., 2003). In chapter 5, MUB theoremwas used to derive analytical expression of the limit moment/load for SE(PB) and C(T) specimen having weld centre crack. Similar limit load expressions were obtained for M(T) specimen having weld centre crack in chapter 6. These limit load expressions were substituted in eq. (7.3) to obtain plastic η-factor (LLD based) for the above-mentioned fracture specimens. Numerical differentiation, using central difference scheme, is used to approximate the first order derivative of limit load with respect to crack size. Apart from limit load, MUB theorem also provides parameters describing the plastic field from which the plastic rotation factor

r_p can be easily obtained. The CMOD based plastic η-factor can then be obtained using eq. (7.4).

7.5 Results

For a pure bending SE(PB) specimen having a weld centre crack the expression of LLD and CMOD based plastic η-factors were obtained as discussed in section 7.4. Comparison of analytical solutions of LLD and CMOD based plastic η-factors with finite element results, obtained by the author, is shown in Figs. 7.2 and 7.3 respectively. Analytical solutions of plastic η-factor for a compact tension C(T) specimen and a middle tension M(T) specimen having weld centre crack were obtained in a similar manner. It may be noted that for a C(T) specimen there is essentially no difference between LLD and CMOD. The effect of weld strength mismatch on plastic η-factor of fracture specimens having weld centre crack was also examined by Kim et al. (2003). These authors used detailed FE analyses to incorporate strength mismatch effects on plastic η-factor. Comparison of proposed plastic η-factors for a C(T) specimen and M(T) specimen with finite element results of Kim et al. (2003) is shown in Fig. 7.4 and Fig. 7.5 respectively.

7.6 Discussion

In this chapter analytical solutions of plastic η-factor are proposed for a SE(PB), C(T) and M(T) specimen having a weld centre crack. The effect of weld strength mismatch ratio M and weld slenderness ratio ψ on plastic η-factor was systematically examined. The proposed solutions of plastic η-factor obtained from MUB theorem were compared with finite element results obtained by the author and those of Kim et al. (2003). In all cases *a/W* was kept as 0.5. Although the analytical limit moment/load solutions were in good agreement with those obtained from FE analysis (see chapter 5 and 6), the analytical solutions of plastic η-factor did not show such a good agreement. The maximum difference noted was about 12%, however, the overall trend was correct. At this point it is worth to mention that Kim et al. (2003) have also presented comparison of plastic η-factors obtained from FE limit load solutions with those obtained directly from detailed FE analysis and similar sort of differences were observed. This does not mean that either the proposed limit load solutions or their partial derivative with respect to crack size are not accurate. This difference may be due to the inherent assumption of load separation criterion that is used to evaluate plastic η-factor from limit load solution, using eq. (7.3).

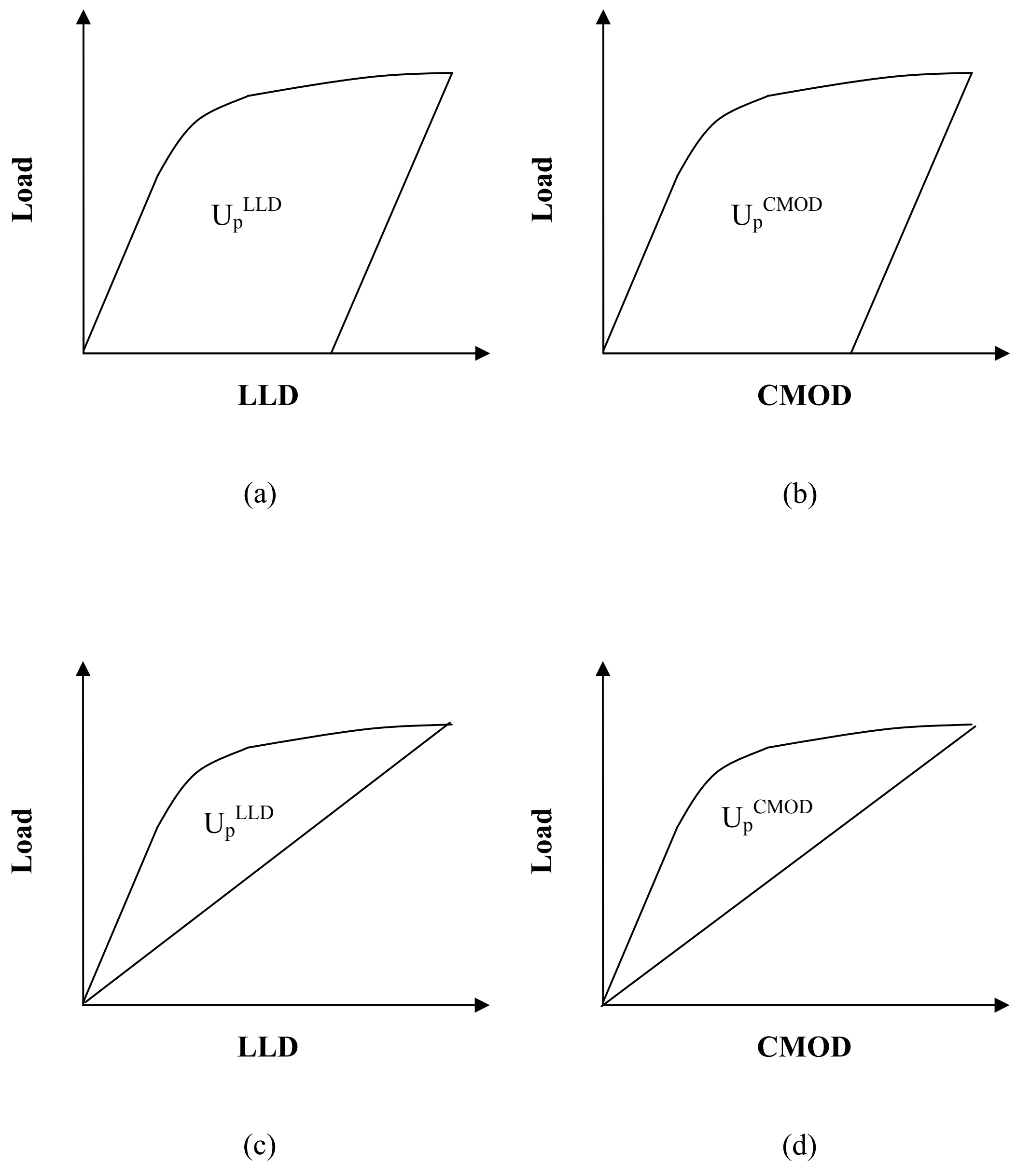

Fig. 7.1: Determination of area under experimental load-displacement records for J-estimation (a and b) plastic area for SE(PB) and C(T) specimens, (c and d) plastic area for M(T) specimen.

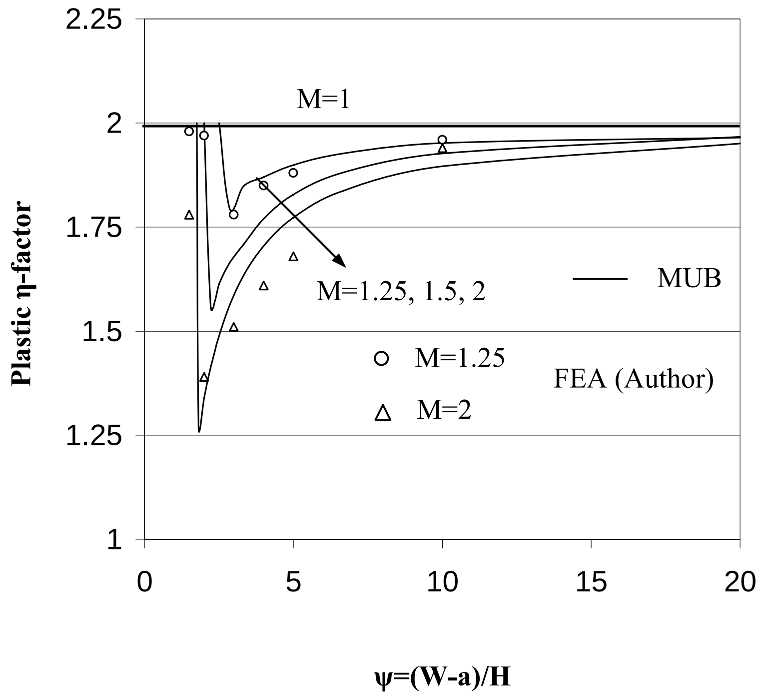

Fig. 7.2: Comparison of LLD based plastic η-factor of SE(PB) specimen having a weld centre crack obtained from MUB theorem with FE results.

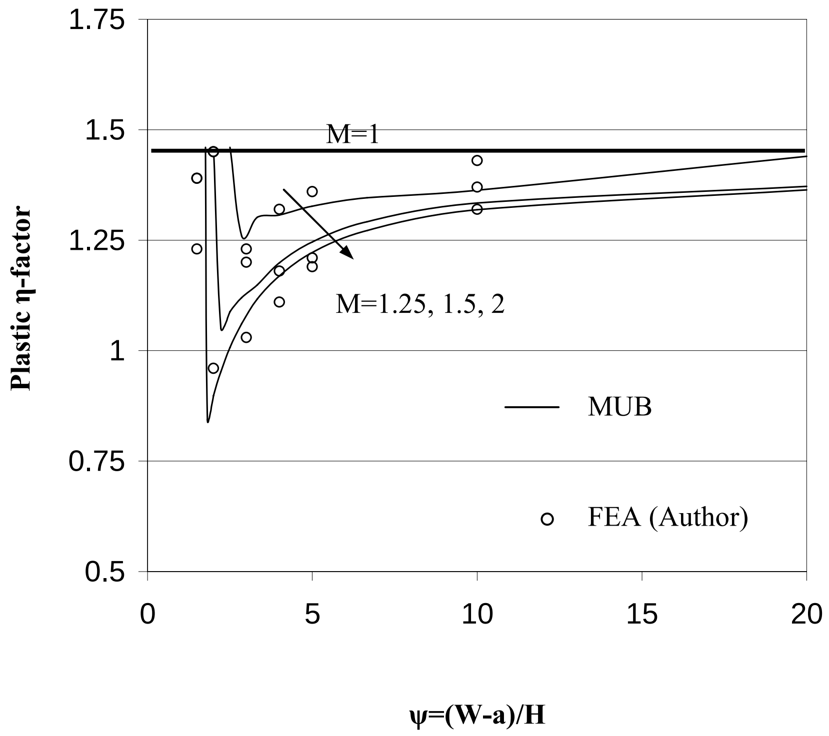

Fig. 7.3: Comparison of CMOD based plastic η-factor of SE(PB) specimen having a weld centre crack obtained from MUB theorem with FE results.

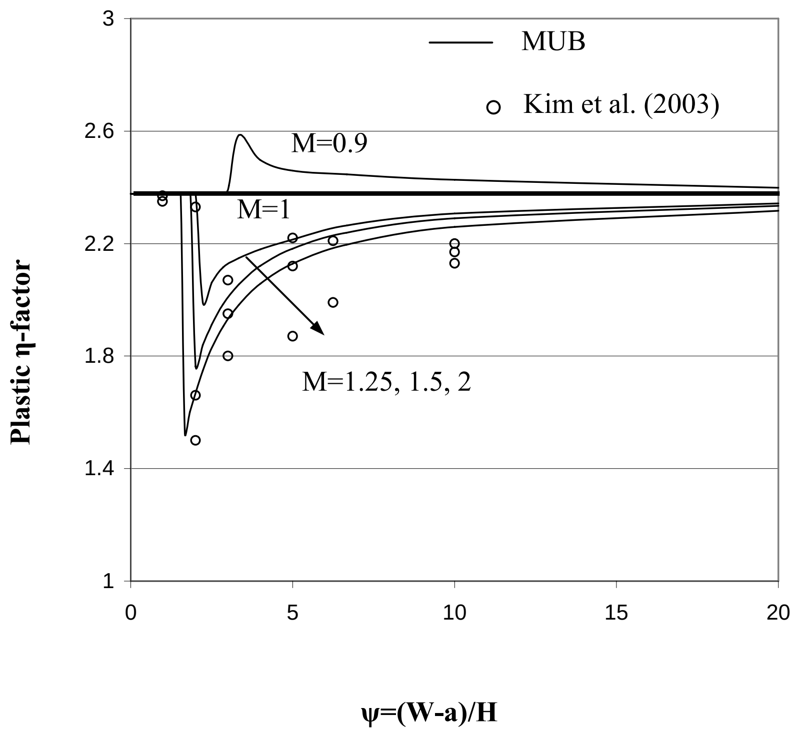

Fig. 7.4: Comparison of CMOD based plastic η-factor of C(T) specimen having a weld centre crack obtained from MUB theorem with FE results of Kim et al. (2003).

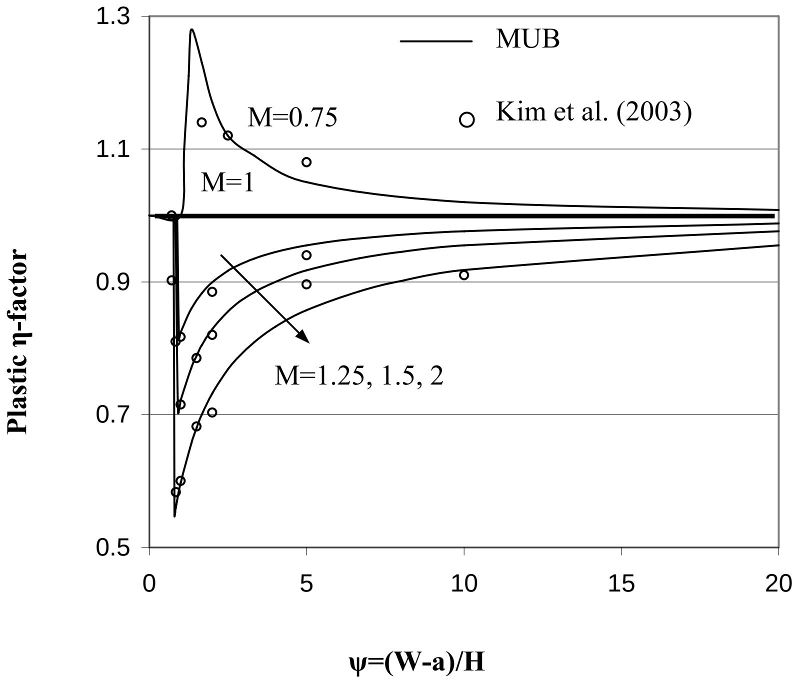

Fig. 7.5: Comparison of CMOD plastic η-factor of M(T) specimen having a weld centre crack obtained from MUB theorem with FE results of Kim et al. (2003).

CHAPTER 8

Characterisation of crack tip stresses in elastic-perfectly plastic material under mode-I loading

8.1 Introduction

Characterisation of crack tip stresses has been an area of active research for many decades. Williams (1957) in his landmark paper showed that the crack tip stress fields in an isotropic elastic material can be expressed as an infinite series where the leading term exhibit a $1/\sqrt{r}$ singularity and the second term is independent of r. Classical fracture mechanics theory neglects all but the singular term and, thus, came the concept of characterisation of crack tip stresses by a single parameter. Although the third and higher order terms of the Williams's series vanish near the crack tip, the second term (that is constant) remains finite and has a strong effect on the stresses in the plastic zone. This second term has been referred in the literature as T-stress. The single parameter characterisation is rigorously correct only for $T > 0$. It is important to note that T-stress is an elastic parameter and has no physical meaning under large scale plasticity. Then, assuming small-strain formulation, Hutchinson (1968), Rice and Rosengren (1968) proposed the dominant term of the singularity field (often referred as HRR solution) for plane strain mode-I crack based on the J-integral (Rice, 1968). Thus, the HRR singularity is the natural extension of one-parameter characterisation concept to a non-linear elastic material. However, it has been realized that the specimen geometry and loading conditions significantly affect the crack tip fields and, thus, the HRR field have limited application to real cracked structures. For a Ramberg-Osgood material model, the crack tip fields in the plastic zone can be expressed in terms of a power series where the HRR solution is the leading term. The higher order terms of this power series were grouped together and its amplitude was denoted as Q by O'Dowd and Shih (1991). Other representative two-parameters that are used to characterise the crack tip stress fields are J-T of Betegon and Hancock (1991) and J-A_2 of Chao et al. (1994).

For a rigid plastic material (non-hardening), slip line fields (SLF) have been extensively used to estimate crack tip stresses in fully plastic state under plane strain condition. Results indicate that for a non-hardening material, under fully-yielded condition, the stresses near the crack tip are not unique but a strong function of specimen geometry and loading condition. An excellent compilation of the various SLF solutions has been given by McClintock (1971). For high constraint geometries like deeply cracked Double Edge Crack Plate in tension (DECP) plasticity completely surrounds the crack tip (Prandtl field) and SLF analysis can be used to obtain crack tip stress distribution over all angles. However, when constraint at the crack tip is not high-enough to cause tensile yielding of the crack flank then an elastic sector appears there (not in all cases as would be discussed later) and SLF analysis can only describe the state of stress in the plastic sectors ahead of the crack tip.

Apart from analytical studies (SLF analysis) detailed numerical (finite element) investigations have been performed to evaluate crack tip stress fields in non-hardening material. For small-scale yielding, Du and Hancock (1991) examined the effects of elastic T-stress on crack tip stress fields for mode-I crack under plane strain condition. They provided an explanation to the existence of incomplete crack tip plasticity in terms of *T*-stress. Under large-scale yielding Lee and Parks (1993) analysed single edge cracked specimen subjected to combined bending and tension. Kim et al. (1996) and Zhu and Chao (2000) performed detailed FE analyses of SENB, M(T) AND DECP specimens. Further comments can be seen in Zhu and Chao (2001). It is important to understand that the two-parameters such as J-Q or J-A_2 characterisation cannot describe the state of stress in the elastic sector near the crack flanks.

To construct the general elastic-plastic crack tip stress field Ibrgimov and Tarasyuk (1976) and Nemat-Nasser and Obata (1984) first discussed the possibility of existence of elastic sector for plane strain mode-I crack in elastic-perfectly plastic material. Then, Li and Hancock (1991) described the crack tip fields under small-scale yielding in terms of plastic sectors and an elastic sector to account for the incomplete crack tip plasticity observed from detailed FE investigations. More details about elastic-plastic crack tip stress fields under mode-II and mixed-mode loading can be found in Zhu and Chao (2001). In the asymptotic solution, Li and Hancock (1991) assumed three different stress sectors near the crack tip, that is, a constant stress sector (plastic), a fan field (plastic) followed by an elastic stress sector near the crack flank. Their 3-sector solution was extended by Zhu and Chao (2001) who, based on available FE results of Kim et al. (1996), Zhu and Chao (2000), proposed that the actual stress field of a stationary crack in elastic-perfectly plastic material under plane strain condition can be described by a 4-sector solution. Closed-form asymptotic solutions of crack tip fields were developed by them. Two undetermined parameters; T_p and T_π were proposed to characterise the state of stress near the crack tip.

The proposed asymptotic solutions were compared with detailed FE results for various fracture specimens with constraint level ranging from high to low.

In this chapter asymptotic crack tip stress fields were developed for a stationary plane strain crack under mode-I loading. Incompressible, elastic-perfectly plastic material with Von-Mises yield criterion was assumed for the present study. Detailed investigations have revealed that in between the two extreme conditions of crack tip constraint, that is, between the fully plastic Prandtl field and the uniform stress field the general elastic-plastic crack tip fields can be completely described by the 5-sector stress solution. The 4-sector field proposed by Zhu and Chao (2001) is a subset of the general elastic-plastic field proposed in this work. It is well known that loss of constraint at the crack tip leads to an elastic sector at the crack flank, thus, leading to incomplete crack tip plasticity. This study has revealed that cases arise where severe loss of crack tip constraint can lead to compressive yielding of crack flank. This particular situation leads to 5-sector stress field where the elastic sector is sandwiched between the two plastic sectors of uniform stress state. Such 5-sector stress field exists in an overmatched weld where the relatively higher strength of weld leads to shielding effect on the crack tip and, thus, leads to loss of crack tip constraint. Detailed 2-D elastic plastic finite element analyses were performed on middle tension M(T), pure bending SE(PB) and C(T) specimens having a weld centre crack to examine the validity of the proposed 5-sector stress field. Both under matched and over matched cases were analysed to simulate a wide range of crack tip constraint. Excellent agreement was obtained between the proposed asymptotic crack tip stress field and finite element results. Detailed studies have revealed that, in the general case of elastic plastic crack tip fields, the T_{π} parameter proposed by Zhu and Chao (2001) cannot be used as a constraint parameter to represent a unique state of stress at the crack tip. A new constraint-indexing parameter T_{CS-2} is proposed which along with T_p parameter, suggested by Zhu and Chao (2001), is capable of representing the entire elastic plastic crack tip stress fields over all angles around a crack tip. Advantages of the proposed T_{CS-2} parameter over the T_π parameter are discussed. It is demonstrated that the proposed constraint parameters are adequate to represent the crack tip constraint arising due to specimen geometry and loading conditions as well as additional constraint that arises due to weld strength mismatch.

8.2 Governing equations

We consider here a stationary crack in an incompressible elastic-perfectly plastic material under plane strain condition. Zhu and Chao (2001) have concluded that constraint has no effect on the stress state ahead of the crack tip for a mode-II crack in an elastic-perfectly plastic material. A similar conclusion was made by Chao and Yang (1996) for a power-law hardening material. In view of the above-mentioned conclusions, only mode-I loading is considered here.

8.2.1 Equilibrium equations

For elastic-perfectly plastic material numerical results of Dong and Pan (1990) have established that that all stress components near the crack tip are bounded and are, thus, functions of polar angle θ only. The equilibrium equations, thus, reduces to ordinary differential equations and can be expressed in polar co-ordinate system, centred at the crack tip, in the following form

$$\frac{d\sigma_{r\theta}}{d\theta}+\sigma_{rr}-\sigma_{\theta\theta}=0 \tag{8.1a}$$

$$\frac{d\sigma_{\theta\theta}}{d\theta}+2\sigma_{r\theta}=0 \tag{8.1b}$$

8.2.2 Plane strain condition

If the elastic response of the material is considered as incompressible then due to constancy of volume in plastic deformation the body is fully incompressible. Thus, plane strain condition is same for both elastic and plastic sectors and can be expressed as

$$\sigma_{33}=\frac{1}{2}\left(\sigma_{11}+\sigma_{22}\right)=\frac{1}{2}\left(\sigma_{rr}+\sigma_{\theta\theta}\right) \tag{8.2}$$

8.2.3 Yield criterion

The Von-Mises yield criterion for plane strain condition can be expressed as

$$\frac{1}{4}\left(\sigma_{rr}-\sigma_{\theta\theta}\right)^{2}+\sigma^{2}{}_{r\theta}=k^{2} \tag{8.3}$$

Here k is $\sigma_y/\sqrt{3}$, where σ_y is the yield strength in tension. The in-plane stress components in the plastic sector can be expressed in terms of a stress function $\psi(\theta)$ (Zhu et al., 1997)

$$\sigma_{rr}(\theta) = \sigma_m(\theta) - k\cos\psi(\theta) \quad (8.4a)$$

$$\sigma_{\theta\theta}(\theta) = \sigma_m(\theta) + k\cos\psi(\theta) \quad (8.4b)$$

$$\sigma_{r\theta}(\theta) = k\sin\psi(\theta) \quad (8.4c)$$

8.2.4 <u>Asymptotic solution in plastic sector</u>

When the in-plane stress components satisfying the yield criterion, that is, eq. (8.3) is substituted in the equilibrium equations, eq. (8.1), the governing equations in plastic sector leads to two different stress solutions near the crack tip. While one corresponds to a constant stress sector (in which the mean stress σ_m is a constant quantity) the other represents fan field (where the mean stress σ_m is a linear function of the polar angle θ).

In constant stress sector

$$\psi(\theta) = 2\theta + \psi_o \quad (8.5a)$$

$$\sigma_m(\theta) = C_1 \quad (8.5b)$$

In fan field

$$\psi(\theta) = \frac{\pi}{2} + n\pi \tag{8.6a}$$

$$\sigma_m(\theta) = -2k\theta\cos(n\pi) + C_2 \tag{8.6b}$$

The constants ψ_o, C_1, C_2 and the integer n in eqs. (8.5) and (8.6) can be determined by boundary and continuity conditions.

8.2.5 Asymptotic solution in elastic sector

In an elastic sector in addition to satisfying the asymptotic equilibrium equations, eq. (8.1), the deformation field has to be compatible. Stresses in such an elastic sector can be finally expressed as (Sham et al., 1999)

$$\sigma_{rr}(\theta) = -A\cos 2\theta - B\sin 2\theta + 2C\theta + D \tag{8.7a}$$

$$\sigma_{\theta\theta}(\theta) = A\cos 2\theta + B\sin 2\theta + 2C\theta + D \tag{8.7b}$$

$$\sigma_{r\theta}(\theta) = A\sin 2\theta - B\cos 2\theta - C \tag{8.7c}$$

The integration constants A, B, C and D can be determined from the boundary and continuity conditions.

8.2.6 Assembly of crack tip sectors

Asymptotic elastic and plastic sectors were assembled in a manner that is consistent with the continuity of tractions, $\sigma_{\theta\theta}$ and $\sigma_{r\theta}$ across sector boundaries, as required by equilibrium condition. However, radial stress σ_{rr} may be discontinuous across the sector boundaries. Asymptotic form of yield criterion, eq. (8.3), may be used to find the two possible values of this radial stress as given below

$$\sigma_{rr} = \sigma_{\theta\theta} \pm 2\sqrt{k^2 - \sigma_{r\theta}{}^2} \tag{8.8}$$

For a centred fan adjoining an elastic, or constant stress sector, $\sigma_{r\theta} = k$. There can thus be no stress jump in σ_{rr} and full continuity of all the stress components is required. Thus the continuity of stress components can be simply expressed as

$$\sigma_{\alpha\beta}\left(\theta^{-}{}_{i}\right) = \sigma_{\alpha\beta}\left(\theta^{+}{}_{i}\right) \tag{8.9}$$

Here θ^{-}_{i} and θ^{+}_{i} correspond to angles just before and after the border-delimitation angle θ_i, respectively.

8.3 Elastic-plastic crack tip stress field under mode-I loading

For a mode-I crack, the stress components are required in the upper half plane ($0 \le \theta \le \pi$). The traction free conditions on the crack flank and symmetric deformation requires that

$$\sigma_{\theta\theta}\left(\pm\pi\right)=0 \qquad \sigma_{r\theta}\left(\pm\pi\right)=0 \qquad \sigma_{r\theta}\left(0\right)=0 \tag{8.10}$$

The most general elastic-plastic crack tip stress field, for an incompressible elastic perfectly-plastic material, actually comprises of 4 plastic sectors and one elastic sector as shown in Fig. 8.1 (a). The 4-sector field, Fig. 8.1(b), is a degenerated version of this general 5-sector stress field.

The proposed 5-sector stress field comprises of a plastic sector of uniform stress just ahead of crack tip ($0\leq \theta\leq \theta_1$), a fan field ($\theta_1\leq\theta\leq \theta_2$), a second constant stress sector ($\theta_2\leq\theta\leq \theta_3$), an elastic sector ($\theta_3\leq\theta\leq \theta_4$) and finally a third constant stress sector adjacent to the crack flank. Here θ_1, θ_2, θ_3 and θ_4 are the border angles separating the two adjacent stress sectors. It is easy to visualise that when $\theta_4=\pi$, the proposed 5-sector field degenerates to the 4-sector stress solution. Since the first 3-sectors in proposed 5 sector field are identical to those of Zhu and Chao (2001) we omit the details and directly express the resulting equations as follows

$$\psi\left(\theta\right)=\begin{cases} 2\theta & 0\leq\theta\leq\theta_1=\dfrac{\pi}{4} \\ \dfrac{\pi}{2} & \theta_1\leq\theta\leq\theta_2 \\ \dfrac{\pi}{2}+2\left(\theta-\theta_2\right) & \theta_2\leq\theta\leq\theta_3 \end{cases} \tag{8.11}$$

$$\sigma_m(\theta) = \begin{cases} k(1+\pi) + T_p & 0 \le \theta \le \theta_1 = \dfrac{\pi}{4} \\ k\left(1 + \dfrac{3}{2}\pi - 2\theta\right) + T_p & \theta_1 \le \theta \le \theta_2 \\ k\left(1 + \dfrac{3}{2}\pi - 2\theta_2\right) + T_p & \theta_2 \le \theta \le \theta_3 \end{cases} \tag{8.12}$$

Here T_p is an undetermined constant in the asymptotic analysis. It has to be evaluated from full-field solution like SLF or finite element analysis. This T_p parameter was defined by Zhu and Chao (2001) as

$$T_p = \sigma_{\theta\theta}{}^{app}(0) - \sigma_{\theta\theta}{}^{\mathrm{Pr}\,andtl}(0) \tag{8.13}$$

Thus, T_p essentially represents the hydrostatic stress ahead of the crack tip and carries the same physical meaning as that of Q proposed by O'Dowd and Shih (1991). The stress components in the second constant stress sector, using eq. (5), are as follows

$$\sigma_{rr}(\theta) = k\left(1 + \frac{3}{2}\pi - 2\theta_2\right) + k\sin 2(\theta - \theta_2) + T_p \tag{8.14a}$$

$$\sigma_{\theta\theta}(\theta) = k\left(1 + \frac{3}{2}\pi - 2\theta_2\right) - k\sin 2(\theta - \theta_2) + T_p \tag{8.14b}$$

$$\sigma_{r\theta}(\theta) = k\cos 2(\theta - \theta_2) \tag{8.14c}$$

In the third constant stress sector, adjacent to crack flank, the stress distribution can be obtained by using the traction free condition on the crack flank, that is,

$$\sigma_{\theta\theta}(\pi) = 0 \qquad\qquad \sigma_{r\theta}(\pi) = 0 \tag{8.15}$$

In terms of stress function, $\psi(\theta)$, the boundary conditions, eq. (8.10) can be expressed as follows

$$\sin\psi(\pi) = 0 \ \sigma_m(\pi) = -k\cos\psi(\pi) \tag{8.16}$$

Thus, in the third constant stress sector ($\theta_4 \le \theta \le \pi$), the general solution can be expressed as

$$\psi(\theta) = 2\theta - \pi + n\pi \tag{8.17}$$

It may be noted that the case n=0 would lead to tensile yielding of the crack flank that happens in case of the Prandtl field. For compressive yielding of crack flank n=1 and the resulting stress function and stress components can be expressed as follows

$$\psi(\theta) = 2\theta \tag{8.18}$$

$$\sigma_{rr}(\theta) = -k(1 + \cos 2\theta) \tag{8.19a}$$

$$\sigma_{\theta\theta}(\theta) = -k(1-\cos 2\theta) \tag{8.19b}$$

$$\sigma_{r\theta}(\theta) = k\sin 2\theta \tag{8.19c}$$

For a fully continuous stress solution around the crack tip, the integration constants (*A*, *B*, *C* and *D*) that describes the stress distribution in the elastic sector can be expressed in terms of the border angles separating the two adjacent stress sectors by using the continuity conditions, eq. (8.9). Omitting the algebraic details, the resulting equations can be expressed as follows

$$B = -k\left[\frac{\cos 2\theta_3\left\{\cos 2(\theta_3-\theta_2)-\sin 2\theta_4\right\}+\sin 2(\theta_3-\theta_2)(\sin 2\theta_3-\sin 2\theta_4)}{1-\cos 2(\theta_4-\theta_3)}\right] \tag{8.20a}$$

$$A = -k\left[\frac{\sin 2(\theta_3-\theta_2)}{\cos 2\theta_3}\right] - B\frac{\sin 2\theta_3}{\cos 2\theta_3} \tag{8.20b}$$

$$C = A\sin 2\theta_4 - B\cos 2\theta_4 - k\sin 2\theta_4 \tag{8.20c}$$

$$D = -A\cos 2\theta_4 - B\sin 2\theta_4 - 2C\theta_4 - k(1-\cos 2\theta_4) \tag{8.20d}$$

Continuity conditions provide two additional equations, which are as follows

$$k\left(1+\frac{3}{2}\pi-2\theta_2\right)+T_p=2C\theta_3+D \tag{8.21}$$

$$2C\theta_4+D=-k \tag{8.22}$$

These two equations are insufficient to solve for three unknowns, that is, θ_2, θ_3 and θ_4. In other words, the T_p parameter alone cannot characterise the crack tip stresses. It may be noted that the T_π parameter proposed by Zhu and Chao (2001) that was used to describe the stress state in the elastic sector near the crack flank (in case of 4-sector field) losses its applicability in the general elastic plastic 5-sector stress solution. For various possible states of stress near the crack tip (for a 5-sector solution) the value of T_π parameter is fixed (T_π=-2k). In view of this limitation of T_π parameter we propose the hydrostatic/mean stress in the second constant stress sector as an independent and additional parameter which in conjunction with T_p parameter is used to describe the general state of stress near the crack tip in an elastic perfectly-plastic material.

In an analogous way to the description of T_p parameter we define the $T_{CS\text{-}2}$ parameter as the difference of mean stress in the actual state of stress from the reference Prandtl field in the second constant stress sector. It may be noted that in a constant stress sector the mean stress is not a function of polar co-ordinate θ (σ_m=constant) and thus the $T_{CS\text{-}2}$ parameter can be defined anywhere in the second constant stress sector.

$$T_{CS-2}=\sigma_m{}^{app}-\sigma_m{}^{\mathrm{Pr}andtl} \tag{8.23a}$$

$$T_{CS-2} = \sigma_m{}^{app} - k \tag{8.23b}$$

In the second constant stress sector ($\theta_2 \le \theta \le \theta_3$) we have

$$\sigma_m = k\left(1 + \frac{3}{2}\pi - 2\theta_2\right) + T_p \tag{8.24}$$

The angular position of the border separating the fan field and the second constant stress sector can be expressed in terms of the two constraint indexing parameters as follows

$$\theta_2 = \frac{3}{4}\pi - \frac{\left(T_{CS-2} - T_p\right)}{2k} \tag{8.25}$$

For a given value of T_p and T_{CS-2} parameter, θ_2 can be obtained from eq. (8.25). Eqs (8.21) & (8.22) can then be used to evaluate the two unknown variables, that is, θ_3 and θ_4. Thus, a complete characterisation of crack tip stresses is possible by means of these two independent constraint indexing parameters.

8.3.1 Special cases of the general 5-sector stress solution

i) A definite mathematical relation exists between the constraint parameters T_p and T_{CS-2} when transition occurs from the 5-sector field to the 4-sector stress field. This limiting condition corresponds to the situation when compressive yielding just initiates at the crack tip. Under this special case $\theta_4 = \pi$ and, thus, following relations can be easily obtained

$$A = k\frac{\cos(\theta_3 - 2\theta_2)}{\sin\theta_3} \tag{8.26a}$$

$$B = -k\frac{\cos 2\theta_2}{1-\cos 2\theta_3} \tag{8.26b}$$

$$C = -B \tag{8.26c}$$

$$D = 2\pi B - A \tag{8.26d}$$

On substituting $\theta_4 = \pi$ in eqs. (21) & (22) and after a few algebraic simplifications the following relations can be easily obtained.

$$-\left(\frac{T_p}{k} + 2 + \frac{3}{2}\pi\right) = 2\frac{(\pi - \theta_3)}{1-\cos 2\theta_3}\cos\left(\theta_3 + \cos^{-1}(\sin\theta_3)\right) - \left(\theta_3 + \cos^{-1}(\sin\theta_3)\right) \tag{8.27a}$$

$$T_{CS-2} = T_p + k\left[\frac{3}{2}\pi - \theta_3 - \cos^{-1}(\sin\theta_3)\right] \tag{8.27b}$$

This mathematical relation simply means that at $\theta_4 = \pi$ the compressive yielding would occur just at the crack flank and T_p and T_{CS-2} parameter are not independent. This is the limiting case up to which the 4-sector stress field is valid. Beyond this condition any further loss of crack tip constraint would spread compressive yielding in the region adjacent to crack flank and the resulting stress distribution cannot be described by the 4-sector field. On the contrary, with a rise in crack tip constraint the crack flank comes under elastic condition and eq. (8.22) is not valid. Thus, T_p and $T_{CS\text{-}2}$ parameter again become independent and can be used to characterise the state of stress near the crack tip. For a given value of T_p and $T_{CS\text{-}2}$ parameter, eq. (8.25) can be used to obtain the border angle θ_2. Eq. (8.21) can then be used to evaluate the border angle θ_3 and hence all the 4 integration constants (A, B, C and D). The complete stress distribution in the elastic sector can be obtained using eq. (8.8). This condition corresponds to the 4-sector solution and for this special case either $T_{CS\text{-}2}$ or T_π in conjunction with T_p parameter can be used to define the crack tip stresses. The following relation exists between the $T_{CS\text{-}2}$ or T_π parameter for the case of 4-sector stress field

$$\frac{T_\pi}{k} = -\left(1 + \frac{1}{\sin\theta_3}\cos\left\{\theta_3 - \frac{3\pi}{2} + \left(\frac{T_{CS-2} - T_p}{k}\right)\right\}\right) \tag{8.28}$$

As demonstrated by Zhu and Chao (2001), for commonly used fracture mechanics specimens, the constraint conditions near the crack tip leads to 4-sector stress solution. Comparison of crack tip stresses obtained from detailed FE analysis of Kim et al. (1996), Zhu and Chao (2000) with the asymptotic 4-sector stress solution in terms of T_p and T_π parameters have already been given by Zhu and Chao (2001). For all such cases the numerical values of T_p, $T_{CS\text{-}2}$ and T_π parameters are provided in Table 8.1. Zhu and Chao

(2001) used the values of T_p and T_π parameters, obtained from FE analysis, to obtain the values of border delimitation angles (θ_2 and θ_3) and, hence, the complete crack tip stress distribution. In the present analysis, we have used the values of T_p and T_{CS-2} parameters to obtain the border delimitation angles (θ_2 and θ_3). Once the angles θ_2 and θ_3 are known T_π parameter can be calculated from stress distribution of the elastic sector using eq. (8.8) or directly from eq. (8.28). Both the approaches yield identical results for crack tip stress distribution.

Table 8.1: Comparison of 4-sector stress field variables in terms of T_π and T_{CS-2} parameters

Specimen Type	T_p **(FEA)**	**4-sector solution in terms of T_π parameters**			**4-sector solution in terms of T_{CS-2} parameters**		
		T_π **(FEA)**	θ_2	θ_3	T_{CS-2} **(FEA)**	θ_2	θ_3
SENB (a/W=0.1)	$-0.969\sigma_o$	$-0.827\sigma_o$	88.5°	110.8°	$-0.032\sigma_o$	88.5°	110.8°
SENB (a/W=0.2)	$-0.588\sigma_o$	$-0.877\sigma_o$	107.4°	143°	$-0.032\sigma_o$	107.4°	143°
SENB (a/W=0.3)	$-0.119\sigma_o$	$-0.352\sigma_o$	128.2°	157.8°	$0.018\sigma_o$	128.2°	157.8°
DECP (a/W=0.5)	$-1.092\sigma_o$	$-0.856\sigma_o$	84°	106°	$-0.064\sigma_o$	84°	106°
M(T) (a/W=0.5)	$-1.577\sigma_o$	$-0.903\sigma_o$	62°	65°	$-0.106\sigma_o$	62°	65°

ii) When θ_2=θ_3 and θ_4=π, the 5-sector field degenerates to the 3-sector stress field of Li and Hancock (1999). For this special case following relation can be easily obtained.

$$\frac{T_p}{k} = \left(2\theta_2 - \frac{3}{2}\pi - 1\right) - \frac{\cos\theta_2}{\sin\theta_2} - 2\frac{(\pi - \theta_2)}{1 - \cos 2\theta_2}\cos 2\theta_2 \tag{8.29}$$

Keeping eqs. (8.29) & (8.25) in view, it becomes obvious that for the case of 3-sector field θ_2 and, hence, $T_{CS\text{-}2}$ parameter are not independent. Thus, for this special case T_p parameter alone can characterise the entire crack tip stress field. This conclusions was already made earlier by Zhu and Chao (2001).

iii) When T_p =0, that is for the case of Prandtl field it can be easily shown that θ_2=$3\pi/4$ and $T_{CS\text{-}2}$=0

iv) When T_p =-(2+π)k, that is for the case of uniform stress field it can be easily shown that θ_2=$\pi/4$ and $T_{CS\text{-}2}$= -2k

8.4 Finite element simulation of crack tip stress fields for different constraint levels in incompressible elastic-perfectly plastic material

In the previous section, 5-sector stress solution was proposed to represent the crack tip stress fields, in an incompressible elastic-perfectly plastic material, in terms of two constraint indexing parameters, that is, T_p and $T_{CS\text{-}2}$. As discussed by Nemat-Nasser and Obata (1984) such an asymptotic analysis cannot be used to evaluate these unknown parameters. To verify the proposed asymptotic 5-sector field detailed full-field FE analyses were performed to simulate a wide range of T_p and T_{CS-2} parameter representing different crack tip constraint levels.

For non-hardening material, detailed SLF analysis (McClintock, 1971) and many numerical studies (Lee and parks, 1993; Kim et al., 1996; Zhu and Chao, 2000) have clearly established the effects of specimen geometry and loading conditions on crack tip stresses. In last one decade considerable work has been done on strength mismatch welds where the difference in plastic properties of base and weld material is accounted. Various numerical (FE) as well as experimental studies have indicated that the strength mismatch between base and weld material has appreciable influence on crack tip stresses. Thus, while analysing these strength mismatch weld it is important to consider constraint effects due to geometry and loading of cracked structure as well as due to material strength mismatching. Within the framework of small-scale yielding Burstow et al. (1998) used the modified boundary layer formulation to investigate the crack tip constraint in strength mismatch weld. The effects of specimen geometry on the crack tip stresses were modelled by varying the magnitude of applied T-stress and the effects of constraint due to strength mismatching were investigated by changing the strength of base material with respect to weld.

In this study detailed 2-D plane strain FE analyses were performed on middle tension M(T) specimen, pure bending specimen SE(PB) and compact tension C(T) specimen under large-scale plasticity (at limit state) to model different crack tip constraint. Only idealised weld without any heat affected zone (HAZ) was considered. Stationary weld centre crack running parallel to the interface of base and weld material was modelled (see Fig. 1.1). The two materials were assumed to have same elastic modulus and

Poisson's ratio but mismatch in their yield strength. The elastic response of base and weld material was modeled as isotropic and almost incompressible (ν=0.49). This small departure from full incompressibility was suggested by Sham et al. (1999) to avoid numerical problems with mesh locking. The effects of geometry were modelled by changing the weld slenderness ratio (ψ) while the strength mismatch effects were incorporated by changing the mismatch ratio (M). These two parameters are defined as follows

$$M = \frac{\sigma_{yw}}{\sigma_{yb}} \tag{8.30}$$

$$\psi = \frac{W-a}{H} = \frac{l}{H} \tag{8.31}$$

Material mismatch ratio M and weld slenderness ratio ψ were systematically varied to create a wide range of crack tip constraint. For over matched welds, representing low crack tip constraint, analyses were performed for $1 \leq M \leq 2$. This range of mismatch covers practically the entire range of over matching that is likely to occur in most engineering applications. Similarly for under matched welds, representing high constraint, FE analyses were performed for $0.25 \leq M \leq 1$. Weld slenderness ratio was also varied ($1.667 \leq \psi \leq 10$) to account for both conventional and narrow gap welds. Fig. 5.10 shows the FE discretisation scheme used in present investigation. To avoid problems associated with incompressibility eight-noded plane strain element with reduced integration were employed in all FE calculations. 16 eight-noded elements comprised the upper-half of crack tip and forty circumferential rings of element are surrounding the crack tip. The innermost ring of the elements has one side collapsed on to the crack tip. All the collapsed nodes get separated after the loading is applied. Due to symmetry only one-quarter of M(T) specimen was modelled. Appropriate symmetric boundary conditions were applied on the two planes of symmetry. This one-quarter model contains about 1400, 8-noded elements and 4000 nodes. The radial extent of the elements in the first ring was $\approx 2x10^{-4}$ b where b denotes the uncracked ligament. The numerical model employs the small-strain formulation. The material was model as isotropic, elastic-plastic obeying the Von-Mises yield criterion. Uniform rigid displacement was applied on the top edge of this FE model and the specimen was loaded to its limit state. Results of crack tip stress fields obtained from detailed FE analyses and their comparison with the proposed 5-sector stress field are presented in the following subsection. For the case of homogeneous M(T) specimens, Zhu and Chao (2000) have presented results of crack tip stresses obtained from detailed FE analyses. In order to investigate the effects of applied loading conditions on crack tip stresses they applied two types of loadings on the top edge of the FE model: one was uniformly distributed applied load and the other was uniform rigid displacement. These two cases were used as a benchmark for the present FE calculations. Excellent agreement was obtained between the two FE investigations (see Fig. 8.2).

8.5 Results

In this section results obtained from detailed elastic-plastic FE analyses are presented. Crack tip stress fields obtained from the proposed asymptotic 5-sector stress fields were compared with the full field FE analyses of middle tension M(T) specimen, pure bending specimen SE(PB) and compact tension C(T) specimen, having a weld centre crack, under large-scale plasticity (at limit state). For all these specimens a/W was kept as 0.5. Detailed comparison of analytical results with FE analyses is presented here only for few representative cases.

8.5.1 Middle tension M(T) specimen

For the case of M(T) specimen having a weld centre crack, the normalised values of constraint-indexing parameters, that is, T_p and $T_{CS\text{-}2}$ obtained directly from FE analyses are provided in Table 8.2. To demonstrate the limitation of T_π parameter, numerical values of this parameter obtained from eq. (8.28) is also provided. It may be mentioned that the T_π parameter obtained from eq. (8.28) was in close agreement with FE results.

Table 8.2: Numerical values of T_p, $T_{CS\text{-}2}$ and T_π parameters for a M(T) specimen having a weld centre crack obtained from FE analyses.

Weld slenderness ratio (ψ)	Mismatch ratio (M)	T_p/k (FEA)	$T_{CS\text{-}2}/k$ (FEA)	T_π/k eq. (8.28)	Crack tip stress field classification
	0.25	0	0	0	Prandtl field
	0.5	-0.371	0.0587	-0.821	4-sector stress field
	0.75	-1.959	-0.0648	-1.45	4-sector stress field
10	0.9	-2.464	-0.3426	-1.60	4-sector stress field

	1.25	-3.027	-0.791	-1.883	4-sector stress field
	1.5	-3.243	-0.952	-2	4-sector stress field
	1.75	-3.443	-1.133	-2	5-sector stress field
	2	-3.611	-1.232	-2	5-sector stress field
5	0.25	0	0	0	Prandtl field
	0.5	-0.376	0.0898	-0.736	4-sector stress field
	0.75	-1.928	-0.0347	-1.433	4-sector stress field
	0.9	-2.439	-0.312	-1.59	4-sector stress field
	1.25	-3.076	-0.782	-1.843	4-sector stress field
	1.5	-3.3	-0.995	-2	4-sector stress field
	1.75	-3.498	-1.165	-2	5-sector stress field
	2	-3.625	-1.247	-2	5-sector stress field
3.33	0.9	-2.574	-0.389	-1.627	4-sector stress field
	1.25	-3.011	-0.729	-1.81	4-sector stress field
	1.5	-3.359	-1.04	-2	4-sector stress field
	1.75	-3.475	-1.113	-2	5-sector stress field
	2	-3.52	-1.18	-2	5-sector stress field
2.5	0.5	-0.401	0.0832	-0.787	4-sector stress field
	0.75	-1.962	-0.0658	-1.45	4-sector stress field
	0.9	-2.452	-0.323	-1.598	4-sector stress field
	1.5	-3.265	-0.979	-2	4-sector stress field
	1.75	-3.32	-1.092	-2	5-sector stress field
	2	-3.34	-1.109	-2	5-sector stress field

1.667	0.25	-1.45	0.199	-1.242	4-sector stress field
	0.5	-1.475	0.09	-1.304	4-sector stress field
	0.75	1.987	-0.0378	-1.44	4-sector stress field
	0.9	-2.559	-0.3893	-1.629	4-sector stress field
	1.25	-3.072	-0.767	-1.825	4-sector stress field
	1.5	-3.213	-0.948	-2	4-sector stress field
	1.75	-3.212	-1.026	-2	5-sector stress field
	2	-3.276	-1.058	-2	5-sector stress field

In Figs. 8.3-8.6 comparison of angular variation of crack tip stress fields obtained from analytical solutions with FE results are presented for a thin weld, described by ψ=10, for various mismatch ratios *M*. The case ψ=10 is representative of welds produced by electron beam welding or by narrow gap welding technique. For a thin highly undermatch weld (Fig. 8.3) it can be seen that the mean stress (constraint) near the crack tip is very high and the full Prandtl field develops near the crack tip. As the degree of overmatch increase (Fig. 8.4) the mean stress near the crack tip decrease and an elastic sector appears near the crack flank. For highly overmatch welds (Fig. 8.5 and 8.6) the mean stress nearly get saturated but plastic yielding in compression starts at the crack flank and the yielded region increases in size with the degree of weld overmatching. For such cases the stress fields, particularly in the backward sector ($90° \leq \theta \leq 180°$), can not be described by the 4-sector stress field. The results obtained from the proposed 5-sector stress fields were in excellent agreement with FE solutions for the entire range of $0° \leq \theta \leq 180°$.

Figs. 8.7-8.9 describes the angular variation of crack tip stress fields for a thick weld (ψ=1.67) for various mismatch ratios M. The observations made are very similar to the case of a thin weld as discussed in previous paragraph.

8.5.2 Pure bending SE(PB) specimen

For the case of SE(PB) specimen having a weld centre crack, the normalised values of the constraint-indexing parameters, that is, T_p and $T_{CS\text{-}2}$ were obtained directly from FE analyses. The angular variation of crack tip stresses obtained from the proposed analytical solutions was compared with FE results for various cases. The effect of strength mismatch ratio M and weld slenderness ratio ψ on the crack tip stress field was very similar to that observed for a M(T) specimen. It was noted that two different cases having different values of the mismatch ratio M and weld slenderness ratio ψ but having nearly same value of the proposed constraint parameters lead to almost similar stress fields. An example of such a case is shown in Fig. 8.10.

8.5.3 Compact tension C(T) specimen

The case of C(T) specimen having a weld centre crack was also analysed. The effect of strength mismatch ratio M and weld slenderness ratio ψ on the crack tip stress field was examined. The conclusions made from the study are very similar to those discussed for the case of SE(PB) specimen.

8.6 Discussion

For mode-I crack in an elastic-perfectly plastic material the general elastic-plastic crack tip stress field is a 5-sector solution that can be completely described by T_p and $T_{CS\text{-}2}$ parameters. For high constraint geometries like DECP $T_p \approx 0$ that leads to complete yielding of the crack tip. For such cases the T_p parameter alone can characterise the crack tip stresses. With the loss of crack tip constraint an elastic sector appears in the region adjacent to crack flank and two independent parameters, that is, T_p and $T_{CS\text{-}2}$ (or T_π) are required for complete description of stress field. The crack tip stresses of most of the commonly used fracture specimens can be completely characterised by means of 4-sector solution. With a further reduction in crack tip constraint, the integration constant A becomes equal to k, the yield criterion gets satisfied on the crack flank, that is, at $\theta=\pi$ and T_π parameter becomes -2k. This is the transition point between the 4-sector and the 5-sector field. Beyond this stage any further loss of crack tip constraint would lead to plastic yielding in the region adjacent to crack flank and the elastic sector gets pressed between the two plastic sectors of uniform stress state. This situation arises in case of over matched welds where the relatively higher strength of weld material produces a shielding effect on the crack tip and thus severely lowers the crack tip constraint. In all such cases the value of T_π parameter remains as -2k and thus the 4-sector solution is incapable to describe the shift of elastic sector as a function of crack tip constraint. From the detailed investigations it appears that the proposed $T_{CS\text{-}2}$ parameter possesses some advantages over the T_π parameter suggested by Zhu and Chao (2001). In the general case of elastic plastic crack tip stress field (5-sector solution) the T_π parameter cannot characterise the crack tip stresses particularly near the crack flank. For the value of $T_\pi = -2k$ many different states of crack tip stresses are possible. While one of the states corresponds to the well-known fully plastic uniform stress field, many other states of stresses are possible for the cases where 5-sector stress solution exists such as in case of over matched M(T) specimen. Thus, while the T_π parameter is valid only for the 4-sector stress field the proposed $T_{CS\text{-}2}$ parameter is applicable for all possible states of crack tip stresses and is, thus, more general. In addition to the above-mentioned aspects it is the apprehension of the writer that $T_{CS\text{-}2}$ parameter may have some influence on the mechanism of fracture. It is widely accepted that two-parameter approaches like J-T (Betegon and Hancock, 1991) and J-Q (O'Dowd and Shih, 1991) bring an improvement over the conventional single parameter (J-based) approach in characterization of fracture toughness. However, they in turn are not adequate enough to fully resolve this issue. These two-parameter approaches are based on the notion that the state of stress in leading sector ($0 \leq \theta \leq 90^\circ$) near the crack tip governs the fracture process. Actually O'Dowd and Shih (1991) proposed this concept based on their numerical study where they demonstrated that the Q-parameter can accurately describe the state of stress in this leading sector. However, no experimental study has yet been reported which clearly shows that the state of stress in the leading sector only governs this fracture process. In light of this, a qualitative statement that an accurate characterization of fracture process requires an accurate description of the state of stress, at least in plastic sectors near the crack tip, is quite plausible. This perspective, thus, supports that $T_{CS\text{-}2}$ parameter is more suitable than T_π parameter evaluated from the elastic sector. In view of this it is felt that $T_{CS\text{-}2}$ parameter in conjunction with T_p parameter is more appropriate for a general characterisation of crack tip stress field in an elastic perfectly plastic material under mode-I loading. Since the present work is concerned with elastic-perfectly plastic material application of the proposed constraint parameters to the actual strain-hardening material is yet to be established. Thus, this work may be looked upon as the first step towards this important issue of fracture characterization from the consideration of crack tip stresses.

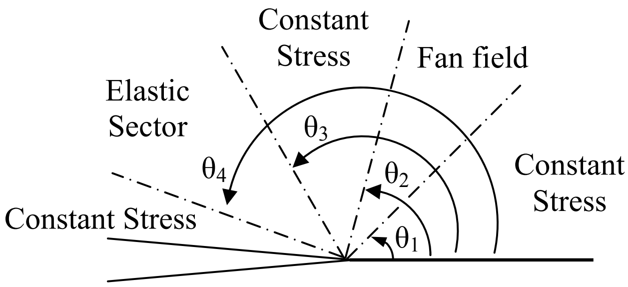

(a)

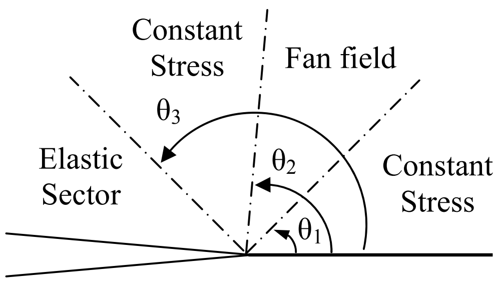

(b)

Fig. 8.1: Description of elastic-plastic crack-tip stress fields under mode I loading by (a) proposed 5-sector field and (b) 4-sector solution of Zhu and Chao (2001).

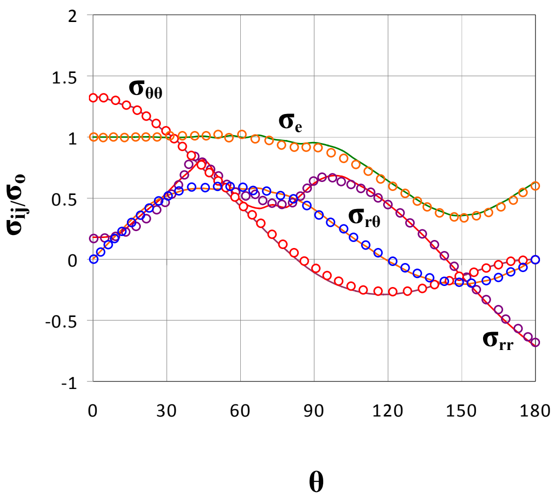

(a)

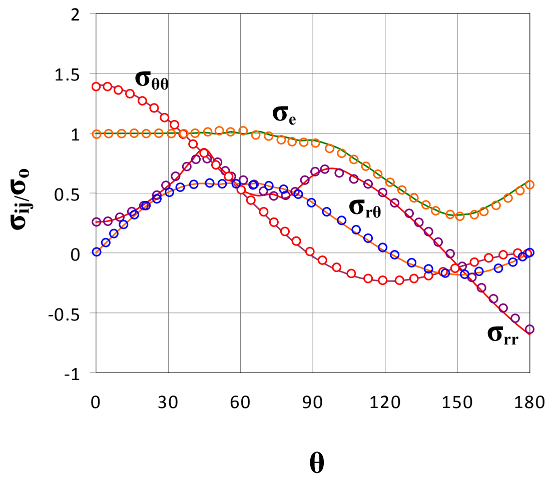

(b)

Fig. 8.2: Comparison of crack-tip stresses for M(T) specimen obtained from present FE analysis with those of Zhu and Chao (2001) (a) under rigid displacement loading condition and (b) under uniformly distributed applied pressure. While continuous line shows present FE results, the open circles refer to FEA of Zhu and Chao (2001).

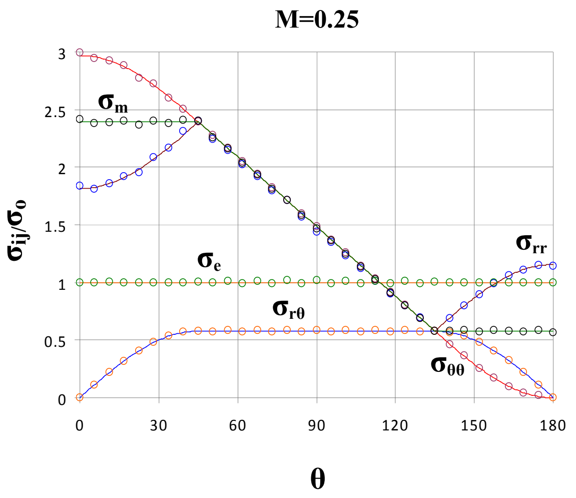

(a)

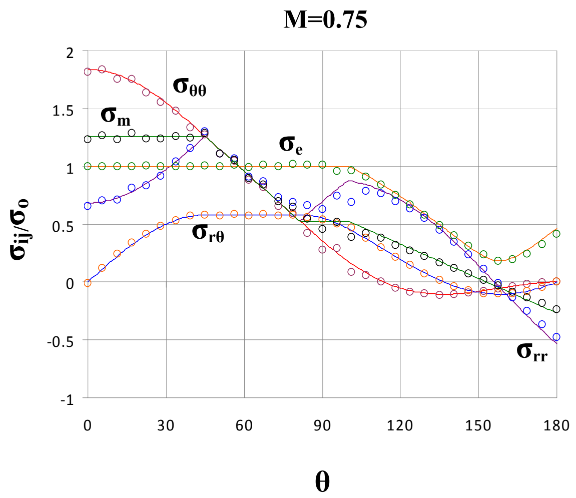

(b)

Fig. 8.3: Comparison of crack-tip stresses for mismatch welded M(T) specimen with ψ=10. (a) M=0.25 and (b) M=0.75. While continuous line shows the results of asymptotic 4-sector stress solution, the open circles refer to FEA.

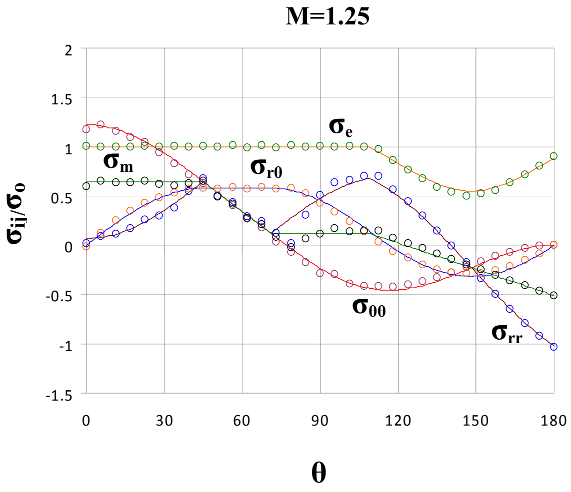

(a)

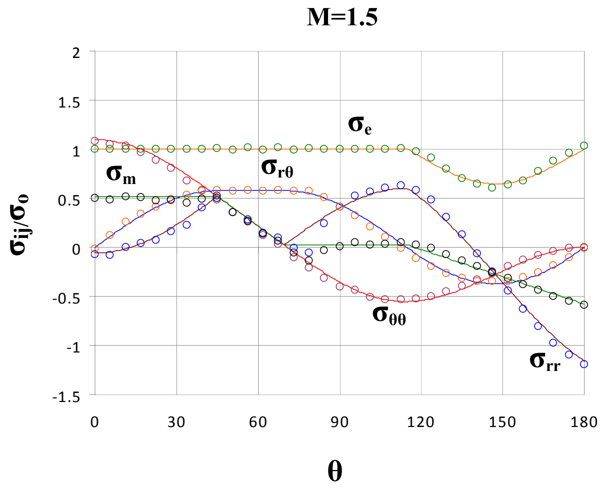

(b)

Fig. 8.4: Comparison of crack-tip stresses for mismatch welded M(T) specimen with ψ=10. (a) M=1.25 and (b) M=1.5 that leads to compressive yielding just on crack flank. While continuous line shows the results of asymptotic 4-sector stress solution, the open circles refer to FEA.

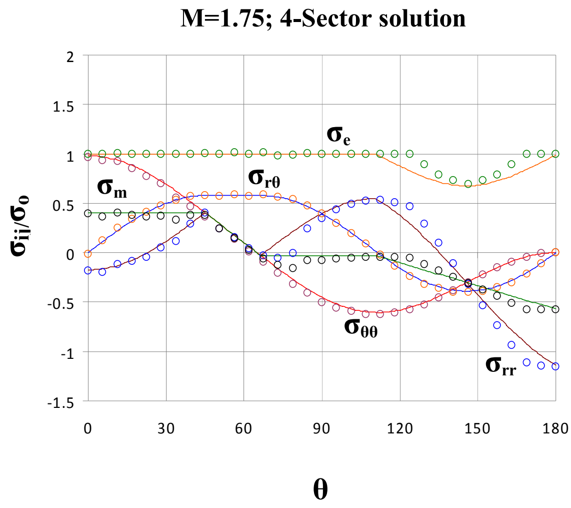

(a)

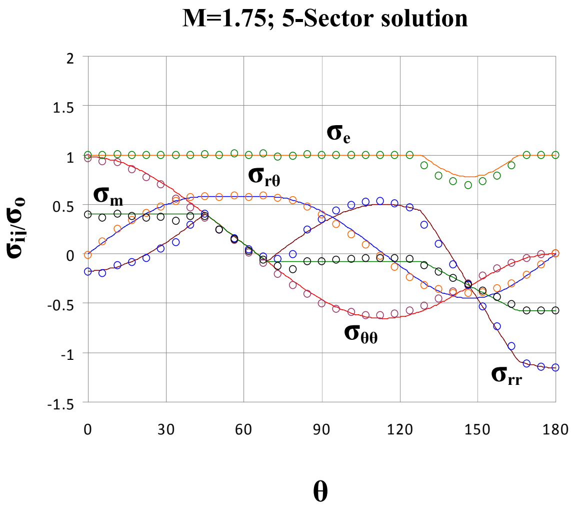

(b)

Fig. 8.5: Comparison of crack-tip stresses for mismatch welded M(T) specimen with ψ=10 and M=1.75. (a) Asymptotic 4-sector stress solution proposed by Zhu and Chao (2001). (b) Proposed 5-sector stress solution. The open circles refer to results obtained from FEA.

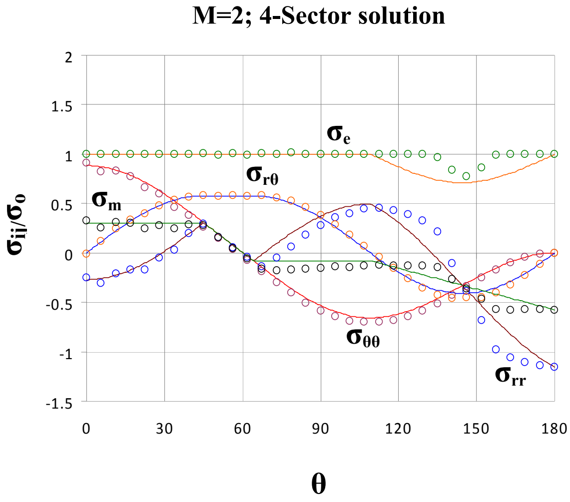

(a)

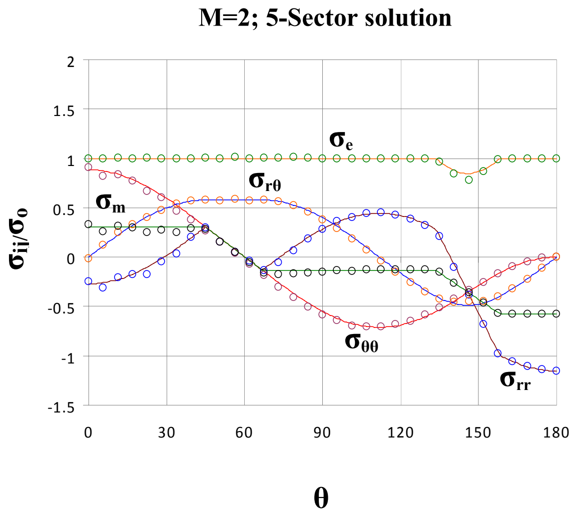

(b)

Fig. 8.6: Comparison of crack-tip stresses for mismatch welded M(T) specimen with ψ=10 and M=2. (a) Asymptotic 4-sector stress solution proposed by Zhu and Chao (2001). (b) Proposed 5-sector stress solution. The open circles refer to results obtained from FEA.

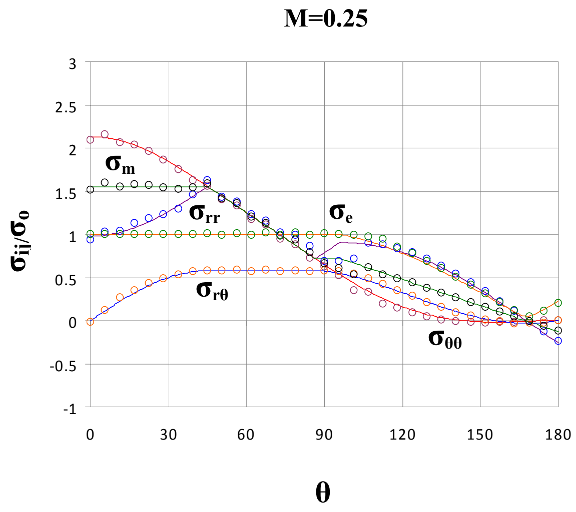

(a)

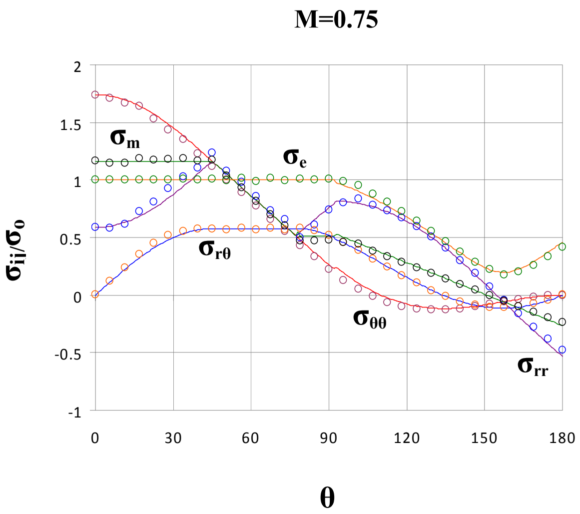

(b)

Fig. 8.7: Comparison of crack-tip stresses for mismatch welded M(T) specimen with ψ=1.67. (a) M=0.25 and (b) M=0.75. While continuous line shows the results of asymptotic 4-sector stress solution, the open circles refer to FEA.

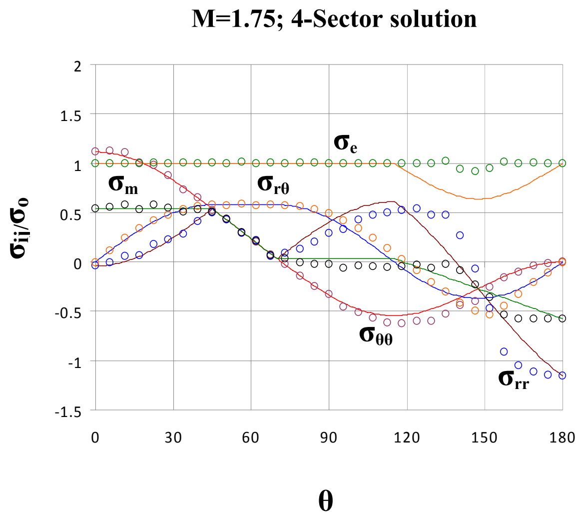

(a)

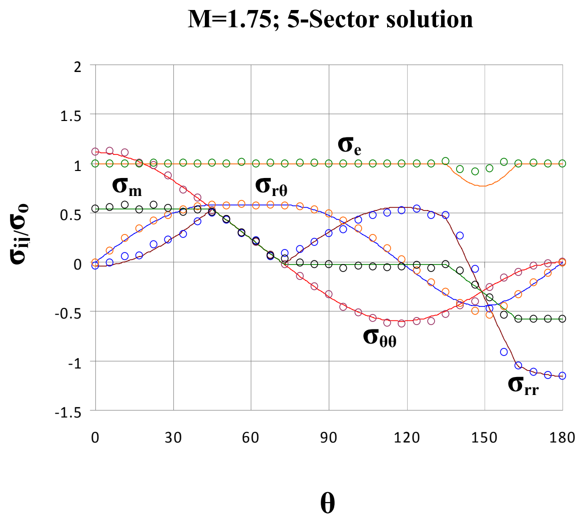

(b)

Fig. 8.8: Comparison of crack-tip stresses for mismatch welded M(T) specimen with ψ=1.67 and M=1.75. (a) Asymptotic 4-sector stress solution proposed by Zhu and Chao (2001). (b) Proposed 5-sector stress solution. The open circles refer to results obtained from FEA.

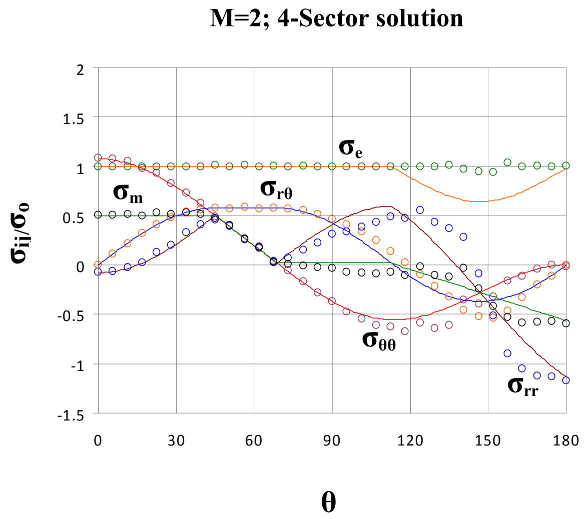

(a)

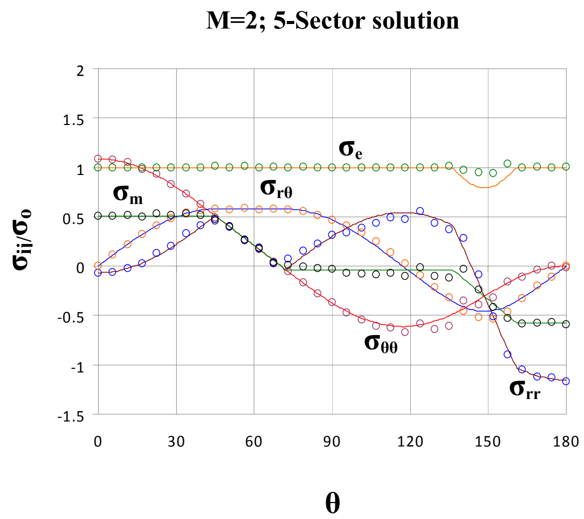

(b)

Fig. 8.9: Comparison of crack-tip stresses for mismatch welded M(T) specimen with ψ=1.67 and M=2. (a) Asymptotic 4-sector stress solution proposed by Zhu and Chao (2001). (b) Proposed 5-sector stress solution. The open circles refer to results obtained from FEA.

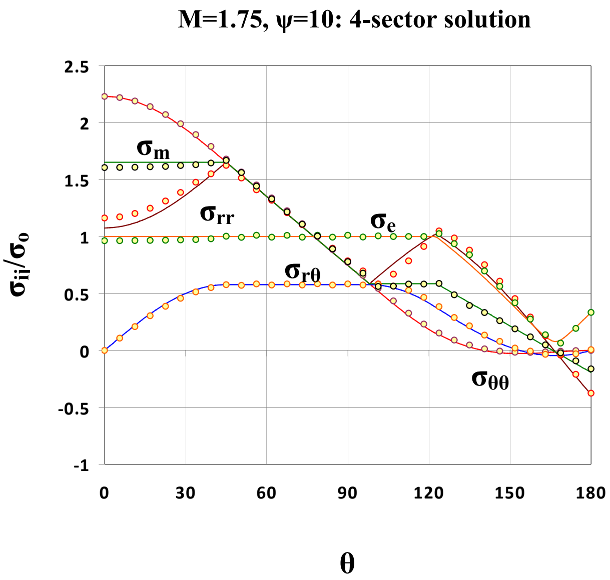

(a)

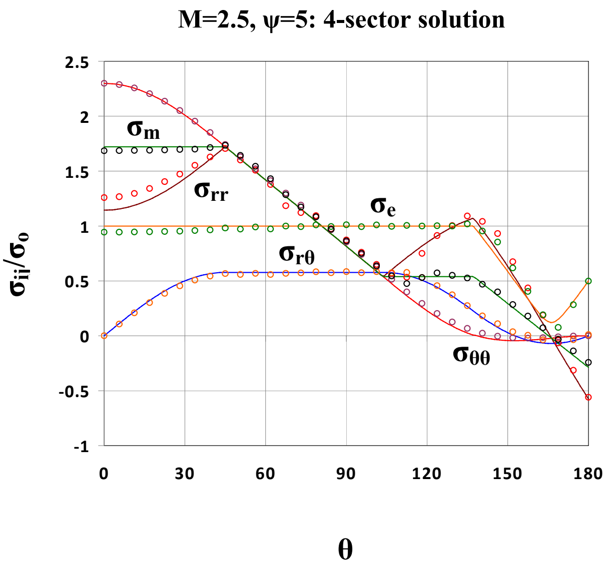

(b)

Fig. 8.10: Comparison of crack-tip stresses for mismatch welded SE(PB) specimen with. (a) T_p/k=-1.28, T_{CS-2}/k=-1.32 and (b) T_p/k=-1.16, T_{CS-2}/k=-1.48. While continuous line shows the results of asymptotic 4-sector stress solution, the open circles refer to FEA.

CHAPTER 9

Conclusions and future work

In this chapter studies performed in this work are summarised. In addition to conclusions further possible extensions of the present study that may be carried out in future are also discussed.

9.1 Conclusions

Salient conclusions drawn from this work are as follows

- The modified upper bound (MUB) theorem of limit analysis for plane strain problems was developed. The proposed theorem is adequate to account weld strength mismatch effects on the fracture mechanics parameters.

- In comparison to slip line fields describing the stress distribution in homogeneous cracked fracture specimens, fields for fracture specimens having a weld centre crack are more complicated. In this work the detailed structure of global plastic fields that occurs in pure bending SE(PB) specimen, compact tension C(T) specimen and middle tension M(T) specimen having a weld centre crack was presented. Proposed fields were confirmed by performing detailed elastic-plastic FE analysis.

- Accurate analytical solutions of the limit load and plastic η-factor of plane strain fracture specimens having a weld centre crack were obtained using the proposed MUB theorem. Proposed analytical solutions were validated by detailed finite element results obtained by the author as well as with those available in literature. Excellent agreement was observed between the two solutions.

- Weld strength mismatch have significant effects on plastic η-factor and, hence, on estimated fracture toughness of weldments. This is particularly more important for overmatched welds which are typically used in various applications and whose fracture toughness may be overestimated by the use of toughness estimation procedures developed for standard homogeneous fracture specimens.

- In between the two extreme conditions of crack tip constraint, that is, between the fully plastic Prandtl field (representing high constraint) and the uniform stress field (representing low constraint) the most general elastic-plastic crack tip fields can be completely described by the 5-sector stress solution proposed in this work. The 4-sector field proposed by Zhu and Chao (2001) is a subset of the general elastic-plastic field proposed in this work

- It is well known that the loss of constraint at the crack tip leads to an elastic sector at the crack flank leading to incomplete crack tip plasticity. This study has revealed that cases arise where the severe loss of crack tip constraint can lead to compressive yielding of crack flank. This particular situation leads to 5-sector stress field where the elastic sector is sandwiched between the two plastic sectors of uniform stress state.

- Detailed studies have revealed that, in the most general case of elastic plastic crack tip fields, the T_π parameter proposed by Zhu and Chao (2001) cannot be used as a constraint indexing parameter to represent a unique state of stress at the crack tip. A new constraint parameter T_{CS-2} is proposed which along with T_p is capable of representing the general elastic plastic crack tip stress fields over all angles around a crack tip.

- The asymptotic variation of crack tip stresses in plane strain fracture specimens having a weld centre crack under mode I loading, for various strength mismatch ratio *M* and weld slenderness ratio ψ, is very similar to what has been observed in different homogeneous fracture specimens. The crack tip stresses for all such cases can be fully described by the proposed 5-sector stress solution.

- Detailed 2-D elastic plastic finite element analyses were performed to examine the validity of the proposed 5-sector stress field for a wide range of crack tip constraint. Excellent agreement was obtained between the proposed asymptotic crack tip stress field and the finite element results.

- For elastic-perfectly plastic material at limit state, the proposed constraint parameters, that is, T_p and T_{CS-2} are adequate to represent the crack tip constraint arising due to specimen geometry and loading conditions as well as the additional constraint arising due to weld strength mismatch. It is demonstrated that two different type of specimens (with different geometries and loading condition) having different weld strength mismatch ratio *M* and weld slenderness ratio ψ but having the same values of the proposed constraint parameters have identical crack tip stress fields. Thus, it seems that once these constraint parameters are available the fracture mechanics assessment of these heterogeneous welds can be carried out in exactly similar way as for homogeneous specimens. Several activities are going on in the author's group to validate this last statement in a comprehensive way.

9.2 Future work

Some of the possible extensions of the work reported in this thesis are listed below

- The present study was based on the assumption of elastic-perfectly plastic (non-hardening) material. Real materials, however, do not satisfy such ideal conditions and show significant strain hardening. In metal forming processes, attempts have been made to incorporate the effect of strain hardening on extrusion pressure etc using mean strain concepts (Johnson and Kudo, 1962). Halling and Mitchell (1967) demonstrated that the SLF pattern of extrusion through a smooth die was not much affected by the form of stress-strain relationship. Thus, it would be worth trying to extend the present study to real strain hardening materials.

- The present work was focused on the problem of a stationary crack lying at the centre of a strength mismatched weld. In an actual weld joint crack may lie, however, anywhere also. The proposed MUB theorem may be used to analyse such cases but the structure of global plastic fields need to be established. Such studies may be carried out in future to analyse the structural integrity of interfacial cracks that can form at the heat affected zone (HAZ) and base metal interface.

Bibliography

Ainsworth, R.A, 1984. The assessment of defects in structures of strain hardening materials. Engineering Fracture Mechanics, 19, 633-642.

Al-Ani, A.M., Hancock, J.W., 1991. J-dominance of short cracks in tension and bending. Journal of Mechanics and Physics of Solids, 39, 23-43.

Alexander, J.M. and Komoly, T.J., 1962. On the yielding of a rigid/plastic bar with an Izod notch. Journal of Mechanics and Physics of Solids, 10, 265-275.

Alexandrov, S., 2010. A limit load solution for a highly weld strength undermatched tensile panel with an arbitrary crack, Engineering Fracture Mechanics, 77, 3368-3371.

Alexandrov, S., Chicanova, N., Kocak, M., 1999. Analytical yield load solution for overmatched centre cracked tension specimen, Engineering Fracture Mechanics, 64, 383-399.

An, G.B., Ohata, M., Toyoda, M., 2003. Effect of strength mismatch and dynamic loading on ductile fracture initiation. Engineering Fracture Mechanics, 70, 1359-1377.

Besson, J., Madi, Y., Motarjemi,A., Kocak, M., Martin, G., Hornet, P., 2005. Crack initiation and propagation close to the interface in a ferrite–austenite joint. Materials Science and Engineering A 397, 84-91.

Betegon, C., Hancock, J.W., 1991. Two-parameter characterization of elastic-plastic crack-tip fields. Journal of Applied Mechanics, 58, 104-l10.

Betegon, C., Penuelas, I., 2006. A constraint based parameter for quantifying the crack tip stress fields in welded joints. Engineering Fracture Mechanics, 73, 1865-1877.

Burstow, M.C. and Ainsworth. R. A., 1995. Comparison of analytical, numerical and experimental solutions to problems of deeply cracked welded joints in bending. Fatigue & Fracture of Engineering Materials & Structures, 18, 221-234.

Burstow, M.C., Howard, I.C., Ainsworth, R.A., 1998. The influence of constraint on crack tip stress fields in strength mismatch welded joints. Journal of the Mechanics and Physics of Solids 46, 845-872.

Cao, H.C., Evans, A.G., 1989. An experimental study of the fracture resistance of bimaterial interfaces. Mechanics of Materials, 7, 295-304.

Chakrabarty, J., 1987. Theory of Plasticity. McGraw-Hill international edition, New York.

Chao, Y.J., Yang, S., 1996. Higher order crack tip fields and its implication for fracture of solids under mode II conditions. Engineering Fracture Mechanics, 55, 777-794.

Chao, Y.J., Yang, S., Sutton, M.A., 1994. On the fracture of solids characterised by one or two parameters: theory and practice. Journal of the Mechanics and Physics of Solids, 42, 629-647.

Chattopadhyay J., Dutta, B.K., Kushwaha, H.S., 2001. Derivation of 'γ' parameter from limit load expressions of cracked component to evaluate J–R curve. International Journal of Pressure Vessels & Piping, 78, 401-27.

Chattopadhyay J., Dutta, B.K., Kushwaha, H.S., 2004. New 'η_{pl}' and 'γ' functions to evaluate J-R curve from cracked pipes and elbows. Engineering Fracture Mechanics, 71, 2635-2660.

Cherepanov, G.P., 1962. The stress state in a heterogeneous plate with slits. Izvestia AN SSSR, OTN, Mekhan, i, Mashin., Vol. 1, 131-137.

Comninou, M., 1977. The interface crack. Journal of Applied Mechanics, 44, 631-636.

Comninou, M., Schmueser, D., 1979. The interface crack in a combined tension-compression and shear field. Journal of Applied Mechanics, 46, 345-348.

de Verdia, L.A., 1989. Applications of EPFM to welding: current trends, Advances in Fracture Research, Vol. 1, ed. by K. Salama and others, Pergamon Press, 223-230.

Donato, G.H.B., Magnabosco, R., Ruggieri, C., 2009. Effects of weld strength mismatch on J and CTOD estimation procedure for SE(B) specimens. International Journal of Fracture, 159, 1-20.

Dong, P., Pan, J., 1990. Plane strain mixed-mode near-tip fields in elastic perfectly plastic solids under small-scale yielding conditions. International Journal of Fracture 45, 243-262.

Dowd, O. and Shih., 1991. Family of crack tip fields characterized by a triaxiality parameter-I: Structure of fields. Journal of Mechanics and Physics of Solids, 39**,** 898-1015.

Drucker, D.C, 1951. A more fundamental approach to plastic stress-stran relations. Proceedings of 1st U.S. National Congress on Applied Mechanics, 487.

Du, Z.Z., Hancock, J.W., 1991. The effect of non-singular stresses on crack tip constraint. Journal of the Mechanics and Physics of Solids 39, 555-567.

Duga. J.J., Fisher, W.H., Buxbaum, R.W., Rosen field, A.R., Burh A.R., Honton. E.J., and McMillan, S.C., 1983. The Economic Effects of Fracture in the United States. NBS Special Publication 647-2, United States, Department of Commerce, Washington, DC.

England, A.H., 1965. A crack between dissimilar media. Journal of Applied Mechanics, 32, 400-402.

Erdogan, F., 1965. Stress distribution in bonded dissimilar materials with cracks. Journal of Applied Mechanics, 32, 403-410.

Eripret, C., Hornet, P., (1992). Prediction of overmatching effects on fracture of stainless steel cracked welds. Proc. Of Shallow Cracks Fracture Mechanics, Cambridge, England.

Eripret, C., Hornet, P., (1994). Prediction of overmatching effects on the fracture of stainless steel cracked welds, Mis-Matching of Welds, ESIS 17. Mechanical Engineering Publications, London, pp. 685-708.

Eripret, C., Hornet, P., (1995). Experimental J evaluation from a load-displacement curve for homogeneous and overmatched SENB or CCT specimens. Fatigue & Fracture of Engineering Materials & Structures, 18, 679-692.

Ernst, H.A., Paris P.C., Rossow M., Hutchinson J.W., 1979. Analysis of load displacement relation to determine J–R curve and tearing instability material properties. In: Smith CW, editor. Fracture Mechanics, ASTM STP 677. Philadelphia: American Society for Testing and Materials, 581-599.

Ernst, H.A., Paris P.C., 1980. Techniques of analysis of load–displacement records by J-integral methods, NUREG/CR-1222, US Nuclear Regulatory Commission.

Ewing, D.J.F., 1968. Calculations on the bending of rigid/plastic notched bars. Journal of Mechanics and Physics of Solids, 16, 205-213.

Ewing, D.J.F. and Richards, C.E., 1974. The yield-point loads of singly-notched pin-loaded tensile strips, Journal of Mechanics and Physics of Solids, 22, 27-36.

Ganti, S., Parks, D.M., 1997. Elastic-plastic fracture mechanics of strength-mismatch interface cracks. In: Mahidhara, R.K., et al. (Eds), Recent Advances in Fracture. The Minerals, Metals and Materials Society, 13-25.

Garwood, S.J., 1985. The measurement of critical values of crack tip opening displacement (COD) and J on parent steels and weldments for use in fracture assessment, in Elastic-Plastic Fracture Mechanics, ed. by L.H. Larsson, D. Reidel Pub. Com., 85-115.

Gordon, J.R., Wang, Y.Y., (1994). The effect of weld metal mismatch on structural integrity assessments. EWI Report J6154-11-94.

Green, A.P., 1953. The plastic yielding of notched bars due to bending. Quarterly Journal of Mechanics and Applied Mathematics, 6, 223-239.

Green, A.P., 1954. A theory of plastic yielding due to bending of cantilevers and fixed-ended beams. Part I. Journal of Mechanics and Physics of Solids, 8, 1-15.

Green, A.P., 1956. The plastic yielding of shallow notched bars due to bending. Journal of Mechanics and Physics of Solids, 4, 259-268.

Green, A.P. and Hundy, B.B., 1956. Initial plastic yielding in notch bend tests. Journal of Mechanics and Physics of Solids, 4, 128-144.

Guo, Q., Keer, L.M., 1990a. A crack at the interface between an elastic-perfectly plastic solid and a rigid substrate. Journal of the Mechanics and Physics of Solids, 38, 843-857.

Guo, Q., Keer, L.M., 1990b. A crack at the interface of two power-law hardening materials-Antiplane case. Journal of the Mechanics and Physics of Solids, 38, 183- 194.

Halling, J., and Mitchell, L.A., 1967. The effect of variation in yield stress on slip line field solutions. International Journal of Production Research, 5, 249-262.

Hao, S., Cornec, A., Schwalbe, K.H., 1997. Plastic stress-strain fields and limit loads of a plane strain cracked tensile panel with a mismatched welded joint. International Journal of Solids & Structures, 34, 297-326.

Hao, S., Schwalbe, K. H., Cornec, A., 2000. The effect of yield strength mismatch on the fracture analysis of welded joints; slip-line field solutions for pure bending. International Journal of Solids & Structures, 37, 5385-5411.

Hencky, H., Zeits. ang. Math. Mech., (1923), Vol.3, Pg. 241.

Hill, R., 1950. The Mathematical Theory of Plasticity. Clarendon Press, Oxford.

Hill, R., 1954. On the limits set by plastic yielding to the intensity of singularities of stress. Journal of Mechanics and Physics of Solids, 2**,** 278-285.

Homma, H., Kanto, Y., Kubo, T., Tanaka, Y., 1995. Crack growth resistance in bimetallic weldment. International Journal of Pressure Vessel and Piping, 63, 225-236.

Hornet, P., Eripret, P., 1995. Experimental J evaluation from a load-displacement curve for homogeneous and overmatched SENB or CCT specimens. Fatigue & Fracture of Engineering Materials & Structures, 18, 679-692.

Hoshide, T., Yamada, A., Tanaka, K., (1982). Evaluation of J-integral under gross and general yieldings and its application to fatigue crack growth. Journal of the Society of Materials Science, 31, 810-816.

Hundy, B.B., 1954. Plane plastic. Metallurgia, 49, 109.

Hutchinson, J.W., 1968. Singular behaviour at the end of a tensile crack in a hardening material. Journal of Mechanics and Physics of Solids, 16**,** 13-31.

Hutchinson, J.W., 1983. Fundamentals of the phenomenological theory of nonlinear fracture mechanics. Journal of applied Mechanics, 105, 1042-1051.

Hutchinson J.W., Paris P.C., 1979. Stability analysis of J-controlled crack growth. In: Elastic-Plastic Fracture, ASTM STP 668. Philadelphia: American Society for Testing and Materials, 37-64.

Hutchinson, J.W., Shih, C.F., 1975. Plastic analysis of mixed mode plane stress crack problems. Recent advances in Engineering Science ed T.S. Chang, (Boston; Scientific Publishers), 245-253.

Ibragimov, V.A., Tarasyuk, N.E., 1976. Asymptotic behaviour of stress state near crack tip in elastic-ideally plastic medium. Izv. AN SSSR, Mechanika Tverdogo Tela 11, 184-185.

Joch, J., Ainsworth, R.A., and Hyde, T.H., 1993. Limit load and J-estimates for idealised problems of deeply cracked welded joints in plane-strain bending and tension. Fatigue & Fracture of Engineering Materials & Structures, 16**,** 1061-1079.

Johnson, W., and Mellor P.B., 1973. Engineering Plasticity. Von Nostrand Reinhold Company, New York.

Johnson, W., and Kudo, H., 1962. The mechanics of metal extrusion. Manchester: Manchester University Press.

Kachanov L.M., 1971. Foundations of the theory of plasticity. North-Holland publishing company, Amsterdam.

Kim, Y.J., 2002a. Estimation of fully plastic crack tip stresses from equilibrium of least upper bound circular arcs. International Journal of Mechanical sciences, 44**,** 881-897.

Kim, Y.J., 2002b. Experimental J estimation equations for single-edge-cracked bars in four-point bend: homogeneous and bi-material specimens. Engineering Fracture Mechanics, 69, 793-811.

Kim, Y.J., Kim, J.S., Schwalbe, K.H., Kim, Y.J., 2003. Numerical investigation on J-integral testing of heterogeneous fracture toughness testing specimens: Part I-weld metal cracks. Fatigue & Fracture of Engineering Materials & Structures, 26 **,** 683-694.

Kim, Y.J., Lin, G., Cornec, A., Schwalbe, K.H., 1996. Fully plastic crack tip fields for plane strain shallow-cracked specimens under pure bending. International Journal of Fracture 78, 21-34.

Kim, Y. J., McClintock F. A., Parks, D.M., 1995. Yield locus in deep, single-face-cracked specimens under combined bending and tension. Journal of Applied Mechanics, 63**,** 1045-1047.

Kim, Y.J., Oh, C.S., 2006. Finite element limit analyses of under-matched tensile specimens. Engineering Fracture Mechanics, 73, 1362-1378.

Kim, Y.J., Schwalbe, K.H., 2001a. Mismatch effect on plastic yield loads in idealised weldments. I. Weld centre cracks, Engineering Fracture Mechanics, 68**,** 163-182.

Kim, Y.J., Schwalbe, K.H., 2001b. Mismatch effect on plastic yield loads in idealised weldments. II. Heat affected zone cracks, Engineering Fracture Mechanics, 68**,** 183-199.

Kim, Y.J., Schwalbe, K.H., 2001c. Compendium of yield load solutions for strength mis-matched DE(T),SE(B) and C(T) specimens, Engineering Fracture Mechanics, 68, 1137-1151.

Kim, Y.J., Schwalbe K.H., 2001d. On experimental J estimation equations based on CMOD for SE(B) specimens. Journal of Testing Evaluation, 2001, 29, 67-71.

Kim Y.J., Schwalbe K.H., 2001e. On the sensitivity of J estimation to materials' stress strain curves in fracture toughness testing using the finite element method. Journal of Testing Evaluation, 29, 18-30.

Kim, Y.J., Schwalbe, K.H., 2004. Numerical analyses of strength mis-match effect on local stresses for ideally plastic material. Engineering Fracture Mechanics, 71, 1177-1199.

Kim, Y.J., Son, B.G., Kim, Y.J., 2004. Elastic-plastic finite element analysis for double-edge cracked tension DE(T) plates. Engineering Fracture Mechanics, 71, 945-966.

Kirk, M.T., Dodds, R.H., 1991. An analytical and experimental comparison of J_i values for shallow through and part through surface cracks. Engineering Fracture Mechanics, 39, 535-551.

Kirk, M.T., Dodds, R.H., 1993. The influence of weld strength mismatch on crack tip constraint in single edge notch specimens. International Journal of Fracture, 63, 297-316.

Koiter, W., 1960. General theorems for elastic-plastic solids, in: Sneddon and Hill (eds.), Progress in solid mechanics Vol. 1, North- Holland.

Landes J.D., Walker H., and Clarke G.A., 1979. Evaluation of estimation procedures used in J-integral testing. In: Elastic-Plastic Fracture, ASTM STP 668. Philadelphia: American Society for Testing and Materials, 266-287.

Larsson, S.G., Carlsson, A.J., 1973. Influence of non-singular stress terms and specimen goemetry on small-scale yielding at crack tips in elastic-plastic materials. Journal of Mechanics and Physics of Solids, 21, 263-277.

Lee, H., Kim, Y.J., 2001. Interfacial crack tip constraints and J-integrals in plastically mismatched bi-materials. Engineering Fracture Mechanics, 68, 1013-1031.

Lee, H., Parks, D.M., 1993. Fully plastic analyses of plane strain single edge cracked specimens subjected to combined tension and bending. International Journal of Fracture, 63, 329-349.

Lei Y, Ainsworth RA, 1997. A J integral estimation method for cracks in welds with mismatched mechanical properties. International Journal of Pressure Vessels & Piping, 70, 237-245.

Lei, Y., Tao, J., Li, P.N., 1999. Limit load and J estimates of a centre cracked plate with an asymmetric crack in a mismatched weld. International Journal of Pressure Vessels & Piping, 76, 747-757.

Li, J., Hancock, J.W., 1999. Mode I and mixed mode fields with incomplete crack tip plasticity. International Journal of Solids & Structures 36, 711-725.

Liechti, K.M., Chai, Y.S., 1992. Asymmetric shielding in interfacial fracture under in-plane shear. Journal of Applied Mechanics, 59, 295-304.

Markov, A.A., 1947. On variational principles in the theory of plasticity. Prikladnaia Matematica I Mekhanika, 11, 339-350.

McClintock, F.A., 1971. Plasticity aspects of fracture. In: Liebowitz, H. (Ed.), Fracture: An advanced Treatise, Vol. 3. Academic Press, New York, pp. 47-225.

Miller, A.G., 1988. Review of limit loads of structures containing defects. International Journal of Pressure Vessel & Piping, 32, 197-327.

Milne, I., Ainsworth, R.A., Dowling, A.R., Stewart, A.T., 1986. Assessment of the integrity of structures containing defects, R/H/R6-Rev.3, CEGB, UK.

Narasimhan, R., Subramanya, H.Y., Patil, S.D., Tandaiya, P., Ramamurty, U., 2009. Stationary crack tip fields in elastic-plastic solids: an overview of recent numerical simulations. Journal of Physics D: Applied Physics, 42, 1-15.

Neale, B.K., 1999. The fracture behaviour of mismatched centre-cracked welded specimens in tension. Engineering Fracture Mechanics, 64**,** 473-484.

Nemat-Nasser, S., Obata, M., 1984. On stress field near a stationary crack tip. Mechanics of Materials 3, 235-243.

O'Dowd, N. P., Shih, C. F., 1991. Family of crack-tip fields characterized by a triaxiality parameter-I. Structure of fields. Journal of the Mechanics and Physics of Solids, 39, 989-1015.

O'Dowd, N.P., Shih, C.F., Stout, M.G., 1992. Test geometries for measuring interfacial fracture toughness. International Journal of Solids and Structures 29, 571–589.

Prager, W., 1955. James Clayton Memorial Lecture, Institute of Mechanical Engineers.

Prager, W., and Hodge, P.G., 1951. Theory of perfectly plastic solids. Wiley, New York.

Prandtl, L., 1920. Ueber die Haerte plastischer Koerper. Goettinger Nachr., math.-phys. Kl. 74-85.

Ranestad, Φ., Zhang, Z. and Thaulow, C., 1997. Quantification of mismatch constraint for an interface crack in an elastic-plastic tri-material system. In: Schwalbe K.H., Kocak, M., editors, Mismatching of interfaces and welds. Germany: GKSS Research Centre Publications. 209-220.

Rice, J.R., 1968. A path independent integral and the approximate analysis of strain concentration by notches and cracks. Journal of Applied Mechanics 35, 379-386.

Rice, J.R., 1972. The line spring model for surface flaws. In Swedlow JL, editor. The surface crack: physical problems and computational solutions, New York. American Society of Mechanical Engineers, 171-185.

Rice, J.R., 1974. Limitations to the small scale yielding approximation for crack tip plasticity. Journal of the Mechanics and Physics of Solids, 22, 17-26.

Rice, J.R., 1988. Elastic fracture mechanics concepts for interfacial cracks. Journal of applied Mechanics, 55, 98-103.

Rice, J.R., Johnson, M.A., 1970. The role of large crack tip geometry changes in plane strain fracture. In: Kannine, M.F., Adler, W.F., Rosenfield, A.R., Jaffee, R.I. (Eds.), Inelastic Behavior of Solids. McGraw-Hill, New York, p. 641.

Rice J.R., Paris P.C., Merkle J.G., 1973. Some further results of J-integral analysis and estimates. In: Progress in Flaw Growth and Fracture Toughness Testing, ASTM STP 536. Philadelphia: American Society for Testing and Materials, 231-245.

Rice, J.R., Rosengren, G.F., 1968. Plane strain deformation near a crack tip in a power-law hardening material. Journal of the Mechanics and Physics of Solids, 16, 1-12.

Rice, J.R., Sih, G.C., 1965. Plane problems of crack in dissimilar media. Journal of Applied Mechanics, 32, 418-423.

Roos E., Eisele U., Silcher H., 1986. A procedure for the experimental assessment of the J-integral by means of specimens of different geometries. International Journal of Pressure Vessels & Piping, 23, 81-93.

Roos E., Eisele U., Silcher H., 1993. Effect of stress state on the ductile fracture behaviour of large scale specimens. Constraint effects in fracture. ASTM STP 1171. E.M. Hackett, K.H. Schwalbe, R.H. Dodds, Eds., American Society for Testing and Materials, Philadelphia, 41-63.

Saxena, A., 2007. Role of nonlinear fracture mechanics in assessing fracture and crack growth in welds. Engineering Fracture Mechanics, 74, 821-838.

Sham, T.L., Li, J., Hancock, J.W., 1999. A family of plane strain crack tip stress fields for interface cracks in strength-mismatched elastic-perfectly plastic solids. Journal of the Mechanics and Physics of Solids, 47, 1963-2010.

Sharma, S.M., Aravas, N.J., 1991. Determination of higher order terms in elastoplastic crack tip solutions. Journal of the Mechanics and Physics of Solids, 39, 1043-1072.

Shih, C.F., 1974. Small scale yielding analysis of mixed mode plane strain crack problems. In: Fracture Analysis, ASTM STP 560, Philadelphia: American Society for Testing and Materials, 187-210.

Shih, C.F., Asaro, R.J., 1988. Elastic-plastic analysis of cracks on bimaterial interfaces: part I-small-scale yielding. Journal of Applied Mechanics 55, 299-316.

Shih, C.F., Asaro, R.J., 1989. Elastic–plastic analysis of cracks on bimaterial interfaces: part II-structures of small-scale yielding fields. Journal of Applied Mechanics 56, 763-779.

Shih, C.F., Asaro, R.J., O'Dowd, N.P., 1991. Elastic-plastic analysis of cracks on bimaterial interfaces: part III-large scale yielding. Journal of Applied Mechanics 58, 450-463.

Shiratori, M., Dodd, B., 1980. Effect of deep wedge-shaped notches of small flank angle on plastic failure. International Journal of Mechanical sciences, 22**,** 127-131.

Shiratori, M., Miyoshi, T., 1980. Evaluation of constraint factor and J-integral for single-edge notched specimen. In: Proceedings of the third international conference on materials, Vol. 3, Cambridge, UK, 425-434.

Sih, G.C., Rice, J.R., 1964. The bending of plates of dissimilar materials with cracks. Journal of applied Mechanics, 31, 477-482.

Sumpter, J.D.G., 1987. J_c determination for shallow notch welded bend specimens. Fatigue & Fracture of Engineering Materials & Structures, 10, 479-493.

Sumpter, J.D.G., 1989. Prediction of critical crack size in plastically strain welded panels. Non linear Fracture Mechanics: Volume II-Elastic-Plastic Fracture, ASTM STP 995, J. D. Landes, A. Saxena and J. G. Merkle (Eds), American Society for Testing and Materials, Philadelphia, PA, 415-432.

Tang, W., Shi, Y.W., 1995. Influence of strength matching and crack depth on fracture toughness of welded joints. Engineering Fracture Mechanics, 51, 649-659.

Varias, A.G., Suo, Z., and Shih C.F., 1991. Ductile failure of a constrained metal foil. Journal of the Mechanics and Physics of Solids 37, 963-986.

Tvergaard, V., Hutchinson, J.W., 1993. The influence of plasticity on mixed mode interface toughness. Journal of the Mechanics and Physics of Solids 41, 1119-1135.

Wang, Y.Y., Gordon, J.R., 1992. The limits of applicability of J and CTOD estimation procedures for shallow-cracked SENB specimens. In: Dawes MG, editor. Shallow crack fracture mechanics, toughness and applications. The welding institute, Abington, Cambridge.

Westergaard, H.M., 1939. Bearing pressures and cracks. Journal of Applied Mechanics, 6, 49-53.

Williams, M.L., 1957. On the stress distribution at the base of a stationary crack. Journal of Applied Mechanics 24, 109-114.

Williams, M.L., 1959. The stresses around a fault or crack in dissimilar media. Bull. Seism. Soc. Am., 49, 199-204.

Willis, J.R., 1971. Fracture mechanics of interfacial cracks. Journal of the Mechanics and Physics of Solids 19, 353-368.

Wu, S.X., Cotterell, B., and Mai, Y.W., 1987. Slip-line field solutions of three-point bend specimens with deep notches. International Journal of Mechanical sciences, 29**,** 557-564.

Xia, L., Wang, T.C., Shih, C.F., 1993. Higher-order analysis of crack tip fields in elastic power-law hardening materials. Journal of the Mechanics and Physics of Solids 41, 665-687.

Zhang, Z.L., Hauge, M., Thaulow, C., 1997a. Two parameter characterization of the near tip stress fields for bi-material elastic-plastic interface crack. International Journal of Fracture, 79, 65-83.

Zhang, Z.L., Hauge, M., Thaulow, C., 1997b. Assessment of material mis-match constraint in a bi-material elastic-plastic interface crack. In: Schwalbe K.H., Kocak, M., editors, Mismatching of interfaces and welds. Germany: GKSS Research Centre Publications. 149-160.

Zhu, X.K., Chao, Y.J., 2000. Fully plastic crack tip fields for CCP and DECP specimens under tension in non-hardening materials. International Journal of Solids and Structures, 37, 577-588.

Zhu, X.K., Chao, Y.J., 2001. Constraint effects on crack tip fields in elastic-perfectly plastic materials. Journal of the Mechanics and Physics of Solids 49, 363-399.

Zhu, X.K., Hwang, K.C., Liu, G.T., 1997. Continuous near-tip fields for a dynamic crack propagating ina power-law elastic-plastic material. International Journal of Fracture, 85, 201-209.

Zywicz, E., Parks, D.M., 1989. Elastic yield zone around an interfacial crack-tip. Journal of Applied Mechanics 56, 577-584.

Zywicz, E., Parks, D.M., 1992. Small-scale yielding interfacial crack-tip fields. Journal of the Mechanics and Physics of Solids 40, 511–536.